「細胞・脳機能研究の融合による神経疾患診断・治療法開発拠点の形成」

平成２３年度～平成２７年度私立大学戦略的研究基盤形成支援事業
研　　究　　成　　果　　報　　告　　書

平成28年5月

学校法人名　順天堂
大　学　名　順天堂大学
研究組織名　老人性疾患病態・治療研究センター
研究代表者　服部　信孝
（順天堂大学大学院医学研究科神経学 教授）

はしがき

順天堂大学大学院医学研究科老人性疾患病態・治療研究センター（老研センター）は、文部科学省「平成23年度私立大学戦略的研究基盤形成支援事業研究プロジェクト」に、「細胞・脳機能研究の融合による神経疾患診断・治療法開発拠点の形成予防・治療法開発拠点の形成」をテーマに応募し、採択された。

老人性疾患病態・治療研究センター（老研センター）では、これまで、パーキンソン病（PD）、アルツハイマー病（AD）等の加齢性神経疾患の分子遺伝学的な研究実績を重ねてきた。特に、遺伝性PDの原因遺伝子としてパーキンを世界で初めて同定し、この遺伝子産物であるパーキン分子がユビキチン-リガーゼ（E3酵素）であることを報告した。この発見が元となり、異常なミトコンドリアの処理にこのパーキン分子が関与すること、すなわち孤発性のPDを含め、その病態と異常なミトコンドリアとの関連性が分子レベルで語れるようになってきた。このような時期に、本研究プロジェクトで5年間（平成23年度～27年度）の支援を受けて、“神経疾患診断・治療法開発を推進するため、優れた臨床実績を生かした私立医系大学独自の基礎臨床連携を強化し、“細胞機能研究”と“画像・生理学的脳機能研究”を融合した新たな研究基盤センターを形成することを目的とした研究を進めることができたことの価値は非常に大きかった。さらに、高齢化社会に入った現在、医療の面から高齢化社会に向き合うことは重要である。特に、疾患病態の解析、診断法の開発、新たな治療法にどこまで切り込めるのか、を課題に５年間、向き合えたことは非常に恵まれていたと考えている。

実際、本プロジェクトでは、ミトコンドリア、タンパク質分解等、老化に深く関わる細胞機能の破綻と修復を疾患モデル動物で研究を進めた。脳機能研究では疾患候補遺伝子と画像変化の関連や、SPECTやPETを用いた分子イメージングなどの、患者を対象とし、新たな知見を得ることができた。ここに、本プロジェクトの成果を報告できることに深く感謝すると共に、私たちが新たに得た知見が少しでも社会的に貢献できたとの評価を頂ければ本望である。

（様式 2）

法人番号	131025
プロジェクト番号	S1101009

平成23年度～平成27年度「私立大学戦略的研究基盤形成支援事業」
研究成果報告書概要

1 学校法人名 順天堂　　2 大学名 順天堂大学

3 研究組織名 老人性疾患病態・治療研究センター

4 プロジェクト所在地 東京都文京区本郷2−1−1

5 研究プロジェクト名 細胞・脳機能研究の融合による神経疾患診断・治療法開発拠点の形成

6 研究観点 研究拠点を形成する研究

7 研究代表者

研究代表者名	所属部局名	職名
服部信孝	大学院医学研究科	教授

8 プロジェクト参加研究者数 11 名 （その他平成27年度の時点で、ポスドク 9名、リサーチアシスタント 3名、連携研究者（奨励研究者23名）、外部連携研究者（兼評価委員） 3名）

9 該当審査区分 理工・情報　　(生物・医歯)　　人文・社会

10 研究プロジェクトに参加する主な研究者

研究者名	所属・職名	プロジェクトでの研究課題	プロジェクトでの役割
服部信孝	大学院医学研究科・神経学・教授	ミトコンドリア，ユビキチン・プロテアソームに着目したパーキンソン病の病態解明と治療戦略	細胞機能標的治療によるパーキンソン病の克服
内山安男	大学院医学研究科・老人性疾患病態・治療研究センター、センター長	オートファジー／リソソームによる神経回路網の品質管理とその破綻	神経疾患における神経回路網の品質管理異常と治療による正常化をイメージングで検証する
櫻井隆	大学院医学研究科・薬理学	βアミロイド産生・分解調節系における細胞内輸送・神経活動依存性の解析	βアミロイド産生・分解系の解析によりアルツハイマー病の病態解明と創薬標的探索を進める
平澤恵理	大学院医学研究科老人性疾患病態治療研究センター・先任准教授	細胞外環境による細胞の分化・増殖の制御	細胞外マトリックス等の条件検討により脳疾患細胞治療に有利な細胞外環境を示す

法人番号	131025
プロジェクト番号	S1101009

樋野興夫	大学院医学研究科・病理・腫瘍学　教授	神経細胞の分化・移動・腫瘍化・幹細胞性−特に結節性硬化症の原因遺伝子 Tsc2 を起点として−	Tsc2 分子の研究成果を生かし神経細胞における腫瘍化と幹細胞性の維持機構を解明する
新井一	大学院医学研究科・脳神経外科学	脳腫瘍発生分子機構における神経細胞の腫瘍化と幹細胞性	グリオーマをモデルとして神経細胞の幹細胞性のメカニズムを標的とした治療を開発する
高久智生	大学院医学研究科・血液学	骨髄幹細胞ニッチ環境研究による成体神経新生メカニズム	骨髄幹細胞ニッチ環境の三次元可視化とその機能解明を行い、成体神経新生システムに応用する。
池田勝久	大学院医学研究科・耳鼻咽喉科学・教授	聴覚・平衡覚にかかわる細胞品質管理機構の正常とその破綻	聴覚・平衡覚にかかわる細胞品質管理機構の可視化、脳機能疾患との関連性を示す
宇賀貴紀	大学院医学研究科・神経生理学・先任准教授	多点電極を用いた神経活動記録法の整備	モデル動物での神経ネットワークを可視化するため、多点電極を用いた神経活動記録法を整備する
青木茂樹	大学院医学研究科・放射線医学・教授	脳の加齢・認知・発達障害の可視化　新規画像診断法の確立	加齢・認知・発達障害による脳機能異常を示す新規画像解析法を開発する
新井平伊	大学院医学研究科・精神医学・教授	アルツハイマー病の発症分子機構解明	アルツハイマー病の発症分子機構を解明し、新規診断・治療技術を発展させる
（共同研究機関等）			
東京都臨床医学総合研究所・理事長・所長	田中啓二	オートファジー不全と神経変性機構解明	オートファジー不全の正常化による神経変性疾患の治療
大阪大学医学系研究科・教授	長澤丘司	免疫担当細胞ニッチ環境の時間的空間的理解	造血幹細胞ニッチ研究成果からの成体神経新生ニッチへの情報提供
慶應義塾大学・医学部・医学部長・生理学教室・教授	岡野　栄之	神経変性疾患における iPS 治療の基盤確立	神経変性疾患における iPS 治療の基盤確立

（様式 2）

法人番号	131025
プロジェクト番号	S1101009

＜研究者の変更状況（研究代表者を含む）＞

旧

ﾌﾟﾛｼﾞｪｸﾄでの研究課題	所属・職名	研究者氏名	プロジェクトでの役割
アルツハイマー病の炎症性 T 細胞の可視化	大学院医学研究科・認知症診断予防治療学・客員教授	田平武	Aβ反応性 T 細胞による神経傷害機構を可視化し、新規診断・治療技術を発展させる

（変更の時期：平成 24 年 4 月 1 日）

新

変更前の所属・職名	変更（就任）後の所属・職名	研究者氏名	プロジェクトでの役割
大学院医学研究科精神・行動科学・教授	大学院医学研究科精神・行動科学・教授	新井 平伊	アルツハイマー病の発症分子機構を解明し、新規診断・治療技術を発展させる
大学院医学研究科細胞・分子薬理学・教授	大学院医学研究科細胞・分子薬理学・教授	櫻井隆	βアミロイド産生・分解系の解析によりアルツハイマー病の病態解明と創薬標的探索を進める

旧

ﾌﾟﾛｼﾞｪｸﾄでの研究課題	所属・職名	研究者氏名	プロジェクトでの役割
発達障害性神経疾患の原因分子探索のための可視化	大学院医学研究科神経生理学・教授	北澤茂	発達障害性神経疾患の原因分子探索のための可視化

（変更の時期：平成 23 年 6 月 30 日）

新

変更前の所属・職名	変更（就任）後の所属・職名	研究者氏名	プロジェクトでの役割
大学院医学研究科神経生理学・教授	大阪大学医学系研究科・教授	北澤茂	発達障害性神経疾患の原因分子探索のための可視化

旧

ﾌﾟﾛｼﾞｪｸﾄでの研究課題	所属・職名	研究者氏名	プロジェクトでの役割
オートファジー／リソソームによる神経回路網の品質管理とその破綻	大学院医学研究科神経機能構造学・教授	内山安男	神経疾患における神経回路網の品質管理異常と治療による正常化をイメージングで検証する

（変更の時期：平成 23 年 4 月 1 日）

法人番号	131025
プロジェクト番号	S1101009

新

変更前の所属・職名	変更（就任）後の所属・職名	研究者氏名	プロジェクトでの役割
大学院医学研究科神経機能構造学・教授	大学院医学研究科老人性疾患病態・治療研究センター・センター長	内山安男	神経疾患における神経回路網の品質管理異常と治療による正常化をイメージングで検証する

11 研究の概要（※ 項目全体を10枚以内で作成）

（1）研究プロジェクトの目的・意義及び計画の概要

老人性疾患病態・治療研究センター（老研センター）では、これまで加齢性神経疾患、特にパーキンソン病(PD)、アルツハイマー病(AD)等で分子遺伝学的な研究実績を重ねてきた。本申請では、神経疾患診断・治療法開発を推進するため、基礎臨床連携を強化し、”細胞機能研究”と”画像・生理学的脳機能研究”を融合した新たな拠点を形成する。細胞機能研究では、タンパク質品質管理と神経新生機構を標的とした治療方法を開発する。具体的には、ミトコンドリア機能、タンパク質分解系機能等、老化に深く関わる細胞機能の破綻と修復を疾患モデル動物で研究する。脳機能研究では疾患候補遺伝子と画像変化（脳体積、白質構造、機能的 MRI 等）の関連や、SPECT や PET を用いた分子イメージングなどの、患者を対象とした知見を得る。これらの臨床研究から、症状特異性の高い新たな遺伝子・標的分子を発見し、細胞機能研究の成果と融合させる。細胞を使った分子生物学的研究と脳科学研究は各々独立して遂行されているが、 神経疾患の診断・治療研究の推進には密接な連携が重要である。本学は老研センター運営を通じ、これを可能として来た。本申請により社会的貢献を果たす拠点を形成できると考えられる。

（2）研究組織

図参照:高齢者におけるさまざまな疾患の原因究明を目的に、「ハイテクリサーチセンター整備事業」の一環としてスタートし、国内外研究機関との連携のもと、研究拠点形成を行ってきた老研センターを基盤施設とする。研究グループは、細胞機能研究と脳機能研究の2つに大きく分け、前者は、(1)細胞の品質管理機構とその破綻の観点から、神経変性疾患等について解析するとともに、(2)細胞の分化・増殖・幹細胞性の観点から、腫瘍学、骨髄幹細胞研究等異分野の知見を統合する。後者では、(3)加齢・認知・発達障害の画像解析の観点から神経変性疾患、発達障害の多様な遺伝リスク因子を少数の表現型に分類するための遺伝画像解析を確立する。特に本学神経放射線科の得意とする神経疾患での拡散テンソルイメージング技術を生かし、早期病変の可視化や薬剤効果判定に寄与するバイオマーカーを開発し、疾患特異性のある新規遺伝子、分子を探索する。代表研究者11名に加え、ポスドク9名（平成27年度現在）、リサーチアシスタント3名（平成27年度現在）、及び内部連携研究者（奨励研究23名（平成27年度））で研究を推進している。他、外部連携者 3 名は、3つの小課題の研究領域における本邦を代表する研究者であり、研究推進の連携と外部評価を依頼している。

法人番号	131025
プロジェクト番号	S1101009

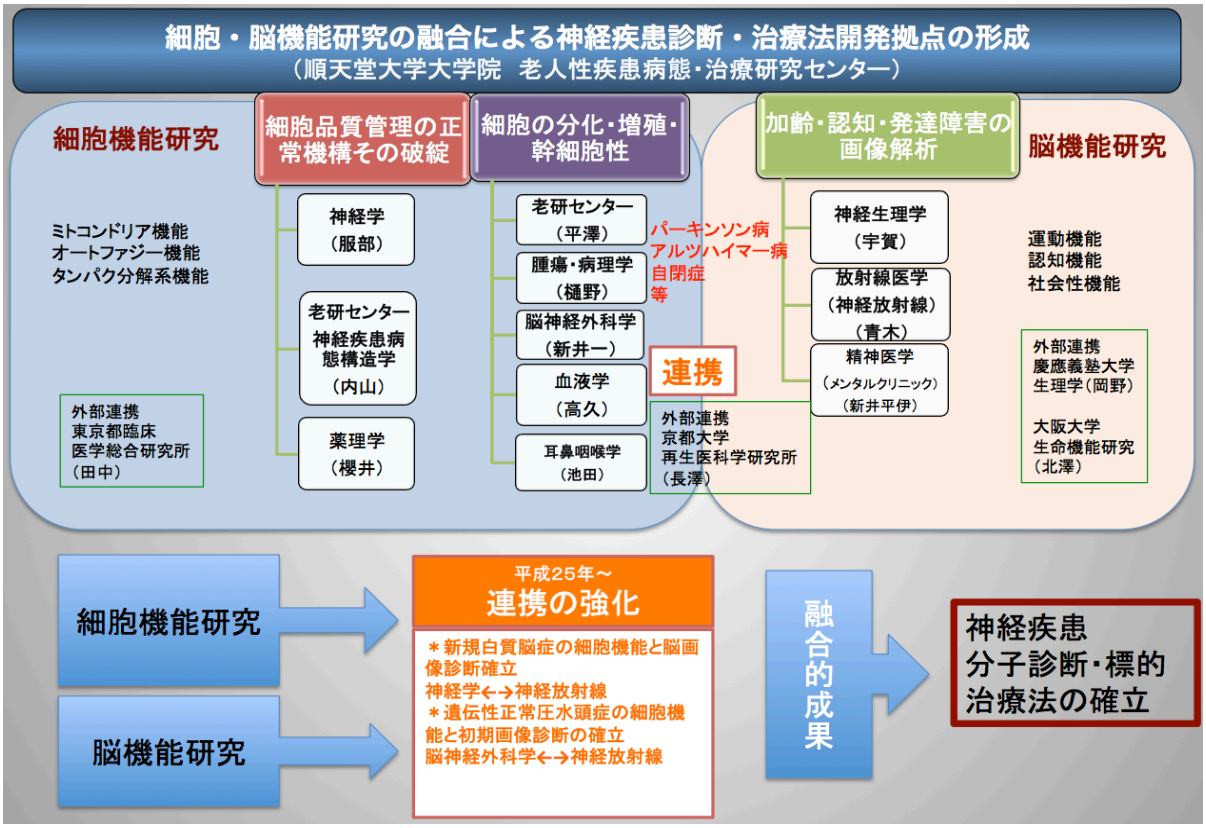

（3）研究施設・設備等

高齢者におけるさまざまな疾患の原因究明を目的に、「ハイテクリサーチセンター整備事業」の一環としてスタートした、老人性疾患病態・治療研究センター（研究施設面積：8，268㎡、使用者数：100 人）を基盤施設とする。細胞機能の正常と異常を評価するため、経時的イメージングを施行するが、1年目に 2 光子顕微鏡（ZeissLSM7DUO NLO、稼働時間数：336h）を整備した。

（4）研究成果の概要　※下記、13及び14に対応する成果には下線及び＊を付すこと。

研究プロジェクトの計画や目的・意義と関連づけて、当初の目標をどれだけ達成したか記述するとともに、新たに得られた知見などについても具体的に記述してください。

（１）細胞の品質管理の正常機構とその破綻

服部グループ：ミトコンドリア，ユビキチン・プロテアソームに着目したパーキンソン病の病態解明と治療戦略

遺伝性パーキンソン病の病態としてオートファジーリソソーム系の関与が有力と成りつつある。これまでに 1）PINK1/Parkin が協調して作用し、損傷ミトコンドリアをクリアランスすること。2）ATP13A2 はリソソーム膜上に局在し恒常性の維持に重要な働きをすることを明らかにしてきた。しかし、in vivo での解析が遅れていた。今回、PINK1 ノックアウトマウス由来の MEF 細胞ではミトコンドリア機能が有意に低下していること（＊108）、ATP13A2 ノックアウトマウスには異常なリソソームが多数蓄積していることを見出した（投稿準備中）。３）一方、常染色体優性遺伝性パーキンソン病の家系から新規原因遺伝子 CHCHD2 を同定した（＊12）。CHCHD2 はミトコンドリアに関連した因子であることから、遺伝性パーキンソン病の病態としてミトコンドリア機能の障害が強く疑われた。４）CHCHD2 と同様に新たな変異遺伝子を見出し、リソソーム酵素活性に関わるどう遺伝子産物の変異タンパク質の解析を鋭意進めている。

内山グループ：オートファジー／リソソームによる神経回路網の品質管理とその破綻

内山ら（小池は内山グループの一員として活動）は、軸索／シナプス前領域におけるオートファジー／リソソーム系の機構をモデルマウスの解析により明らかにし、カテプシンCやDNaseIIの特異的

法人番号	131025
プロジェクト番号	S1101009

な局在を(＊159,161)、Atg8のほ乳類ホモログの一つであるGABARAPのトランスジェニックマウスを作成し、LC3（細胞体と樹状突起）と異なり、軸索初節への局在を（＊158）明らかにした。リソソームの膜タンパク質であるLAMP2を欠損する症例（ダノン病症候群）と欠損マウスの中枢神経系における形態解析したこと(＊13,160)、選択的オートファジーのアダプタータンパク質であるp62とNBR1は、オリゴマーを形成し、細胞体と樹状突起に局在するが、軸索には侵入できないこと、N端側にあるその責任ドメインを除くと単量体となり軸索にも侵入すること、さらに、オートファジー関連因子の中で唯一膜タンパク質であるAtg9aを脳特異的に欠損させた所、軸索が正常に伸展せず、脳梁や前交連の形成が障害されることが分かった（**39、論文はrevise中)。これまで、酸性条件下に対して感受性を持つ蛍光色素と耐性の蛍光色素をつないだ蛍光を用いてオートファゴソームの成熟性を検討していたが、十分ではなかった。私たちは、この条件を完全に克服する蛍光色素、pHluorin-mKate tandem fluorescence proteinを開発した。これにLC３を付加したしたタンパク質は、オートファゴソームの成熟化の良いマーカーとなる（*17）。また、服部らと共同したCHCHD2がミトコンドリアにあることを明らかにした（*12)。

櫻井グループ：βアミロイド産生・分解系調節機構の可視化解析

アルツハイマー病の病理に中心的な役割を果たすβアミロイド（Aβ)は、ミクロドメインにおけるアミロイド前駆体タンパク質(APP)のβ・γ切断により産生される。BACE1 によるβ切断が起こる初期エンドソームの輸送障害とβ切断亢進が孤発性アルツハイマー病の初期変化とされているが、その機序は明らかではない。また、BACE1 阻害薬は治療戦略として有望であるが、APP 以外の BACE1 基質の切断抑制による副作用発現が懸念される。切断端認識抗体を用いた BACE1 基質切断の可視化により、創薬標的となる APP 特異的β切断制御因子を見出すことを目的としてミクロドメインを解析した。その結果、エンドソーム輸送を制御する APP 結合蛋白質を見出し、エンドソーム障害及び APP 選択的なβ切断制御に関与することを明らかにした（**10)。現在、病態との関連、治療標的としての可能性について検討を進めている（特許出願)。また、βアミロイドによる神経障害に関わる代謝型グルタミン酸受容体について、他種受容体とのヘテロダイマー形成によるシグナル制御機構を明らかにした(*3,170)。

（２）細胞の分化・増殖・幹細胞性

平澤グループ：細胞外環境による細胞の分化・増殖の制御

成体神経新生領域である脳室下帯（SVZ）に存在する新規基底膜様構造 fractone と血管周細胞のネットワーク構造が、発生や成体神経新生に重要なニッチ環境を提供すると考えて、これまでに、FGF2 が fractone に存在するパールカンとヘパラン硫酸鎖を介し結合することを報告したが（Stem Cells 2007)、本研究では、ヘパラン硫酸プロテオグリカンであるパールカンを欠損する SVZ 及び neurosphere では、FGF2 投与による神経幹細胞の増殖率が有意に抑制されることを明らかにした（*115,171）。さらに、老化による fractone の構造、および構成タンパク質種および糖鎖修飾の変化を確認し（*36）、それによる神経新生シグナルの分子機構を検討した（論文投稿準備中)。さらに、青木グループ（放射線医学）と共同して、自閉症モデルマウスの拡散テンソル MRI 画像解析と透明化標本による３D 画像を比較検討して、新たなバイオマーカー開発手法を提示した（*34)。

樋野グループ：神経細胞の分化・移動・腫瘍化・幹細胞性−特に結節性硬化症の原因遺伝子 Tsc2 を起点として−

Eker ラット由来(*54,119,120,174,175)の胚盤胞より ES 細胞株を樹立し(*55)、多能性マーカー遺伝子発現や、胚様体および奇形腫における分化能を調べ、*Tsc2* ホモ欠損型細胞は野生型細胞と同様に三胚葉由来の組織形成能を示すが、Eker ラットの腎腫瘍に類似した異常腺管構造を発生することがわかった(＊106,107,154,155,156)。Tsc2+/+ Eker ラット胎児線維芽細胞からはアルカリホスファターゼ陽性の iPS 細胞様コロニーが多数得られる条件において、Tsc2-/- Eker ラット胎児線維芽細胞からはコロニーが全く形成されなかった。従って、ラットにおいて Tsc2 欠損は多能性幹細胞へのリプログラミングを阻害すると考えられた。Tsc2 欠損によって惹起される mTORC1 活性の亢進がリプログラミング阻害の主要因である可能性を考え、山中 4 因子の導入後、mTOR 阻害剤であるラパマイシン存在下で iPS 様細胞の樹立を試みた。まず既に樹立した Eker ラットの ES 細胞を用いて、ES 細胞の増殖に影響無しに mTORC1 経路の阻害を認めるラパマイシン濃度を探った。この前実験により得られた濃度に準じて、Tsc2-/- Eker ラット胎児線維芽細胞からの iPS 細胞樹立過程でラパマイシンを加えるも、コロニー形成の割合に変化は認められなかった。これらの結果から、少なくとも誘導期間のみの mTORC1 抑制ではリプログラミング能は回復しないものと推察された。

新井（一）グループ：脳腫瘍発生分子機構における神経細胞の腫瘍化と幹細胞性、正常圧水頭症病

法人番号	131025
プロジェクト番号	S1101009

態の可視化
悪性脳腫瘍の腫瘍化過程と腫瘍幹細胞の解析による治療介入の検討として、特に小児悪性脳腫瘍および成人神経膠腫を中心に、腫瘍細胞からの遺伝子情報の抽出と腫瘍幹細胞抽出培養の手技および方法を確立し、遺伝子も同定した。MRI 拡散強調画像と拡散 kurtosis 画像を用いて、正常圧水頭症における皮質脊髄路への影響を検討し、水頭症では、皮質脊髄路は神経線維と垂直方向に圧排され軸索が伸展された状態であることを明らかにした。(*123,178)

高久グループ：骨髄幹細胞ニッチ環境研究による成体神経新生メカニズム
３D イメージング手法により、ヘパラン硫酸プロテオグリカン（HSPG）が網状構造として存在することを示し、そのノックアウトマウスを用いて骨髄内の細胞構成につきフローサイトメトリーにて検証している。Agrin の欠損マウスの解析から、agrin は造血幹細胞維持に重要な役割を持つことが明らかとなった。

池田グループ：聴覚・平衡覚にかかわる細胞品質管理機構の正常とその破綻
これまでの研究では、遺伝性難聴モデル Cx26 優性阻害変異マウスの新規病態（*126）や Cx26 欠損マウスにおけるギャップ結合複合体の崩壊（*127）という新たな分子病態を発見し,他の遺伝子 POU3F4 変異での難聴も共通の分子病態を持つことを明らかにした（*125)。更に骨髄間葉系幹細および人工多能性幹（iPS）細胞を用いた新規細胞移植法をアデノ随伴ウイルス（AAV）による Cx26 遺伝子導入と複合的に応用することにより高音領域を有意に聴力改善させることに成功した(*68)。また 新生仔マウス蝸牛への AAV 局所投与により Cx26 欠損マウスの聴力を有意に改善させることに成功した（*66)。

（３）加齢・認知・発達障害の画像解析

青木グループ：脳の加齢・認知・発達障害の可視化　新規画像診断法の確立
脳の加齢変化を in vivo で観察できる方法として脳 MRI の 3DT1 強調像が J-ADNI などの大規模スタディーで用いられているが、最近では拡散テンソルなどの拡散 MRI が脳の白質路の定量評価や connectivity の評価が可能なため、追加されることが多い（ADNI3)。青木らは、拡散テンソルや次世代拡散解析の手法の開発(*153,210)、validation(*90)を行い、種々の疾患における feasibility study(*149,151,140,186,207,209,246)を行い、脳の微細構造の変化を in vivo で種々の病態で観察できることを報告した。拡散 MRI の種々の手法は validation が必要なため、平澤、Kerever らの協力で MRI と透明化した脳との対比を種々の施設の MRI を借用して行った（*34）。全脳解析や広い範囲の拡散テンソルトラクトグラフィーなど MRI が有用な点も多いと考えられた。

宇賀、北沢グループ：多点電極を用いた神経活動記録法の整備
北澤グループ（大阪大学）は、自閉症スペクトラム障害患者の解析で、映像視聴時に、自閉症スペクトラム障害患者では、瞬きが健常者と比較して同期していないことを解明した（*285)。また、触覚手がかりのみを用いて物体形状を判断する課題では、自閉症スペクトラム障害患者が健常者と比較して成績が優位であったことを解明した（*286)。宇賀らは、マカクザルでの多点電極記録法を用いた柔軟な判断の神経基盤の解明を行った。状況に応じて柔軟に判断をし、多様な選択を行うことはヒトの重要な認知機能のひとつである。本研究では、相同な機能を持つ霊長類において、神経活動を直接計測し、その神経基盤の解明に注力した。2 つのルール（運動方向を判断する、奥行きを判断する）をランダムに切り替えるタスクスイッチ課題を用い、判断が形成される LIP 野では、運動方向、奥行き情報が共に時間的に蓄積され、ルールに依存して情報蓄積のゲインが調整されていることを解明した。統合失調症早期病態を反映すると言われているケタミン（NMDA 受容体拮抗薬）低用量全身投与により、ルールに依存した情報蓄積のゲイン調節過程に障害が現れることを解明した。

新井（平伊）グループ：アルツハイマー病の発症分子機構解明
AD 発症に関与が示されている Apolipoprotein E 遺伝子や Apolipoprotein D 遺伝子異常が発症リスクに影響を与えていること（＊193)、DLB 症例の幻視症状に Ramelteon が有効であること（＊195)、高齢者うつ病における AD 発症と血清アミロイド蛋白の相関があること（＊261）を報告した。さらに、アルコール多飲歴のあるアルツハイマー病患者群では、その発症要因に COMT 遺伝子、KIBRA 遺伝子の関与が示唆されたこと(*74,129)、レビー小体病患者群では、早期から heart rate variability(心拍変異度)の異常が認められること(*88)、寛解期にあるうつ病患者群では、高次機能障害が残存することが再発のリスクであること、を明らかにした(*137)。

法人番号	131025
プロジェクト番号	S1101009

＜優れた成果があがった点＞

（１）細胞品質管理の正常機構とその破綻

服部グループは、１）PINK1/Parkin が協調して作用し、損傷ミトコンドリアをクリアランスすること(*108)、２)常染色体優性遺伝性パーキンソン病の家系から規原因遺伝子 CHCHD2 を同定し、CHCHD2 はミトコンドリアに関連した因子であることから、遺伝性パーキンソン病の病態としてミトコンドリア機能の障害があることを示した(*12)。内山グループは、１）オートファゴソームの成熟化のマーカーとなる pHluorin-mKate2-tagged human LC3 (PK-hLC3)を開発した(*17)。２）LAMP2 を欠損する神経細胞においてオートアジー／リソソーム系の異常を明らかにし(*13,160)。櫻井らは、１）エンドソーム輸送を制御する APP 結合蛋白質を見出し、エンドソーム障害及び APP 選択的なβ切断制御に関与することを明らかにした(**10)。２）病態と関連し、治療標的になるとして、特許出願（特願 2014-132309）した。

（２）細胞の分化・増殖・幹細胞性

新井（一）らは、MRI 拡散強調画像と拡散 kurtosis 画像を用いて、正常圧水頭症における皮質脊髄路への影響を検討し、水頭症では、皮質脊髄路は神経線維と垂直方向に圧排されることを明らかにした。池田らは、Cx26 欠損マウスにおけるギャップ結合複合体の崩壊（*127）という新たな分子病態を発見し、共同研究で Cx27 の遺伝子治療による難聴治療法の開発を実施した(*66)。

（３）加齢・認知・発達障害の画像解析

青木らは、拡散テンソルや次世代拡散解析の手法の開発（*153）、validation(*90)を行い、種々の疾患における feasibility study(*151,190,246)を行うことで、脳の微細構造の変化を in vivo で種々の病態で観察できることを報告し、拡散テンソル MRI の所見を確かめるために、平澤らの協力で 透明化標本を用いて免疫組織化学的にも検討した（*34）。青木らの拡散テンソル MRI で得られた所見を組織学的、さらには細胞構造学的レベルで検証する実験系が開発された。自閉症モデルマウス脳を MRI 撮像後透明化し、免疫組織染色を行い脳全体の画像を比較することが可能になった（Zeiss 780Duo の活用)。

＜課題となった点＞

本研究プロジェクトではそれぞれの目的を達成できたと考えている。疾患の原因遺伝子の解析、病態解析や疾患の診断法については大きな飛躍を示すことができた。しかし、治療法の開発については、各グループで積極的に取り組んだが、十分な結果は得られたいない。明確な成果としては、難聴の原因遺伝子の一つ Cx26 による遺伝子治療の可能性を示すにとどまった。また、ここの研究グループで目標に掲げた内容についての達成に至っていないグループも見られたが、現在も、またこれからもこの目的に沿った研究を続ける予定である。

＜自己評価の実施結果と対応状況＞

本研究プロジェクトによって、各グループにおいて多くの成果を得ることができた。これらの成果は、本プロジェクトおいて使用し得た研究費をもとに得られたものである。具体的に得た成果については下記に記す。

（１）細胞の品質管理の正常機構とその破綻

服部らは、ミトコンドリアやリソソームに関連する遺伝子異常を有するパーキンソン病患者の家系を明らかにし、その異常タンパク質産物の病態解析を進め、かなりの程度、プロジェクトを進行することができた。現在、パーキンソン病の新たな原遺伝子を同定し、その変異タンパク質の病態解析を進めている。内山らは、オートファジーとリソソーム関連疾患モデルの解析を進め一定の成果を収めた。現在、ATG9A や p62/NBR1 に関する解析結果を論文にまとめ、一部は投稿した（現在 revise 中)。さらに、ノックインマウスを用いて、ATG9A や DFCP1 の局在を検討している。櫻井らは、中間評価時点の自己評価ではアミロイド前駆体タンパク質(APP)の輸送・切断における新規制御タンパク質の調節機構解析が課題であった。モデルマウスと初代培養神経細胞に加え、両者をつなぐ新たなモデルとして脳スライス培養系を確立した。その結果をもとにモデルマウス及び培養細胞を中心に解析を進めることで機能解析が進み、調節機構の一部が明らかとなりつつある。

（２）細胞の分化・増殖・幹細胞性

平澤らは、ヘパラン硫酸プロテオグリカンが神経発生にどのように関わるかについて、成果を収めてきた。老化による fractone の構造、および構成タンパク質種および糖鎖修飾の変化を解析報告したが、それによる神経新生シグナルの分子機構を検討している。樋野らは、*Tsc2*+/+ Eker ラット胎児線維芽細胞と、*Tsc2*-/- Eker ラット胎児線維芽細胞のコロニー形成能の差から、mTORC1 活性の亢

法人番号	131025
プロジェクト番号	S1101009

進がリプログラミングを阻害すると考えられた。ラパマイシン投与下の樹立実験により、誘導期間のmTORC1 抑制のみでは変化がないことから、この実験系が腫瘍抑制遺伝子変異とリプログラミングの分子機構の関連を調べる上で、大変有用であると考えられた。今後、本モデルを用いた、「神経分化のオミックス解析と新規治療薬開発」が期待される。高久らは、造血幹細胞ニッチにおける、細胞外マトリックスの関与について検証する目的で、各種骨髄細胞におけるマトリックス欠損マウスを作製し解析を行った。その結果、ニッチ構成細胞における細胞外マトリックス欠損により、造血幹細胞維持機構の機能低下が原因と考えられる造血幹細胞が有意に減少している事を明らかにした。池田らは、本研究では遺伝性難聴における最大の原因である Cx26 の遺伝子変異における発症原因となる分子病態メカニズムを解明した。さらに新たな遺伝子治療法を開発することにより、この分子病態の進行を抑え、聴力を回復させる方法の開発に成功した。これらの成果を中心に本研究はおおむね順調に進行した。新井（一）らは、神経放射線科と共同して、特発性正常圧水頭症(iNPH)の画像バイオマーカーの探索を目的に、Diffusion MRI の各種方法を用いて行った。その結果、対照と比較して、iNPH では白質の細胞外液が増加し、錐体路の軸索が伸展していることを捉えることができた。これらの結果を国際紙に報告した。

（３）加齢・認知・発達障害の画像解析

青木らは、研究の進展状況と、その広報について自己評価を行った。脳のDiffusion tensor imagingと次世代の拡散MRIを中心としたMRIの解析において、研究期間内に十分な成果が得られ、学会、研究会での発表や論文作成を行った。発展途上にある次世代拡散MRIの、新たな解析法であるNeurite Orientation and dispersion and density imaging (NODDI)をいち早く導入できた。宇賀・北澤らは、ヒトにおける自閉症スペクトラムの解析で一定の成果を得るとともに、マカクザルを用いた研究でも、柔軟な判断機能に関する神経基盤を明らかにできた。新井（平）らは、アルツハイマー病と比較して、パーキンソン病、レビー小体病の検体収集が捗らず、統計学的パワー値が不十分であった。実験手技の問題よりは臨床医がもっと積極的に検体収集を行う必要があると思われた。研究員各員がアルツハイマー病以外でも、医師-患者関係を早い段階から構築し、DNA提供の同意をいただけるよう、指導を行っている。

＜外部（第三者）評価の実施結果と対応状況＞

３人の外部委員から評価をもらい、おおむね良好との評価を頂いた。

（１）東京都医学総合研究所・理事長/所長・田中啓二氏：高齢化社会に突入した今日、加齢に伴う様々な疾病が急増しているが、中でも脳・神経系の破綻を原因とする老人性疾患は増加の一途を辿っている。そして知能低下を主症状とするアルツハイマー病・レビー小体型認知症や運動機能劣化が顕在化するパーキンソン病などの老人性疾患は、生活の質 QOL の激しい低下やそれに伴う多大な介護費用が発生するなど、大きな社会・国家問題となっている。これらの老人性疾患は、病気の発症を完全に阻止できなくても、発症の進行を部分的に抑制、例えば発症時期を５年間程度遅らせることができれば、未曾有に拡大している社会的損失が大きく軽減されることは、国内外での学術的分析から鋭く指摘されており、この観点からも高次脳機能障害の早期診断・原因解明と治療法開発は、医学・生命科学領域における急務の課題となっている。

このような状況を踏まえると、本プロジェクト「細胞・脳機能研究の融合による神経疾患診断・治療法開発拠点の形成」は、非常に重要かつ時宜にかなった優れたプログラムであり、その研究成果の社会への波及効果が大きく期待される事業であった。本事業の拠点組織には、基礎研究及び臨床研究に携わる多くの研究者・医師たちが有機的に融合して、大きな成果を挙げたと総括できる。事業は（１）細胞の品質管理の正常機構の破綻、（２）細胞の分化・増殖・幹細胞性、（３）加齢・認知・発達障害の画像解析の３課題にカテゴライズされたグループから構成されているが、相互に情報交換や技術の提携が合理的に運営され、相加的・相乗的効果を育んだと判断できる。特筆される研究成果として例を挙げると、家族性パーキンソン病（PD）の研究では、世界で研究が進んでいる PINK1 と Parkin がミトコンドリアの品質管理に関わることの解明に成功したことや新規な PD 遺伝子 CHCHD2 の発見など、総じてして世界を先導する研究となっている。またオートファジーやリソソームに関する、卓越した形態学解析技術に基づいた神経管理網の品質管理研究、アルツハイマー病の成因である□アミロイド産出機序の可視化、そして細胞外マトリックスの作動機構、結節性硬

法人番号	131025
プロジェクト番号	S1101009

化症の原因 遺伝子 Tsc2 のニューロンにおける働きの解明、臨床治療に有用な脳障害の可視化による新規画像診断法の確立や聴覚などに関わる細胞品質管理機構の可視化技術の開発などが挙げられる。そしてこれらの優れた研究が、実に多くの論文として数々の上流誌に発表されてきたことも本事業の特徴であると総評できる。

このように本プロジェクトでは、基礎的な新規の病気遺伝子の発見から、実践的に臨床応用できる病態解析技術の開発まで多岐に亘り、得られた研究成果が未来医療への架け橋となる可能性を示唆すると共に、すでに実際の患者に適用され臨床の現場で役に立っていることを想起すると、本事業は比類ないレベルに達しており、学術的に高く評価できる。今後さらに基礎系研究者と臨床系研究者の連携が合理的に機能すれば、様々な老人性疾患の発症機序解明と予防・治療法開発へ向けての大きな力となって発展すること、そして次世代の脳科学研究を牽引するような新しいテーマと人材の発掘に大きく貢献することが期待できる。

（２）慶應義塾大学医学部長・岡野栄之氏：本研究グループは、アルツハイマー病やパーキンソン病などの加齢性神経変性疾患を対象にして、我が国そして世界のトップレベルの研究者が参画し、基礎から臨床の緊密な連携の基に、coordinateされている。特に、服部教授、内山教授の強力なリーダーシップの基、研究手法としては、微細形態にも力点を置いた細胞生物学的アプローチと、個体レベルでのシステム神経科学や画像解析を含む機能的なアプローチが見事に融合している。家族性パーキンソン病の新規の遺伝子の同定（Funayama et al., Lancet Neurol, 2015）などの画期的な論文を始めとして、発表業績も年々良くなっているものと評価できる。

（３）大阪大学医学系研究科・教授・長澤丘司：概ね良好に研究が行われている。特に、常染色体優先遺伝性パーキンソン病の家系から、ミトコンドリアに関連する新規の原因遺伝子CHCHD2を同定した成果は特に優れている。また、本事業の特色の一つである細胞外マトリックスの研究では、パールカンを構成因子とする神経幹細胞を維持する微小環境（ニッチ）の候補であるFractoneに関する研究は独創性があり、進展している他、骨髄の造血微小環境（ニッチ）でAgrinに注目している研究は優れた着眼で、発展が期待される。また、上皮細胞の細胞間チャネル分子として知られるConnexin26が内耳上皮細胞のギャップジンクションの形成に必須であるとの知見も重要である。

＜研究期間終了後の展望＞

本プロジェクトが終了してからは、他の競争的資金を利用したり、同資金の獲得を目指し、本研究を継続する。また、これらの継続研究では、本研究プロジェクトで得た機器を利用する。

（１）細胞の品質管理の正常機構とその破綻

服部らは、多くの患者から得られた血液細胞を基に、iPS 細胞の樹立を試みている。また、膜輸送障害によりリソソーム機能が引き起こされる可能性を明らかにする。本研究により小胞体をはじめとした膜輸送障害がパーキンソン病の病態に関わることが明らかになることが期待できる。内山らは､本研究で作成したオートファジー関連因子の中で唯一膜タンパク質である Atg9A の KO マウスとノックインマウスを用いて、軸索神経終末領域で起きるオートファゴソーム形成に関わる因子が、どのように細胞体から終末部に送られるのかを解析し、オートファゴソーム形成機序を明らかにする。櫻井らは、本研究期間中にアミロイド前駆体タンパク質(APP)の細胞内輸送と切断・アミロイド産生を制御するタンパク質の機能解析を行い、APP との相互作用部位を明らかにした。相互作用ドメイン・ペプチドは、アルツハイマー病の最初期変化でありβアミロイド過剰産生につながるエンドソーム輸送障害を改善することから、これを基盤としてより副作用の少ない新たな治療戦略の開発を目指している。

（２）細胞の分化・増殖・幹細胞性

平澤らは、本プロジェクト終了後には、他の競争的資金を活用して老化脳における成体神経新生能力の向上を目指し、脳室内への分子化合物の投与や、糖鎖修飾方法の確立、細胞治療の新規技術開発を目指す。また、青木らとの共同研究による新規サロゲートマーカーの開発は､」日立研究所、放医研、東京医科歯科大学など外部とも連携を開始し、動物実験から臨床応用への技術開発を目指す。樋野らは、*Tsc2*+/+ Eker ラット胎児線維芽細胞と、*Tsc2*−/− Eker ラット胎児線維芽細胞のコロニー

法人番号	131025
プロジェクト番号	S1101009

形成能の差から、mTORC1 活性の亢進がリプログラミングを阻害すると考えられた。ラパマイシン投与下の樹立実験により、誘導期間のmTORC1 抑制のみでは変化がないことから、この実験系が腫瘍抑制遺伝子変異とリプログラミングの分子機構の関連を調べる上で、大変有用であると考えられた。今後、本モデルを用いた、「神経分化のオミックス解析と新規治療薬開発」が期待される。高久らは、造血機構におけるマトリックスの関与に関しては、マウスモデルでの血管内皮細胞におけるマトリックス欠損により、生体で造血幹細胞の優位な減少を認めている。ニッチ機構の機能低下による幹細胞数の低下が疑われ、今後はそのメカニズムについての検証を行う予定である。池田らは、本研究では遺伝性難聴の分子病態に基づいた遺伝子治療法、細胞治療法等の治療法開発を遺伝子改変動物を用いて行った。今後は臨床応用の実現にむけ、患者 iPS 細胞から内耳前駆細胞を分化誘導し、同細胞を遺伝子治療、ゲノム編集等により修復することを目指す。新井（一）らは、本研究で得られた、画像バイオマーカーを用いた、前向き多施設共同件研究を行い、これらのバイオマーカーの感度および特異度を算出し、その結果を基に特発性正常圧水頭症患者の治療予後の改善に継なげたい。

（３）加齢・認知・発達障害の画像解析

青木らは、本研究において解析法を導入し、報告した種々の神経疾患や正常における変化、モデルマウスでの知見につき、症例を増やして、予後との関係や、薬剤反応性のイメージングバイオマーカとしての有用性などを検討し、それを広く普及させていく。新たな疾患や疾患モデルマウスにおける検討を行っていく。宇賀・北澤らは、本プロジェクトの解析結果を生かしさらに、自閉症スペクトラムや霊長類の判断の基礎となる神経構造の解明を目指す。新井（平）らは、神経症状を有する認知症患者さんの多くが、脳神経内科も併診して、治療を受けている実態が明らかとなった。本研究を通じて、本期間が終了後も脳神経内科と協働して、遺伝子研究を行う礎が確立された。今後は、向精神薬、抗パーキンソン病薬も治療反応性などについてもどのような遺伝学的背景があるのか、検討を行うこととしている。

＜研究成果の副次的効果＞

服部らは、膜輸送障害がリソソーム機能異常を引き起こすことでパーキンソン病の病態に関わることを明らかにすることにより創薬に繋がり、最終的には根本治療の発見に寄与する効果がある。櫻井らは、、特許出願（「アルツハイマー病予防治療薬のスクリーニング法」高杉展正、櫻井隆、清水瑠奈、特願 2014-132309、学校法人順天堂、平成 26 年 6 月 27 日）を行った。青木らは、特許ではないが、脳 MRI の種々の解析を一括して行うパイプラインを作成し、希望する研究者に配布している。さらに、新井一学長は、本プロジェクトに参加した多くの研究グループを中心に神経懇話会を立ち上げ、最新の情報についての学内外の研究者に紹介していただき、神経研究の情報交換、研究費取得に関する意見交換を実施している。

12 キーワード（当該研究内容をよく表していると思われるものを8項目以内で記載してください。）

（1）パーキンソン病　（2）アルツハイマー病　（3）オートファジー
（4）ミトコンドリア　（5）コネキシン　（6）拡散テンソル MRI 画像
（7）遺伝子解析　（8）細胞外間基質

13 研究発表の状況（研究論文等公表状況。印刷中も含む。）

上記、11(4)に記載した研究成果に対応するものには＊を付すこと。

＜雑誌論文＞

２０１５年グループ（１）

1. Kurosawa M, Matsumoto G, Sumikura H, Hatsuta H, Murayama S, Sakurai T, Shimogori T, Hattori N, Nukina N : Serine 403-phosphorylated p62/SQSTM1 immunoreactivity in inclusions of neurodegenerative diseases. Neurosci Res,103,64-70, 2016
2. Hashimoto M, Nara T, Enomoto M, Kurebayashi N, Yoshida M, Sakurai T, Mita T, Mikoshiba K: A Dominant Negative Form of Inositol 1,4,5-Trisphosphate Receptor Induces Metacyclogenesis and

法人番号	131025
プロジェクト番号	S1101009

Increases Mitochondrial Density in Trypanosoma cruzi. Biochem Biophys Res Commun, 466: 475-480, 2015
*3. Kamikubo Y, Tabata T, Sakairi, H, Hashimoto Y, Sakurai T: Complex formation and functional interaction between adenosine A1 receptor and type-1 metabotropic glutamate receptor, J Pharmacol Sci, 128, 125-130, 2015
4. Takano S, Tsuzuki T, Murayama T, Sakurai T, Fukuda H, Arisawa M, Shuto S: Synthesis of 7-Deaza-cyclic Adenosine-5'-diphosphate-carbocyclic-ribose and Its 7-Bromo Derivative as Intracellular Ca2+-Mobilizing Agents. J Org Chem,80, 6619-6627, 2015
5. Murayama T, Kurebayashi N, Yamazawa T, Oyamada H, Suzuki J, Kanemaru K, Oguchi K, Iino M, Sakurai T: Divergent Activity Profiles of Type 1 Ryanodine Receptor Channels Carrying Malignant Hyperthermia and Central Core Disease Mutations in the Amino-terminal Region. PLoS ONE, 10, e0130606, 2015
6. Kurosawa M, Matsumoto G, Kino Y, Okuno M, Kurosawa-Yamada M, Washizu C, Taniguchi H, Nakaso K, Yanagawa T, Warabi E, Shimogori T, Sakurai T, Hattori N, Nukina N: Depletion of p62 reduces nuclear inclusions and paradoxically ameliorates disease phenotypes in Huntington's model mice. Hum Mol Genet, 24 1092-1105, 2015
7. Sunabori T, Koike M, Asari A, Oonuki Y, Uchiyama Y : Suppression of ischemia-induced hippocampal pyramidal neuron death by hyaluronan tetrasaccharide through inhibition of toll-like receptor 2 signaling pathway. Am J Pathol, in press, 2016
8. Shibata M, Koike M, Kusumi K, Sato N, Uchiyama U : A specific tripeptidyl substrate for tripeptidyl peptidase activity is effectively hydrolyzed by alanyl aminopeptidase/aminopeptidase N/CD13 in the rat kidney. Arch Histol Cytol, 76,1-8, 2016
9. Yamamoto-Nonaka K, Koike M, Asanuma K, Takagi M, Oliva Trejo JA, Seki T, Hidaka T, Ichimura K, Sakai T, Tada N6 Ueno T, Uchiyama Y, Tomino Y : Cathepsin D in podocytes is important in the pathogenesis of proteinuria and CKD. J Am Soc Nephrol, in press, 2016
10. Xie C, Ginet V, Sun Y, Koike M, Zhou K, Li T, Li H, Li Q, Wang X, Uchiyama Y, Truttmann AC, Kroemer G, Puyal J, Blomgren K, Zhu C : Neuroprotection by selective neuronal deletion of autophagy-related gene 7 in neonatal brain injury. Autophagy, 12, 410-423, 2016
11. Rinchai D, Riyapa D, Buddhisa S, Utispan K, Titball RW, Stevens MP, Stevens JM, Ogawa M, Tanida I, Koike M, Uchiyama Y, Ato M, Lertmemongkolchai: Macroautophagy is essential for killing of intracellular Burkholderia pseudomallei in human neutrophils. Autophagy, 11, 748-755 , 2015
*12. Funayama M, Ohe K, Amo T, Furuya N, Yamaguchi J, Saiki S, Li Y, Ogaki K, Ando M, Yoshino H, Tomiyama H, Nishioka K, Hasegawa K, Saiki H, Satake W, Mogushi K, Sasaki R, Kokubo Y, Kuzuhara S, Toda T, Mizuno Y, Uchiyama Y, Ohno K, Hattori N: CHCHD2 mutations in autosomal dominant late-onset Parkinson's disease: a genome-wide linkage and sequencing study. Lancet Neurol, 14 274-282 , 2015
13. Furuta A, Kikuchi H, Fujita H, Yamada D, Fujiwara Y, Kabuta T, Nishino I, Wada K, Uchiyama Y: Property of Lysosomal Storage Disease associated with Midbrain Pathology in the CNS of LAMP-2-deficient Mice. Am J Pathol 185, 1713-1723, 2015
14. Nori S, Okada Y, Nishimura S, Ssaki T, Itakura G, Kobayashi Y, Renault-Mihara F, Shimizu A, Koya I, Yoshida R, Kudoh J, Koike M, Uchiyama Y, Ikeda E, Toyama Y, Nakamura M, Okano H: Long-Term Safety Issues of iPSC-Based Cell Therapy in a Spinal Cord Injury Model: Oncogenic Transformation with Epithelial Mesenchymal Transition. Stem Cell Rep, 4, 1-14, 2015
15. Uemura N, Koike M, Ansai K, Kinoshita M, Fujiwara-Ishikawa T, Matsui H, Naruse K, Sakamoto N, Uchiyama Y, Todo T, Takeda S, Yamakado H, Takahashi R:Axonal accumulation of alpha-synuclein in Gaucher disease model of medaka (Oryzias latipes) does not contribute to neurodegeneration. Pros Genetics, 10, 1371, 2015
16. Nanao T, Koike M, Yamaguchi J, Sasaki M, Uchiyama Y : Cellular localization and tissue distribution of endogenous DFCP1 protein.Biomed Res, 36, 121-133, 2015
*17. Tanida I, Ueno T, Uchiyama Y : A Super-Ecliptic, pHluorin-mKate2, Tandem Fluorescent Protein-Tagged Human LC3 for the Monitoring of Mammalian Autophagy. PLoS ONE, 9, e110600, 2015
18. Nakamura R, Sone J, Atsuta N, Tohnai G, Watanabe H, Yokoi D, Nakatochi M, Watanabe H, Ito M, Senda J, Katsuno M, Tanaka F, Li Y, Izumi Y, Morita M, Taniguchi A, Kano O, Oda M, Kuwabara S, Abe K, Aiba I, Okamoto K, Mizoguchi K, Hasegawa K, Aoki M, Hattori N, Tsuji S, Nakashima K, Kaji R, Sobue G; Japanese Consortium for Amyotrophic Lateral Sclerosis Research (JaCALS). Next-generation sequencing of 28 ALS-related genes in a Japanese ALS cohort. Neurobiol Aging, 39, 219.e1-8, 2016
19. Hatano T, Saiki S, Okuzumi A, Mohney RP, Hattori N : Identification of novel biomarkers for

法人番号	131025
プロジェクト番号	S1101009

Parkinson's disease by metabolomic technologies. J Neurol Neurosurg Psychiatry, 87, 295-301, 2016
20. Yamada D, Saiki S, Furuya N, Ishikawa K, Imamichi Y, Kambe T, Fujimura T, Ueno T, Koike M, Sumiyoshi K, Hattori N : Ethambutol neutralizes lysosomes and causes lysosomal zinc accumulation. Biochem Biophys Res Commun, 471, 109-16. 2016
21. Takamura S, Ikeda A, Nishioka K, Furuya H, Tashiro M, Matsushima T, Li Y, Yoshino H, Funayama M, Morinobu S, Hattori N : Schizophrenia as a prodromal symptom in a patient harboring SNCA duplication. Parkinsonism Relat Disord. pii: S1353-8020(16)30028-1, 2016
22. Conedera S, Apaydin H, Li Y, Yoshino H, Ikeda A, Matsushima T, Funayama M, Nishioka K, Hattori N : FBXO7 mutations in Parkinson's disease and multiple system atrophy. Neurobiol Aging, pii: S0197-4580(16)00004-X, 2016
23. Ueno Y, Tanaka R, Yamashiro K, Shimada Y, Kuroki T, Hira K, Urabe T, Hattori N. Impact of BNP on cryptogenic stroke without potential embolic sources on transesophageal echocardiography. J Neurol Sci, 359, 287-92, 2015
24. Ogaki K, Koga S, Heckman MG, Fiesel FC, Ando M, Labbé C, Lorenzo-Betancor O, Moussaud-Lamodière EL, Soto-Ortolaza AI, Walton RL, Strongosky AJ, Uitti RJ, McCarthy A, Lynch T, Siuda J, Opala G, Rudzinska M, Krygowska-Wajs A, Barcikowska M, Czyzewski K, Puschmann A, Nishioka K, Funayama M, Hattori N, Parisi JE, Petersen RC, Graff-Radford NR, Boeve BF, Springer W, Wszolek ZK, Dickson DW, Ross OA : Mitochondrial targeting sequence variants of the CHCHD2 gene are a risk for Lewy body disorders. Neurology, 85, 2016-25, 2015
25. Tanaka R, Yamashiro K, Okuma Y, Shimura H, Nakamura S, Ueno Y, Tanaka Y, Miyamoto N, Tomizawa Y, Nakahara T, Furukawa Y, Watada H, Kawamori R, Hattori N, Urabe T : Effects of Pioglitazone for Secondary Stroke Prevention in Patients with Impaired Glucose Tolerance and Newly Diagnosed Diabetes: The J-SPIRIT Study. J Atheroscler Thromb, 22, 1305-16, 2015
26. Matsumoto SE, Motoi Y, Ishiguro K, Tabira T, Kametani F, Hasegawa M, Hattori N: The twenty-four KDa C-terminal tau fragment increases with aging in tauopathy mice: implications of prion-like properties. Hum Mol Genet, 24, 6403-16, 2015
27. Yamashiro K, Tanaka R, Hoshino Y, Hatano T, Nishioka K, Hattori N : The prevalence and risk factors of cerebral microbleeds in patients with Parkinson's disease. Parkinsonism Relat Disord. 21, 1076-81, 2015
28. Fuse A, Furuya N, Kakuta S, Inose A, Sato M, Koike M, Saiki S, Hattori N: VPS29 VPS35 intermediate of retromer is stable and may be involved in the retromer complex assembly process. FEBS Lett, 589, 1430-6, 2015
29. Vaikath NN, Majbour NK, Paleologou KE, Ardah MT, van Dam E, van de Berg WD, Forrest SL, Parkkinen L, Gai WP, Hattori N, Takanashi M, Lee SJ, Mann DM, Imai Y, Halliday GM, Li JY, El-Agnaf OM : Generation and characterization of novel conformation-specific monoclonal antibodies for α-synuclein pathology. Neurobiol Dis, 79, 81-99, 2015
30. Imai Y, Kobayashi Y, Inoshita T, Meng H, Arano T, Uemura K, Asano T, Yoshimi K, Zhang CL, Matsumoto G, Ohtsuka T, Kageyama R, Kiyonari H, Shioi G, Nukina N, Hattori N, Takahashi R : The Parkinson's Disease-Associated Protein Kinase LRRK2Modulates Notch Signaling through the Endosomal Pathway. PLoS Genet, 11, e1005503, 2015
31. Funayama M, Hattori N: CHCHD2 and Parkinson's disease-Authors' reply.Lancet Neurol, 14, 682-3, 2015
32. Funayama M, Ohe K, Amo T, Furuya N, Yamaguchi J, Saiki S, Li Y, Ogaki K, Ando M, Yoshino H, Tomiyama H, Nishioka K, Hasegawa K, Saiki H, Satake W, Mogushi K, Sasaki R, Kokubo Y, Kuzuhara S, Toda T, Mizuno Y, Uchiyama Y, Ohno K, Hattori N: CHCHD2 mutations in autosomal dominant late-onset Parkinson's disease: a genome-wide linkage and sequencing study. Lancet Neurol, 14, 274-82 , 2015
33. Nonaka R, Iesaki T, de Vega S, Daida H, Okada T, Sasaki T, and Arikawa-Hirasawa E: Perlecan deficiency causes endothelial dysfunction by reducing the expression of endothelial nitric oxide synthase. Physiol Rep, 27, e12272, 2015
*34. Kerever A, Kamagata K, Yokosawa S, Otake Y, Ochi H, Yamada T, Hori M, Kamiya K, Nishikori A, Aoki S, Arikawa-Hirasawa E: See-through Brains and Diffusion Tensor MRI Clarified Fiber Connections. A Magnetic Resonance in Medical Sciences, 14, 159-62, 2015
35. Iwata S, Ito M, Nakata T, Noguchi Y, Okuno T, Ohkawara B, Masuda A, Goto T, Adachi M, Osaka H, Nonaka R, Arikawa-Hirasawa E, Ohno K.: A missense mutation in domain III in HSPG2 in Schwartz–Jampel syndrome compromises secretion of perlecan into the extracellular space. Neuromuscul Disord. 8, 667-71, 2015
*36. Kerever A, Yamada T, Suzuki Y Mercier F, Arikawa-Hirasawa, E: Fractone aging in the subventricular zone of the lateral ventricle. Journal of Chemical Neuroanatomy, 5, 66-67, 2015

法人番号	131025
プロジェクト番号	S1101009

37. Ning L, Xu Z, Furuya N, Nonaka R, Yamada Y, Arikawa-Hirasawa E: Perlecan inhibits autophagy to maintain muscle homeostasis in mouse soleus muscle. Matrix Biol, 48, 26-35, 2015
38. de Vega S, Hozumi K, Suzuki N, Nonaka R, Seo E, Takeda A, Ikeuchi, T Nomizu, Yamada Y, Arikawa-Hirasawa E: Identification of Peptides Derived from the C-terminal Domain of Fibulin-7 Active for Endothelial Cell Adhesion and Tube Formation Disruption. Peptide Science, 106,184-195,2015
39. Yamada S, Ishikawa M, Miyajima M, Atsuchi M, Kimura T, Kazui H, Mori E,SINPHONI-2 Investigators (Appendix): SINPHONI-2 Investigators Appendix: Disease duration: the key to accurate CSF tap test in iNPH.Acta Neurol Scand DOI:10.1111/ane.12580, 2016
40. Uchiyama Y, Nakashima M, Watanabe S, Miyajima M, Taguri M, Miyatake S, Miyake N, Saitsu H, Mishima H, Kinoshita A, Arai H, Yoshiura K, Matsumoto N: Ultra-sensitive droplet digital PCR for detecting a low-prevalence somatic GNAQ mutation in Sturge-Weber syndrome.Sci Rep, 6, 22985, 2016
41. Yoshihara A, Fukatsu M, Hoshi K, Ito H, Nollet K, Yamaguchi Y, Ishii R, Tokuda T, Miyajima M, Arai H, Kato T, Furukawa K, Arai H, Kikuchi A, Takeda A, Ugawa Y, Hashimoto Y: Subgroup differences in "brain-type" transferrin and α-synuclein in Parkinson's disease and multiple system atrophy. J Biochem, mvw015, 2016
42. Kazuhide Iizuka, Tomomasa Yokomizo, Naoki Watanabe, Motomi Osato, Tomoiku Takaku and Norio Komatsu: Whole-mount analysis of hematopoietic development in the mouse embryonic head. PLOS ONE, リバイス中, 2016
*43. Kageyama H, Miyajima M, Ogino I, Nakajima M, Shimoji K, Fukai R, Miyake N, Nishiyama K, Mastumoto N, Arai H: Panventriculomegaly with a wide foramen of Magendi and a large cisterna magna.J Neurosurg, 1-9,2015
44. Tsutsumi S, Ogino I, Miyajima M, Ito M, Arai H, Yasumoto Y: Cerebrospinal fluid drainage through the diploic and spinal epidural veins.J Anat, 227,297-301,2015
45. Nakajima M, Miyajima M, Ogino I, Akiba C, Sugano H, Hara T, Fusegi K, Karagiozov K, Arai H: Cerebrospinal fluid biomarkers for prognosis of long-term cognitive treatment outcomes in patients with idiopathic normal pressure hydrocephalus. J Neurol Sci, 357, 88-95, 2015
46. Kazui H, Miyajima M, Mori E, Ishikawa M: Lumboperitoneal shunt surgery for idiopathic normal pressure hydrocephalus (SINPHONI-2): an open-label randomized trial.Lancet Neurol, 14, 585-594, 2015
47. Moriya M, Miyajima M, Nakajima M, Ogino I, Arai H: Impact of cerebrospinal fluid shunting for idiopathic normal pressure hydrocephalus on the amyloid cascade. PLoS One, 10, e0119973, 2015
48. Schultz M, Kimura T, Akiyama O, Shimoji K, Spors B, Miyajima M, Thomale UW: Endoscopic and microsurgical treatment of Sylvian fissure arachnoid cysts – clinical and radiological outcome.World Neurosurg. 84, 327-336, 2015
49. Komuro Y, Shimizu A, Shimoji K, Miyajima M, Arai H: Posterior cranial vault distraction osteogenesis with barrel stave osteotomy in the treatment of craniosynostosis. Neurol Med Chir (Tokyo), 55, 617-623, 2015
50. Miyajima M, Nakajima M, Ogino I, Kunichika M, Arai H: An autopsy case of long-standing overt ventriculomegaly in adults (LOVA) –neuropathhological investing-. J Hydrocephalus, 7, 2015
51. Miyajima M, Kazui H, Mori E, Ishikawa M:One-Year Outcome in Patients with Idiopathic Normal-Pressure Hydrocephalus: Comparison of Lumbo-Peritoneal Shunt to Ventriculo-Peritoneal Shunt. J Neurosurg, Feb, 1-10, 2016
52. Hori M, Kamiya K, Nakanishi A, Fukunaga I, Miyajima M, Nakajima M, Suzuki M, Suzuki Y, Irie R, Kamagata K, Arai H, Aoki S: Prospective estimation of mean axon diameter and extra-axonal space of the posterior limb of the internal capsule in patients with idiopathic normal pressure hydrocephalus before and after a lumboperitoneal shunt by using q-space diffusion MRI. Eur Radiol, Dec, DOI:10.1007/s00330-015-4162-9, 2015
53. Miyajima M, Arai H: Evaluation of the production and absorption of cerebrospinal fluid. Neurol Med Chir (Tokyo), 55, 647-656, 2015
*54. Sugiura H., Yasuda S., Katsurabayashi S., Kawano H., Endo K., Takasaki K., Iwasaki K., Ichikawa M., Kobayashi T., Hino O. and Yamagata K: Rheb actvation disrupts spine synapse formation through accumulation of syntenin in tuberous sclerosis complex. Nature Communications, (DOI: 10.1038/ncomms7842), 6,6842 , 2015
*55. Ito Y., Kawano H., Kanai F., Nakamura E., Tada N., Takai S., Horie S., Arai H., Kobayashi T. & Hino O: Establishiment of Tsc2-deficient rat embryonic stem cells. Int. J Oncology, 46, 1944-1952, 2015
56. Einama T, Kawamata F, Kamachi H, Nishihara H, Homma S, Matsuzawa F, Mizukami T, Konishi Y, Tahara M, Kamiyama T, Hino O, Taketomi A., Todo S: Clinical impacts of mesothelin expression in

法人番号	131025
プロジェクト番号	S1101009

gastrointestinal carcinomas. World J, Gastrointestinal Pathophysiology, in press

57. Aizawa Y, Shirai T, Kobayashi T, Hino O, Tsujii Y, Inoue H, Kazami M, Tadokoro T, Suzuki T, Kobayashi K. and Yamamoto Y: The tuberous sclerosis complex model Eker (TSC2+/-) rat exhibits hyperglycemia and hyperketonemia due to decreased glycolysis in the liver. Archives of Biochemistry and Biophysics (doi: 10.1016/j.abb. 2015.10.019) 590, 48-55,2016
58. Kawano H., Ito Y., Kanai F., Nakamura E., Tada N., Takai S., Horie S., Kobayashi T. and Hino O: Aberrant differentiation of Tsc2-deficient teratomas associated with activation of the mTORC1-TFE3 pathway. Oncology Reports, 34,2251-2258, 2015
59. Imai M. and Hino O: "Environmental carcinognensis-100th anniversary of creating cancer."Cancer Science (doi: 10.1111/cas.12798), 27-Aug, 2015
60. Horimoto Y., Arakawa A., Tanabe M., Kuroda K., Matsuoka J., Igari F., Himuro T., Yoshida Y., Tokuda E., Shimizu H., Hino O. and Saito M: Menstrual cycle could affect Ki67 expression in estrogen receptor-positive breast cancer patients. J. Clin. Pathol, (doi:10.1136/jclinpath-2015-203085),Oct 68(10), 825-8295, 2015
61. Saeki H., Suzuki C, Yamasaki S, Hashizume A, Izumi H, Suzuki F, Ishi K, Nojima M. and Hino O: Cotyledonoid dissecting leiomyoma of the uterus: report of two case. Arch. Gynecology and Obstetrics (DOI 10.1007/s00404-014-3406-2), 291, 357-361, 2015
62. Anzai, T., Fukunaga, I., Hatakeyama, K., Fujimoto, A., Kobayashi, K., Nishikawa, A., Aoki, T., Noda, T., Minowa, O., Ikeda, K., and Kamiya, K: Deformation of the Outer Hair Cells and the Accumulation of Caveolin-2 in Connexin 26 Deficient Mice. PloS one, 10, e0141258,2015
63. Hiroko Okada, Kazusaku Kamiya., Takashi Iizuka and Katsuhisa Ikeda: Postnatal Development and Maturation of the Vestibular Organ in Dominant-Negative Connexin 26 Transgenic Mouse. J Otol Rhinol, S1, 37-40, 2015
64. Ikeda, K., Misawa, S., and Kusunoki, T: Comparative bactericidal activity of four fluoroquinolones against Pseudomonas aeruginosa isolated from chronic suppurative otitis media.BMC ear, nose, and throat disorders, 15, 5, 2015
65. Kazusaku Kamiya, Ichiro Fukunaga, Kaori Hatakeyama and Katsuhisa Ikeda: Connexin26 regulates assembly and maintenance of cochlear gap junction macromolecular complex for normal hearing AIP Conference Proceedings, 1703, 30018;1-3, 2015
*66. IizukaT., KamiyaK., GotohS., SugitaniY., SuzukiM., NodaT., MinowaO., and IkedaK: Perinatal Gjb2 gene transfer rescues hearing in a mouse model of hereditary deafness. HUMAN MOLECULAR GENETICS, 24, 3651-3661,2015
67. Kazusaku Kamiya, Keiko Karasawa, Kazuma Kobayashi, Asuka Miwa and Katsuhisa Ikeda: Differentiation of iPS Cells to Cochlear Cells are Regulated Depending on the Part of Cocultured Organs. Otology & Rhinology, S1,34-36, 2015
*68. Kazusaku Kamiya : Inner ear cell therapy targeting hereditary deafness by activation of stem cell homing factors. Frontiers in Pharmacology. 6, 2, 2015

２０１５年グループ（３）

69. Hirano A, Ohara T, Takahashi A, Aoki M, Fuyuno Y, Ashikawa K, Morihara T, Takeda M, Kamino K, Oshima E, Okahisa Y, Shibata N, Arai H, Akatsu H, Ikeda M, Iwata N, Ninomiya T, Monji A, Kitazono T, Kiyohara Y, Kubo M, Kanba S: A genome-wide association study of late-onset Alzheimer's disease in a Japanese population. Psychiatr Genet, 25,139-46,2015
70. Nagata T, Kobayashi N, Ishii J, Shinagawa S, Nakayama R, Shibata N, Kuerban B, Ohnuma T, Kondo K, Arai H, Yamada H, Nakayama K: Association between DNA Methylation of the BDNF Promoter Region and Clinical Presentation in Alzheimer's Disease. Dement Geriatr Cogn Dis Extra, 5, 64-73, 2015
71. Chiba Y, Fujishiro H, Ota K, Kasanuki K, Arai H, Hirayasu Y, Sato K, Iseki E:Clinical profiles of dementia with Lewy bodies with and without Alzheimer's disease-like hypometabolism. Int J Geriatr Psychiatry, 30, 316-23, 2015
72. Yoshita M, Arai H, Arai H, Arai T, Asada T, Fujishiro H, Hanyu H, Iizuka O, Iseki E, Kashihara K, Kosaka K, Maruno H, Mizukami K, Mizuno Y, Mori E, Nakajima K, Nakamura H, Nakano S, Nakashima K, Nishio Y, Orimo S, Samuraki M, Takahashi A, Taki J, Tokuda T, Urakami K, Utsumi K, Wada K, Washimi Y, Yamasaki J, Yamashina S, Yamada M.Diagnostic accuracy of 123I-meta-iodobenzylguanidine myocardial scintigraphy in dementia with Lewy bodies: a multicenter study. PLoS One, 10, e0120540, 2015
73. Arai H, Sumitomo K, Sakata Y, Daidoji K, Takase T, Toyoda T.Disease state changes and safety of long-term donepezil hydrochloride administration in patients with Alzheimer's disease: interim results from the long-term, large-scale J-GOLD study in Japan. Psychogeriatrics, Jun 26,

法人番号	131025
プロジェクト番号	S1101009

doi:10.1111/psyg.12130,2015

*74. Kawai E, Shibata N, Nagata T, Shinagawa S, Tgai K, Ohnuma T, Shimazaki H, Toda A, Kasanuki K, Takayama T, Suzuki A, Nakayama K, Yamada H, Arai H: Genetic Association Between KIBRA Polymorphism and Alzheimer's Disease with in a Japanese Population. Neuromolecular Med, 17, 170-7, 2015

75. Ayako Suzuki, Nobuto Shibata, Koji Kasanuki, Tomoyuki Nagata, Shunichiro Shinagawa, Nobuyuki Kobayashi, Tohru Ohnuma, Yoshihide Takeshita, Eri Kawai, Toshiki Takayama, Kenya Nishioka, Yumiko Motoi, Nobutaka Hattori, Kazuhiko Nakayama, Hisashi Yamada, Heii Arai: Genetic association between presenilin 2 polymorphisms and Alzheimer's disease and dementia of Lewy body type in a Japanese population. Dementia and Geriatric Cognitive Disorders extra, 印刷,2016

76. Ota K, Fujishiro H, Kasanuki K, Kondo D, Chiba Y, Murayama N, Arai H, Sato K, Iseki E: Prediction of later clinical course by a specific glucose metabolic pattern in non-demented patients with probable REM sleep behavior disorder admitted to a memory clinic: A case study. Psychiatry Res. 28;248, 151-8,2016

77. Kobayashi N, Shinagawa S, Nagata T, Shimada K, Shibata N, Ohnuma T, Kasanuki K, Arai H, Yamada H, Nakayama K, Kondo K: Development of Biomarkers Based on DNA Methylation in the NCAPH2/LMF2 Promoter Region for Diagnosis of Alzheimer's Disease and Amnesic Mild Cognitive Impairment. PLoS One, 11(1), e0146449, 2016

78. Ohnuma T, Toda A, Kimoto A, Takebayashi Y, Higashiyama R, Tagata Y, Ito M, Ota T, Shibata N, Arai H: Benefits of use, and tolerance of, medium-chain triglyceride medical food in the management of Japanese patients with Alzheimer's disease: a prospective, open-label pilot study. Clin Interv Aging, 11, 29-36,2016

79. Kimoto A, Kasanuki K, Kumagai R, Shibata N, Ichimiya Y, Arai H.Serum insulin-like growth factor-I and amyloid beta protein in Alzheimer's disease: relationship with cognitive function. Psychogeriatrics. doi: 10.1111/psyg.12149, 2015

80. Kondo D, Hino H, Shibuya K, Fujisawa K, Kosaka K, Hirayasu Y, Yamamoto R,Kasanuki K, Minegishi M, Sato K, Hosokawa M, Arai T, Arai H, Iseki E.An autopsied case of corticobasal degeneration showing severe cerebral atrophy over a protracted disease course of 16 years. Neuropathology, 35(3), 280-8,2015

81. Iwanami T, Maeshima H, Baba H, Satomura E, Namekawa Y, Shimano T, Suzuki T, Arai H: Psychomotor agitation in major depressive disorder is a predictive factor of mood-switching. J Affect Disord, 170, 185-9, 2015

82. Arai H, Umemura K, Ichimiya Y, Iseki E, Eto K, Miyakawa K, Kirino E, Shibata N, Baba H, Tsuchiwata S: Safety and pharmacokinetics of bapineuzumab in a single ascending-dose study in Japanese patients with mild to moderate Alzheimer's disease. Geriatr Gerontol Int, Jun 4, doi: 10.1111/ggi.12516,2015

83. Arai H, Sumitomo K, Sakata Y, Daidoji K, Takase T, Toyoda T: Disease state changes and safety of long-term donepezil hydrochloride administration in patients with Alzheimer's disease: interim results from the long-term, large-scale J-GOLD study in Japan. Psychogeriatrics, doi: 10.1111/psyg.12130, 2015

84. Nomoto H, Baba H, Satomura E, Maeshima H, Takebayashi N, Namekawa Y, Suzuki T, Arai H: Serum brain-derived neurotrophic factor levels and personality traits in patients with major depression. BMC Psychiatry, 15,33, 2015

85. Asano T, Baba H, Kawano R, Takei H, Maeshima H, Takahashi Y, Suzuki T, Arai H:Temperament and character as predictors of recurrence in remitted patients with major depression: A 4-year prospective follow-up study. Psychiatry Res, 225,322-25, 2015

86. Arai H, Suzuki H, Yoshiyama T: Vanutide cridificar and the QS-21 adjuvant in Japanese subjects with mild to moderate Alzheimer's disease: results from two phase 2 studies. Curr Alzheimer Res, 12, 242-54, 2015

87. Ota K, Murayama N, Kasanuki K, Kondo D, Fujishiro H, Arai H, Sato K, Iseki E: Visuoperceptual assessments for differentiating dementia with Lewy bodies and Alzheimer's disease: illusory contours and other neuropsychological examinations.Arch Clin Neuropsychol, 30, 256-63, 2015

*88. Kasanuki K, Iseki E, Fujishiro H, Ando S, Sugiyama H, Kitazawa M, Chiba Y, Sato K, Arai H: Impaired heart rate variability in patients with dementia with Lewy bodies: Efficacy of electrocardiogram as a supporting diagnostic marker. Parkinsonism Relat Disord, 21, 749-54, 2015

89. Watanabe T, Hanajima R, Shirota Y, Tsutsumi R, Shimizu T, Hayashi T, Terao Y, Ugawa Y, Katsura

法人番号	131025
プロジェクト番号	S1101009

M, Kunimatsu A, Ohtomo K, Hirose S, Miyashita Y, Konishi S: Effects of rTMS over presupplementary motor area on fronto-basal-ganglia network activity during stop-signal task. J Neurosci, 35, 4813-4823, 2015

*90. Kamagata K, Shimoji K, Hori M, Nishikori A, Tsuruta K, Yoshida M, Kamiya K, Irie R, Suzuki M, Kyogoku S, Suzuki Y, Sato N, Aoki S: Intersite Reliability of Diffusion Tensor Imaging on Two 3T Scanners. Magn Reson Med Sci, 14(3), 227-233, 2015

91. Runge VM, Aoki S, Bradley WG Jr, Chang KH, Essig M, Ma L, Ross JS, Valavanis A:Magnetic Resonance Imaging and Computed Tomography of the Brain-50 Years of Innovation, With a Focus on the Future. Invest Radiol, 50, 551-6, 2015

92. Katagiri N, Pantelis C, Nemoto T, Zalesky A, Hori M, Shimoji K, Saito J, Ito S, Dwyer DB, Fukunaga I, Morita K, Tsujino N, Yamaguchi T, Shiraga N, Aoki S, Mizuno M.A longitudinal study investigating sub-threshold symptoms and white matter changes in individuals with an 'at risk mental state' (ARMS).Schizophr Res, 162, 7-13,2015

93. Tachibana Y, Obata T, Yoshida M, Hori M, Kamagata K, Suzuki M, Fukunaga I, Kamiya K, Yokoyama K, Hattori N, Inoue T, Aoki S:Analysis of normal-appearing white matter of multiple sclerosis by tensor-based two-compartment model of water diffusion. Eur Radiol, 25, 1701-7, 2015

94. Sato K, Ishigame K, Ying SH, Oishi K, Miller MI, Mori S: Macro- and microstructural changes in patients with spinocerebellar ataxia type 6: assessment of phylogenetic subdivisions of the cerebellum and the brain stem. JNR Am J Neuroradiol, 36, 84-90, 2015

95. Suzuki M, Bachelet-Violette L, Rouzet F, Beilvert A, Autret G, Maire M, Menager C, Louedec L, Choqueux C, Sabourat P, Haddad O, Chauvierre C, Chaubet F, Michel JB, Serfaty JM, Letourneur D: Ultrasmall superparamagnetic iron oxide nanoparticles coated with fucoidan for molecular MRI of intraluminal thrombus. Nanomedicine,10, 73-87,2015

２０１４年グループ（1）

96. Inoue H, Murayama T, Tashiro M, Sakurai T, Konishi M: Mg2+- and ATP-dependent inhibition of TRPM7 by oxidative stress.Free Radic Biol Med, 72, 257-266, 2014

97. Kamiya K, Yum SW, Kurebayashi N, Muraki M, Ogawa K, Karasawa K, Miwa A, Guo X, Gotoh S, Sugitani Y, Yamanaka H, Ito-Kawashima S, Iizuka T, Sakurai T, Noda T, Minowa O, Ikeda K: Assembly of the cochlear gap junction macromolecular complex requires connexin 26. J Clin Invest, 124, 1598-1607,2014

98. Suyama M, Koik M, Asaoka D, Mori H, Oguro M, Ueno T, Nagahara A, Watanabe S, Uchiyama Y: Increased immunoreactivity of cathepsins in the rat esophagus under chronic acid reflux esophagitis. J Histochem Cytochem, 62, 645-660, 2014

99. Sakuraba M, Murata J, Teruyama R, Kamiya K, Yamaguchi J, Okano Y, Uchiyama Y, Ikeda K: Spatotemporal expression of TRPM4 in the mouse cochlea. J Neurosci Res, 92, 1409-1418, 2014

100. Ueshima S, Nishida T, Koike M, Matsuda H, Sawa Y, Uchiyama Y: Nirtic oxide-mediated injury of interstitial cells of Cajal and intestinal dysmotility under endotoxemia. Biomed Res, 35, 251-262, 2014

101. Bartolomé A, Kimura-Koyanagi M, Asahara S, Guillén C, Teruyama K, Inoue H, Shimizu S, Kanno A, García-Aguilar A, Koike M, Uchiyama Y, Benito M, Noda T, Kido Y: Pancreatic β cell failure mediated by mTORC1 hyperactivity and autophagic Pancreatic β cell failure mediated by mTORC1 hyperactivity and autophagic impairment. Diabetes, 63, 2996-3008, 2014

102. Nakafuku-Fukuda M, Hirata T, Keto Y, Yamano M, Yokoyama T, Uchiyama Y: Inhibitory effect of the selective secretion 5-HT receptor antagonist ramosetron on duodenal acidification-induced gastric hypersensitivity in rats. Eur J Pharmacol, 731,88-92, 2014

103. Yamanaka T, Tosaki A, Kurosawa M, Matsumoto G, Koike M, Uchiyama Y, Maity SN, Shimogori T, Hattori N, Nukina N: NF-Y inactivation causes atypical neurodegeneration characterized by ubiquitin and p62 accumulation and endoplasmic reticulum disorganization. Nat Commun , 10, 1038, 2014

104. Yokono M, Takasu T, Hayashizaki Y, Mitsuoka K, Kihara R, Muramatsu Y, Miyoshi S, Tahara A, Kurosaki E, Li Q, Tomiyama H, Sasamata M, Shibasaki M, Uchiyama Y: SGLT2 selective inhibitor ipragliflozin reduces body fat mass by increasing fatty acid oxidation in high-fat diet-induced obese rats.Eur J Pharmaco,727, 66-74, 2014

105. Awazawa M, Futami T, Sakada M, Kaneko K, Ohsugi M, Nakaya K, Terai A, Suzuki R, Koike M, Uchiyama Y, Kadowaki T, Ueki K: Deregulation of Pancreas-Specific Oxidoreductin ERO1β in the Pathogenesis of Diabetes Mellitus. Mol Cell Biol, 34,1290-1299, 2014

*106. Kashima J, Shintani-Ishida K, Nakajima M, Maeda H, Unuma K, Uchiyama Y, Yoshida K: Immunocytochemical study of the autophagy marker microtubule-associated protein 1 light chain 3

法人番号	131025
プロジェクト番号	S1101009

in normal and steatotic human livers. Hepatol Res,44, 779-787,2014

*107. Shiba-Fukushima K, Arano T, Matsumoto G, Inoshita T, Yoshida S, Ishihama Y, Ryu KY, Nukina N, Hattori N, Imai Y: Phosphorylation of mitochondrial polyubiquitin by PINK1 promotes Parkin mitochondrial tethering. PLoS Genet, 10, e1004861,2014

*108. Shiba-Fukushima K, Inoshita T, Hattori N, Imai Y: Lysine 63-linked polyubiquitination is dispensable for Parkin-mediated mitophagy. J Biol Chem, 289, 33131-6, 2014

109. Amo T, Saiki S, Sawayama T, Sato S, Hattori N: Detailed analysis of mitochondrial respiratory chain defects caused by loss of PINK1.Neurosci Lett, 580 37-40, 2014

110. Shiba-Fukushima K, Inoshita T, Hattori N, Imai Y: PINK1-mediated phosphorylation of Parkin boosts Parkin activity in Drosophila.PLoS Genet, 10, e1004391, 2014

111. Hattori N, Saiki S, Imai Y: Regulation by mitophagy.Int J Biochem Cell Biol, 53, 147-50, 2014

112. Furuya N, Ikeda S, Sato S, Soma S, Ezaki J, Oliva Trejo JA, Takeda-Ezaki M, Fujimura T,Arikawa-Hirasawa E, Tada N, Komatsu M, Tanaka K, Kominami E, Hattori N, Ueno T : PARK2/Parkin-mediated mitochondrial clearance contributes to proteasome activation during slow-twitch muscle atrophy via NFE2L1 nuclear translocation. Autophagy, 10, 631-41, 2014

113. Hattori N: Cerebral organoids model human brain development and microcephaly. Mov Disord, 29, 185, 2014

114. Hattori N, Saiki S, Imai Y:Regulation by mitophagy.Int J Biochem Cell Biol, 53, 147-50, 2014

２０１４年グループ（２）

*115. Kerever A Mercier F, Nonaka R, de Vega S, Oda Y, Zalc B, Okada Y, Hattori N, Yamada Y, Arikawa-Hirasawa: Perlecan is required for FGF-2 signaling in the neural stem cell niche. Stem Cell Res, 12, 492-505,2014

116. Ning L, Kurihara H, de Vega S,* Ichikawa-Tomikawa n, Xu Z,Nonaka R, Kazuno S, Yamada Y, Miner JH, Arikawa-HirasawA E : Laminin α1 regulates age-related mesangial cell proliferation and mesangial matrix accumulation through the TGFβ pathway The American Journal of Pathology. The American Journal of Pathology, 184, 1683-94, 2014

117. Nakajima M, Miyajima M, Ogino I, Sugano H, Akiba C, Domon N, Karagiozov KL, Arai H : Use of External Lumbar Cerebrospinal Fluid Drainage and Lumboperitoneal Shunts with Strata NSC Valves in Idiopathic Normal Pressure Hydrocephalus. World Neurosurg, 83, 387-393, 2014

118. Tsutsumi S, Ogino I, Miyajima M, Nakamura M, Yasumoto Y, Arai H, Ito M: Cranial Arachnoid Protrusions and Contiguous Diploic Veins in CSF Drainage. AJNR Am J Neuroradiol, 35, 1735-1739, 2014

*119. Yasuda S., Sugiura H., Katsurabayashi S., Shimada T., Tanaka H., Takasaki K., Iwasaki K., Kobayashi T., Hino O. and Yamagata K: Activation of Rheb, but not of MTORC1, impairs spine synapse morphogenesis in tuberous sclerosis complex. Science Rep. 4, 5155, 2014

*120. Shiono M., Kobayashi T., Takahashi R., Ueda M., Ishikawa C. and Hino O: Transgenic expression of the N525S-tuberin variant in Tsc2 mutant (Eker) rats causes dominant embryonic lethality. Scientific Reports, 4, 5927, 2014

121. Nakajima M, Miyajima M, Ogino I, Sugano H, Akiba C, Domon N, Karagiozov KL, Arai H: Use of External Lumbar Cerebrospinal Fluid Drainage and Lumboperitoneal Shunts with Strata NSC Valves in Idiopathic Normal Pressure Hydrocephalus. World Neurosurg, 83, 387-393, 2014

122. Tsutsumi S, Ogino I, Miyajima M, Nakamura M, Yasumoto Y, Arai H, Ito M: Cranial Arachnoid Protrusions and Contiguous Diploic Veins in CSF Drainage. AJNR Am J Neuroradiol, 35, 1735-1739, 2014

*123. Kamiya K, Hori M, Miyajima M, Nakajima M, Suzuki Y, Kamagata K, Suzuki M, Arai H, Ohtomo K, Aoki S: Axon diameter and intra-axonal volume fraction of the corticospinal tract in idiopathic normal pressure hydrocephalus measured by q-space imaging. PLoS One, 9, e103842, 2014

124. SakurabaM., MurataJ., TeruyamaR., KamiyaK., YamaguchiJ., OkanoH., UchiyamaY., and IkedaK: Spatiotemporal expression of TRPM4 in the mouse cochlea. JOURNAL OF NEUROSCIENCE RESEARCH, 92, 1409-1418, 2014

*125. KidokoroY., KarasawaK., MinowaO., SugitaniY., NodaT., IkedaK., and KamiyaK.: Deficiency of transcription factor Brn4 disrupts cochlear gap junction plaques in a model of DFN3 non-syndromic deafness. PLoS One, 9, 9, 2014

*126. InoshitaA., KarasawaK., FunakuboM., MiwaA., IkedaK., and KamiyaK.: Dominant negative connexin26 mutation R75W causing severe hearing loss influences normal programmed cell death in postnatal organ of Corti. BMC GENETICS, 15, 1, 2014

*127. Kamiya, K., Yum, S. W., Kurebayashi, N., Muraki, M., Ogawa, K., Karasawa, K., Miwa, A., Guo, X., Gotoh, S., Sugitani, Y., Yamanaka, H., Ito-Kawashima, S., Iizuka, T., Sakurai, T., Noda, T.,

法人番号	131025
プロジェクト番号	S1101009

Minowa, O., and Ikeda, K.: Assembly of the cochlear gap junction macromolecular complex requires connexin 26. The Journal of clinical investigation, 124, 1598-1607, 2014

128. Kazusaku Kamiya, Vincent Michel, Fabrice Giraudet, Brigitte Riederer, Isabelle Foucher, Samantha Papal, Isabelle Perfettini, Sebastien Le Gal, Elisabeth Verpy, Weiliang Xia, Ursula Seidler, Maria-Magdalena Georgescu, Paul Avan, Aziz El-Amraouia, Christine Petit: An unusually powerful mode of low-frequency sound interference due to outer hair cell hair bundle defects unveiled in Nherf1-/- mice. Proc Natl Acad Sci U S A, 111, 9307-12, 2014

*129. Shibata N, Nagata T, Tagai K, Shinagawa S, Ohnuma T, Kawai E, Kasanuki K, Shimazaki H, Toda A, Tagata Y, Nakada T, Nakayama K, Yamada H, Arai H: Association between the catechol-O-methyltransferase polymorphism Val158Met and Alzheimer's disease in a Japanese population. Int J Geriatr Psychiatry, 30, 927-33, 2014

130. Kohno K, Baba H, Inoue T, Nakai Y, Toyomaki A, Suzuki T, Hatano K, Arai H, Terao T: Dose-dependent effects of light on hyperthymic temperament. J Affect Disord, 162, 26-29, 2014

131. Kasanuki K, Iseki E, Kondo D, Fujishiro H, Minegishi M, Sato K, Katsuse O, Hino H, Kosaka K, Arai H: Neuropathological investigation of hypocretin expression in brains of dementia with Lewy bodies. Geriatr Gerontol Int, 569, 68-73, 2014

132. Komatsu M, Shibata N, Ohnuma T, Kuerban B, Tomson K, Toda A, Tagata Y, Nakada T, Shimazaki H, Arai H: Polymorphisms in the aldehyde dehydrogenase 2 and dopamine hydroxylase genes are not associated with Alzheimer's disease. J Neural Transm, 121, 427-32, 2014

133. Chiba Y, Iseki E, Fujishiro H, Ota K, Kasanuki K, Arai H, Hirayasu Y, Sato K: Primary visual cortical metabolism and rapid eye movement sleep behavior disorder in dementia with Lewy bodies. Psychiatry Clin Neurosci, 68, 137-44, 2014

134. Arai H, Ichimiya Y, Shibata N, Nakajima T, Sudoh S, Tokuda T, Sujaku T, Yokokawa S, Hoshii N, Noguchi H, Bille A: Safety and tolerability of immune globulin intravenous (human), 10% solution in Japanese subjects with mild to moderate Alzheimer's disease. Psychogeriatrics, 14, 165-74, 2014

135. Baba H, Kohno K, Inoue T, Nakai Y, Toyomaki A, Suzuki T, Hatano K, Arai H, Terao T: The effects of mental state on assessment of bipolar temperament. J Affect Disord, 161, 1-3, 2014

136. Ota K, Iseki E, Murayama N, Chiba Y, Fujishiro H, Kasanuki K, Manabe Y, Arai H, Sato K: Three presenile patients in which neuropsychological and neuroimaging examinations suggest possible progression to dementia with Lewy bodies. Psychogeriatrics, 14, 72-80, 2014

*137. Nagane A, Baba H, Nakano Y, Maeshima H, Hukatsu M, Ozawa K, Suzuki T, Arai H: Comparative study of cognitive impairment between medicated and medication-free patients with remitted major depression: Class-specific influence by tricyclic antidepressants and newer antidepressants. Psychiatry Res, 218, 101-105, 2014

138. Kumano H, Uka T: Visual impairment by surrounding noise is due to interactions among stimuli in the higher-order visual cortex. J Neurophysiol, 112, 620-630, 2014

139. Katsura M, Hirose S, Sasaki H, Mori H, Kunimatsu A, Ohtomo K, Jimura K. Konishi S: Decreased fronto-temporal interaction during fixation after memory retrieval. PLoS ONE, 9, e110798, 2014

140. Jimura K, Hirose S, Kunimatsu A, Ohtomo K, Koike Y, Konishi S: Late development of brain-behavior correlations during response inhibition. Neuroscience, 274, 383-392, 2014

141. Hirose S, Jimura K, Kunimatsu A, Abe O, Ohtomo K, Miyashita Y, Konishi S: Changes in cerebro-cerebellar interaction during response inhibition after performance improvement. Neuroimage, 99, 142-148, 2014

142. Watanabe T, Hanajima R, Shirota Y, Ohminami S, Tsutsumi R, Terao Y, Ugawa Y, Hirose S, Miyashita Y, Konishi S, Kunimatsu A, Ohtomo K: Bidirectional effects on inter-hemispheric resting-state functional connectivity induced by excitatory and inhibitory repetitive transcranial magnetic stimulation: Bidirectional effects on inter-hemispheric resting-state functional connectivity induced by excitatory and inhibitory repetitive transcranial magnetic stimulation. Human Brain Mapping, 35, 1896-1905, 2014

143. Watanabe T, Kan S, Koike T, Misaki M, Konishi S, Miyauchi S, Miyashita Y, Masuda N: Network-dependent modulation of brain activity during sleep. Neuroimage, 98, 1-10, 2014

144. Watanabe T, Hirose S, Wada H, Imai Y, Machida T, Shirouzu I, Konishi S, Miyashita Y, Masuda N: Energy landscapes of resting-state brain networks. Frontiers in Neuroinformatics, 8, 12, 2014

145. Goto M, Abe O, Aoki S, Hayashi N, Miyati T, Takao H, Matsuda H, Yamashita F, Iwatsubo T, Mori H, Kunimatsu A, Ino K, Yano K, Ohtomo K: Influence of Parameter Settings in Voxel-based Morphometry 8. Using DARTEL and Region-of-interest on Reproducibility in Gray Matter Volumetry. Mehods In Med, 54, 171-8, 2014

146. Goto M, Kunimatsu A, Shojima M, Mori H, Abe O, Aoki S, Hayashi N, Gonoi W, Miyati T, Ino K, Yano K, Saito N, Ohtomo K: Depiction of branch vessels arising from intracranial aneurysm sacs:

法人番号	131025
プロジェクト番号	S1101009

Time-of-flight MR angiography versus CT angiography. Clin Neurol Neurosurg, 126, 177-84, 2014

147. Hayakawa YK, Sasaki H, Takao H, Hayashi N, Kunimatsu A, Ohtomo K, Aoki S: Depressive symptoms and neuroanatomical structures in community-dwelling women: A combined voxel-based morphometry and diffusion tensor imaging study with tract-based spatial statistics. Neuroimage Clin, 4, 481-7, 2014
148. Hori M, Tsutsumi S, Yasumoto Y, Ito M, Suzuki M, Tanaka FS, Kyogoku S, Nakamura M, Tabuchi T, Fukunaga I, Suzuki Y, Kamagata K, Masutani Y, Aoki S: Cervical spondylosis: Evaluation of microstructural changes in spinal cord white matter and gray matter by diffusional kurtosis imaging. Magn Reson Imaging, 32, 428-32, 2014
*149. Hori M, Yoshida M, Yokoyama K, Kamagata K, Kumagai F, Fukunaga I, Kamiya K, Suzuki M, Masutani Y, Hamasaki N, Suzuki Y, Kyogoku S, Hattori N, Aoki S: Multiple sclerosis: Benefits of q-space imaging in evaluation of normal-appearing and periplaque white matter. Magn Reson Imaging, 32, 625-629, 2014
150. Ishii K, Ito K, Nakanishi A, Kitamura S, Terashima A: Computer-assisted system for diagnosing degenerative dementia using cerebral blood flow SPECT and 3D-SSP: a multicenter study. Jpn J Radiol, 32, 383-90, 2014
*151. Kamiya K, Hori M, Miyajima M, Nakajima M, Suzuki Y, Kamagata K, Suzuki M, Arai H, Ohtomo K, Aoki S: Axon diameter and intra-axonal volume fraction of the corticospinal tract in idiopathic normal pressure hydrocephalus measured by q-space imaging. PLoS One, 9, e103842, 2014
152. Katsura M, Suzuki Y, Hata J, Hori M, Sasaki H, Akai H, Mori H, Kunimatsu A, Masutani Y, Aoki S, Ohtomo K: Non-Gaussian diffusion-weighted imaging for assessing diurnal changes in intervertebral disc microstructure. J Magn Reson Imaging, 40, 1208-14, 2014
*153. Masutani Y, Aoki S: Fast and robust estimation of diffusional kurtosis imaging (DKI) parameters by general closed-form expressions and their extensions. Magn Reson Med Sci, 13, 97-115, 2014
*154. Kamagata K, Hori M, Kamiya K, Suzuki M, Nishikori A, Kumagai F, Yoshida M, Kyogoku S, Aoki S: Diffusion MR Imaging of White Matter Pathways. Visualization and Quantitative Evaluation. Juntendo Medical Journal, 60, 100-106, 2014

２０１３年グループ（１）

*155. Okura H., Kobayashi T., Koike M., Ohsawa M., Zhang D., Arai H., Uchiyama Y. and Hino O: Tuberin activates and controls the distribution of Rac1 via association with p62 and ubiquitin through the mTORC1 signaling pathway. Int. J. Oncology, 43, 447-456, 2013
*156. Adachi T, Takahara K, Taneo J, Uchiyama Y, Inaba K : Particle size of latex beads dictates IL-1β production mechanism. PLos One, 8, e68499, 2013
157. Matsui H, Sato F, Sato S, Koike M, Taruno Y, Saiki S, Funayama M, Ito H,Taniguchi Y, Uemura N, Toyoda A, Sakaki Y, Takeda S, Uchiyama Y, Hattori N,Takahashi R: ATP13A2 deficiency induces a decrease in cathepsin D activity, fingerprint-like inclusion body formation, and selective degeneration of dopaminergic neurons. FEBS Lett, 587, 1316-25, 2013
*158. Koike M, Tanida I, Nanao N, Tada N, Iwata J, Ueno T, Kominami E, Uchiyama Y: Enrichment of GABARAP relative to LC3 in the axonal initial segments of neurons. PLos One, 8, e63568, 2013
*159. Ohkouchi S, Shibata M, Sasaki M, Koike M, Safig P, Peters C, Nagata S, Uchiyama Y: Biogenesis and proteolytic processing of lysosomal DNase II. PLoS One, 8, e59148, 2013
*160. Furuta A, Wakabayashi K, Haratake J, Kikuchi H, Kabuta T, Mori F, Tokonami F, Katsumi Y, Tanioka F, Uchiyama Y, Nishino I, Wada K: Lysosomal storage and advanced senescence in the brain of LAMP-2-deficient Danon disease. Acta Neuropathol, 125, 459-461, 2013
161. Koike M, Shibata M, Ezaki J, Peters C, Saftig P, Kominami E, Uchiyama Y: Differences in expression patterns of cathepsin C/dipeptidyl peptidase I in normal, pathological and aged mouse central nervous systems. Eur J Neurosci, 37, 816-30, 2013
*162. Hayakawa N, Shiozaki M, Shibata M, Koike M, Uchiyama Y, Matsuura M, Gotow T: Resveratrol affects undifferentiated and differentiated PC12 cells differently, particularly with respect to possible differences in mitochondrial and autophagic functions. Eur J Cell Bio, 92, 30-43, 2013
163. Nonomura K, Yamaguchi Y, Hamachi M, Koike M, Uchiyama Y, Nakazato K, Mochizuki A, Sakaue-Sawano A, Miyawaki A, Yoshida H, Kuida K, Miura M: Local apoptosis modulates early mammalian brain development through the elimination of morphogen-producing cells. Dev Cell, 27, 621-634, 2013
164. Abe H, Uchida T, Hara A, Mizukami H, Komiya K, Koike M, Shigihara N, Toyofuku Y, Ogihara T, Uchiyama Y, Yagihashi S, Fujitani Y, Watada H: Exendin-4 improves beta cell function in autophagy-deficient beta cells. Endicrinology, 154, 4512-24, 2013

法人番号	131025
プロジェクト番号	S1101009

165. Sakata K, Ohmuraya M, Araki K, Suzuki C, Ida S, Hashimoto D, Wang J, Uchiyama Y, Baba H, Yamamura K: Generation and analysis of serine protease inhibitor Kazal type 3-Cre driver mice. Exp Animals, 63, 45-53, 2013
166. Tsuzuki T, Sakaguchi N, Kudoh T, Takano S, Uehara M, Murayama T, Sakurai T, Hashii M, Higashida H, Weber K, Guse AH, Kameda T, Hirokawa T, Kumaki Y, Potter BV, Fukuda H, Arisawa M, Shuto S: Design and Synthesis of Cyclic ADP-4-Thioribose as a Stable Equivalent of Cyclic ADP-Ribose, a Calcium Ion-Mobilizing Second Messenger. Angew Chem Int Ed Engl, 52, 6633-7, 2013
167. Shoji K, Murayama T, Mimura I, Wada T, Kume H, Goto A, Ohse T, Tanaka T, Inagi R, van der Hoorn FA, Manabe I, Homma Y, Fukayama M, Sakurai T, Hasegawa T, Aburatani H, Kodama T, Nangaku M: Sperm-associated antigen 4, a novel hypoxia-inducible factor 1 target, regulates cytokinesis, and its expression correlates with the prognosis of renal cell carcinoma. Am J Pathol, 182, 2191-2203, 2013
168. Hashimoto M, Enomoto M, Morales J, Kurebayashi N, Sakurai T, Hashimoto T, Nara T, Mikoshiba K: Inositol 1,4,5-Trisphosphate Receptor Regulates Replication, Differentiation, Infectivity, and Virulence of the Parasitic Protist Trypanosoma cruzi. Molecular Microbiology, 87, 1133-50, 2013
169. Sugihara M, Odagiri F, Suzuki T, Murayama T, Nakazato Y, Unuma K, Yoshida K, Daida H, Sakurai T, Morimoto S, Kurebayashi N: Usefulness of Running Wheel for Detection of Congestive Heart Failure in Dilated Cardiomyopathy Mouse Model. PLoS One, 8, e55514, 2013
*170. Kamikubo Y, Shimomura T, Fujita Y, Tabata T, Kashiyama T, Sakurai T, Fukurotani K, Kano M: Functional cooperation of metabotropic adenosine and glutamate receptors regulates postsynaptic plasticity in the cerebellum. J Neurosci, 33, 18661-18671, 2013

２０１３年グループ（２）

*171. Douet V, Arikawa-Hirasawa E Mercier F: Fractone-heparan sulfates mediate FGF-2 stimulation of cell proliferation in the adult subventricular zone. Cell Prolif, 46, 137-145, 2013
172. Nakazawa N, Miyahara K, Okawada M, Yamataka A, Suzuki R, Akazawa C, Tomikawa-Ichikawa N, Arikawa-Hirasawa E: Laminin-1 promotes enteric nervous system development in mouse embryo. Pediatr Surg Int. Pediatr Surg Int, 29, 1205-8, 2013
173. Suzuki N, Numakawa T,Joshua Chou J, de Vega, S, Mizuniwa C, Sekimoto K, Adachi N, Kunugi N, Arikawa-Hirasawa E, Yamada Y, Akazawa C: Teneurin-4 promotes cellular protrusion formation and neurite outgrowth through focal adhesion kinase signaling. The FASEB Journal, 28, 1386-97, 2013
*174. Ohsawa M., Kobayashi T., Okura H., Igarashi T., MizuguchiM. and Hino O: TSC1 controls distribution of actin fibers through its effect on function of Rho family of small GTPases and regulates cell migration and polarity. Plos One, 8, e54503-54516, 2013
*175. Okura H., Kobayashi T., Koike M., Ohsawa M., Zhang D., Arai H., Uchiyama Y. and Hino O: Tuberin activates and controls the distribution of Rac1 via association with p62 and ubiquitin through the mTORC1 signaling pathway. Int. J. Oncology, 43, 447-456, 2013
176. Miyajima M, Nakajima M, Ogino I, Miyata H, Motoi Y, Arai H: Soluble amyloid precursor protein α in the cerebrospinal fluid as a diagnostic and prognostic biomarker for idiopathic normal pressure hydrocephalus. Eur J Neurol, 20, 236-242, 2013
177. Watanabe M, Miyajima M, Ogino I, Nakajima M, Arai H: Cerebellar Purkinje Cells Exhibit Increased Expression of HMGB-1 and Apoptosis in Congenital Hydrocephalic H-TxRats. Neurosurgery, 72, 459-467, 2013
*178. Nakanishi A, Fukunaga I, Hori M, Masutani Y, Takaaki H, Miyajima M, Aoki S: Microstructural changes of the corticospinal tract in idiopathic normal pressure hydrocephalus: a comparison of diffusion tensor and diffusional kurtosis imaging. Neuroradiology, 55, 971-976, 2013
179. Hoshi K, Kariya Y, Nara K, Ito H, Matsumoto K, Nagae M, Yamaguchi Y, Nakajima M, Miyajima M, Arai H, Kuno A, Narimatsu H, Shirotani K, Hashimoto Y: Lectin-dependent inhibition of antigen-antibody reaction: application for measuring α2,6-sialylated glycoforms of transferrin. J Biochem, 154, 229-232, 2013
180. Miyajima M, Nakajima M, Motoi Y, Moriya M, Sugano H, Ogino I, Nakamura E, Tada N, Kunichika M, Arai H: Leucine-rich α2-glycoprotein is a novel biomarker of neurodegenerative disease in human cerebrospinal fluid and causes neurodegeneration in mouse cerebral cortex. PLoS One, 8, e74453, 2013
181. 神谷和作: 遺伝性難聴への内耳細胞治療法開発：幹細胞ホーミング機構を応用した遺伝性難聴に対する内耳細胞治療法の開発，日本薬理学雑誌（Folia Pharmacol. Jpn), 141, 191-4, 2013

法人番号	131025
プロジェクト番号	S1101009

182. Gianluca Esposito, Sachine Yoshida, Ryuko Ohnishi, Yousuke Tsuneoka, Maria del Carmen Rostagno, Susumu Yokota, Shota Okabe, Kazusaku Kamiya, Mikio Hoshino, Masaki Shimizu, Paola Venuti, Takefumi Kikusui, Tadafumi Kato, Kumi O. Kuroda K: Infant Calming Responses During Maternal Carrying In Humans and Mice. Current Biology, 23, 739-45, 2013
183. Nomura N, Kamiya K, Ikeda K, Yui N, Chiga M, Sohara E, Rai T, Sakaki S, Uchida S: Treatment with 17-allylamino-17-demethoxygeldanamycin ameliorated symptoms of Bartter syndrome type IV caused by mutated Bsnd in mice. Biochem Biophys Res Commun, 441, 544-9, 2013
184. Mitani A, Sasaki R, Oizumi M, Uka T: A leaky-integrator model as a control mechanism underlying flexible decision making during task switching. PLoS ONE, 8, e59670, 2013
185. Kumano H, Uka T: Neuronal mechanisms of visua l perceptual learning. Behavioral Brain Research, 249, 75-80, 2013
*186. Kamagata K, Tomiyama H, Motoi Y, Kano M, Abe O, Ito K, Shimoji K, Suzuki M, Hori M, Nakanishi A, Kuwatsuru R, Sasai K, Aoki S, Hattori N: Diffusional kurtosis imaging of cingulate fibers in Parkinson disease: Comparison with conventional diffusion tensor imaging. Magn Reson Imaging, 31, 1501-1506, 2013
187. Nakanishi A, Fukunaga I, Hori M, Masutani Y, Takaaki H, Miyajima M, Aoki S: Microstructural changes of the corticospinal tract in idiopathic normal pressure hydrocephalus: a comparison of diffusion tensor and diffusional kurtosis imaging. Neuroradiology, 55, 971-6, 2013
188. Fukunaga I, Hori M, Masutani Y, Hamasaki N, Sato S, Suzuki Y, Kumagai F, Kosuge M, Hoshito H, Kamagata K, Shimoji K, Nakanishi A, Aoki S, Senoo A: Effects of diffusional kurtosis imaging parameters on diffusion quantification. Radiol Phys Techno, 6, 343-8, 2013
189. Shimoji K, Abe O, Uka T, Yasmin H, Kamagata K, Asahi K, et al: White matter alteration in metabolic syndrome: diffusion tensor analysis. Diabetes care. Diabetes care: 36, 696-700, 2013
*190. Kamagata K, Motoi Y, Tomiyama H, Abe O, Ito K, Shimoji K, et al: Relationship between cognitive impairment and white-matter alteration in Parkinson's disease with dementia: tract-based spatial statistics and tract-specific analysis. Eur Radiol, 23, 1946-55, 2013
191. Goto M, Abe O, Aoki S, Hayashi N, Miyati T, Takao H, et al. Diffeomorphic Anatomical Registration Through Exponentiated Lie Algebra provides reduced effect of scanner for cortex volumetry with atlas-based method in healthy subjects. Neuroradiology, 55, 869-75, 2013
192. Shibata N, Motoi Y, Tomiyama H, Ohnuma T, Kuerban B, Tomson K, Komatsu M, Shimazaki H, Hattori N, Arai H: Lack of Genetic Associations of PPAR-γ and PGC-1α with Alzheimer's Disease and Parkinson's Disease with Dementia. Dement Geriatr Cogn Dis Extra, 3, 161-7, 2013
*193. Shibata N, Nagata T, Shinagawa S, Ohnuma T, Shimazaki H, Komatsu M, Kuerban B, Tomson K, Nakayama K, Yamada H, Arai H: Genetic association between APOA1 and APOD polymorphisms and ALZHEIMER 's disease in a Japanese population. J Neural Transm, 120, 1599-603, 2013
194. Nagata T, Shinagawa S, Kuerban B, Shibata N, Ohnuma T, Arai H, Nakayama K, Yamada H: Age-Related Association between Apolipoprotein E ε4 and Cognitive Function in Japanese Patients with Alzheimer's Disease. Dement Geriatr Cogn Dis Extra, 3, 66-73, 2013
*195. Kasanuki K, Iseki E, Nishida Y, Fujishiro H, Chiba Y, Sato K, Arai H: Effectiveness of Ramelteon for Treatment of Visual Hallucinations in Dementia With Lewy Bodies: A Report of 4 Cases. J Clin Psychopharmacol, 33, 581-583, 2013
196. Murayama N, Iseki E, Tagaya H, Ota K, Kasanuki K, Fujishiro H, Arai H, Sato K: Intelligence or years of education: which is better correlated with memory function in normal elderly Japanese subjects. Psychogeriatrics, 13, 9-16, 2013
197. Maeshima H, Baba H, Nakano Y, Satomura E, Namekawa Y, Takebayashi N, Nomoto H, Suzuki T, Mimura M, Arai H: J Time course for memory dysfunction in early-life and late-life major depression: A longitudinal study from the Juntendo university mood disorder project. Affect Disord, 151, 66-70, 2013
198. Namekawa Y, Baba H, Maeshima H, Nakano Y, Satomura E, Takebayashi N, Nomoto H, Suzuki T,Arai H: Heterogeneity of elderly depression: increased risk of Alzheimer's disease and Aβ protein metabolism. Prog Neuropsychopharmacol Biol Psychiatry, 43, 203-8, 2013
199. Kurita H, Maeshima H, Kida S, Matsuzaka H, Shimano T, Nakano Y, Baba H, Suzuki T, Arai H:Serum dehydroepiandrosterone (DHEA) and DHEA-sulfate (S) levels in medicated patients with major depressive disorder compared with controls. J Affect Disord, 146, 205-12, 2013
200. Toda A, Tagata Y, Nakada T, Komatsu M, Shibata N, Arai H: Changes in Mini-Mental State Examination score in Alzheimer's disease patients after stopping habitual drinking. Psychogeriatrics,13, 94-8, 2013
201. Kumano H, Uka T: Responses to random dot motion reveal prevalence of pattern-motion selectivity in area MT. J Neurosci, 33, 15161-15170, 2013

法人番号	131025
プロジェクト番号	S1101009

202. Mitani A, Sasaki R, Oizumi M, Uka T: A leaky-integrator model as a control mechanism underlying flexible decision making during task switching. PLoS One, 8, e59670, 2013
203. Kumano H, Uka T: Neuronal mechanisms of visual perceptual learning. Behavioral Brain Research, 249, 75-80, 2013
204. Hirose S, Watanabe T, Wada H, Imai Y, Machida T, Shirouzu I, Miyashita Y, Konishi S: Functional relevance of micromodules in the human association cortex delineated with high-resolution fMRI. Cerebral Cortex, 23, 2863-2871, 2013
205. Hirose S, Kimura H. M, Jimura K, Kunimatsu A, Abe O, Ohtomo K, Miyashita Y, Konishi S: Dissociable temporo-parietal memory networks revealed by functional connectivity during episodic retrieval. PLoS One, 8, e71210, 2013
206. Watanabe T, Hirose S, Wada H, Imai Y, Machida T, Shirouzu I, Konishi S, Miyashita Y, Masuda N: A pairwise maximuNature Communicationsm entropy model accurately describes resting-state human brain networks, 4, 1370, 2013
*207. Kamagata K, Tomiyama H, Motoi Y, Kano M, Abe O, Ito K, Shimoji K, Suzuki M,Hori M, Nakanishi A, Kuwatsuru R, Sasai K, Aoki S, Hattori N: Diffusional kurtosis imaging of cingulate fibers in Parkinson disease: comparison with conventional diffusion tensor imaging. Magn Reson Imaging, 31, 1501-6, 2013
208. Nakanishi A, Fukunaga I, Hori M, Masutani Y, Takaaki H, Miyajima M, Aoki S: Microstructural changes of the corticospinal tract in idiopathic normal pressure hydrocephalus: a comparison of diffusion tensor and diffusional kurtosis imaging. Neuroradiology, 55, 971-976, 2013
*209. Kamagata K, Motoi Y, Tomiyama H, Abe O, Ito K, Shimoji K, Suzuki M, Hori M, Nakanishi A, Sano T, Kuwatsuru R, Sasai K, Aoki S, Hattori N: Relationship between cognitive impairment and white-matter alteration in Parkinson's disease with dementia: tract-based spatial statistics and tract-specific analysis. Eur Radiol, 23, 1946-55, 2013
*210. Hori M, Fukunaga I, Masutani Y, Taoka T, Kamagata K, Suzuki Y, Aoki S. Visualizing non-Gaussian diffusion: clinical application of q-space imaging and diffusional kurtosis imaging of the brain and spine. Magn Reson Med Sci, 11, 221-33, 2013

２０１２年グループ（１）

211. Shiba-Fukushima K, Imai Y, Yoshida S, Ishihama Y, Kanao T, Sato S, Hattori N: PINK1-mediated phosphorylation of the Parkin ubiquitin-like domain primes mitochondrial translocation of Parkin and regulates mitophagy. Sci Rep, 2, 1002, 2012
212. Ujiie S, Hatano T, Kubo S, Imai S, Sato S, Uchihara T, Yagishita S, Hasegawa K, Kowa H, Sakai F, Hattori N: LRRK2 I2020T mutation is associated with tau pathology. Parkinsonism Relat Disord, 18, 819-23, 2012
213. Saiki S, Sato S, Hattori N: Molecular pathogenesis of Parkinson's disease: update. J Neurol Neurosurg Psychiatry, 83, 430-6, 2012
214. Ando M, Funayama M, Li Y, Kashihara K, Murakami Y, Ishizu N, Toyoda C, Noguchi K, Hashimoto T, Nakano N, Sasaki R, Kokubo Y, Kuzuhara S, Ogaki K, Yamashita C, Yoshino H, Hatano T, Tomiyama H, Hattori N: VPS35 mutation in Japanese patients with typical Parkinson's disease. Mov Disord, 27, 1413-7, 2012
215. Piao X, Komazawa-Sakon S, Nishida T, Koike M, Piao JH, Ehlken H, Kurihara H, Hara M, van Rooijen N, Schütz G, Ohmuraya M, Uchiyama Y, Yagita H, Okumura K, He YW, Nakano H: c-FLIP maintains tissue homeostasis by preventing apoptosis and programmed necrosis. Sci Signal, 5, ra93, 2012
216. Tashiro Y, Urushitani M, Inoue H, Koike M, Uchiyama Y, Komatsu M, Tanaka K, Yamazaki M, Abe M, Misawa H, Sakimura K, Ito H, Takahashi R: Motor Neuron-specific Disruption of Proteasomes, but not Autophagy, Replicates Amyotrophic Lateral Sclerosis. J Biol Chem, 287, 42984-94, 2012
217. Unno T, Wakamori M, Koike M, Uchiyama Y, Ishikawa K, Kubota H, Yoshida T, Sasakawa H, Peters C, Mizusawa H, Watase K: Development of Purkinje cell degeneration in a knockin mouse model reveals lysosomal involvement in the pathogenesis of SCA6. Proc Natl Acad Sci USA, 109, 17693-8, 2012
218. Sekine S, Kanamaru Y, Koike M, Nishihara A, Okada M, Kinoshita H, Kamiyama J, Maruyama J, Uchiyama Y, Ishihara N, Takeda K, Ichijo H: Rhomboid protease PARL mediates the mitochondrial membrane potential loss-induced cleavage of PGAM5. J Biol Chem, 287, 34635-45, 2012
219. Imaizumi Y, Okada Y, Akamatsu W, Koike M, Kuzumaki N, Hayakawa H, Nihira T, Kobayashi T, Ohyama M, Sato S, Takanashi M, Funayama M, Hirayama A, Soga T, Hishiki T, Suematsu M, Yagi

法人番号	131025
プロジェクト番号	S1101009

T, Ito D, Kosakai A, Hayashi K, Shouji M, Nakanishi A, Suzuki N, Mizushima N, Amagai M, Uchiyama Y, Mochizuki H, Hattori N, Okano H: Mitochondrial dysfunction associated with increased oxidative stress and α-synuclein accumulation in PARK2 iPSC-derived neurons and postmortem brain tissue. Mol Brain, 6, 35, 2012

220. Klionsky D,Uchiyama, Y et al. Guidelines for the use and interpretation of assays for monitoring autophagy. Atuophagy, 8, 445-544, 2012
221. Suzuki T, Shioya T, Murayama T, Sugihara M, Odagiri F, Nakazato Y, Nishizawa H, Chugun A, Sakurai T, Daida H, Morimoto S, Kurebayashi N: Multistep Ion Channel Remodeling and Lethal Arrhythmia Precede Heart Failure in a Mouse Model of Inherited Dilated Cardiomyopathy. PLoS One, 7, e35353, 2012
222. Kakizawa S, Yamazawa T, Chen Y, Ito A, Murayama T, Oyamada H, Kurebayashi N, Sato O, Watanabe M, Mori N, Oguchi K, Sakurai T, Takeshima H, Saito N, Iino M: Nitric oxide-induced calcium release via ryanodine receptors regulates neuronal function. EMBO J, 31, 417-428, 2012

２０１２年グループ（２）

223. Ichikawa-Tomikawa N, Ogawa J, Douet V, Xu Z, Kamikubo Y, Sakurai,T, Kohsaka S, Chiba H, Hattori H, Yamada Y, and Arikawa-Hirasawa E: Laminin a1 is essential for mouse cerebellar development. Matrix Biol, 311, 17–28, 2012
224. Mercier F, Arikawa-Hirasawa E: Heparan sulfate niche for cell proliferation in the adult brain. Neuroscience Letters, 510, 67-72, 2012
225. Yoshinaga H, Sakoda,S Good JM, Takahashi MP, Kubota T, Arikawa-Hirasawa E, Nakata T, Ohno K, Kitamura T, Kobayashi K, and Ohtsuka Y: A novel mutation in SCN4A causes severe myotonia and school-age-onset paralytic episodes. Journal of the Neurological Science, 315, 15-9, 2012
226. Ishijima M, Suzuki N, Hozumi K, Matsunobu T, Kosaki K, Kaneko H, Hassell JR, Arikawa-Hirasawa E, Yamada Y: Perlecan modulates VEGF signaling and is essential for vascularization in endochondral bone formation. Matrix Biol, 31, 234-245, 2012
227. Ishijima M, Suzuki N, Hozumi K, Matsunobu T, Kosaki K, Kaneko H, Hassell JR, Arikawa-Hirasawa E, Yamada Y: Perlecan modulates VEGF signaling and is essential for vascularization in endochondral bone formation. Matrix Biol, 31, 234-245, 2012
228. Suzuki N, Fukushi M, Kosaki K, Doyle AD, de Vega S, Yoshizaki K, Akazawa C, Arikawa-Hirasawa E, Yamada Y: Teneurin-4 is a novel regulator of oligodendrocyte differentiation and myelination of small-diameter axons in the CNS. J Neurosci, 32, 11586-99, 2012
229. Futami I, Ishijima M, Kaneko H, Tsuji K, Ichikawa-Tomikawa N, Sadatsuki R, Muneta T, Arikawa-Hirasawa E, Sekiya I, Kaneko K: Isolation and Characterization of MultipotentialMesenchymal Cells from the Mouse Synovium. PLoS ONE, 7, e45517, 2012
230. Douet V, Arikawa-Hirasawa E, Mercier F: Fractone-heparan sulfates mediate BMP-7 inhibition of cell proliferation in the adult subventricular zone. Neurosci Lett, 528, 120-125, 2012
231. Sato A., Kasai S., Kobayashi T., Takamatsu Y., Hino O., Ikeda K. and Mizuguchi M: Rapamycin reverses impaired social interaction in mouse models of tuberous sclerosis complex. Nature Communications, 2295, 1-9, 2012
232. Goncharova E.A., Goncharov D.A., Fehrenbach M., Khavin I., Ducka B., Hino O., Colby T.V., Merrilees M.J., Haczku A., Albelada S.M. and Krymskaya V: Preventing of alveolar destruction and airspace enlargement in a mouse Model of pulmonary lymphangioleiomyomatosis (LAM). Science Translational Medicine, 4, 1-10, 2012
233. Shimizu A, Komuro Y, Miyajima M, Arai H: Familial nonsyndromic craniosynostosis with specific deformity of the cranium. J Neurosurg Pediatr, 10, 560-564, 2012
234. Mori E, Ishikawa M, Kato T, Kazui H, Miyake H, Miyajima M, Nakajima M, Hashimoto M, Kuriyama N, Tokuda T, Ishii K, Kaijima M, Hirata Y, Saito M, Arai H: Guidelines for management of idiopathic normal pressure hydrocephalus: second edition.
235. Ueda A, Shimizu A, Natori Y, Sonoue H, Komuro Y, Miyajima M, Arai H: Expression of transforming growth factor-β1, -β2, and -β3 in plagiocephalic fused and patent coronal suture. J Craniofac Surg, 23, 755-757, 2012
236. Kakuda N, Shoji M, Arai H, Furukawa K, Ikeuchi T, Akazawa K, Takami M, Hatsuta H, Murayama S, Hashimoto Y, Miyajima M, Arai H, Nagashima Y, Yamaguchi H, Kuwano R, Nagaike K, Ihara Y: Japanese Alzheimer's Disease Neuroimaging Initiative: Altered γ-secretase activity in mild cognitive impairment and Alzheimer's disease. EMBO Mol Med, 4, 344-352, 2012
237. Miyajima M, Shimoji K, Watanabe M, Nakajima M, Ogino I, Arai H: Role of artificial cerebrospinal fluid as perfusate in neuroendoscopic surgery: a basic investigation. Acta Neurochir Suppl, 113, 103-7, 2012

法人番号	131025
プロジェクト番号	S1101009

238. Nakajima M, Miyajima M, Ogino I, Watanabe M, Hagiwara Y, Segawa T, Kobayashi K, Arai H: Brain localization of leucine-rich α2-glycoprotein and its role. Acta Neurochir Suppl. 113, 97-101, 2012
239. Watanabe M, Miyajima M, Nakajima M, Arai H, Ogino I, Nakamura S, Kunichika M: Expression analysis of high mobility group box-1 protein (HMGB-1) in the cerebral cortex, hippocampus, and cerebellum of the congenital hydrocephalus (H-Tx) rat. Acta Neurochir Suppl, 113, 91-96, 2012
240. Futakawa S, Nara K, Miyajima M, Kuno A, Ito H, Kaji H, Shirotani K, Honda T, Tohyama Y, Hoshi K, Hanzawa Y, Kitazume S, Imamaki R, Furukawa K, Tasaki K, Arai H, Yuasa T, Abe M, Arai H, Narimatsu H, Hashimoto Y: A unique N-glycan on human transferrin in CSF: a possible biomarker for iNPH. Neurobiol Aging, 33, 1807-1815, 2012
241. Hiroko Okada, Takashi Iizuka, Hideki Mochizuki, Tomoko Nihira, Kazusaku Kamiya, Ayako Inoshita, Hiromi Kasagi, Misato Kasai, Katsuhisa Ikeda: Gene transfer targeting mouse vestibule using adenovirus and adeno-associated virus vectors. Otology & Neurotology, 33, 655-9, 2012

２０１２年グループ（３）

242. Uka T, Sasaki R, Kumano H: Change in choice-related response modulation in area MT during learning of a depth-discrimination task is consistent with task learning. J Neurosci, 32, 13689-13700, 2012
243. Kumano H, Uka T: Reduction in receptive field size of macaque MT neurons in the presence of visual noise. J Neurophysiol, 108, 215-216, 2012
244. 宇賀貴紀，熊野弘紀: 奥行き知覚. Clinical Neuroscience, 8, 894-896, 2012
245. Shimoji K, Aoki S, Nakanishi A, Suzuki M, Hori M, Sato S, et al: Distribution of estimated glomerular filtration rate (eGFR) values in patients receiving contrast-enhanced magnetic resonance imaging. Jpn J Radiol, 30, 116-9, 2012
*246. Kamagata K, Motoi Y, Abe O, Shimoji K, Hori M, Nakanishi A, et al. White matter alteration of the cingulum in Parkinson disease with and without dementia: evaluation by diffusion tensor tract-specific analysis. AJNR, 33, 890-5, 2012
247. Hori M, Fukunaga I, Masutani Y, Taoka T, Kamagata K, Suzuki Y, et al.: Visualizing non-Gaussian diffusion: clinical application of q-space imaging and diffusional kurtosis imaging of the brain and spine. MRMS, 113, 221-33, 2012
248. Hori M, Fukunaga I, Masutani Y, Nakanishi A, Shimoji K, Kamagata K, et al.: New diffusion metrics for spondylotic myelopathy at an early clinical stage. Eur Radiol, 22, 1797-802, 2012
249. Hattori T, Sato R, Aoki S, Yuasa T, Mizusawa H.: Different patterns of fornix damage in idiopathic normal pressure hydrocephalus and Alzheimer disease. AJNR, 33, 274-9, 2012
250. Hattori T, Orimo S, Aoki S, Ito K, Abe O, Amano A, et al.: Cognitive status correlates with white matter alteration in Parkinson's disease. Human brain mapping, 33, 727-39, 2012
251. Hattori T, Ito K, Aoki S, Yuasa T, Sato R, Ishikawa M, et al.: White matter alteration in idiopathic normal pressure hydrocephalus: tract-based spatial statistics study. AJNR, 33, 97-103, 2012
252. Goto M, Miyati T, Abe O, Takao H, Kurosu T, Hayashi N, et al.: Repeatability of measured brain volume by atlas-based method using T1-weighted image. Journal of digital imaging, 25, 173-8, 2012
253. Goto M, Abe O, Miyati T, Kabasawa H, Takao H, Hayashi N, et al.: Influence of signal intensity non-uniformity on brain volumetry using an atlas-based method. Korean journal of Radiology, 13, 391-402, 2012
254. Goto M, Abe O, Miyati T, Aoki S, Takao H, Hayashi N, et al.: Association between iron content and gray matter missegmentation with voxel-based morphometry in basal ganglia. JMRI, ISSN: 1053-1807, 958-62, 2012
255. Goto M, Abe O, Kabasawa H, Takao H, Miyati T, Hayashi N, et al.: Effects of image distortion correction on voxel-based morphometry, Magnetic resonance in medical sciences, 11, 27-34, 2012
256. Ohnuma T, Nakamura T, Takebayashi Y, Hanzawa R, Kitazawa M, Higashiyama R, Takeda M, Thompson K, Komatsu M, Shimazaki H, Shibata N, Arai H.: No Associations Found between PGBD1 and the Age of Onset in Japanese Patients Diagnosed with Sporadic Alzheimer's Disease. Dement Geriatr Cogn Dis Extra, 2, 496-502, 2012
257. Shibata N, Motoi Y, Tomiyama H, Ohnuma T, Kuerban B, Tomson K, Komatsu M, Hattori N, Arai H.: Lack of genetic association of the UCHL1 gene with Alzheimer's disease and Parkinson's disease with dementia. Dement Geriatr Cogn Disord, 33, 250-254, 2012
258. Kasanuki K, Iseki E, Fujishiro H, Yamamoto R, Higashi S, Minegishi M, Togo T, Katsuse O, Uchikado H, Furukawa Y, Hino H, Kosaka K, Sato K, Arai H.: J Neuropathological investigation of the hypometabolic regions on positron emission tomography with [18F] fluorodeoxyglucose in

法人番号	131025
プロジェクト番号	S1101009

patients with dementia with Lewy bodies. Neurol Sci, 15, 111-119, 2012

259. Maeshima H, Baba H, Nakano Y, Satomura E, Namekawa Y, Takebayashi N, Suzuki T, Mimura M,Arai H.: Residual memory dysfunction in recurrent major depressive disorder--a longitudinal study fromJuntendo University Mood Disorder Project. J Affect Disord, 143, 84-88, 2012
260. Takebayashi N, Maeshima H, Baba H, Nakano Y, Satomura E, Kita Y, Namekawa Y, Nomoto H, Suzuki T, Arai H.: Duration of last depressive episode may influence serum BDNF levels in remitted patients with major depression. Depress Anxiety, 29, 775-779, 2012
*261. Baba H, Nakano Y, Maeshima H, Satomura E, Kita Y, Suzuki T, Arai H.: Metabolism of amyloid-β protein may be affected in depression. J Clin Psychiatry, 73, 115-120, 2012
262. Nakano T, Kato N, Kitazawa S: Superior haptic-to-visual shape matching in autism spectrum disorders. Neurophychologia, 50, 696-703, 2012

２０１１年グループ（１）

263. Sato S, Hattori N: Genetic mutations and mitochondrial toxins shed new light on the pathogenesis of Parkinson's disease. Parkinsons Dis, 123, 19-26, 2011
264. Kawajiri S, Saiki S, Sato S, Hattori N: Genetic mutations and functions of PINK1. Trends Pharmacol Sci. 32. 573-80. 2011
265. Usami Y, Hatano T, Imai S, Kubo S, Sato S, Saiki S, Fujioka Y, Ohba Y, Sato F, Funayama M, Eguchi H, Shiba K, Ariga H, Shen J, Hattori N: DJ-1 associates with synaptic membranes. Neurobiol Dis, 43, 651-62, 2011
266. Kuwahara Y, Oikawa T, Ochiai Y, Roudkenar MH, Fukumoto M, Shimura T, OhtakeY, Ohkubo Y, Mori S, Uchiyama Y, Fukumoto M: Enhancement of autophagy is a potential modality for tumors refractory to radiotherapy. Cell Death Dis, 30, e177, 2011
267. Shiozaki M, Hayakawa N, Shibata M, Koike M, Uchiyama Y, Gotow T: Closer association of mitochondria with lipid droplets in hepatocytes and activation of Kupffer cells in resveratrol-treated senescence-accelerated mice. Histochem Cell Biol, 136, 475-89, 2011
268. Nori S, Okada Y, Yasuda A, Tsuji O, Takahashi Y, Kobayashi Y, Fujiyoshi K, Koike M, Uchiyama Y, Ikeda E, Toyama Y, Yamanaka S, Nakamura M, Okano H: Grafted human-induced pluripotent stem-cell-derived neurospheres promote motor functional recovery after spinal cord injury in mice. Proc Natl Acad Sci USA, 108, 16825-30, 2011
269. Uchida Y, Hasegawa J, Chinnapen D, Inoue T, Okazaki S, Kato R, Wakatsuki S, Misaki R, Koike M, Uchiyama Y, Iemura S, Natsume T, Kuwahara R, Nakagawa T, Nishikawa K, Mukai K, Miyoshi E, Taniguchi N, Sheff D, Lencer WI, Taguchi T, Arai H: Intracellular phosphatidylserine is essential for retrograde membrane traffic through endosomes. Proc Natl Acad Sci USA, 108, 15846-51, 2011
270. Koyanagi M, Asahara A, Matsuda T, Hashimoto N, Shigeyama Y, Shibutani Y, Hosooka T, Inoue H, Matsumoto H, Koike M, Uchiyama Y, NodaT, Seino S, Kasuga M, Kido Y: Ablation of TSC2 enhances insulin secretion by increasing the number of mitochondria through activation of mTORC1. PLoS One, 6, e23238, 2011
271. Murayama T, Kurebayashi N, Oba T, Oyamada H, Oguchi K, Sakurai T, Ogawa Y: Role of amino-terminal half of the S4-S5 linker in the RyR1 channel gating. J. Biol. Chem, 286, 35571-35577, 2011
272. Suzuki N, Hasegawa-Moriyama M, Takahashi Y, Kamikubo Y, Sakurai T, Inada E: Lidocaine attenuates the development of diabetic-induced tactile allodynia by inhibiting microglial activation. Anesthesia & Analgesia, 113, 941-946, 2011

２０１１年グループ（２）

273. Ning L, Ishijima M, Kaneko H, Kurihara H, Arikawa-Hirasawa E, Kubota M, Liu L, Xu Z, Futami I, Yusup A, Miyahara K, Xu S, Kaneko K, Kurosawa H：Correlations between both the expression levels of inflammatory mediators and growth factor in medial perimeniscal synovial tissue and the severity of medial knee osteoarthritis. International orthopaedics, 35, 831-838, 2011
274. Chyba M, Mercier F, RaderJ, Douet V Arikawa-Hirasawa E, Kwon YC, Kodama R: Dynamic mathematical modeling of cell-fractone interactions. Journal of Math-for-Industry, 3, 79–88, 2011
275. 神谷和作 池田勝久：多能性幹細胞を用いた遺伝性難聴に対する内耳細胞治療法の開発 Inner ear cell therapy for hereditary deafness with multipotent stem cells. 日本臨床　特集・幹細胞治療, 69, 2215-2219, 2011
276. Hayashi C, Funayama M, Li Y, Kamiya K, Kawano A, Suzuki M, Hattori N, Ikeda K: Prevalence of GJB2 causing recessive profound non-syndromic deafness in Japanese children. Int J Pediatr Otorhinolaryngol, 75, 211-4, 2011

法人番号	131025
プロジェクト番号	S1101009

277. Yan D, Kamiya K (co-first), Ouyang XM, Liu XZ: Analysis of subcellular localization of Myo7a, Pcdh15 and Sans in Ush1c knockout mice. Int J Exp Pathol, 92, 66-71, 2011

２０１１年グループ（３）

278. Sasaki R, Uka T: Psychophysical evidence for contraction of the range of spatial integration as a mechanism for filtering out spatial noise in a random dot motion display. Vision Res, 51, 1979-1985, 2011
279. Shibata N, Ohnuma T, Kuerban B, Komatsu M, Arai H: Genetic association between ghrelin polymorphisms and Alzheimer's disease in a Japanese population. Dement Geriatr Cogn Disord, 32, 178-181, 2011
280. Shibata N, Ohnuma T, Kuerban B, Komatsu M, Baba H, Arai H: Genetic Association between Akt1 Polymorphisms and Alzheimer's Disease in a Japanese Population. Int J Alzheimers Dis, 2011, 762471, 2011
281. Komatsu M, Shibata N, Kuerban B, Ohnuma T, Baba H, Arai H: Genetic association between clusterin polymorphisms and Alzheimer's disease in a Japanese population. Psychogeriatrics, 11, 14-18, 2011
282. Reitz C, Cheng R, Rogaeva E, Lee JH, Tokuhiro S, Zou F, Bettens K, Sleegers K, Tan EK, Kimura R,Shibata N, Arai H, Kamboh MI, Prince JA, Maier W, Riemenschneider M, Owen M, Harold D, Hollingworth P, Cellini E, Sorbi S, Nacmias B, Takeda M, Pericak-Vance MA, Haines JL, Younkin S, Williams J, van Broeckhoven C, Farrer LA, St George-Hyslop PH, Mayeux R: Meta-analysis of the association between variants in SORL1 and Alzheimer disease. Arch Neurol, 68, 99-106, 2011
283. Utumi Y, Iseki E, Murayama N, Nozawa M, Kumagai R, Matsubara Y, Ichimiya Y, Arai H: Effect of Rikkunshi-to on appetite loss found in elderly dementia patients: a preliminary study. Psychogeriatrics, 11, 34-39, 2011
284. Higashi S, Moore DJ, Minegishi M, Kasanuki K, Fujishiro H, Kabuta T, Togo T, Katsuse O, Uchikado H, Furukawa Y, Hino H, Kosaka K, Sato K, Arai H, Wada K, Iseki E: Localization of MAP1-LC3 in vulnerable neurons and Lewy bodies in brains of patients with dementia with Lewy bodies. J Neuropathol Exp Neurol, 70, 264-280, 2011
*285. Satomura E, Baba H, Nakano Y, Maeshima H, Suzuki T, Arai H: Correlations between brain-derived neurotrophic factor and clinical symptoms in medicated patients with major depression. J Affect Disord, 135, 332-335, 2011
*286. Nakano T, Kato N, Kitazawa S: Lack of eyeblink entrainments in autism spectrum disorders. Neurophychologia, 49, 2784-2790, 2011

＜図書＞

1. 特発性正常圧水頭症の診療. 宮嶋雅一、新井一, 金芳堂, 2014 年
2. Annual Review 神経 2014. 宮嶋雅一、新井一, 中外医学社, 290, 2014 年
3. 別冊日本臨床　神経症候群（第２版）X 脊髄・脊椎疾患. 宮嶋雅一、中島円、新井一, 日本臨床社, 876, 2014 年
4. Uchiyama Y, Kominami E: Autophagy regulates lipid droplet formation and adipogenesis. In: Lipid metabolism. Ed by Rodrigo Valenzuela Baez. InTech, Chapter 7, pp149-162, 2013
5. PARK9(ATP13A)の病態とリソソーム機能障害、医学のあゆみ. 佐藤栄人、服部信孝, 医歯薬出版（株）, 4, 2013 年
6. microRNA 診断　神経変性疾患に関与する miRNA とその臨床応用への可能性(解説/特集). 今居　譲、服部信孝, メディカルドゥ, 4, 2012 年
7. パーキンソン病の基本的知識]パーキンソン病の遺伝学と遺伝子診断の手順, GP レジデントのためのパーキンソン病テキストブック. 服部信孝, アルタ出, 11, 2012 年
8. パーキンソン病の基本　診断・治療の前に押さえておきたい基礎知識　パーキンソン病の原因は? 佐藤 栄人, 日本医事新報社, 4, 2012 年
9. パーキンソン病・アルツハイマー型認知症、コエンザイム Q10 の基礎と応用. 頼高朝子、服部信孝, 編者:日本コエンザイム Q 協会、発行所:丸善プラネット㈱、発売所:丸善出版(株), 8, 2015 年
10. ７．大脳変性疾患、II　錐体外路系疾患、1～9. 服部信孝, 監修；平山惠造、編集；廣瀬源二郎、田代邦雄、葛原茂樹、臨床神経内科学、第 6 版 1 刷、pp409-433, 2016 年 2 月 15 日、南山堂, 25, 2016 年
11. ***Komatsu M, Koike M, Ichimura Y, Uchiyama Y: Genetic mouse models for elucidation of

法人番号	131025
プロジェクト番号	S1101009

autophagy-lysosomal systems in neurons under physiologic and pathologic conditions. In Ed. Zhenyu yue, Charleen T Chu: Autophagy of the nervous system – Cellular self-digestion in neurons and neurological diseases. World Scientific, Chapter 8, pp175-204, 2012

12. リソソーム内の分解機構」オートファジー　生命をささえる細胞の自己分解システム. 内山安男 、小池正人, 化学同人, 9, 2012 年

＜学会発表＞

２０１５年グループ（１）

1. 山名智人、上窪裕二、井上由理子、櫻井隆. 海馬ニューロンに対するナノシリカ粒子の細胞毒性, 第 93 回日本生理学会大会, 2016 年 3 月, 札幌
2. 村山尚、呉林なごみ、小川治夫、鈴木純二、金丸和典、飯野正光、櫻井隆. 2 型リアノジン受容体チャネルゲーティングにおける S4-S5 リンカーの役割, 第 93 回日本生理学会大会, 2016 年 3 月, 札幌
3. 上窪裕二、新里和恵、橋本祥江、櫻井隆. β セクレターゼによるシナプス形成と機能の制御, 第 89 回日本薬理学会年会, 2016 年 3 月, 横浜
4. 山名智人、上窪裕二、井上由理子、櫻井隆. シリカナノ粒子は海馬神経細胞に対して酸化ストレスを引き起こす, 第 89 回日本薬理学会年会, 2016 年 3 月, 横浜
5. 村山尚、呉林なごみ、小川治夫、鈴木純二、金丸和典、飯野正光、櫻井隆. 2 型リアノジン受容体チャネルゲーティングにおける S4-S5 リンカーの役割, 第 89 回日本薬理学会年会, 2016 年 3 月, 横浜
6. Kamikubo Y, Tabata T, Sakurai T. Bidirectional interaction between adenosine A1 receptor and type-1 metabotropic glutamate receptor. Neuroscience 2015. 2015 年 10 月, Chicago, USA
7. Takasugi N, Sakurai T. The analysis of endosomal proteins, which specifically interact with APP-βCTF. Neuroscience 2015, 2015 年 10 月, Chicago, USA
8. 上窪 裕二、山名智人、櫻井 隆. GPCR 複合体形成による神経機能の制御, 第 129 回日本薬理学会関東部会（部会長：櫻井隆）及びシンポジウム「神経変性疾患の新たな治療戦略と創薬」順天堂大学本郷キャンパス、2013 年 10 月 19 日、東京
9. 村山　尚、呉林なごみ、山澤徳志子、小山田英人、鈴木純二、金丸和典、小口勝司、飯野正光、櫻井　隆. 1 型リアノジン受容体チャネルに対する中央領域疾患変異の効果, 「遺伝性パーキンソン病の分子病態を基盤としたバイオマーカーの開発」順天堂大学医学部神経学講座 佐藤栄人、第 129 回日本薬理学会関東部会シンポジウム、順天堂大学本郷キャンパス、2013 年 10 月 19 日、東京

＊＊10. 高杉展正、新家瑠奈、櫻井隆. APP-βCTF に特異的に結合するエンドソームタンパク質の解析, 第 88 回日本薬理学会年会, 2015 年 3 月, 名古屋

11. 秋元貴至、村山尚、樫山拓、上窪裕二、橋本祥江、市川宗厳、豊島陽子、櫻井隆. シュードタイプバキュロウイルスを用いた疾患変異ダイニン重鎖の神経細胞への発現, 第 88 回日本薬理学会年会, 2015 年 3 月, 名古屋
12. 坂入伯駿、上窪裕二、櫻井隆. 代謝型グルタミン酸受容体 1 型はアデノシン A1 受容体のシグナルを制御する, 第 88 回日本薬理学会年会, 2015 年 3 月, 名古屋
13. 村山尚、呉林なごみ、山澤徳志子、小山田英人、鈴木純二、金丸和典、小口勝司、飯野正光、櫻井隆. 1 型リアノジン受容体チャネル活性に対する中央領域疾患変異の効果, 第 88 回日本薬理学会年会, 2015 年 3 月, 名古屋
14. Murayama T, Kurebayashi N, Yamazawa T, Oyamada H, Suzuki J, Kanemaru K, Oguchi K, Iino M, Sakurai T. Effects of MH and CCD mutations in the central region on RyR1 channels. Biophysical Society 59th annual meeting, 2015 年 2 月, Baltimore, Maryland, USA
15. 佐藤栄人、小池正人、舩山学、金井数明、新井公人、内山安男 、服部信孝. 遺伝子パーキンソン病 PARK9(ATP13A2)の分子機構とリソソームの障害, 第 55 回日本神経学会, 2014 年 5 月, 福岡
16. 真鍋 彩、西岡 健弥、李 元哲、吉野 浩代、舩山 学、松島 隆史、上野 真一、栗田 尚英、上野 祐司、本井 ゆみ子、服部 信孝. The analyze of three pedigrees with MAPT N279K mutation accompanying DAT-scan、変性疾患 [AP-02] 2015 年ポスター, 第 56 回日本神経学会総会, 2015

法人番号	131025
プロジェクト番号	S1101009

年 5 月，新潟
17. 平 健一郎、上野 祐司、田中 亮太、黒木 卓馬、島田 佳明、山城 一雄、卜部 貴夫、服部 信孝．The expression of axonal growth inhibitors in the peri-infarct area in rat brain、変性疾患 ［Pe-017］ポスター(英語)，第 56 回日本神経学会総会，2015 年 5 月，新潟
18. 福嶋 佳保里、荒野 拓、松本 弦、井下 強、吉田 繁、石濱 泰、貫名 信行、服部 信孝．リン酸化 63K ポリユビキチン鎖は Parkin をミトコンドリアに局在化させる、［O-51］口演，第 56 回日本神経学会総会，2015 年 5 月，新潟
19. 松島 隆史、西岡 健弥、山城 一雄、李 元哲、島田 佳明、吉野 浩代、舩山 学、田中 亮太、本井 ゆみ子、服部 信孝．Cliniogenetic study of CADASIL pedigrees with notch3 mutation、変性疾患 ［Pe-018］ポスター，第 56 回日本神経学会総会，2015 年 5 月，新潟
20. 森 聡生、王子 悠、奥住 文美、波田野 琢、今居 譲、久保 紳一郎、服部 信孝．Parkinson's disease-associated mutations of PLA2G6 alters the membrane dynamics、［Pe-057］ポスター(英語)，第 56 回日本神経学会総会，2015 年 5 月 ，新潟
21. 山城 一雄、田中 亮太、上野 祐司、卜部 貴夫、山城 雄一郎、野本 康二、高橋 琢也:、辻 浩和、朝原 崇、服部 信孝．Gut microbiota in patients with ischemic stroke、［O-19］口演，第 56 回日本神経学会総会，2015 年 5 月，新潟
22. 奥住文美、波田野 琢、斉木臣二、舩山 学、服部信孝．Serum metabolomics revealed several metabolic markers of Parkinson's disease、［Pe-056］ポスター(英語)，第 56 回日本神経学会総会，2015 年 5 月，新潟
23. 小林愛美、波田野 琢、中島明日香、城 崇之、奥住文美、下 泰司、服部信孝．パーキンソン病の自然史、［P-161］ポスター(日本語)，第 56 回日本神経学会総会，2015 年 5 月，新潟
24. Hatano T, Saiki S, Okuzumi A, Hattori N. Identification of novel biomarkers for Parkinson's disease by metabolomics technologies, 19th International Congress of Parkinson's Disease and Movement Disorders, 2015 年 6 月，San Diego, CA, USA
25. Inoshita T, Hosaka Y, Imai Y, Hattori N. Parkinson's disease-associated proteins Vps35 and LRRK2 regulate synaptic vesicle dynamics, Oral Session, 第 38 回日本神経科学大会，2015 年 7 月，神戸
26. 服部信孝．脳内環境における封入体形成のメカニズム：封入体と神経細胞死の関連性について（演題名：新規遺伝性パーキンソン病からの解析から），文科省科研費補助金「新学術領域研究」 脳内環境：恒常性維持機構とその破綻、平成 27 年度夏のワークショップ，2015 年 9 月，軽井沢
27. Funayama M, Hattori N. CHCHD2 is novel gene for autosomal dominant Parkinson's disease, -Neurodegenerative disorders in cells to animals- Symposium "At the Bench", 10th Annual Genetic Epidemiology of Parkinson's Disease Consortium (GEO-PD), 2015 年 10 月,東京
28. Sato S, Hattori N. Pathological perspective on autophagy lysosome pathway in Parkinson's disease, -Neurodegenerative disorders in cells to animals-, Symposium "At the Bench", 10th Annual Genetic Epidemiology of Parkinson's Disease Consortium (GEO-PD), 2015 年 10 月，東京
29. 波田野 琢、斉木臣二、奥住文美、Mohney Robert、服部信孝．パーキンソン病患者の血清メタボローム解析（ポスター），第 9 回パーキンソン病・運動障害疾患コングレス，2015 年 10 月，東京
30. 舩山 学、服部 信孝．CHCHD2 は家族性パーキンソン病の新規原因遺伝子である，第 9 回パーキンソン病・運動障害疾患コングレス，2015 年 10 月，東京
31. Hattori N, Funayama M. Clinicogenetic study of CHCHD2 in patients with autosomal dominant familial Parkinson's disease, Poster, XXII World Congress of Neurology, World Congress of Neurology 2015, 2015 年 11 月，Santiago, Chili
32. Mori A, Hatano T, Imai Y, Oji Y, Kubo S, Yamamoto K, Murakami M, Hattori N. Parkinson's disease-associated mutations of PLA2G6 alters the membrane dynamics, 5th Asian and Oceanian Parkinson's Disease and Movement Disorders Congress, 2016 年 3 月，Manila, Philippines
33. Yamashiro K, Tanaka R, Hoshino Y, Taku Hatano T, Nishioka K, Hattori N. The prevalence

法人番号	131025
プロジェクト番号	S1101009

and risk factors of cerebral microbleeds in patients with Parkinson’s disease, 5th Asian and Oceanian Parkinson’s Disease and Movement Disorders Congress, 2016 年 3 月, Manila, Philippines

34. 佐藤 栄人, 服部 信孝. パーキンソン病の発症メカニズムと相互関連 遺伝性パーキンソン病とミトコンドリア品質管理の破綻　これまでの展開と今後の課題, 第 8 回パーキンソン病・運動障害疾患コングレス, 2014 年 10 月, 京都
35. 佐藤栄人. オートファジー欠損マウスはパーキンソン病のモデルとなりうるか、セッション 7 生理・病態（3）, 第 8 回オートファジー研究会、第 2 回新学術「オートファジー」班会議, 2014 年 11 月, 札幌
36. Yasuo Uchiyama. Cell death and autophagy, The 24th International Symposium on Morphological Science, 2015 年 9 月, Istanbul
37. Yasuo Uchiyama. The LC3 conjugation system is involved in lipid droplet formation, The 2nd Congress, International Academy of Sportology, 2015 年 9 月, Tokyo
38. Yasuo Uchiyama. Autophagy in central nervous system neurons-The LC3 conjugation system is involved in lipid droplet formation-, The 2nd congerss, International Academy of Spotology, 2015 年 9 月, Tokyo
39. 内山安男. 神経細胞におけるリソソームタンパク質分解とその破綻, 第１２１回日本解剖学会総会・学術集会, 2016 年 3 月, 郡山

２０１５年グループ（2）

40. 山田泰平、Aurelien Kerever、鈴木佑治、, 平澤（有川）恵理. 老化マウス脳室下帯における細胞外マトリックス構造の変化と FGF-2 シグナル伝達, 第 47 回日本結合組織学会学術大会, 2015 年 5 月, 東京
41. 鈴木佑治、Aurelien Kerever、山田泰平、平澤（有川）恵理. 老化マウス海馬における細胞外マトリックス構成の変化, 第 47 回日本結合組織学会学術大会, 2015 年 5 月, 東京
42. 多賀　祐喜、石島　旨章、平澤（有川）　恵理、田中　啓友、水野　一乗、楠畑　雅、服部　俊治. 安定同位体標識コラーゲンを用いた血中、尿中のコラーゲン由来因子の高精度定量分析, 第 47 回日本結合組織学会学術大会, 2015 年 5 月, 東京
43. S. de Vega, K. Hozumi, N. Suzuki, R. Nonaka, E. Seo, A. Takeda, T. Ikeuchi, M. Nomizu, Y. Yamada, and E. Arikawa-Hirasawa. Synthetic Peptides Derived from the C-terminal Fibulin-type Domain of Fibulin-7: Role in Endothelial Cell Adhesion, 第 47 回日本結合組織学会学術大会, 2015 年 5 月, 東京
44. Aurelien Kerever Taihei Yamada, and Eri Arikawa-Hirasawa. Aging of the extracellular matrix structure fractone in the mouse subventricular zon, 第 47 回日本結合組織学会学術大会, 2015 年 5 月, 東京
45. 平澤恵理、寧亮、古屋徳彦、野中里紗、服部信孝. Schwartz-Jampel 症候群の原因遺伝子、パールカンの筋オートファジーへの関与, 第 56 回日本神経学会学術大会, 2015 年 5 月, 新潟
46. Yuji Suzuki,Aurelien Kerever,Taihei Yamada, and Eri Arikawa-Hirasawa. Extracellular matrix aging in mouse hippocampus, 第 38 回日本神経科学大会, 2015 年 7 月, 神戸
47. Kazusaku Kamiya, Ichiro Fukunaga, Kaori Hatakeyama, Toru Aoki, Ayumi Fujimoto, Atena Nishikawa,Takashi Anzai, Osamu Minowa, Katsuhisa Ikeda. Cochlear gap junction plaque, stabilized macromolecular complex composed of specific connexins, 52nd Inner Ear Biology Workshop, 2015 年 9 月, イタリアローマ
48. Takashi Anzai, Kazusaku Kamiya, Katsuhisa Ikeda. Caveolins accumulates at the organ of Corti in GJB2 associated deafness, 52nd Inner Ear Biology Workshop, 2015 年 9 月, イタリアローマ
49. Kaori Hatakeyama, Katsuhisa Ikeda, Kazusaku Kamiya. Reproduction of various types of cochlear gap junction plaques in human cell line, 52nd Inner Ear Biology Workshop, 2015 年 9 月, イタリアローマ
50. Ichiro Fukunaga, Kaori Hatakeyama,Toru Aoki, Atena Nishikawa, Ayumi Fujimoto, Osamu Minowa, Katsuhisa Ikeda, Kazusaku Kamiya. Differentiation of mouse iPS cell into

法人番号	131025
プロジェクト番号	S1101009

Cx26-positive cell and formation of inter cellular Cx26-gap junction plaque, 52nd Inner Ear Biology Workshop, 2015 年 9 月, イタリアローマ

51. Kazusaku Kamiya, Ichiro Fukunaga. Restoration og Cochlear Gap Junction for GJB2, Association for Research in Otolaryngology (ARO), 39th Annual MidWinter Meeting, 2016 年 2 月, 米国サンディエゴ
52. Toru Aoki, Katsuhisa Ikeda, Kazusaku Kamiya. Generation of induced pluripotent stem cells form connexin26 conditional knock out mouse, Association for Research in Otolaryngology (ARO), 39th Annual MidWinter Meeting, 2016 年 2 月, 米国サンディエゴ
53. Ichiro Fukunaga, Kaori Hatakeyama, Toru Aoki, Ayumi Fujimoto, Atena Nishikawa, Katsuhisa Ikeda, Kazusaku Kamiya. Differentiation of mouse iPS cell into Cx26-positive cell and formation of inter cellular Cx26-gap junction plaque, Association for Research in Otolaryngology (ARO), 39th Annual MidWinter Meeting, 2016 年 2 月, 米国サンディエゴ
54. Takashi Anzai, Kazusaku Kamiya, Katsuhisa Ikeda. Deformation of the Outer Hair Cells and the Accumulation of Caveolin-2 in Connexin 26-Deficient Mice, Association for Research in Otolaryngology (ARO), 39th Annual MidWinter Meeting, 2016 年 2 月, 米国サンディエゴ
55. Ayumi Fujimoto, Ichiro Fukunaga, Kaori Hatakeyama, Toru Aoki, Atena Nishikawa, Katsuhisa Ikeda, Kazusaku Kamiya. Induction of iPS cell differetiation into Connexin26 positive cells with gap junction plaques using cochlear feeder cell, Association for Research in Otolaryngology (ARO), 39th Annual MidWinter Meeting, 2016 年 2 月, 米国サンディエゴ
56. Kaori Hatakeyama, Katsuhisa Ikeda, Kazusaku Kamiya. Various cochlear gap junction plaque reproduced in human cell line, Association for Research in Otolaryngology (ARO), 39th Annual MidWinter Meeting, 2016 年 2 月, 米国サンディエゴ
57. 神谷和作. GJB2 変異遺伝性難聴に対する細胞治療・遺伝子治療法の開発, 第 15 回日本再生医療学会総会, 2016 年 3 月, 大阪市
58. 福永一朗、畠山佳欧里、青木徹、藤本あゆみ、西川貴菜、美野輪治、池田勝久、神谷和作. iPS 細胞からの Connexin26 発現細胞への分化誘導と細胞間ギャップ結合プラークの構築, 第 15 回日本再生医療学会総会, 2016 年 3 月, 大阪市
59. 青木徹、福永一朗、畠山佳欧里、藤本あゆみ、西川貴菜、美野輪治、池田勝久、神谷和作. コネキシン 26 欠損マウスからの iPS 細胞の樹立, 第 15 回日本再生医療学会総会, 2016 年 3 月, 大阪市
60. 藤本あゆみ、福永一朗、畠山佳欧里、青木徹、西川貴菜、池田勝久、神谷和作. 内耳フィーダー細胞を用いた iPS 細胞の分化誘導による Cx26 ギャップ結合形成細胞の樹立, 第 15 回日本再生医療学会総会, 2016 年 3 月, 大阪市

２０１５年グループ（3）

61. Uka T. Neural mechanisms of flexibility in perceptual decision making, 第 38 回日本神経科学大会, 2015 年 7 月, 神戸
62. Konishi S. Neuroimaging study of quadripulse stimulation (QPS), 第 56 回日本神経学大会, 2015 年 5 月, 新潟
63. Uka T, Mitani A, Sasaki R. Movement-specific employment of sensory signals as a basis for rapid task switching, 第 92 回日本生理学会, 2015 年 3 月, 神戸
64. Konishi S. Neuroimaging study of combined fMRI and QPS, 日本臨床生理学会, 2015 年 11 月, 大阪
65. Konishi S. Human brain mapping of autonomic functions, 2nd Congress, International Academy of Sportology, 2015 年 9 月, 順天堂
66. Katsura M., Hirose S., Jimura K., Mori H., Kunimatsu A., Ohtomo K., Konishi S. Fronto-temporal interaction during fixation after memory retrieval, Human Brain Mapping Conference, 2015 年 6 月, Hawaii
67. Nao Takano, Michimasa Suzuki, Ryusuke Irie, Munetaka Yamamoto, Kanako Kumamaru, Masaaki Hori, Hidenori Oishi, Shigeki Aoki, Hajime Arai. Usefulness of Non-Contrast Enhanced

法人番号	131025
プロジェクト番号	S1101009

Magnetic Resonance Angiography Using Silent Scan for Follow-Up after Y Stent-Assisted Coil Embolization for Basilar Tip Aneurysms, European Society of Radiology Annual Meeting, 2016年3月, Vienna, Austria

68. Kanako Sato, Aurelien Krever, Koji Kamagata, Ryuji Sakakibara, Hitoshi Terada, Shigeki Aoki. Understanding microstructure of the brain with advanced diffusion tensor imaging and comparing with pathological findings, European Society of Radiology Annual Meeting, 2016年3月, Vienna, Austria
69. Kouhei Kamiya, Ryusuke Irie, Koji Kamagata, Masaaki Hori, Yuichi Suzuki, Harushi Mori, Akira Kunimatsu, Shigeki Aoki, Kuni Ohtomo. Impact of axon undulation on the estimation of dMRI metrics: Monte-Carlo simulation study on conventional diffusion tensor ellipsoids and NODDI, European Society of Radiology Annual Meeting, 2016年3月, Vienna, Austria
70. Nojiri R, Tsurushima Y, Ishigame K, Kumamaru K, Hori M, Murata K. Interslice Leakage Artifact Caused by Multi-band Echo Planar Imaging. Influence of Multichannel Coils and Leakage Reduction Technique, European Society of Radiology Annual Meeting, 2016年3月, Vienna, Austria
71. Tsurushima Y, Nojiri R, Ishigame K, Kumamaru K, Hori M, Murata K. Evaluation of PETRA (pointwise encoding time reduction with radial acquisition)-MRA for carotid artery visualization, European Society of Radiology Annual Meeting, 2016年3月, Vienna, Austria
72. M. Hori, R. Nojiri, Y. Tsurushima, K. Murata, K. Tsuruta, K. Kumamaru, K. Ishigame, and S. Aoki. High-resolution Diffusional Kurtosis Fractional Anisotropy Mapping for Discrimination between Vasogenic Edema and Tumor-Infiltration, European Society of Radiology Annual Meeting, 2016年3月, Vienna, Austria
73. Ayaz Aghayev, Andreas Giannopoulos, Tianxi Cai, Kanako K. Kumamaru, Michael L. Steigner, Dimitris Mitsouras, Frank J. Rybicki III. The Gravitational Gradient (GG), Defined as the Dependent Divided by Independent Region of Interest (ROI) Attenuation in Abdominal Aortic Aneurysms (AAA), Strongly Predicts Rapid Aneurysm Growth in Patients with Less Intramural Thrombus, 101st Radiological Society of North America annual meeting, 2015年11月, Chicago, IL, USA
74. Leonid Chepelev, Amir Imanzadeh, Andreas Giannopoulos, Tatiana Kelil, Peter C. Liacouras, Beth A. Ripley, Tianrun Cai, Kanako K. Kumamaru, Frank J. Rybicki III, Gerald T. Grant, Dimitris Mitsouras. 3D printing in Radiology, 101st Radiological Society of North America annual meeting, 2015年11月, Chicago, IL, USA
75. Tianrun Cai, Kurt Schultz, Kanako K. Kumamaru, Amir Imanzadeh, Frank J. Rybicki III, Dimitris Mitsouras. The Remnant Standard Tessellation Language (STL) Volume is a Novel Metric for 3D Printing Quality and the Remnant STL Volume Used to Validate 3D Printing from CT Images of Bone at Reduced Radiation Dose, 101st Radiological Society of North America annual meeting, 2015年11月, Chicago, IL, USA
76. Christina Andica、Akifumi Hagiwara, Masaaki Hori, Saori Shiota, Mariko Yoshida, Kanako Sato, Yuko Takahashi, Kanako Kumamaru, Michimasa Suzuki, Atsushi Nakanishi, Misaki Nakazawa, Kouhei Tsuruta, Shigeki Aoki. Synthetic MRI: an old concept becomes practical, 10th AOCNR, 2015年11月, Fukuoka, Japan
77. Akifumi Hagiwara, Christina Andica, Masaaki Hori, Saori Shiota, Mariko Yoshida, Kanako Sato, Yuko Adachi, Kanako Kumamaru, Michimasa Suzuki, Atsushi Nakanishi, Misaki Nakazawa, Kouhei Tsuruta, and Shigeki Aoki. Contrast-enhanced Synthetic MRI for the Detection of Brain Metastases, 10th AOCNR, 2015年11月, Fukuoka, Japan
78. Takamura K, Fujimoto S, Kondo T, Kumamaru K, Kawaguchi Y, Suda S, Matsumori R., Kato E, Hiki M, Takase S, Rybicki FJ, Daida H. Prognostic Value of Coronary CT Angiography and Coronary Artery Calcium Score Performed Before Revascularization, American Heart Association, 88th Scientific Session, American Heart Association, 88th Scientific Session, Orland, FL, USA
79. Kumamaru KK, Saboo SS. Gonzalez-Quesada, George E, Hussain Z, Dunne R, Bedayat A,

法人番号	131025
プロジェクト番号	S1101009

Aghayev A, Wake N, Khandelwal A, Imanzadeh A, Bhivasankar R, Hunsaker AR, Rybicki FJ. CT Findings-based Risk Scoring System for Mortality Prediction after Acute Pulmonary Embolism, 10th Annual Scientific Meeting of the Society of Cardiovascular Computed Tomography, 2015年7月, Las Vegas, USA

80. Kanako Sato, Koji Kamagata, Ryuji Sakakibara, Hitoshi Terada, Shigeki Aoki. Neurite orientation dispersion and density imaging in patients with spinocerebellar ataxia type 6, 21st Annual Meeting of the Organization for Human Brain Mapping, 2015年7月, Honolulu, Hawaii
81. A Nishikori, K Tsuruta, K Kamagata, T Hatano, A Okuzumi, M Hori, M Suzuki, S Aoki, A Seno. Detection of Microstructural Changes of Nigra-Striatum Dopaminergic Neurons in Parkinson's Disease using High Resolution DWI, ISMRM 23rd Annual Meeting & Exhibition, 2015年5月, Toronto, Canada
82. Yuichi Suzuki, Kouhei Kamiya, Masaki Katsura, Akira Kunimatsu, Harushi Mori, Akitake Mukasa, Katsuya Maruyama, Yasushi Watanabe, Takeo Sarashina, Kenji Ino, Masami Goto, Jiro Sato, Keiichi Yano, Nobuhito Saito, Kuni Ohtomo. NODDI analyses can demonstrate differences of tissue microstructure between brain metastasis and meningioma, ISMRM 23rd Annual Meeting & Exhibition, 2015年5月, Toronto, Canada
83. Kouhei Kamiya, Yuichi Suzuki, Shota Tanaka, Akitake Mukasa, Masaaki Hori, Harushi Mori, Akira Kunimatsu, Nobuhito Saito, Shigeki Aoki, and Kuni Ohtomo. Discrimination between tumor-infiltration and vasogenic edema using non-gaussian diffusion MRI techniques: preliminary experience, ISMRM 23rd Annual Meeting & Exhibition, 2015年5月, Toronto, Canada
84. Kouhei Kamiya, Yuichi Suzuki, Shiori Amemiya, Naoto Kunii, Kensuke Kawai, Harushi Mori, Akira Kunimatsu, Nobuhito Saito, Shigeki Aoki, and Kuni Ohtomo. Machine learning approach for lateralization of temporal lobe epilepsy utilizing DTI structural connectome, ISMRM 23rd Annual Meeting & Exhibition, 2015年5月, Toronto, Canada
85. K.Tsuruta、R.Irie、M.Hori、I.Fukunaga、Y.Masutani、K.Kamiya、A.Nishikori、M.Yoshida、M.Suzuki、M.Miyajima、M.Namajima、K.Kamagata、H.Arai、A.Nakanishi、S.Aoki、A.Seno. Neurite Orientation Dispersion and Density Imaging could show the microstractual changes of Cortico-Spinal Tract in patients with Idiopathic Normal Pressure Hydrocephalus, ISMRM 23rd Annual Meeting & Exhibition, 2015年5月, Toronto, Canada
86. Masaki Katsura, Yuichi Suzuki, Akihiro Kasahara, Harushi Mori, Akira Kunimatsu, Yoshitaka Masutani, Masaaki Hori, Shigeki Aoki, and Kuni Ohtomo. Non-Gaussian diffusion weighted imaging for assessing degenerative changes in intervertebral disc composition, ISMRM 23rd Annual Meeting & Exhibition, 2015年5月, Toronto, Canada
87. Rachael LeeAnn Deardorff, Emilie T McKinnon, Tara Eckenrode Sokolowski, Jens H Jensen, Masaaki Hori, Varan Govind, and Joseph A Helpern. Kurtosis Imaging Network: a Collaborative, Open-Source Imaging Database, ISMRM 23rd Annual Meeting & Exhibition, 2015年5月, Toronto, Canada
88. Masaaki Hori, Ryuji Nojiri, Katsutoshi Murata, Yuichi Suzuki, Koji Kamagata, Mariko Yoshida, Kouhei Tsuruta, Keiichi Ishigame, and Shigeki Aoki. Optimization of Spinal Cord NODDI Protocol with Multi-band EPI for Clinical Use, ISMRM 23rd Annual Meeting & Exhibition, 2015年5月, Toronto, Canada
89. K Kamagata, M Hori, A Nishikori, K Tsuruta, A Okuzumi, T Hatano, K Kamiya, N Hattori, S Aoki. High-resolution Neurite Orientation Dispersion and Density Imaging in the substantia nigra of de novo Parkinson disease, ISMRM 23rd Annual Meeting & Exhibition, 2015年5月, Toronto, Canada
90. 鶴田航平, 鎌形康司, 本井ゆみ子, 堀正明, 鈴木通真, 下地啓五, 村田渉, 上田亮, 中澤美咲, 佐藤秀二, 濱崎望, 小西清貴, 芳士戸治義, 服部信孝, 青木茂樹. アルツハイマー病とレビー小体型認知症における拡散テンソル画像によるヒト・コネクトームを用いたネットワーク解析, 平成２７年度老人性疾患病態・治療研究センター研究発表会, 2016年3月, 東京

法人番号	131025
プロジェクト番号	S1101009

91. 村田渉,鎌形康司,波田野琢,奥住文美,堀正明,鈴木通真,下地啓五,浜崎望,佐藤秀二,鶴田航平,上田亮, 中澤美咲, 芳士戸治義, 服部信孝,青木茂樹. NODDI を用いたパーキンソン病における基底核変性の評価:ドパミントランスポーターSPECT との関連, 平成２７年度老人性疾患病態・治療研究センター研究発表会, 2016 年 3 月, 東京
92. 中澤美咲,萩原彰文,堀正明,クリスティナ アンディカ、鶴田航平、高野直、川崎英生、濱崎望、佐藤秀二、隈丸加奈子、芳士戸治義、貝原雄、Marcel Warntjes、青木茂樹. 造影後 Synthetic MRI による転移性脳腫瘍の検出能の評価, 平成２７年度老人性疾患病態・治療研究センター研究発表会, 2016 年 3 月, 東京
93. 鎌形康司, Aurelien Kerever, 横沢俊, 堀正明, 鶴田航平, 田川一彦, 岡澤均, 平澤恵理, 青木茂樹. Quantitative Histological Validation of Diffusion Tensor MRI by Two-Photon Microscopy of Cleared Mouse Brain, 第 18 回日本ヒト脳機能マッピング学会, 2016 年 3 月, 京都
94. 鎌形康司、波田野琢、奥住文美、阿部修、下地啓五、鈴木通真、堀正明、隈丸加奈子、鶴田航平、服部信孝、青木茂樹. 神経突起イメージングを用いたパーキンソン病における灰白質変性の検討, 第 45 回日本神経放射線学会, 2016 年 2 月, 山形
95. 鈴木通真、高野直、入江隆介、堀正明、隈丸加奈子、鎌形康司、山本宗孝、大石英則、青木茂樹. Y stent, 第 45 回日本神経放射線学会, 2016 年 2 月, 山形
96. 萩原彰文、堀正明、中澤美咲、クリスティナ アンディカ、鶴田航平、高野直、川崎英生、濱崎望、佐藤秀二、青木茂樹. 造影後 Synthetic MRI による転移性脳腫瘍の検出能の評価, 第 45 回日本神経放射線学会, 2016 年 2 月 18 日～20 日, 山形
97. 原祥子, 田中洋二, 稲次基希, 石井賢二, 前原健寿, 堀正明, 青木茂樹, 成相直. pCASL と NODDI を用いた もやもや病の脳血流および微細構造の評価, 第 45 日本神経放射線学会, 2016 年 2 月 18 日～20 日, 山形
98. 中澤美咲、川崎英生、佐藤秀二、濱崎望、高野直、熊谷文孝、萩原彰文、堀正明、青木茂樹、妹尾敦史. Synthetic MRI による定量血の基礎的検討と転移性脳腫瘍への応用, 第 39 回日本脳神経 CI 学会総会, 2016 年 1 月, 東京
99. 村田渉, 鎌形康司, 波田野琢, 奥住文美, 堀正明, 鈴木通真, 鶴田航平, 服部信孝, 青木茂樹, 妹尾淳史. パーキンソン病における神経変性の評価：NODDI 定量値と DAT-SPECT との関連, 第 39 回日本脳神経 CI 学会総会, 2016 年 1 月, 東京
100. 鶴田航平、鎌形康司、本井ゆみ子、下地啓五、神谷昂平、堀正明、鈴木通真、村田渉、青木茂樹、妹尾淳史. 脳白質の拡散テンソル構造的ネットワーク解析による Alzheimer's Disease と Dementia with Lewy Bodies の評価, 第 39 回日本脳神経 CI 学会総会, 2016 年 1 月, 東京
101. 髙野直、鈴木通真、山本宗孝、堀正明、大石英則、青木茂樹、新井一. Y stent assisted coil embolization 後のフォローアップにおける Silent MRA の有用性, 第 39 回日本脳神経 CI 学会総会, 2016 年 1 月, 東京
102. Hagiwara Akifumi, Anwarjan Yusup, Koji Kamagata, Muneaki Ishijima, Haruka Kaneko, Lizu Liu, Liang Ning, Ryo Sadatsuki, Shinnosuke Hada, Mayuko Kinoshita, Ippei Futami, Kazuo Kaneko, Shigeki Aoki. Bone marrow lesions, subchondral bone cysts and subchondral bone attrition are associated with histological synovitis in patients with end-stage knee osteoarthritis : a cross-sectional study, 第 27 回日本骨軟部放射線研究会, 2016 年 1 月, 東京
103. 髙野直、佐藤秀二、濱崎望、川崎英生、芳士戸 治義:静音型.MRangiography における撮像時間短縮の検討 第 43 回日本放射線技術学会秋季学術大会,2015 年 10 月,盛岡
104. 髙野直、鈴木通真、山本宗孝、堀正明、大石英則、青木茂樹.Silent MRA におけるセルデザインの異なる頭蓋内ステントの描出能の検討,第 31 回 NPO 法人日本脳神経血管内治療学会学術総会,2015 年 11 月,岡山
105. 竹田和良、松元まどか、緒方洋輔、米田恵子、村上祐樹、村山航、下地啓五、花川隆、松元健二、中込和幸.統合失調症患者における内発的動機づけ変容の行動制御への影響,第 37 回日本生物学的精神医学会・第 45 回日本神経精神薬理学会合同年会,2015 年 9 月,東京
106. 原田健一郎、松尾幸治、中島麻美、樋口文宏、樋口尚子、柴田朋彦、芳原輝之、中野雅之、大脇孝治、綿貫俊夫、松原敏郎、古川又一、藤田悠介、下地 啓五、松永尚文、山形弘隆、渡邉義

法人番号	131025
プロジェクト番号	S1101009

文.高齢うつ病患者における内側前頭-辺縁系の構造異常,第 37 回日本生物学的精神医学会・第 45 回日本神経精神薬理学会合同年会,2015 年 9 月,東京

107.村田渉、鎌形康司、波田野琢、奥住文美、堀正明、鈴木通真、下地啓五、 濱崎望、佐藤秀二、鶴田航平、中澤美咲、上田亮、服部信孝 、青木茂樹 、妹尾淳史. NODDI を用いたパーキンソン病における基底核変性の評価：ドパミントランスポーター SPECT との関連,第 43 回日本磁気共鳴医学会大会,2015 年 9 月,東京

108.福永一星、堀正明、増谷佳孝、濱崎望、佐藤秀二、熊谷文孝、鶴田航平、鎌形康司、鈴木由里子、伊藤憲之、小美野高志、堂領和彦、芳士戸治義、青木茂樹 .拡散時間が Diffusional kurtosis imaging（DKI）の定量値に与える影響,第 43 回日本磁気共鳴医学会大会,2015 年 9 月,東京

109.濱崎望、堀正明、佐藤秀二、川崎英生、高野直、鈴木由里子、芳士戸治義、 青木茂樹 .Reference scan が Multi band に及ぼす影響,第 43 回日本磁気共鳴医学会大会,2015 年 9 月,東京

110.藤本進一郎、川口裕子、松森理枝、高村和久、比企誠、宮内克己、隈丸加奈子、近藤 武、代田浩之.安定狭心症診断戦略における冠動脈 CT の新しい位置づけ ,第 63 回日本心臓病学会学術集会,2015 年 9 月,横浜

111.中澤美咲、萩原彰文、クリスティナアンディカ、堀正明、鶴田航平、高野直、熊谷文孝、濱崎望、佐藤秀二、川崎英生、鎌形康司、吉田茉莉子、村田渉、上田亮、青木茂樹 、妹尾淳史.Synthetic MR の使用経験,第 43 回日本磁気共鳴医学会大会,2015 年 9 月,東京

112.鶴田航平、立花泰彦、神谷昂平、入江隆介、鎌形康司、堀正明、鈴木通真、中西淳、佐藤秀二、濱崎望、服部信孝 、青木茂樹 、妹尾淳史.異方性を考慮した拡散尖度画像を推定する手法(eDKI)の臨床応用に関する検討,第 43 回日本磁気共鳴医学会大会,2015 年 9 月,東京

113.鶴田航平、鎌形康司、本井ゆみ子、堀正明、鈴木通真、下地啓五、上田亮、中澤美咲、村田渉、佐藤秀二、濱崎望、熊谷文孝、服部信孝 、青木茂樹 、妹尾淳史.グラフ理論を用いたネットワーク解析による Alzheimer's Disease と Dementia with Lewy Bodies の評価,第 43 回日本磁気共鳴医学会大会,2015 年 9 月,東京

114.髙野直、鈴木通真、佐藤秀二、濱崎望、川崎英生、芳士戸治義、山本宗孝、堀正明、大石英則、青木茂樹 .Silent MRA における 2 種類の頭蓋内ステントの描出能の検討,第 43 回日本磁気共鳴医学会大会,2015 年 9 月,東京

115.佐藤秀二、高野直、川崎英生、濱崎望、熊谷文孝、鈴木通真、芳士戸治義、堀正明、青木茂樹 .静音型 MR angiography における狭窄血管ファントムの描出検討,第 43 回日本磁気共鳴医学会大会,2015 年 9 月,東京

116.熊谷文孝、鎌形康司、奥住文美、波田野琢、佐藤秀二、濱崎望、川崎英生、鶴田航平、堀正明、服部信孝 、青木茂樹 ,fMRI を用いたパーキンソン病患者における両側協調運動時の脳機能活動の変化,第 43 回日本磁気共鳴医学会大会,2015 年 9 月,東京

117.川崎英生、熊谷文孝、濱崎望、佐藤秀二、堀正明、青木茂樹 .Synthetic MRI 及び従来法での T1 値 , T2 値の比較検討 ,第 43 回日本磁気共鳴医学会大会,2015 年 9 月,東京

118.鎌形康司、波田野琢、鶴田航平、奥住文美、堀正明、鈴木通真、下地啓五、濱崎望、佐藤秀二、上田亮、服部信孝 、青木茂樹 .拡散テンソル構造的ネットワーク解析を用いたパーキンソン病における脳内ネットワーク変容 の解,第 43 回日本磁気共鳴医学会大会,2015 年 9 月,東京

119. 加藤悦郎、藤本進一郎、松森理枝、Rani Bhivasankar 、隈丸加奈子 、川口裕子、高村和久、Frank J Rybicki、Dimitrios Mitsouras.Evaluation of 64-Multidetector Row CT Angiography Transluminal Attenuation Gradient for the Detection of Significant Coronary Artery Disease,Determined by Fractional Flow Reserve,第 24 回日本心血管インターベンション学会,2015 年 7 月,福岡

120.中澤美咲、鶴田航平、堀正明、萩原彰文、高野直、熊谷文孝、濱崎望、佐藤秀二、川崎英生、鎌形康司、吉田茉莉子、村田渉、上田亮、青木茂樹 、妹尾淳史.Synthetic MR の使用経験 Advanced CT・MR 2015,2015 年 6 月,軽井沢

121.上田亮、鶴田航平、堀正明、錦織瞭、鎌形康司、神谷昂平、下地啓五、吉田茉莉子、萩原彰文、熊谷文孝、中澤美咲、村田渉、青木茂樹 、妹尾淳史.パーキンソン病患者と健常者の拡散テンソルを用いた connectome の比較,Advanced CT・MR 2015,2015 年 6 月,軽井沢

122.髙野直、鈴木通真、佐藤秀二、濱崎望、川崎英生、芳士戸治義、山本宗孝、堀正明、大石英則、青木茂樹 .Silent MRA における 2 種類の頭蓋内ステントの信号強度比の変化,Advanced CT・MR

法人番号	131025
プロジェクト番号	S1101009

2015,2015 年 6 月,軽井沢
123. 神谷昂平、鈴木雄一、田中将太 、武笠晃丈、堀正明、森墾、國松聡、青木茂樹 、大友邦.腫瘍周囲の T2WI 高信号域における、DKI・NODDI 定量値の初期検討：腫瘍浸潤 vs 血管原性浮腫,第 74 回日本医学放射線学会総会,2015 年 4 月,横浜
124. Ryusuke Irie, Michimasa Suzuki, Munetaka Yamamoto, Nao Takano, Yasuo Suga, Masaaki Hori, Koji Kamagata, Mariko Yoshida, Hidenori Oishi, Shigeki Aoki.Magnetic resonance angiography using silent scan after stent-assisted coil embolization for posterior circulation aneurysms,第 74 回日本医学放射線学会総会,2015 年 4 月,横浜
125. 隈丸加奈子, Saboo S, Cai T, Gonzalez-Quesada C, George E, Hussain Z, Dunne R, Bedayat A, Aghayev A, Wake N, Imanzadeh A, Bhivasankar R, Hunsaker AR, Rybicki FJ.包括的 CT 所見に基づいたスコアリングによる肺塞栓後の死亡予測,第 74 回 日本医学放射線学会総会,2015 年 4 月,横浜
126. 隈丸加奈子, Hiraku Kumamaru, Brian T. Bateman, Jun Liu, Laurence D. Higgins, Frank J. Rybicki, Elisabetta Patorn.米国大規模入院データベースを用いた股／膝関節置換術後の肺塞栓 CT 利用のばらつきの解析,第 74 回日本医学放射線学会総会,2015 年 4 月,横浜
127. 隈丸加奈子, Hiraku Kumamaru, Brian T. Bateman, Jun Liu, Laurence D. Higgins, Frank J. Rybicki, Elisabetta Patorn.米国大規模入院データベースを用いた股／膝関節置換術後の肺塞栓 CT 利用のばらつきの解析,第 74 回 日本医学放射線学会総会,2015 年 4 月,横浜
128. 隈丸加奈子, Cai T, Mitsouras D, Imanzadeh A, George E, Schultz K, Grant GT, Liacouras PC, Steigner M, Bueno E, Pomahac B, Rybicki FJ,顔面骨 CT の 3D プリンティングにおける被ばく低減と逐次近似法の検討,第 74 回 日本医学放射線学会総会,2015 年 4 月,横浜
129. 隈丸加奈子, Bedayat A, Bhivasankar R, Cai T, George E, Imanzadeh A, Hussain Z, Dunne R, Hunsaker AR, Rybicki FJ.肺塞栓 CT レポート内の診断の曖昧さと患者アウトカムの関連解析,第 74 回 日本医学放射線学会総会,2015 年 4 月,横浜

２０１４年グループ（1）
130. 上窪裕二、坂入伯駿、田端俊英、櫻井隆.アデノシン A1 受容体と代謝型グルタミン酸受容体の複合体形成と機能的相互作用,第 131 回日本薬理学会関東部会,2014 年 10 月,横浜
131. 村山尚、呉林なごみ、山澤徳志子、小山田英人、鈴木純二、金丸和典、小口勝司、飯野正光、櫻井隆.1 型リアノジン受容体における中央領域疾患変異体の機能解析,第 131 回日本薬理学会関東部会,2014 年 10 月,横浜
132. 上窪裕二、櫻井隆.海馬スライス培養系を用いた β セクレターゼ活性の解析,第 35 回日本神経科学大会,2014 年 9 月,横浜
133. 高杉展正、新家瑠奈、上窪裕二、櫻井隆.APP-βCTF に特異的に結合するエンドソーム蛋白質の解析,第 87 回日本薬理学会年会,2014 年 3 月,仙台
134. 村山 尚, 呉林なごみ, 山澤徳志子, 小山田英人, 鈴木純二, 金丸和典, 竹森 重, 小口勝司, 飯野正光, 櫻井隆.1 型リアノジン受容体 N 末疾患変異はカルシウムチャネル活性に多様な影響を及ぼす,第 87 回日本薬理学会年会,2014 年 3 月,仙台
135. 上窪裕二, 櫻井隆.アデノシン A1 受容体と代謝型グルタミン酸受容体の相互作用による小脳シナプス可塑性の制御,第 87 回日本薬理学会年会,2014 年 3 月,仙台
136. 村山尚, 呉林なごみ, 山澤徳志子, 小山田英人, 鈴木純二, 金丸和典, 竹森重, 小口勝司, 飯野正光, 櫻井隆.1 型リアノジン受容体チャネルに対する N 末疾患変異の効果,第 91 回日本生理学会大会,2014 年 3 月,鹿児島
137. Murayama T, Kurebayashi N, Yamazawa T, Oyamada T, Takemori T, Oguchi K, Sakurai T.Effects of amino-terminal disease-associated mutations on the CICR activity of RyR1 channel.,Biophysical Society 58th Annual Meeting,2014 年 2 月,San Francisco, CA, USA
138. 佐藤栄人、小池正人、舩山学、金井数明、新井公人、内山安男 、服部信孝.遺伝子パーキンソン病 PARK9(ATP13A2)の分子機構とリソソームの障害,第 55 回日本神経学会,2014 年 5 月,福岡
139. 佐藤 栄人, 服部信孝.パーキンソン病の発症メカニズムと相互関連 遺伝性パーキンソン病とミトコンドリア品質管理の破綻,これまでの展開と今後の課題,第 8 回パーキンソン病・運動障

法人番号	131025
プロジェクト番号	S1101009

害疾患コングレス,2014 年 10 月,京都
140. 佐藤栄人.オートファジー欠損マウスはパーキンソン病のモデルとなりうるか、セッション 7 生理・病態（３）,第 8 回オートファジー研究会、第 2 回新学術「オートファジー」班会議,2014 年 11 月,札幌
141. 内山安男.神経系におけるオートファジー,第５５回日本組織細胞化学会総会シンポジウム,2014 年 9 月,松本
142. 内山安男,オートファジーと認知症 特別講演,第２０回近畿老年期認知症研究会,2014 年 7 月,大阪
**143. 内山安男.リソソーム蓄積症とオートファジー. 学術教育講演,第１１９回日本解剖学会総会･全国学術集会,2014 年 3 月,栃木
144. 内山安男.神経細胞の極性とオートファジー,第１９回グリアクラブ特別講演,2014 年 2 月,新潟

２０１４年グループ（２）

145. Masakazu Miyajima.Clinical complexity of hydrocephalus and parkinsonism: Optimal balance between medical and surgical management ,4th Asian and Oceanian Parkison's Disease and Movement Disorders Congress,2014 年 11 月,Pattaya
146. Masakazu Miyajima.Long-term outcome in patients with idiopathic normal-pressure hydrocephalus treated with lumbo-peritoneal shunt: a multicentre prospective study (SINPHONI-2),Hydrocephalus 2014,2014 年 9 月,Bristol
147. Satoshi Adachi, Akihide Kondo.髄芽腫における MGMT メチル化解析,日本脳腫瘍学会,2014 年 11 月,千葉
148. Tomoko Kurimoto, Akihide Kondo.O6-methylguanine-DNAmethyltransferase (MGMT) in medulloblastomaInternational Symposium on Pediatric Neuro-Oncology,2014 年 6 月,Singapore
149. Kazusaku Kamiya, Keiko Karasawa, Asuka Miwa, Osamu Minowa, Megumi Funakubo1, Katsuhisa Ikeda.″The activation of stem cell homing factors highly induce the cochlear invasion of bone marrow mesenchymal stem cells.Association for Research in Otolaryngology (ARO), 37th MidWinter Meeting,2014 年 2 月,米国サンディエゴ
150. Risa Nonaka, Takafumi Iesaki, Susana de Vega, Yoshihiko Yamada, Eri Arikawa-Hirasawa.The role of the extracellular matrix protein Perlecan in the arterial wall,Experimental Biology ,2014 年 5 月,San Diego CA USA
151. Eri Arikawa-Hirasawa .Role of Perlecan in Neurogenesis and Ageing Gordon Research Conference on proteoglycan ,2014 年 7 月,New Hampshire, USA
152. Risa Nonaka, Takafumi Iesaki, Susana de Vega., Aurerien Kerever, Yoshihiko Yamada, Eri Arikawa-Hirasawa.Perlecan-deficient Mutation Impairs Homeostasis and Wound Healing in Mouse Corneal Epithelium,Gordon Research Conference on proteoglycan ,2014 年 7 月,New Hampshire, USA
153. Takenori Inomata, Toru Matsunaga, Nobuyuki Ebihara, Akira Murakami, Eri Arikawa-Hirasawa.Gordon Research Conference on proteoglycan ,2014 年 7 月,New Hampshire, USA
154. 平澤恵理、岩田哲、野中里紗、服部信孝、中田智彦、伊藤美佳子、大野欽司.Schwartz-Jampel 症候群の原因遺伝子、パールカンの機能部分欠損変異の機能解析 ,第 55 回日本神経学会学術大会,2014 年 5 月,福岡
155. 野中里紗、家崎貴文、Susana de Vega、Aurelien Kerever、山田 吉彦、平澤（有川）恵理.大動脈構造や機能におけるパールカンの役割,第 46 回日本結合組織学会・第 61 回マトリックス研究会合同学術集会,2014 年 6 月,名古屋

２０１４年グループ（３）

156. Suda Y, Kumano H, Uka T.LIP neurons accumulate relevant information depending on task demand,第 37 回日本神経科学大会,2014 年 9 月,横浜

法人番号	131025
プロジェクト番号	S1101009

２０１３年グループ（1）

157. 佐藤栄人、里　史明、松井秀彰、小池正人、金井数明、斉木臣二、舩山　学、武田俊一、内山安男、高橋良輔、服部信孝.若年発症パーキンソン病原因遺伝子産物 ATP13A2 の機能解析,第 54 回日本神経学会学術大会,2013 年 5 月,東京
158. 佐藤栄人、服部信孝.ATP13A2(PARK9)の機能解析,第 54 回日本神経学会総会,2013 年 5 月,東京
159. 佐藤栄人、服部信孝.ATP13A2 ノックアウトマウスの機能解析　　神経変性班　班会議(中野班),2013 年 12 月,東京
160. 佐藤栄人,服部信孝.PARK9(ATP13A2)の分子病態とリソソームの障害,神経変性疾患に関する調査研究班,平成 25 年度　班会議,2013 年 12 月,東京
161. 佐藤栄人、服部信孝.遺伝性パーキンソン病とオートファジーリソソームの障害,第 129 回日本薬理学会関東部会,2013 年 10 月,東京
162. 佐藤栄人、服部信孝.遺伝性パーキンソン病とミトコンドリア品質管理の障害,世界生物学的精神医学会国際会議,2013 年 6 月,京都
163. 内山安男.ロテオリシスによる生体制御：極性のあるニューロンへのリソソソーム／オートファゴソームの局在について,第 133 年会日本薬学会シンポジウム,2013 年 3 月,横浜
164. 上窪裕二、櫻井 隆.海馬スライス培養標本を用いた β-セクレターゼ機能の評価,第 128 回日本薬理学会関東部会,2013 年 7 月,東京
165. 上窪裕二、櫻井 隆.海馬切片培養標本を用いた β-セクレターゼの解析,第 36 回日本神経科学大会 Neuro2013,2013 年 6 月,京都
166. 坂入伯駿,上窪裕二,櫻井 隆.異種 GPCR 間の相互作用による神経伝達の制御,第 90 回日本生理学会大会,2013 年 3 月,東京
167. 村山尚、呉林なごみ、小山田英人、鈴木純二、金丸和典、小口勝司、飯野正光、櫻井隆.1 型リアノジン受容体チャネルに対する疾患変異の多様な効果,第 86 回日本薬理学会,2013 年 3 月,福岡
168. 樫山拓、上窪裕二、櫻井 隆.切断端認識抗体を用いたニューレグリン 1 の BACE1 切断依存的細胞間シグナル伝達の解析,第 86 回日本薬理学会年会,2013 年 3 月,福岡
169. 上窪裕二、櫻井 隆.海馬切片培養標本を用いたアミロイド β 産生の評価　,第 86 回日本薬理学会年会,2013 年 3 月,福岡
170. 坂入伯駿, 上窪裕二, 櫻井隆.GPCR 複合体形成によるシグナル伝達制御,第 129 回日本薬理学会関東部会,2013 年 10 月,東京

２０１３年グループ（2）

171. 河野春奈、伊藤敬孝、金井富三夫、中村衣理、多田昇弘、小林敏之、樋野興夫.Eker ラット ES 細胞および iPS 細胞による腎癌発生メカニズムの解析,第 101 泌尿器科学会総会,2013 年 4 月,札幌
172. 伊藤敬孝、河野春奈、金井富三夫、中村衣里、多田昇弘、新井一、小林敏之、樋野興夫.Tsc2 欠損ラット ES 細胞を用いた mTOR 経路関連神経疾患の病態解明,老研発表会,順天堂大学, 2013 年 2 月,東京
173. Akihide Kondo.The seeking of the stem cell characters in oligo-glial tumors,The Neuro-Oncology Symposium ,2013 年 9 月,Taiwan
174. 近藤聡英.Oligo-glial tumor における Tumor stem cell.,第 22 回 J.K.W フォーラム,2013 年 4 月,東京
175. Masakazu Miyajima.Leucine-rich α-glicoprotein (LRG) is a novel biomarker of neurogenerative disease in human cerebrospinal fluid and causes neurodegeneration in mouse cerebral cortex.,Hydrocephalus 2013,2013 年 6 月,Athens
176. Kamiya K, Karasawa K, Osamu Minowa, Ikeda K.Connexin26 mutations that cause hereditary deafness lead to macromolecular complex degradation of cochlear gap junction plaques,Association for Research in Otolaryngology (ARO),36th MidWinter Meeting, 2013 年 2 月,米国,ボルチモア
177. 宮嶋雅一.髄液の産生と吸収の再考,日本脳神経外科学会,第７２回学術総会,2013 年 10 月横浜

法人番号	131025
プロジェクト番号	S1101009

178. Masakazu Miyajima. Leucine-rich α2-glycoprotein (LRG) is a novel biomarker of neurogenerative disease in human cerebrospinal fluid and causes neurodegeneration in mouse cerebral cortex.,Hydrocephalus 2013,2013 年 7 月,Athens
179. Masakazu Miyajima. Guideline for management of iNPH and results of Japan Shunt Registry., 韓国機能脳神経外科学会,2013 年 3 月,釜山
180. Mario Suzuki, Akihide Kondo. Oligodendroglial tumors における腫瘍幹細胞と遺伝子変異の関係,日本脳腫瘍学会,2013 年 11 月,広島
181. ″神谷和作,美野輪治,池田勝久 .幹細胞ホーミング分子機構を応用した効率的内耳細胞治療法の開発,第 23 回　日本耳科学会学術集会,2013 年 11 月,宮崎市
182. Kazusaku Kamiya, Keiko Karasawa, Takashi Anzai, Kana Harada, Kazuma Kobayashi, Osamu Minowa, Katsuhisa Ikeda. Cell therapy for hereditary deafness with bone marrow mesenchymal stem cell and the activation of stem cell homing.,国際幹細胞学会 (ISSCR),2013 年 9 月,イタリアフィレンツェ″
183. Kazusaku Kamiya, Keiko Karasawa, Takashi Anzai, Kana Harada, Kazuma Kobayashi, Osamu Minowa, Katsuhisa Ikeda. Cell therapy for hereditary deafness with bone marrow mesenchymal stem cell and the activation of stem cell homing.,50th Inner Ear Biology Workshop,2013 年 9 月,スペインマドリッド
184. 野中里紗、家崎貴文、Susana de Vega、山田吉彦、平澤 (有川) 恵理 .ヘパラン硫酸プロテオグリカン、パールカンの内皮依存性血管拡張における役割,第 36 回日本分子生物学会年会,2013 年 12 月,神戸
185. Arikawa-Hirasawa E, Douet V, Alarcon VB, Kerver A, Mercier F,. Fractone niche for neuroepithelial and neural stem cell proliferation,Society for Neuroscience annual meeting,2013 年 11 月,San Diego CA USA
186. Kerver A , Yamada Y, Nonaka R, Mercier F, Arikawa-Hirasawa E. Age-related alteration of extracellular matrix in the subventricular zone of the lateral ventricles.,Society for Neuroscience annual meeting Society for Neuroscience annual meeting ,2013 年 11 月,San Diego CA USA
187. Susana de Vega, Nobuharu Suzuki, Risa Nonaka, Takako Sasaki, Patricia Forcinito, Yoshihiko Yamada, Eri Arikawa-Hirasawa . Interaction of the C-terminal region of fibulin-7 with endothelial cells: a potential role in angiogenesis ,36th MBSJ ,2013 年 12 月,神戸

２０１３年グループ（３）

188. Suda Y, Kumano H, Uka T. Dynamics of sensory information accumulation in LIP during task switching.,43rd Annual Meeting of the Society for Neuroscience, San Diego, CA, USA,2013 年 11 月,San Diego, CA, USA
189. Kumano H, Uka T. Characteristics of trial-to-trial spike count variability in MT neurons are consistent with bottom-up components of decision related response modulation.,Neuroscience 2013,2013 年 11 月,San Diego
190. Suda Y, Kumano H, Uka T. Dynamics of sensory information accumulation in LIP during task switching.,Neuroscience 2013,2013 年 11 月,San Diego
191. Uka T. Studying flexible decision making using perceptual decisions. The 9th Asia-Pacific conference on vision,2013 年 7 月,Suzhou, China
192. Kumano H, Uka T. Is decision related response modulation of sensory neurons due to bottom-up or top-down signal?: Analysis of trial-to-trial spike count variability in MT neurons.,第 36 回日本神経科学大会,2013 年 6 月,京都
193. Konishi S. Neural mechanisms of memory retrieval revealed by fMRI,第 36 回日本神経科学大会,2013 年 6 月,京都
194. Kumano H, Uka T. Characteristics of trial-to-trial spike count variability in MT neurons are consistent with bottom-up components of decision related response modulation.,43rd Annual Meeting of the Society for Neuroscience,2013 年 11 月,San Diego, USA

法人番号	131025
プロジェクト番号	S1101009

195. Kumano H, Uka T. Is decision related response modulation of sensory neurons due to bottom-up or top-down signal?: Analysis of trial-to-trial spike count variability in MT neurons., 第 36 回日本神経科学大会, 2013 年 6 月, 京都

２０１２年グループ（1）

196. 石川景一, 斉木臣二, 今道洋子, 佐藤栄人, 河尻澄宏, 李元哲, 服部信孝. ペリー症候群の原因遺伝子産物ダイナクチンの機能解析 , 第 53 回日本神経学会学術大会, 2012 年 5 月, 東京
197. Imai Y, Shiba-Fukushima K, Yoshida S, Ishihama Y, Hattori N, PINK1-mediated phosphorylation of the Parkin ubiquitin-like domain primes mitochondrial translocation of Parkin: an initial step of mitophagy., 第 35 回日本分子生物学会年会 ワークショップ「オートファジーによる分解の諸相」, 2012 年 12 月, 福岡
198. Imai Y. PINK1-mediated phosphorylation of the Parkin ubiquitin-like domain primes mitochondrial translocation of Parkin and regulates mitophagy, The 17th Takeda Science Foundation Symposium on Bioscience, 2012 年 12 月, 大阪
199. 江口博人、今泉美佳、坂口勇ケネス、佐藤栄人、舩山学、柴佳保里、斉木臣二、波田野琢、久保紳一郎、永松信哉、服部信孝. Parkin ノックアウトマウスにおける分泌異常の検討, 第 6 回パーキンソン病・運動障害疾患コングレス(MDSJ), 2012 年 10 月, 京都
200. Eguchi Hiroto, Ohara-Imaizumi M, Tsukaguchi K, Sato S, Funayama M, Saiki S, Hatano T, Kubo S, Nagamatsu S, Hattori N. Parkin dysfunction results in defective depolarization-induced exocytosis and reorganization of the cytoskeleton, 16th International Congress of Parkinson's Disease and Movement Disorder, 2012 年 6 月, Dublin, Ireland
201. Yasuo Uchiyama. Characteristic differences between Purkinje cells specifically deficient in cathepsin D and Atg7 , 6th International Symposium on Autophagy （招待講演）, 2012 年 10 月, 沖縄
202. Yasuo Uchiyama. Imaging of intracellular organelles with special reference to the lysosome in neurons and its loss of function., In: Japan-Korea Information Exchange Program on Technologies of Analysis 2012 （招待講演）, 2012 年 9 月, 幕張
203. Yasuo Uchiyama. Hyaluronan tetrasaccharide rescues hippocampal pyramidal neuron death after hypoxic-ischemic injury., 14th International Congress of Histochemistry and Cytochemistry（招待講演）, 2012 年 8 月, 京都
204. 内山安男. リソソーム蓄積症とオートファジー, 蛋白研セミナー「神経疾患の克服に向けて」(招待講演）, 2012 年 3 月, 大阪
205. Yasuo Uchiyama. Cell death and autophagy., Opening Lecture in XXII International Symposium on Morphological Sciences （招待講演）, 2012 年 2 月, Sau Paolo, Brasil
206. 樫山拓、上窪裕二、櫻井 隆. 切断端特異的抗体を用いた BACE1 依存的ニューレグリン 1 切断による細胞間シグナル伝達の解析, 第 127 回日本薬理学会関東部会, 2012 年 10 月, 東京
207. 村山 尚、大田啓貴、櫻井 隆. ダイニンアダプターBicaudal-D2 の細胞周期依存的核膜局在の分子機構 , 第 50 回日本生物物理学会年会, 2012 年 9 月, 名古屋
208. 上窪裕二、櫻井 隆. mGluR1-アデノシン A1 受容体相互作用とシグナル・クロストーク, 第 35 回日本神経科学大会, 2012 年 9 月, 愛知
209. 村山尚、呉林なごみ、大羽利治、小山田英人、小口勝司、櫻井隆、小川靖男. 1 型リアノジン受容体の S4-S5 リンカーはチャネルゲーティングを調節する, 第 89 回日本生理学会大会 , 2012 年 3 月, 松本
210. 上窪裕二, 櫻井 隆. アデノシン A1 受容体と 1 型代謝型グルタミン酸受容体の複合体形成によるシグナル・クロストーク, 第 85 回日本薬理学会年会, 2012 年 3 月, 京都
211. 村山尚、呉林なごみ、大羽利治、小山田英人、小口勝司、小川靖男、櫻井隆. 1 型リアノジン受容体 S4-S5 リンカーはチャネルゲーティングを調節する, 第 85 回日本薬理学会年会, 2012 年 3 月, 京都
212. 樫山拓、櫻井隆. BACE1 依存的ニューレグリン 1 切断による隣接細胞間シグナル伝達の切断端抗体を用いた解析, 第 85 回日本薬理学会年会, 2012 年 3 月, 京都

法人番号	131025
プロジェクト番号	S1101009

213. Murayama T, Kurebayashi N, Oba T, Oyamada H, Oguchi K, Sakurai T, Ogawa Y. Role of amino-terminal half of the S4-S5 linker in the RyR1 channel gating., Biophysical Society 56th Annual Meeting , Feb, 2012, San Diego
214. de Vega S, Arikawa-Hirasawa E, Yamada Y. Fbln7-d3, a fragment of the ECM protein fibulin-7, a potential inhibitor of Angiogenesis., 45th JSDB- 64th JSCB Meeting (Japanese Society for Developmental Biology & Cell Biology Joint Meeting, 2012 年 5 月 Kobe Japan
215. Kerever A, Mercier F, Oda Y and Arikawa-Hirasawa E. Perlecan is necessary for the maintenance of CD133 expressing neural stem cells in the subventricular zone., the International Society for Stem Cell Research (ISSCR) 10th Annual Meeting, 2012 年 6 月, Yokohama, Japan
216. Mercier F, Douet V , Arikawa-Hirasawa E. Heparan sulfate connective tissue niche for the regulation of stem cell proliferation in the adult brain, International Society for Stem Cell Research (ISSCR) 10th Annual Meeting , 2012 年 6 月, Yokohama, Japan
217. Risa Nonaka, Takafumi Iesaki, Susana de Vega, Yoshihiko Yamada, Eri Arikawa-Hirasawa. Role of perlecan, a heparan sulfate proteoglycan, in aortic endothelial cell activity in response to arterial tension in vitro, 35th MBSJ , 2012 年 12 月, Fukuoka Japan
218. Kerever A, De Vega S, Nonaka R, Mercier F, Oda Y and Arikawa-Hirasawa E. Perlecan is an essential component of the neurogenic niche. , 35th MBSJ , 2012 年 12 月, Fukuoka Japan
219. Ning L, Kurihara H, Ichikawa-Tomikawa N, Yamada Y, and Arikawa-Hirasawa E. Laminin α1 deficiency causes abnormal increase in mesangial cell proliferation and matrix production, 35th MBSJ , 2012 年 12 月, Fukuoka Japan
220. Nakazawa N, Miyahara K, Okawada M, Liu Y, Akazawa C, Yamataka A, Arikawa-Hirasawa E. Laminin-1 promotes neuronal development in mouse embryonic gut., XXVth International Symposium on Paediatric Surgical Research, 2012 年 9 月, London, UK
221. 河野春奈、伊藤敬孝、金井富三夫、中村衣里、高井節夫、多田昇弘、樋野興夫. Generation and analysis of Tsc2-deficient rat embryonic stem cells., 第 35 回日本分子生物学会年会, 2012 年 12 月, 福岡
222. 伊藤敬孝、河野春奈、高井節夫、新井一、小林敏之、樋野興夫. Eker ラットからの Tsc2 欠損型杯性幹細胞の樹立, 第 71 回日本癌学会学術総会, 2012 年 9 月, 札幌
223. 伊藤敬孝、河野春奈、金井冨三夫、多田昇弘、小林敏之、樋野興夫. Elucidation of pathogenesis using Tsc2-deficient rat embryonic stem cells., 文部科学省科学研究費補助金 新学術領域 「がん研究分野の特性等を踏まえた支援活動」, 平成 24 年度がん若手研究者ワークショップ, 2012 年 9 月, 長野
224. 鈴木まりお、近藤聡英. Oligodendroglial tumors における腫瘍幹細胞と遺伝子変異の関係, 第 30 回日本脳腫瘍学会, 2012 年 11 月, 広島
225. Akihide Kondo. The molecular biological comparisons between original, recurrent tumors, and primary culture cells from Atypical Teratoid / Rhabdoid Tumor, International Pediatric Neuro-Oncology meeting, 2012 年 6 月, Toronto, Canada
226. 安田肇. 3D image analysis of the bone marrow extracellular matrix, 第 74 回日本血液学会, 2012 年 10 月, 京都
227. Kamiya K, Karasawa K, Osamu Minowa, Ikeda K. Connexin26 mutations that cause hereditary deafness lead to macromolecular complex degradation of cochlear gap junction plaque, EMBO meeting2012, 2012 年 9 月, フランス, ニース
228. 神谷和作、美野輪治、池田勝久. 遺伝子改変難聴モデル動物による内耳細胞治療法の開発, 第 22 回日本耳科学会シンポジウム, 2012 年 10 月, 名古屋
229. 神谷和作、池田勝久. 遺伝子改変難聴モデル動物による内耳細胞治療法の開発, 第 74 回耳鼻咽喉科臨床学会シンポジウム, 2012 年 7 月, 東京
230. Kazusaku Kamiya, Miho Muraki, Kana Ogawa, Katsuhisa Ikeda. Cell therapy for hereditary hearing loss with stem cell homing factors, 第 85 回日本薬理学会シンポジウム講演, 2012 年 3 月, 京都

法人番号	131025
プロジェクト番号	S1101009

231. Kumano H, Uka T. Contribution of spatial summation properties within receptive field to the apparent contraction of receptive field size of MT neurons when presented with noise, 第 35 回日本神経科学大会, 2012 年 9 月, 名古屋
232. Saruwatari M, Uka T, Kitazawa S. Pre-saccadic shifts of receptive fields in medial superior temporal area neurons. , 第 35 回日本神経科学大会, 2012 年 9 月, 名古屋

２０１１年グループ（１）

233. Yasuo Uchiyama. Ischemic neuron death and autophagy., Opening Lecture in 10th Japan-China Joint Meeting of Histochemistry and Cytochemistry, 2011 年 10 月, 北京
234. 村山尚、呉林なごみ、大羽利治、小山田英人、小口勝司、小川靖男、櫻井隆. １型リアノジン受容体チャネルゲーティングにおける S4-S5 リンカーの役割, 第 125 回日本薬理学会関東部会, 2011 年 10 月, 船橋
235. 上窪裕二, 藤田洋介, 下村岳司, 宮島隆彰, 田端俊英, 袋谷賢吉, 狩野方伸, 櫻井 隆. アデノシン A1 受容体と代謝型グルタミン酸受容体の相互作用による小脳 LTD の 調節, 第 34 回日本神経科学大会(Neuroscience2011), 2011 年 9 月, 横浜
236. 長谷川麻衣子、高橋良佳、鈴木尚生子、櫻井 隆、稲田英一. PPAR-γ アゴニスト rosiglitazone のマクロファージを介した鎮痛効果, 日本麻酔科学会第 58 回学術集会, 2011 年 5 月, 神戸
237. 鈴木尚生子、長谷川麻衣子、櫻井 隆、稲田英一. 糖尿病性ニューロパチーにおけるリドカインのミクログリアを介した鎮痛効果, 日本麻酔科学会第 58 回学術集会, 2011 年 5 月, 神戸

２０１１年グループ（２）

238. Kamiya K, Muraki M, Ogawa K, IKEDA K. Cochlear Gap Junction Plaque is Disrupted by connexin26 Mutation, 48th Inner Ear Biology Workshop2011, 2011 年 9 月, ポルトガルリスボン
239. Kamiya K, Muraki M, Ogawa K, IKEDA K. Cochlear Gap Junction Plaque is Disrupted by connexin26 Mutation, EMBO meeting2011 , 2011 年 9 月, オーストリア, ウイーン
240. 神谷和作、池田勝久. コネキシン２６遺伝子変異による蝸牛ギャップ結合プラークの崩壊, 第 21 回日本耳科学会総会・学術講演会, 2011 年 6 月, 沖縄
241. 神谷和作、村木美帆、小川佳奈、池田勝久. コネキシン 26 変異による内耳ギャップ結合プラークの崩壊-遺伝性難聴の新規分子病態, 第 63 回日本細胞生物学会, 2011 年 6 月, 札幌
242. 神谷和作、池田勝久. コネキシン２６遺伝子欠損マウスにおける蝸牛ギャップ結合プラークの解析, 第 112 回日本耳鼻咽喉科学会総会・学術講演会, 2011 年 5 月, 京都

２０１１年グループ（３）

243. Saruwatari M, Uka T, Kitazawa S. Temporo-spatial dynamics of perisaccadic directional selectivity in areas MT and MST of the macaque monkey revealed by motion reverse correlation., 41st Annual Meeting of the Society for Neuroscience, 2011 年 11 月, Washington, DC, USA
244. Saruwatari M, Uka T, Kitazawa S. Temporo-spatial dynamics of perisaccadic directional selectivity in the medial temporal area of the macaque monkey: application of a motion reverse correlation method, 第 34 回日本神経科学大会, 2011 年 9 月, 横浜
245. Mitani A, Oizumi M, Sasaki R, Uka T. A bounded leaky integrator model can explain variations in reaction time during task switching., 第 34 回日本神経科学大会, 2011 年 9 月, 横浜
246. Kumano H, Uka T. Transfer of choice-related response modulation across visual fields during learning of a depth-discrimination task., 第 34 回日本神経科学大会, 2011 年 9 月, 横浜

法人番号	131025
プロジェクト番号	S1101009

＜研究成果の公開状況＞（上記以外）

シンポジウム・学会等の実施状況、インターネットでの公開状況等

＜既に実施しているもの＞

第１回　公開シンポジウム

細胞・脳機能研究の融合による神経疾患診断・治療法開発拠点の形成

日時　平成２３年１０月１３日（木）

場所　順天堂大学老人性疾患病態・治療研究センター１０号館１階　カンファレンスルーム

拠点概要

順天堂大学神経機能構造学・教授　内山安男　細胞品質管理機構とその破綻

順天堂大学分子病理病態学・教授　樋野興夫　細胞の分化・増殖・幹細胞性

順天堂大学神経学・教授　服部信孝　加齢・認知・発達障害の脳画像解析

細胞機能、脳機能研究の現状

慶應義塾大学生理学教室・教授 岡野栄之

京都大学再生医学研究所・教授 長澤岳司

東京大学精神神経科・教授 笠井清登

大阪大学生命機能研究科・教授 北澤茂

東京都臨床医学総合研究所・所長　田中啓二

2. 第 41 回日本耳鼻咽喉科感染症研究会・第 35 回日本医用エアロゾル研究会（会長:池田勝久）2011 年 9 月 2 日～3 日
3. 第 74 回 耳鼻咽喉科臨床学会総会・学術講演会（会長:池田勝久）2012 年 7 月 5 日～6 日
4. 第 31 回耳鼻咽喉科ニューロサイエンス研究会（会長:池田勝久、事務局長：神谷和作）2013 年 8 月 24 日
5. 第 14 回日本在宅医学大会・第 16 回日本在宅ケア学会学術集会（会長：服部信孝・脳神経内科）2012 年 3 月 17、18 日、東京
6. 第 5 回順天堂・東京女子医大ジョイントカンファレンス（JJJC）（会長：服部信孝・脳神経内科）、順天堂大学、2012 年 4 月 10 日、東京
7. プレスリリース、2012 年 12 月 19 日 9：00、文部科学省にてプレスリリース、若年性パーキンソン病の原因遺伝子である Parkin と PINK1 の解析から、同疾患の発症に関わる新規メカニズムを発見。2012 年 12 月 19 日 19:00、日経バイオテクオンラインに掲載　（脳神経内科）
8. 第 129 回日本薬理学会関東部会（部会長：櫻井 隆）シンポジウム：神経変性疾患の新たな治療戦略と創薬
9. 「遺伝性パーキンソン病の分子病態を基盤としたバイオマーカーの開発」順天堂大学医学部神経学講座　佐藤 栄人、平成 25 年 10 月 19 日、　順天堂大学本郷キャンパス
10. 第 43 回日本磁気共鳴医学会大会（大会長：青木茂樹）国際シンポジウム：　神経・精神疾患の定量評価とバイオマーカ（仮題）
11. International Symposium on Mitochondria 2013, The 13th Conference of Japanese Society of Mitochondrial Research and Medicine (J-mit), Chairman: Nobutaka Hattori, Dept.Neurology, Roppongi Academyhills 49, Nov 6-7, 2013, Tokyo Japan
12. Nobutaka Hattori; Advisory board, The 9th International Congress on Mental Congress on Mental Disorders & other Non-Motor features in Parkinson's Disease and Related Disorders,

法人番号	131025
プロジェクト番号	S1101009

Seoul, Apr 18, 2013, Korea
http://www2.kenes.com/mdpd/Pages/Home.aspx

13. 服部信孝；開会・閉会の辞、総合司会、市民公開フォーラム、明日のために知っておきたいパーキンソン病治療の今、よみうりホール、2013 年 4 月.28 日、東京
14. 服部信孝；新聞掲載、手足震え、動作鈍くなるパーキンソン病－薬工夫で生活の質向上、朝日新聞　2013 年 9 月 10 日朝刊, p 34 生活面
15. Nobutaka Hattori; President & Symposium Chairperson, International Symposium on Mitochondria 2013, The 13th Conference of Japanese Society of Mitochondrial Research and Medicine (J-mit), Roppongi Academyhills 49, Nov 6-7, 2013, Tokyo Japan
http://www.j-mit.org/sub6-kako.html（ミトコンドリア学会ホームページ・過去の学術集会より）
16. 服部信孝；パーキンソン病・最新治療のいま！、パーキンソン病と上手に付き合う、第 8 回パーキンソン病市民公開講座 in 会津、会津若松ワシントンホテル、 2014 年 6 月 15 日、会津若松市
17. 服部信孝；TV シンポジウム- パーキンソン病とつきあう ～治療・リハビリ・生活環境～、2014 年 9 月 20 日（土)、14:00-14:59 放送、NHK Eテレ
18. 舩山学、服部信孝；プレスリリース、遺伝性パーキンソン病の原因遺伝子を新たに発見～ミトコンドリア発の新しいパーキンソン病発症メカニズムを提唱～、文部科学省、2015 年 1 月 28 日、東京
http://www.juntendo.ac.jp/graduate/pdf/news15.pdf
19. 服部信孝；講演、あきらめないパーキンソン病を目指して～いつまでも元気にいられるために～、神経疾患ブレインバンク 第 14 回市民講演会、国立精神・神経医療研究センター ユニバーサルホール、2015 年 2 月 8 日、東京
20. 服部信孝；講演、市民公開講座、第 56 回日本神経学会学術大会 新潟学会学術大会、日報ホール、2015 年 5 月 21 日、新潟
21. 服部信孝；顧問・講演、第 1 回日本パーキンソン病コングレス JPC、水戸京成テル、2015 年 6 月 24 日～25 日、水戸
http://www.juntendo-neurology.com/jpc/
22. Nobutaka Hattori; the Course Director, MDS-AOS Basic Scientists Summer school 2015, the Akihabara Convention Hall, Aug 6-8, 2015, Tokyo Japan
http://www.movementdisorders.org/MDS/Education/Past-Courses/Basic-Scientists-Summer-School-Tokyo.htm
23. 今居 譲、服部信孝. プレスリリース、晩発性パーキンソン病で神経変性がゆっくり進行するメカニズムを解明、～細胞内輸送における LRRK2 の役割～、順天大学、2015 年 9 月 11 日、東京
http://www.juntendo.ac.jp/graduate/pdf/news20.pdf
http://www.asahi.com/and_M/information/pressrelease/CATP201573525.html
24. Nobutaka Hattori; the Chairman, the 10th Annual GEoPD Meeting in Tokyo,Roppongi Academyhills 49, Oct. 1-2, 2015, Tokyo Japan
http://www.geopdtyo.org/index.html
25. 第 14 回日本正常圧水頭症学会（会長：宮嶋雅一・脳神経外科）2013 年 2 月 9 日、東京
26. 日本脳神経外科学会第 73 回学術総会（会長：新井 一・脳神経外科）2014 年 1 月 9 日～11 日、東京

法人番号	131025
プロジェクト番号	S1101009

27. 第 1 回日本結節性硬化症学会、日時：平成 25 年 11 月 1 日（金）場所：東京ガーデンパレスホテル、順天堂大学　病理・腫瘍学　教授　樋野興夫（学会長、理事長）
28. 第 2 回日本結節性硬化症学会、日時：平成 26 年 11 月 15 日（土)、場所：東京大学 、順天堂大学 病理・腫瘍学 教授　樋野興夫（理事長）
    日本結節性硬化症学会ホームページ：
    http://jstsc.kenkyuukai.jp/special/index.asp?id=8468
29. 43 回日本磁気共鳴医学会大会　2015 年 9 月 10－12 日（東京）
30. 脳 MRI 画像チュートリアル　2015 年 1 月（東京大学）
31. 脳 MRI 画像チュートリアル・サテライトシンポジウム：　於第 35 回日本神経科学大会　2012 年 9 月（名古屋）
32. 第 27 回　頭頚部放射線研究会　2014 年 9 月 27 日（神戸）
33. 2014 年 3 月 4 日日経産業新聞「遺伝性難聴の仕組みを解明　順天堂大など」
34. 2014 年 3 月 4 日時事通信「遺伝性難聴の要因解明＝新薬開発に貢献期待―順天堂大など］
35. 2014 年 3 月 4 日日経プレスリリース「順天堂大と理化学研究所、遺伝性難聴の原因メカニズムを解明」
36. 2014 年 6 月 19 日医療 NEWS QLifePro 2014 年 6 月 19 日「順天堂大　聴毛配列異常で高音が低く誤認識される新聴覚障害を発見」
37. 2014 年 7 月 4 日科学新聞　「高音が 2 オクターブも低音に誤認識される　順天堂大　新しいタイプの聴覚障害を発見」
38. 2015 年 4 月 7 日 NHK ニュースおはよう日本 先天性難聴マウスで遺伝子治療成功
39. 2015 年 4 月 7 日毎日新聞　遺伝子治療に道　順天堂大・理研、マウス実験成功
40. 2015 年 4 月 7 日読売新聞　遺伝子治療で難聴予防　研究チーム、マウスで成功
41. 2015 年 4 月 12 日日本経済新聞「遺伝子治療で難聴改善　順天堂大学などマウスで成功」
42. 2015 年 5 月 14 日朝日新聞「遺伝性難聴のマウス　聴力を回復　順天堂大学」
43. Nobutaka Hattori; Chair, MDS/Asian & Oceanian Section/MDS-AOS Officers(2015-2017), the International Parkinson and Movement Disorder Society
    http://www.movementdisorders.org/MDS/MDS-AOS-Officers-2015-2017.htm
44. 服部信孝；講演、市民公開講座「パーキンソン病の次世代治療」、第３３回日本神経治療学会総会、名古屋国際会議場、2015 年 11 月 28 日、名古屋
45. 佐藤栄人；講演、神経変性疾患の原因と治療、第 8 回平成 27 年度都医学研都民講座、一橋講堂、平成 28 年 2 月 5 日、東京
    http://www.metro.tokyo.jp/INET/BOSHU/2015/02/22p2j101.htm
46. 服部信孝；パーキンソン病市民公開講座 in 会津、2016 年 6 月 5 日、会津若松市
47. 第 8 回日本水頭症脳脊髄液学会(会長：宮嶋雅一・脳神経外科)2015 年 11 月 22 日
48. 第 3 回　日本結節性硬化症学会、日時：平成 27 年 11 月 17 日（土）場所：JR 東京総合病院、順天堂大学　病理・腫瘍学　教授　樋野興夫（理事長）
49. ホームページ：
    http://www.juntendo.ac.jp/graduate/laboratory/labo/shinkei/index.html（神経学）
    http://www.juntendo.ac.jp/graduate/laboratory/labo/shinkei_kozo/index.htm（神経生物学・形態学）
    http://pharmacology.sakura.ne.jp/jp/research/microdomain_res/microdomain_ res.html（薬理学）
    http://www.juntendo.ac.jp/graduate/laboratory/labo/rojinsei_shikkan/index.html（老人性疾患病態・治療研究センター）

法人番号	131025
プロジェクト番号	S1101009

http://www.juntendo.ac.jp/graduate/laboratory/labo/bunshi_byori/index.htm（病理・腫瘍学）
http://www.juntendo.ac.jp/graduate/laboratory/labo/nouge/index.html（脳神経外科）
http://www.juntendo.ac.jp/hospital/clinic/ketsuekinaika/index.html（血液学）
http://www.juntendojibi.com/（耳鼻咽喉科学）
http://square.umin.ac.jp/physiol1/member.html（生理学第一）
http://www.juntendo.ac.jp/graduate/laboratory/labo/hoshasen/index.html（放射線 医学）
http://www.juntendo.ac.jp/graduate/laboratory/labo/seishin/index.html（精神医学）
http://square.umin.ac.jp/Brainbnk/link.html(包括型脳科学研究推進支援ネットワーク)
http://www.mri-surescan.com/dbs/training/index.html(脳深部刺激用条件付き MRI 対応神経刺激システム)
http://square.umin.ac.jp/~HN_Rad/gakujyutsu.htm（頭頸部放射線研究会）

＜これから実施する予定のもの＞

1. 第 2 回日本パーキンソン病コングレス（会長：岡田芳子、顧問：服部信孝、高橋良輔）2017 年 4 月 15 日～16 日、東京
2. 第 35 回日本認知症学会学術集会（会長:新井平伊　精神・行動科学）2016 年 12 月 1 日～12 月 3 日、東京
3. 第 46 回日本神経放射線学会（会長：　青木茂樹・放射線科）　2017 年 2 月 17-19 日　東京

14 その他の研究成果等

樋野興夫：結節性硬化症センターの立ち上げ（順天堂大学）

研究の成果として、特許出願＊（「アルツハイマー病予防治療薬のスクリーニング法」高杉展正、櫻井隆、清水瑠奈、特願 2014-132309、学校法人順天堂、平成 26 年 6 月 27 日）を行った。

日立製作所　中央研究所　拡散尖度画像を用いたパーキンソン病の早期診断法の開発　平成 26 年～27 年 6 月

法人番号	131025
プロジェクト番号	S1101009

15 「選定時」及び「中間評価時」に付された留意事項及び対応

＜「選定時」に付された留意事項＞

該当なし。

＜「選定時」に付された留意事項への対応＞

該当なし。

＜「中間評価時」に付された留意事項＞

1. 共焦点レーザースキャンニング顕微鏡（Zeiss LSM780DUO/NLO）の使用時間のみではなくその使用によってどのような効果があったかについて記載してください。
2. 研究成果の実用化に向けた努力について記載してください。

＜「中間評価時」に付された留意事項への対応＞

1. ZeissLSM7DUO/NLO 機は、高解像の共焦点レーザーと 高速ライブイメージング機能を持つ DUO に２光子顕微鏡機能を搭載した多機能顕微鏡として主として神経細胞機能の解析のために購入された。本機器の使用については、高い解像度を活かし多くの発表論文にプロジェクト名と共に機器名が記載されている.

深い焦点面を特徴とする２光子顕微鏡機能を活用し、近年国内外で大きな注目を集めた透明脳技術をいち早く取り入れ、脳 MRI 画像との比較という新しい分野を立ち上げ、ヒト疾患における MRI 画像診断と病理診断を結びつける研究成果をあげつつあることは特記すべきことである。また、神経生細胞のオートファジー等の細胞機能変化をリアルタイムで可視化し解析を進め、論文発表を準備している。

２．研究成果の実用化に向けた努力について：拡散テンソル MRI 画像と遺伝子解析は、多くの疾患の診断解析に利用されている。その効果が、新井（一）グループの水頭症の解析にも見られる。服部らは、遺伝子解析で得た家族性パーキンソン病の現遺伝子の一つを新たに見出し、その局在がミトコンドリアにあることから疾患の原因としてミトコンドリア障害がキーとなることを明らかにできた。さらに難聴の遺伝子治療に、コネキシン２６が利用され、実験的に効果があることが示された。これらの結果は、本プロジェクト研究の過程で得られたもので、診断と治療に展開されることが期待される。

本研究期間における研究によって得られた新たな知見等の成果

本研究プロジェクトは、高齢者におけるさまざまな疾患の原因究明を目的に、「ハイテクリサーチセンター整備事業」の一環としてスタートし、国内外研究機関との連携のもと、研究拠点形成を行ってきた老研センターを基盤施設において行われた。

本研究の目指す目的に沿った研究:

本研究は、ﾐﾄｺﾝﾄﾞﾘｱ機能、ﾀﾝﾊﾟｸ質分解系機能等老化に深く関わる細胞機能や、神経新生、神経変性疾患及び発達障害の分子機構に焦点を当て、神経疾患診断と根治的治療を戦略的に目指す。このため、下記の3つのグループ体制で、目的にあった研究を実行した。本研究で得た成果を、交付申請書に記載した内容に沿って、記載した。

（１）細胞の品質管理の正常機構とその破綻

服部グループ：ミトコンドリア，ユビキチン・プロテアソームに着目したパーキンソン病の病態解明と治療戦略

内山グループ：オートファジー／リソソームによる神経回路網の品質管理とその破綻

櫻井グループ：βアミロイド産生・分解系調節機構の可視化解析

（２）細胞の分化・増殖・幹細胞性

平澤グループ：細胞外環境による細胞の分化・増殖の制御

樋野グループ：神経細胞の分化・移動・腫瘍化・幹細胞性−特に結節性硬化症の原因遺伝子 Tsc2 を起点として−

新井(一)グループ：脳腫瘍発生分子機構における神経細胞の腫瘍化と幹細胞性、正常圧水頭症病態の可視化

高久グループ:骨髄幹細胞ニッチ環境研究による成体神経新生メカニズム

池田グループ：聴覚・平衡覚にかかわる細胞品質管理機構の正常とその破綻

（３）加齢・認知・発達障害の画像解析

青木グループ:脳の加齢・認知・発達障害の可視化　新規画像診断法の確立

宇賀、北沢グループ:多点電極を用いた神経活動記録法の整備

新井(平伊)グループ：アルツハイマー病の発症分子機構解明

具体的に各グループの中で、研究成果がどのようにして出てきたかを以下に述べる。

服部らは、プロジェクトの開始時に、異常ﾐﾄｺﾝﾄﾞﾘｱの除去(ﾐﾄﾌｧｼﾞｰ)と PD の発症について研究成果をあげており、新たな治療標的として確立する、との目標を設定した。本プロジェクトでは、1) PINK1/Parkin が協調して作用し、損傷ミトコンドリアをクリアランスすること（FEBS Letter, 2010)を提示し、東京都医学研（松田氏）との共同研究で Parkin のリン酸化についての研究へと発展した。また、PINK1 ノックアウトマウス由来の MEF 細胞ではミトコンドリア機能が有意に低下していること(＊108)を明らかにした。さらに、2) ATP13A2 はリソソーム膜上に局在し恒常性の維持に重要な働きをすることを明らかにしてきた。ATP13A2 の KO マウスの解析から、リソソームに ceroid-lipofuscin の蓄積症（主にミトコンドリアの ATP synthase のサブユニット c）を惹起することから、Batten 病でよく知られる、神経性seroid-lipofuscin 蓄積症の原因遺伝子でもあることを明らかにした（現在論文投稿中)。一方、３）常染色体優性遺伝性パ PD の家系から新規原因遺伝子 CHCHD2 を同定した(＊12)。CHCHD2 はミトコンドリアに局在することから、同オルガネラに関わる因子であると予想され、同遺伝子変異による PD の病態としてミトコンドリア機能の障害が強く疑われた。すなわち、孤発性の PD を考える上で重要な所見となるミトコンドリアの障害が遺伝性疾患でも明らかになった点は非常に大きな成果であると考えられる。本研究成果に基づき、新たな PD の原因となる遺伝子変異を見出し現在、その病態解析を進め、これまでの成果と合わせて創薬の検討を進める所まで進展することができた。このように、服部らの研究成果は、今後の PD 研究の主流をなすもので、本プロジェクトの中で最もインパクトの強い成果と考えている。

内山らは、小池研究員のプロジェクトの責任者である関係上、本プロジェクトの開始直後から、研究に参画した。PD や AD の病態とオートファジーについては、これまで数多くの研究がなされているが、モデル動物を用いた研究では不明な点も多く残されている。実際、内山らは、これまでにリソソームカテプシン D（CD）欠損マウスは神経性セロイドリポフスチン蓄積症のモデルマウスであり、CD が中枢神経系の恒常性の維持に重要であること明らかにしてきた(Uchiyama et al., 2008, 2009; ***12)。これらの事実を踏まえ、本プロジェクトでは、神経疾患における神経回路網の品質管理異常と治療による正常化をイメージングで検証することを目指した。その結果、１）カテプシン C や DNaseII の特異的な局在(＊159,161)、２）Atg8 のほ乳類ホモログの一つである GABARAP のトランスジェニックマウスを作成し、LC3（細胞体と樹状突起）と異なり GABARAP が軸索初節への局在すること（＊158)、を明らかにした。また、３）リソソームの膜タンパク質である LAMP2 を欠損する症例（ダノン病症候群）と欠損マウスの

中枢神経系における形態解析をした（＊13,160)。４）CD を欠損するマウス脳で調べると、選択的オートファジーのアダプタータンパク質である p62 と NBR1 は、オリゴマーを形成し、細胞体と樹状突起に局在するが、軸索には侵入できないこと、N 端側にあるその責任ドメインがあることが分かった（現在、論文投稿準備中)。さらに、５）オートファジー関連因子の中で唯一膜タンパク質である Atg9a を欠損した脳では、細胞体でオートファジーは抑制されるが、時間経過と共に抑制作用が減少すること、一方、軸索の変化は時間と共に障害の度合いが進展すると共に、初代培養神経細胞の軸索伸展が阻害されること、脳梁や前交連の形成が障害されることが分かった（**39、現在、論文の revise 中)。６）これまで、酸性条件下に対して感受性を持つ蛍光色素と耐性の蛍光色素をつないだ蛍光を用いてオートファゴソームの成熟性を検討できる蛍光色素、pHluorin-mKate tandem fluorescence protein を開発し、LC３に付加したタンパク質は、オートファゴソームの成熟化の良いマーカーとなることを示した（*17）。また、７）服部らと共同した CHCHD2 がミトコンドリアにあることを明らかにした（*12)。

櫻井らは、田平らの研究目的である AD における炎症反応と T 細胞の可視化に関する研究を実質的に発展させるために本プロジェクトに参入した。櫻井らは、β アミロイド産生・分解系の解析によりアルツハイマー病の病態解明と創薬標的探索を目指した。これまでの研究でよく知られているように、アルツハイマー病の病理に関わるβアミロイド（Aβ)は、アミロイド前駆体タンパク質(APP)のβ・γ切断により産生される。しかし、BACE1 によるβ切断が起こる初期エンドソームの輸送障害とβ切断亢進が孤発性アルツハイマー病の初期変化とされているが、その機序は明らかではない。それ故、切断端認識抗体を用いた BACE1 基質切断の可視化により、創薬標的となる APP 特異的β切断制御因子を見出すことを目的としてミクロドメインを解析し、１）エンドソーム輸送を制御する APP 結合蛋白質を見出し、エンドソーム障害及び APP 選択的なβ切断制御に関与することを明らかにした（**10)。現在、病態との関連、治療標的としての可能性について検討を進めている（特許出願)。また、２）βアミロイドによる神経障害に関わる 代謝型グルタミン酸受容体について、他種受容体とのヘテロダイマー形成によるシグナル制御機構を明らかにした(*3,170)。櫻井らは、本プロジェクトの研究目的にあった研究を目指し、病的なAβペプチドの産生に関わるベータ部位での切断に関わる BACE1 の制御因子を見出したことは本プロジェクトの成果の一つと考える。

平澤らは、神経細胞の分化・増殖・移動に着目した腫瘍化・幹細胞性の理解を進めることを目指した。細胞外マトリックス等の条件検討により脳疾患細胞治療に有利な細胞外環境を見いだすことが重要である。平澤らは、これまでに成体神経新生領域である脳室下帯（SVZ）に存在する新規基底膜様構造 fractone と血管周細胞のネットワーク構造が、発生や成体神経新生に重要なニッチ環境を提供すると考えて、これまでに、FGF2 が fractone に存在するパールカンとヘパラン硫酸鎖を介し結合することを報告した（Stem Cells 2007)。本プロジェクトでは、１）ヘパラン硫酸プロテオグリカンであるパールカンを欠損する SVZ 及び neurosphere では、FGF2 投与による神経幹細胞の増殖率が有意に抑制されることを明らかにした（*115,171）。を確認し（*36）、それによる神経新生シグナルの分子機構を検討した（論文投稿準備中)。平澤らは、青木グループ（放射線医学）と共同して、自閉症モデルマウスの拡散テンソル MRI 画像解析と透明化標本による３D 画像を比較検討して（Zeiss 共焦点レーザー顕微鏡７８０)、新たなバイオマーカー開発手法を提示した（*34)、ことは連携研究を重要視する本プロジェクトに沿った成果である。

樋野らは、Tsc2 分子の研究成果を生かし神経細胞における腫瘍化と幹細胞性の維持機構を解明することを目指した。本プロジェクトを通して、1)Eker ラット由来(*54,119,120,174,175)の胚盤胞より ES 細胞株を樹立し(*55)、２）多能性マーカー遺伝子発現や、胚様体および奇形腫における分化能を調べ、*Tsc2* ホモ欠損型細胞は野生型細胞と同様に三胚葉由来の組織形成能を示すが、Eker ラットの腎腫瘍に類似した異常腺管構造を発生すること（＊106,107,154,155,156)、を明らかにした。これまでに、神経細胞における腫瘍化と幹細胞性については、今後の課題として残った。これを実現するための一過程として、Tsc2-/- Eker ラット胎児線維芽細胞からの iPS 細胞樹立を試みているが、未だ条件決定に至っていない。しかしながら、この実験系が腫瘍抑制遺伝子変異とリプログラミングの分子機構の関連を調べる上で、大変有用であり、今後課題として、本モデルを用いた、「神経分化のオミックス解析と新規治療薬開発」を目指している。

新井（一）らは、グリオーマをモデルとして神経細胞の幹細胞性のメカニズムを標的とした治療を開発することを目指した。本プロジェクトでは、この目標に沿って研究を進め、１）悪性脳腫瘍の腫瘍化過程と腫瘍幹細胞の解析による治療介入の検討として、特に小児悪性脳腫瘍および成人神経膠腫を中心に、腫瘍細胞からの遺伝子情報の抽出と腫瘍幹細胞抽出培養の手技および方法を確立し、遺伝子も同定した。さらに、２）MRI 拡散強調画像と拡散 kurtosis 画像を用いて、正常圧水頭症における皮質脊髄路への影響を検討し、水頭症では、皮質脊髄路は神経線維と垂直方向に圧排され軸索が伸展された状態であることを明らかにした。(*123,178)

高久らは、骨髄幹細胞ニッチ環境の三次元可視化とその機能解明を行い、成体神経新生システムに応用することを目指した。実際には、３D イメージング手法により、ヘパラン硫酸プロテオグリカン（HSPG）が網状構造として存在することを示し、そのノックアウトマウスを用いて骨髄内の細胞構成につきフローサイトメトリーにて検証している。Agrin の欠損マウスの解析から、agrin は造血幹細胞維

持に重要な役割を持つことが明らかとなった。今後これらの成果をもとに、神経新生の理解に応用する予定である。

池田らは、聴覚・平衡覚にかかわる細胞品質管理機構の可視化、脳機能疾患との関連性を示すことを目指した。本プロジェクトでは、１）遺伝性難聴モデル Cx26 優性阻害変異マウスの新規病態 (*126) や Cx26 欠損マウスにおけるギャップ結合複合体の崩壊 (*127) という新たな分子病態を発見し，２）他の遺伝子 POU3F4 変異での難聴も共通の分子病態を持つことを明らかにした (*125)。さらに、３）骨髄間葉系幹細および人工多能性幹（iPS）細胞を用いた新規細胞移植法をアデノ随伴ウイルス（AAV）による Cx26 遺伝子導入と複合的に応用することにより高音領域を有意に聴力改善させることに成功した (*68)。また 新生仔マウス蝸牛への AAV 局所投与により Cx26 欠損マウスの聴力を有意に改善させることに成功した (*66)。池田らは、このように聴覚の分子病態像の一つを明らかにし、遺伝子治療の元となる実験も進め、治療法の開発の手がかりを得たことは、次に繋がるインパクトの高い成果と考える。

青木らのグループは、加齢・認知・発達障害による脳機能異常を示す新規画像解析法を開発することを目指した。実際、脳の加齢変化を in vivo で観察できる方法として脳 MRI の 3DT1 強調像が J-ADNI などの大規模スタディーで用いられているが、最近では拡散テンソルなどの拡散 MRI が脳の白質路の定量評価や connectivity の評価が可能なため、追加されることが多い（ADNI3)。青木らは、１）拡散テンソルや次世代拡散解析の手法の開発 (*153,210) 、validation(*90)を行い、２）種々の疾患における feasibility study(*149,151,140,186,207,209,246)を行い、脳の微細構造の変化を in vivo で種々の病態で観察できることを報告した。３）拡散 MRI の種々の手法は validation が必要なため、平澤、Kerever らの協力で MRI と透明化した脳との対比を種々の施設の MRI を借用して行った (*34) 。全脳解析や広い範囲の拡散テンソルトラクトグラフィーなど MRI が有用な点も多いと考えられた。このように、青木らは、目標に掲げた、診断技術の開発に大いに貢献した点は、インパクトの高い成果と考える。

北澤らは、発達障害性神経疾患の原因分子探索のための可視化をめざした。定量診断法の開発を目指し、自閉症スペクトラム障害やパーキンソン病における行動と脳機能の定量化・可視化の技術開発を進めることを研究内容とした。本プロジェクトでは、１）自閉症スペクトラム障害患者の解析で、映像視聴時に、自閉症スペクトラム障害患者では、瞬きが健常者と比較して同期していないことを解明した(*286)。また、２）触覚手がかりのみを用いて物体形状を判断する課題では、自閉症スペクトラム障害患者が健常者と比較して成績が優位であったことを解明した (*287)。実際に、北澤らは、自閉症スペクトラムの患者を解析して、診断のための成果を得た。**宇賀らは**、モデル動物での神経ネットワークを可視化するため、多点電極を用いた神経活動記録法を整備することを目指した。実際、マカクザルでの多点電極記録法を用いた柔軟な判断の神経基盤の解明を行い、相同な機能を持つ霊長類において、神経活動を直接計測し、その神経基盤の一端を明らかにした。

新井(平)らは、アルツハイマー病の発症分子機構を解明し、新規診断・治療技術を発展させることを目指した。本プロジェクトでは、**１)**AD 発症に関与が示されている Apolipoprotein E 遺伝子や Apolipoprotein D 遺伝子異常が発症リスクに影響を与えていること（＊193)、２）DLB 症例の幻視症状に Ramelteon が有効であること（＊195)、３）高齢者うつ病における AD 発症と血清アミロイド蛋白の相関があること（＊261）を報告した。さらに、４）アルコール多飲歴のあるアルツハイマー病患者群では、その発症要因に COMT 遺伝子、KIBRA 遺伝子の関与が示唆されたこと(*74,129)、５）レビー小体病患者群では、早期から heart rate variability(心拍変異度)の異常が認められること(*88)、６）寛解期にあるうつ病患者群では、高次機能障害が残存することが再発のリスクであること、を明らかにした(*137)。このように、新井らは、AD を中心に診断に繋がる一定の成果を得ることができた。

以上のように、本プロジェクトでは、各グループが申請書に記載した、たそれぞれの目標を達成すべく努力し、上記の成果を得た。

主要論文

CHCHD2 mutations in autosomal dominant late-onset Parkinson's disease: a genome-wide linkage and sequencing study

Manabu Funayama, Kenji Ohe, Taku Amo, Norihiko Furuya, Junji Yamaguchi, Shinji Saiki, Yuanzhe Li, Kotaro Ogaki, Maya Ando, Hiroyo Yoshino, Hiroyuki Tomiyama, Kenya Nishioka, Kazuko Hasegawa, Hidemoto Saiki, Wataru Satake, Kaoru Mogushi, Ryogen Sasaki, Yasumasa Kokubo, Shigeki Kuzuhara, Tatsushi Toda, Yoshikuni Mizuno, Yasuo Uchiyama, Kinji Ohno, Nobutaka Hattori

Summary

Background **Identification of causative genes in mendelian forms of Parkinson's disease is valuable for understanding the cause of the disease. We did genetic studies in a Japanese family with autosomal dominant Parkinson's disease to identify novel causative genes.**

Methods **We did a genome-wide linkage analysis on eight affected and five unaffected individuals from a family with autosomal dominant Parkinson's disease (family A). Subsequently, we did exome sequencing on three patients and whole-genome sequencing on one patient in family A. Variants were validated by Sanger sequencing in samples from patients with autosomal dominant Parkinson's disease, patients with sporadic Parkinson's disease, and controls. Participants were identified from the DNA bank of the Comprehensive Genetic Study on Parkinson's Disease and Related Disorders (Juntendo University School of Medicine, Tokyo, Japan) and were classified according to clinical information obtained by neurologists. Splicing abnormalities of *CHCHD2* mutants were analysed in SH-SY5Y cells. We used the Fisher's exact test to calculate the significance of allele frequencies between patients with sporadic Parkinson's disease and unaffected controls, and we calculated odds ratios and 95% CIs of minor alleles.**

Findings **We identified a missense mutation (*CHCHD2*, 182C>T, Thr61Ile) in family A by next-generation sequencing. We obtained samples from a further 340 index patients with autosomal dominant Parkinson's disease, 517 patients with sporadic Parkinson's disease, and 559 controls. Three *CHCHD2* mutations in four of 341 index cases from independent families with autosomal dominant Parkinson's disease were detected by *CHCHD2* mutation screening: 182C>T (Thr61Ile), 434G>A (Arg145Gln), and 300+5G>A. Two single nucleotide variants (–9T>G and 5C>T) in *CHCHD2* were confirmed to have different frequencies between sporadic Parkinson's disease and controls, with odds ratios of 2·51 (95% CI 1·48–4·24; p=0·0004) and 4·69 (1·59–13·83, p=0·0025), respectively. One single nucleotide polymorphism (rs816411) was found in *CHCHD2* from a previously reported genome-wide association study; however, there was no significant difference in its frequency between patients with Parkinson's disease and controls in a previously reported genome-wide association study (odds ratio 1·17, 95% CI 0·96–1·19; p=0·22). In SH-SY5Y cells, the 300+5G>A mutation but not the other two mutations caused exon 2 skipping.**

Interpretation ***CHCHD2* mutations are associated with, and might be a cause of, autosomal dominant Parkinson's disease. Further genetic studies in other populations are needed to confirm the pathogenicity of *CHCHD2* mutations in autosomal dominant Parkinson's disease and susceptibility for sporadic Parkinson's disease, and further functional studies are needed to understand how mutant CHCHD2 might play a part in the pathophysiology of Parkinson's disease.**

Funding **Japan Society for the Promotion of Science; Japanese Ministry of Education, Culture, Sports, Science and Technology; Japanese Ministry of Health, Labour and Welfare; Takeda Scientific Foundation; Cell Science Research Foundation; and Nakajima Foundation.**

Introduction

Parkinson's disease (MIM 168600), which is caused by the death of dopaminergic neurons in the substantia nigra, is the second most common neurodegenerative disorder. Symptoms mainly involve movement, including resting tremor, rigidity, bradykinesia, and postural instability. Most Parkinson's disease cases are sporadic; only about 11% of patients with Parkinson's disease have one or more first-degree relatives diagnosed with Parkinson's disease.[1] Nevertheless, identification of causative genes in rare familial cases can shed new light on the cause of Parkinson's disease. Most monogenic forms of neurodegenerative diseases are autosomal dominant; however, so far, only six genes have been identified for autosomal dominant forms of familial Parkinson's disease.[2–4]

Although the exact mechanisms of dopaminergic cell death are still unclear, discovery of causative genes for Parkinson's disease has enabled several processes to be proposed, such as impairments in protein degradation, oxidative stress, and mitochondrial dysfunction.[5] We aimed to identify a novel causative gene for familial

Lancet Neurol 2015

Published Online February 4, 2015 http://dx.doi.org/10.1016/S1474-4422(14)70266-2

Research Institute for Diseases of Old Age (M Funayama PhD, H Yoshino PhD, Prof Y Uchiyama MD, Prof N Hattori MD) **and Department of Research and Therapeutics for Movement Disorders** (N Furuya PhD), **Graduate School of Medicine, Juntendo University, Tokyo, Japan; Division of Neurogenetics, Center for Neurological Diseases and Cancer, Nagoya University Graduate School of Medicine, Nagoya, Japan** (K Ohe MD, Prof K Ohno MD)**; Training Program of Leaders for Integrated Medical System for Fruitful Healthy-Longevity Society (LIMS), Kyoto University Graduate School of Medicine, Kyoto, Japan** (K Ohe)**; Department of Applied Chemistry, National Defense Academy, Yokosuka, Japan** (T Amo PhD)**; Department of Cellular and Molecular Neuropathology** (J Yamaguchi MSc, Prof Y Uchiyama)**, Department of Neurology** (M Funayama, N Furuya, S Saiki MD, Y Li MD, K Ogaki MD, M Ando MD, H Tomiyama MD, K Nishioka MD, Prof Y Mizuno MD, Prof N Hattori)**, and Center for Genomic and Regenerative Medicine** (K Mogushi PhD)**, Juntendo University School of Medicine, Tokyo, Japan; Department of Neurology, National Hospital Organization, Sagamihara National Hospital, Sagamihara, Japan** (K Hasegawa MD)**; Department of Neurology, Tazuke Kofukai Medical Research Institute and Kitano Hospital, Osaka, Japan** (H Saiki MD)**; Division of**

Neurology and Molecular Brain Science, Kobe University Graduate School of Medicine, Kobe, Japan (W Satake MD, Prof T Toda MD)**; Department of Neurology, Mie University Graduate School of Medicine** (R Sasaki MD) **and Kii ALS/PDC Research Center, Mie University Graduate School of Regional Innovation Studies** (Prof Y Kokubo MD)**, Tsu, Japan; and Department of Neurology and Medicine, School of Nursing, Suzuka University of Medical Science, Suzuka, Japan** (Prof S Kuzuhara MD)

Correspondence to: Prof Nobutaka Hattori, Department of Neurology, Juntendo University School of Medicine, 2-1-1 Hongo, Bunkyo-ku, Tokyo 113-8421, Japan
nhattori@juntendo.ac.jp

Parkinson's disease by whole-genome and exome sequencing with next-generation sequencing.

Methods

Study design and participants

Participants were selected from the DNA bank of the Comprehensive Genetic Study on Parkinson's Disease and Related Disorders (CGSPD). The CGSPD bank in the Department of Neurology at Juntendo University School of Medicine (Tokyo, Japan) collects DNA and RNA of patients with typical Parkinson's disease, patients with atypical parkinsonism, and control participants for use in case-control studies, replication studies, and the discovery of novel genetic factors for Parkinson's disease. The CGSPD DNA bank stores samples from over 3500 patients with Parkinson's disease and about 800 controls.

We selected patient and control samples according to the following criteria: participants who had a completed clinical data sheet, participants with no known pathogenic mutations for Parkinson's disease, and participants with no parental consanguinity. Patients who seemed to have an autosomal recessive mode of inheritance were excluded, as were those with a family member with Parkinson's disease but an unknown mode of inheritance. We classified patients who had affected family members in at least two consecutive generations (including the index patient) as having autosomal dominant Parkinson's disease and the remaining patients as having sporadic Parkinson's disease. All patients were diagnosed by neurologists according to the Parkinson's UK Brain Bank clinical diagnostic criteria.[6] Controls, who were hospital staff and volunteers recruited during annual medical check-ups for metabolic syndrome, were confirmed by study neurologists (RS, YK, and SK) to be free of neurological disease. All participants were classed as Japanese according to self-reported racial and ethnic data.

For **ExonPrimer** see http://ihg.gsf.de/ihg/ExonPrimer.html

The study was approved by the ethics committee of Juntendo University School of Medicine and all participants gave written informed consent for inclusion in CGSPD, of which this study is a part.

Procedures

For one index patient in our DNA bank, DNA were available for patients with Parkinson's disease and unaffected family members in three generations (family A). Thus, we did linkage analysis and next-generation sequencing to identify a candidate gene in this family. We collected DNA samples from all members of family A who consented to genetic testing (eight affected and five unaffected individuals from family A; figure 1A) and confirmed that they did not have known Parkinson's disease causative gene mutations (appendix). All participants in family A were genotyped using a Genome-Wide human SNP Array 6.0 (Affymetrix, Santa Clara, CA, USA), and we did multipoint parametric linkage analyses with single nucleotide polymorphism (SNP) high throughput linkage analysis system (SNPHitLink)[7] and Merlin software.[8] We selected three patients (A-III-1, A-III-6, and A-III-17) with maximum genetic distance for exome sequencing and one patient (A-II-18) for whole-genome sequencing to complement the regions of difficulty captured by exome sequencing. We did whole-genome sequencing by 100 bp paired-end sequencing on HiSeq2000 (Illumina, San Diego, CA, USA). Sample preparation for exome sequencing was done using the SureSelect Human All Exon Kit (Agilent Technologies, Santa Clara, CA, USA), and samples were subjected to 75 bp paired-end sequencing on a GenomeAnalyzer IIx (Illumina). We did read alignment to the reference human genome (UCSC hg19) with Burrows-Wheeler Aligner version 0.5.9.[9] Single nucleotide variants (SNVs) and indels were detected in each participant by use of SAMtools version 0.1.16.[10] The variants identified by next-generation sequencing were filtered according to the following criteria: location in regions with positive log of odds greater than 1 (appendix); absence from dbSNP132; location in exons or splice sites; being carried in the heterozygous state; prediction to be non-synonymous or cause aberrant splicing; confirmation by Sanger sequencing; and not noted in our unaffected Japanese controls.

We analysed genomic sequences from index cases with autosomal dominant Parkinson's disease, patients with sporadic Parkinson's disease, and control participants by Sanger sequencing with the Applied Biosystems 3130 and 3730 Genetic Analyzer (Life Technologies, Carlsbad, CA, USA) to validate the candidate genes. Primers for Sanger sequencing were designed using ExonPrimer (appendix). The sample size needed for validation was decided on the basis of a previous genetic study that identified a causal gene for neurodegenerative disease and that included 212 controls and data from public databases for the validation of novel variants.[11] We used 1000 Genomes (1089 individuals), dbSNP138, the Human Genetic Variation Database (1208 individuals), and the National Heart, Lung, and Blood Institute (NHLBI) Exome Sequencing Project (ESP) database (6503 individuals) as public databases for the validation.

For cell culture and transfection, cells were seeded onto tissue culture plates for 5 days (SK-N-SH and SH-SY5Y cells) or 24 h (HeLa cells) before transfection. SH-SY5Y cells were used for splicing assays, SK-N-SH cells were used for localisation assays, and HeLa cells were used for splicing, localisation, and immunoelectron microscopy analyses. Cultured cells were transfected using Lipofectamine 2000 reagent (Life Technologies), according to the manufacturer's recommendations.

For splicing analysis, we cloned wild-type and mutant genomic *CHCHD2* DNA fragments (182C>T, 300+5G>A, and 434G>A) into pCR-Blunt II-TOPO vector (Life Technologies) and then transferred them to *Kpn*I-*Xho*I sites in pcDNA3.1/myc-His-A (Life Technologies), generating pcDNA3.1-CHCHD2 (wild-type, 182C>T, 300+5G>A, and 434G>A). *CHCHD2* exon 2 (wild-type

See Online for appendix

and 300+5G>A) with flanking intronic sequence (52 nucleotides upstream and 14 nucleotides downstream) was subcloned into pSPL3,[12] generating pSPL3-CHCHD2 (to analyse abberant exon 2 splicing of 300+5G>A). Total RNA was extracted 24 h after transfection using TRI Reagent (Life Technologies) followed by RQ1 DNase (Promega, Madison, WI, USA) treatment. cDNA was synthesised with random primers using Superscript II reverse transcriptase (Life Technologies) or ReverTra Ace (TOYOBO, Osaka, Japan). Two primer pairs were used for amplification to detect mutation-induced exon skipping of the transfected pcDNA splicing minigene (appendix). α-^{32}P-uridine triphosphate-labelled RNA was synthesised in the 5′ splice site of *CHCHD2* exon 2 using the Riboprobe in-vitro transcription system (Promega) with a PCR-amplified fragment, according to the manufacturer's instructions. We did an RNA-electrophoretic mobility

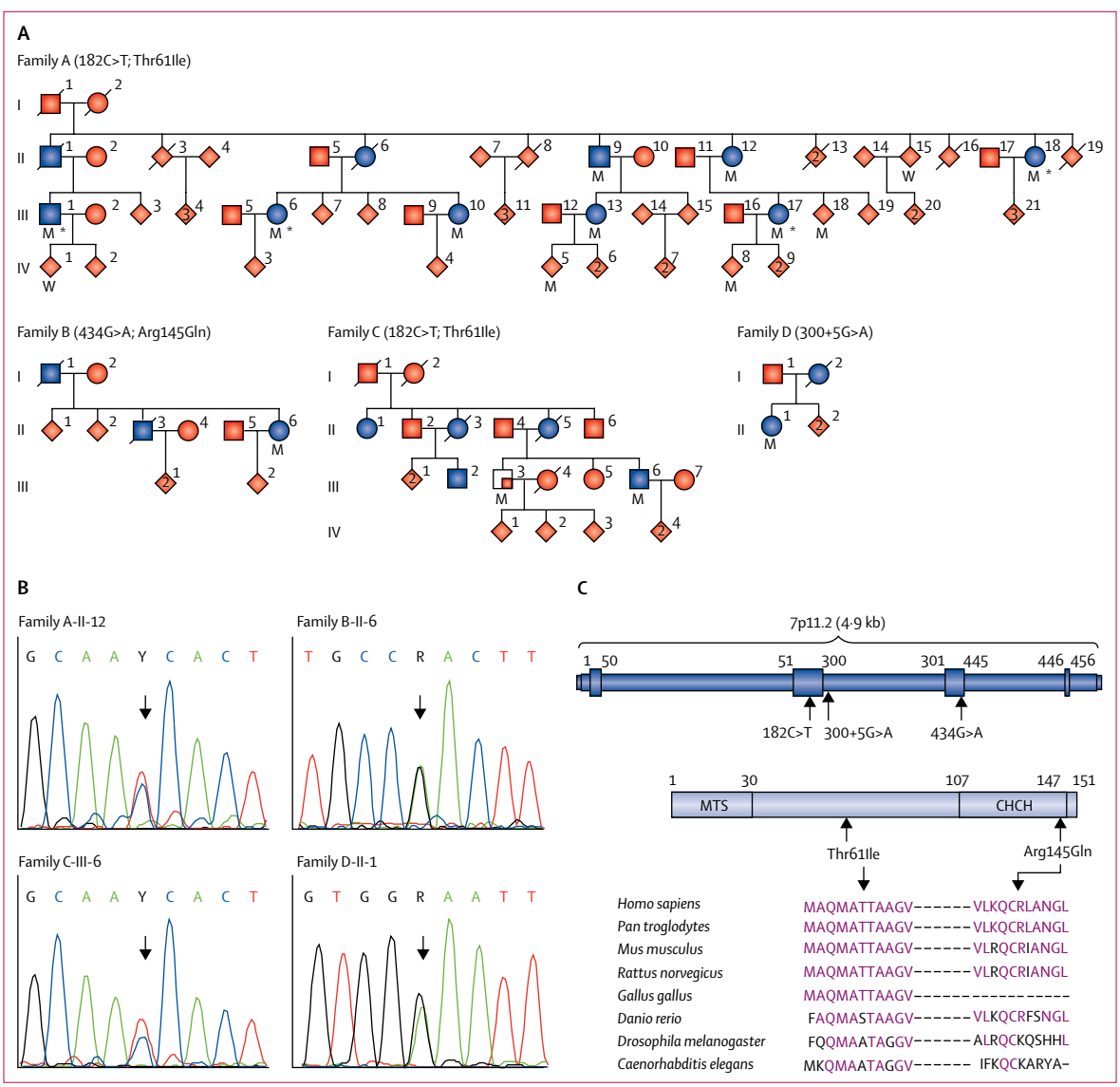

***Figure 1: CHCHD2* mutations in four Japanese families with autosomal dominant Parkinson's disease**
(A) Pedigrees of families with *CHCHD2* mutations. M=heterozygous *CHCHD2* mutation. W=wild-type. Blue symbols represent affected individuals. Red symbols represent unaffected individuals. Numbers within red symbols represent number of unaffected offspring. The quarter-filled symbol represents an individual with essential tremor. Squares represent men. Circles represent women. Diamonds represent sex masked to protect privacy of unaffected individuals. Lines through symbols represent deceased individuals. *Participants analysed by next-generation sequencing. (B) Sequence electropherograms of identified *CHCHD2* mutations. Arrows=mutated bases. (C) Schematic representation of the *CHCHD2* locus and CHCHD2 structure. Genomic locations of identified *CHCHD2* mutations are shown in the upper part of the panel. Boxes on the line represent exons. Aminoacid locations of mutations and sequence alignment with various species are shown in the lower part. NCBI RefSeq accession numbers are as follows: *Homo sapiens*, NP_057223.1; *Pan troglodytes*, XP_003318501.1; *Mus musculus*, NP_077128.2; *Rattus norvegicus*, NP_001015019.1; *Gallus gallus*, NP_001006218.1; *Danio rerio*, NP_957061.1; *Drosophila melanogaster*, NP_573196.1; and *Caenorhabditis elegans*, NP_497826.1. CHCH=coiled-coil-helix-coiled-coil-helix domain. MTS=mitochondrial targeting sequence.

shift assay as described by Ohe and colleagues.[13] The appendix provides probe information, details of antibodies used, and supplemental methods.

Statistical analysis

SNPs with a Hardy–Weinberg equilibrium p value greater than 0·05, a minimum call rate of 1 in controls, a maximum confidence greater than 0·02, a minimum interval of 100 kb, and a minimum minor allele frequency of 0·2 were selected using SNPHitLink. We did parametric multipoint linkage analysis using Merlin software, with a disease frequency of 0·0001. The phenotypes of unaffected siblings and children of patients were described as 0 (missing phenotypes). We did case-control studies using the genotype data of ten variants that were detected in sporadic Parkinson's disease or controls, or both. We used the Fisher's exact test to calculate the significance of allele frequencies between patients with sporadic Parkinson's disease and unaffected controls. We calculated odds ratios (ORs) and 95% CIs of minor alleles found in this study using JMP 8 (SAS Institute, Drive Cary, NC, USA). In association analyses, we used the Bonferroni correction to adjust for multiple testing (ten tests), after which p values of 0·005 or lower were regarded as statistically significant, as detailed in a previous study.[14]

Role of the funding source

The funders of the study had no role in study design, data collection, data analysis, data interpretation, or writing of the report. MF and NH had full access to all the data in the study and had final responsibility for the decision to submit for publication. The other authors had access to all data except for the sequence data acquired from next-generation sequencing, to protect the privacy of personal data.

	Number of participants	Age at onset (years)	Age at sampling (years)	Women:men ratio
Autosomal dominant Parkinson's disease	340	51·42 (13·81, 8–83)	57·99 (13·29, 17–85)	1·27
Sporadic Parkinson's disease	517	48·94 (15·11, 5–88)	57·38 (14·53, 12–92)	1·06
Controls	559	NA	58·74 (11·72, 28–89)	1·57

Data are mean (SD, range) unless otherwise specified. 340 patients were from different, independent, families, whereas family A included eight affected and five unaffected individuals; thus, family A is not included here. NA=not applicable.

Table 1: **Characteristics of participants for additional mutation screening**

	Number of variants
Total variants	2 312 760
In the linkage region	200 075
Not in db132	38 969
In exon or splice site	1018
Heterozygous	304
Predicted to be damaging*	10
Validated by Sanger sequencing	1
Not in 559 controls	1

*Predicted to be non-synonymous or cause aberrant splicing.

Table 2: **Variant filtering**

Results

The mean age at onset of the participating patients in family A (eight patients) was 55·5 years (SD 4·8; range 48–61). For validation and case-control analysis, we obtained DNA samples from 340 additional index patients with autosomal dominant Parkinson's disease, 517 patients with sporadic Parkinson's disease, and 559 controls (16 hospital staff and 543 volunteers recruited during medical check-ups; table 1).

Using next-generation sequencing, we detected a cumulative total of over 2·3 million variants in the four patients who were assessed (table 2; appendix). Our filtering criteria were satisfied by only one variant (table 2; appendix). The heterozygous 182C>T (Thr61Ile) mutation in coiled-coil-helix–coiled-coil-helix domain containing 2 (*CHCHD2*; RefSeq accession number NM_016139.2) cosegregated with Parkinson's disease in family A as assessed by Sanger sequencing of eight affected and five unaffected individuals (figure 1A and B). *CHCHD2* is located on chromosome 7p11.2 and contains four exons that encode 151 aminoacids with a predicted N-terminal mitochondrial targeting sequence (figure 1C). To validate the results of the initial genome-wide linkage analysis of family A (appendix), we did parametric multipoint linkage analysis using six microsatellites mapped to the 5′ and 3′ flanking regions of *CHCHD2*. Parametric multipoint linkage analysis by Merlin yielded a maximum log of odds score of 3·009 at D7S506 (appendix). Additionally, we did two-point linkage analysis using the 182C>T mutation as a genetic marker with a frequency of 0·0018 (1 in 560; 559 controls were sequenced in this study). As a result, the maximum log of odds score was 3·004.

To confirm whether *CHCHD2* is associated with autosomal dominant Parkinson's disease, we screened 340 index cases with autosomal dominant Parkinson's disease by Sanger sequencing and detected three additional patients with *CHCHD2* variants (families B–D; figure 1A and B). None of the three variants were noted in the 559 unaffected Japanese controls (table 3). None of the three variants detected in this study were found in 1000 Genomes, the Human Genetic Variation Database (table 3), the NHLBI ESP, or dbSNP138 (data not shown). Although the Thr61Ile variant was identified in patients from families A and C, independent founders were estimated by haplotype analysis (appendix). Altogether, we identified two missense mutations (182C>T, Thr61Ile, and 434G>A, Arg145Gln) and one splice-site mutation (300+5G>A) from four independent families with autosomal dominant Parkinson's disease.

	Variant		rs number	Alternative minor allele frequency					Sporadic PD *vs* controls	
	cDNA	Aminoacid		Autosomal dominant PD (n=340)	Sporadic PD (n=517)	Controls (n=559)	1000 Genomes	HGVD[15]	OR (95% CI)*	p value†
chr7:56174117	–11G>A	5′UTR	rs200226056	0·000	0·000	0·00099	0·0014	ND	..	..
chr7:56174115	–9T>G	5′UTR	rs10043	0·041	0·048	0·020	0·13	0·044	2·51 (1·48–4·24)	0·0004
chr7:56174102	5C>T	Pro2Leu	rs142444896	0·035	0·018	0·004	0·008	0·013	4·69 (1·59–13·83)	0·0025
chr7:56172172	51-4A>G	Splice site	Unknown	0.000	0·00097	0·005	ND	0·004	0·19 (0·02–1·66)	0·1189
chr7:56172171	51-3C>T‡	Splice site	rs201791644	0·002	0·00097	0·000	0·00046	0·003	..	..
chr7:56172037	182C>T	Thr61Ile	Novel	0·006	0·000	0·000	ND	ND	..	..
chr7:56171964	255T>A	Ser85Arg	rs182992574	0·002	0·000	0·000	0·00092	0·002	..	..
chr7:56171914	300+5G>A	Splice site	Novel	0·002	0·000	0·000	ND	ND	..	..
chr7:56170571	434G>A	Arg145Gln	Novel	0·002	0·000	0·000	ND	ND	..	..
chr7:56169419	*125G>A	3′UTR	rs8406	0·041	0·048	0·027	0·13	ND	1·85 (1·16–2·94)	0·0112

..=not calculated because the genotypes of all of the patients with sporadic PD or controls were the major allele. HGVD=Human Genetic Variation Database.[15] ND=no data were found in database. OR=odds ratio. PD=Parkinson's disease. UTR=untranslated region. *Calculated for the minor allele. †Fisher's exact test. ‡Did not cosegregate in an autosomal dominant PD family.

Table 3: **Alternative minor allele frequencies of identified *CHCHD2* variants**

Thr61 and Arg145 are conserved residues among vertebrates (figure 1C), suggesting these sites may be of functional importance. The substitutions Thr61Ile and Arg145Gln are predicted to be pathogenic or disease causing by Polyphen2,[16] MutationTaster,[17] and SIFT.[18] Furthermore, we analysed the 300+5G>A mutation using Human Splicing Finder (version 2.4.1)[19] to predict whether it affects *CHCHD2* splicing. The 300+5G>A mutation at the 5′ splice site decreased the Human Splicing Finder score from 88·2 to 76·0, and the MaxEnt score from 6·71 to 1·62. The SD-score[20] similarly predicted that 300+5G>A causes aberrant splicing and is likely to be a splicing mutation.

To assess whether any of the mutations affect splicing in the human SH-SY5Y neuroblastoma cell line, we cloned wild-type and mutant full-length (4921 bp) genomic DNA fragments into the pcDNA3.1 mammalian expression vector. As shown in figure 2A, exon 2 splicing was not affected by pcDNA-*CHCHD2* wild-type, 182C>T, or 434G>A, but the 300+5G>A mutation caused exon 2 skipping. None of the clones affected exon 3 splicing (appendix).

We further analysed the 300+5G>A mutation in HeLa cells by inserting *CHCHD2* exon 2 and flanking introns between the two proprietary constitutive exons of a modified exon-trapping vector, pSPL3. In this heterologous context, the 300+5G>A mutation caused *CHCHD2* exon 2 exclusion (figure 2B). The exon 2-excluded mRNA generated a premature termination codon 24 nucleotides upstream of the last exon junction, and thus should be resistant to non-sense-mediated mRNA decay. The band with intermediate mobility between the exon-containing and exon-skipped bands was sequenced and shown to result from activation of an upstream cryptic-5′ splice site at position 161 in *CHCHD2* exon 2. This mRNA was predicted to be subject to non-sense-mediated mRNA decay due to a premature termination codon generated 98 nucleotides upstream of the last exon junction. We tested U1 small nuclear ribonucleoprotein (snRNP) binding to wild-type and 300+5G>A mutant 5′ splice sites with RNA electrophoresis mobility shift assays. We noted decreased U1 snRNP-binding in HeLa nuclear extracts for 300+5G>A compared with wild-type 5′ splice site RNA (figure 2C, lanes 4 and 8). We verified the mobility of the complex using purified U1 snRNP.[13] Database searches for a truncating mutation in *CHCHD2* detected a non-sense SNV, Tyr99Stop, in 1000 Genomes and dbSNP138 databases, with an allelic frequency of one in 2178. No other protein-truncating mutations were registered in the Human Genetic Variation Database or the NHLBI ESP database. This is a rare non-sense SNV and we are unable to say whether it is related to pathogenicity in Parkinson's disease or other diseases.

To investigate whether *CHCHD2* might be a susceptibility gene for sporadic Parkinson's disease, we sequenced all *CHCHD2* exons, including splice junctions, in 517 patients with sporadic Parkinson's disease and 559 controls. Two SNVs had significantly different frequencies (–9T>G, OR 2·51, 95% CI 1·48–4·24, p=0·0004; and 5C>T, 4·69, 1·59–13·83, p=0·0025; table 3). The frequencies of several variants in the control participants were slightly different to those in public databases (table 3). To confirm the link between *CHCHD2* variants and risk of sporadic Parkinson's disease, we examined a previously reported genome-wide association study on sporadic Parkinson's disease in Japanese people.[21] Although one SNP (rs816411) was found on the intron of *CHCHD2*, there was no significant difference in its frequency between patients and control participants in this genome-wide association study (OR 1·17, 95% CI 0·96–1·19, p=0·22, Cochran-Armitage trend test).[21]

For the **UniProt database** see http://www.uniprot.org

CHCHD2 has a predicted N-terminal mitochondrial targeting sequence according to the UniProt database; therefore, we investigated whether CHCHD2 is located in mitochondria. Western blot analysis of subcellular fractions revealed that endogenous CHCHD2 is present in mitochondria (appendix). Furthermore, findings from confocal microscopy studies showed that exogenously expressed CHCHD2 localises to mitochondria, whereas CHCHD2 that has had the mitochondrial targeting sequence deleted does not (appendix). Immunoelectron microscopy and trypsin digestion assays showed that CHCHD2 is mainly localised in the intermembrane space (appendix). No localisation differences were noted between wild-type and missense mutants (appendix).

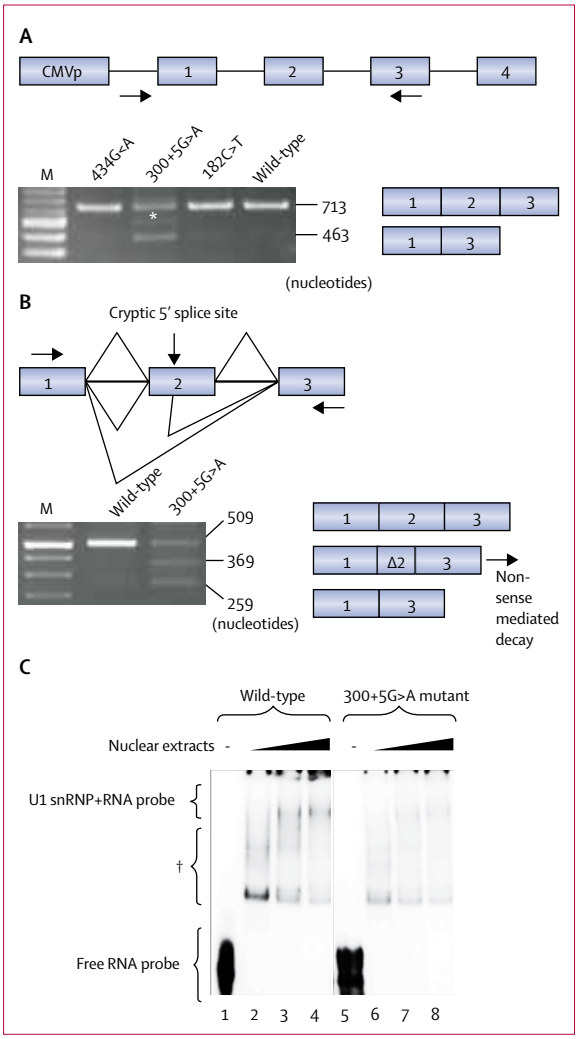

Figure 2: **Splicing assay of *CHCHD2* 300+5G>A**
(A) pcDNA-*CHCHD2*- 300+5G>A induced exon 2 skipping in SH-SY5Y cells, whereas 434G>A, 182C>T, or wild-type did not. *A faint band with intermediate mobility was present between exon 2-containing and exon 2-excluded bands. (B) pSPL3-*CHCHD2*-exon 2- 300+5G>A generated an exon 2-skipped transcript and a transcript with partial exon 2-inclusion via activation of an upstream cryptic 5′ splice site (arrow above exon 2). The arrows next to exons 1 and 3 show the position of primers used in the analyses. Triangles above the gene schematic denote normal splicing between exons 1 and 2, and 2 and 3, which results in a transcript with all three exons shown as a transcript bar below; the two triangles immediately below the line refer to the middle transcript bar with partial exon 2, and the lowest triangle refers to the lowest transcript bar with completely skipped exon 2. Numbers on the right side of the electrophoresis bands show their size. (C) Binding of *CHCHD2* exon 2-wild-type and 300+5G>A-mutant 5′ splice sites to U1 snRNP was measured using increasing amounts of HeLa nuclear extracts (3 μg, 6 μg, and 12 μg). Binding of the 5′ splice site probe to U1 snRNP was compromised with HeLa nuclear extracts. CMVp=cytomegalovirus promoter. M=100 bp DNA marker. snRNP=small nuclear ribonucleoprotein. †Bandshift of incomplete U1snRNP complexes.

Table 4 summarises the clinical features of the patients with *CHCHD2* mutations. The mean age at onset of Parkinson's disease was 56·2 years (SD 8·1, range 40–67). Although a patient from family C (C-III-3; figure 1), who was examined and from whom DNA was collected after additional mutation screening with 340 index cases, mainly showed only upper limb tremor-like essential tremor, other patients presented with typical parkinsonian features, including bradykinesia, rigidity, and gait disturbance, with symptoms responsive to levodopa that are consistent with the UK Brain Bank Parkinson's disease criteria.[6] Additionally, we detected three asymptomatic carriers with heterozygous 182C>T (Thr61Ile) mutations (A-III-18, A-IV-5, and A-IV-8). Their ages at sampling were 55 years, 56 years, and 35 years, respectively.

Discussion

In this study, we show that the heterozygous 182C>T (Thr61Ile) mutation in *CHCHD2* cosegregated with Parkinson's disease in a Japanese family with autosomal dominant Parkinson's disease. We identified three *CHCHD2* variants, none of which was present in controls, and our findings suggest that *CHCHD2* is a novel gene for autosomal dominant Parkinson's disease (panel).

CHCHD2 belongs to the CHCHD protein family, which are small proteins (about <18 kDa) containing twin cysteine-x9-cysteine motifs. CHCHD proteins localise to the mitochondrial intermembrane space via the Mia40 and Erv1 disulphide relay system.[24] Proteins with the cysteine-x9-cysteine motif are involved in biogenesis and regulation of enzymes in the mitochondrial respiratory chain, from yeast to mammals.[24] In particular, CHCHD2 seems to be closely linked to cytochrome c oxidase (COX), because COX2 protein concentrations and COX activity are affected by *CHCHD2* knock down.[22,23] Moreover, CHCHD2 acts as an antiapoptotic factor in cancer cells.[25] Although further functional studies are needed to investigate how mutant CHCHD2 plays a part in Parkinson's disease in mitochondria, the combination of previously reported CHCHD2 functions and our findings suggest that mitochondrial respiration is the link to Parkinson's disease.

We identified *CHCHD2* mutations not only in patients with Parkinson's disease, but also in a patient with essential tremor from the same family. Although we do not have any dopamine transporter scan data to check for any evidence of a dopaminergic deficit, an association

	A-II-9	A-II-12	A-II-18	A-III-1	A-III-6	A-III-10	A-III-13	A-III-17	B-II-6	C-III-3	C-III-6	D-II-1
Sex	M	W	W	M	W	W	W	W	W	M	M	W
Age at onset (years)	60	61	55	57	59	49	55	48	67	10	40	67
Age at examination (years)	83	81	69	67	63	50	57	58	72	50	43	68
Disease duration (years)	23	20	14	10	4	1	2	10	5	40	3	1
Initial symptoms	Resting tremor	Bradykinesia	Bradykinesia	Bradykinesia	Resting tremor	Resting tremor	Bradykinesia	Resting tremor	Resting tremor	Fine tremor	Resting tremor	Gait disturbance
Hoehn and Yahr stage (on/off)	5/5	4/ND	ND/ND	3/ND	3/3	2/ND	2/ND	3/ND	3/4	ND/ND	2/ND	ND/3
Resting tremor	+	+	+	+	+	+	–	+	+	+ (fine tremor)	+	–
Bradykinesia	+	+	+	+	+	+	+	+	–	–	+	+
Rigidity	+	+	+	+	+	+	+	+	–	–	+	+
Postural instability	–	–	+	+	+	–	+	+	–	–	–	+
Asymmetry at onset	+	–	+	+	+	+	+	–	+	–	+	+
Clinical response to levodopa	+	ND	+	+	+	ND	+	+	+	ND	+	ND
Wearing off	–	ND	+	–	+	ND	–	+	–	ND	–	ND
On/off phenomenon	–	ND	–	–	–	ND	–	–	+	ND	–	ND
Levodopa-induced dyskinesia	–	ND	+	–	+	ND	–	–	–	ND	–	ND
Hyper-reflexia	–	–	–	–	+	+	–	–	+	–	–	+
Orthostatic hypotension	–	–	–	–	+	–	+	–	–	–	–	–
Constipation	–	+	+	+	+	–	+	–	–	–	–	+
Depression	–	–	–	–	–	–	–	–	–	–	–	+
Smell disturbance	–	–	–	–	–	–	–	–	–	–	–	+

All patients also had gait disturbance. No patients had urinary urgency, hallucinations, delusion, dementia, mental retardation, rapid eye movement sleep behaviour disorder, or restless legs syndrome. M=man. ND=not done. W=woman. –=not present. +=present.

Table 4: **Clinical characteristics of patients with *CHCHD2* mutations**

between essential tremor and Parkinson's disease has been suggested by many clinical, epidemiological, neuroimaging, and genetic studies.[26] Additionally, a large family from Arkansas, USA, with Parkinson's disease, essential tremor, and restless legs syndrome has been reported.[27] *CHCHD2* mutations might be identified in this family, but to our knowledge the family has not been tested for *CHCHD2* mutations. We could not make any conclusions regarding the relation between essential tremor and *CHCHD2* mutations because only one patient with essential tremor and a *CHCHD2* mutation was detected in this study. Further studies are needed to identify whether *CHCHD2* is involved in both Parkinson's disease and essential tremor, or whether essential tremor happens to coincide with Parkinson's disease in the same family because of reduced penetrance. Recent studies have reported that *CHCHD2* expression is increased in neural stem cell lines derived from a patient with Huntington's disease (MIM 143100) and in HEK-293 cells under hypoxic conditions (4% oxygen).[22,28,29] Based on these observations, *CHCHD2* might be involved in various neurodegenerative diseases and cerebral infarction (MIM 601367).

Causative genes for mendelian forms of Parkinson's disease play an important part in mitochondrial clearance, and the clearance of damaged mitochondria is a key mechanism in the pathogenesis of Parkinson's disease and needs to be better understood. *PARK2* (MIM 602544) and *PINK1* (MIM 608309) are well known causative genes for early-onset autosomal recessive Parkinson's disease. Findings from functional studies have revealed that Parkin E3 ubiquitin ligase is fully activated by PINK1-dependent phosphorylation of both Parkin and ubiquitin on damaged mitochondria in the first phase of PINK1/parkin-mediated mitophagy.[30,31] MIX17 (YMR002W), the yeast homolog of CHCHD2, is regulated by the ubiquitin-proteasome system.[32] Although there has been no evidence of a relation between CHCHD2 and mitophagy, whether CHCHD2 is involved in PINK1/parkin-mediated mitophagy should be investigated.

Although the Thr61Ile mutation of *CHCHD2* was confirmed in independent probands and cosegregates with Parkinson's disease, the Arg145Gln and splicing (300+5G>A) mutations were found in only one patient in a small family with autosomal dominant Parkinson's disease. Whether or not these two mutations are linked to Parkinson's disease remains unclear. We would have liked to confirm these findings by undertaking mutation screening of patients and unaffected members of families B and D, but unfortunately the patients in this study declined access to other family members. Furthermore, we could not collect RNA samples from patients with 300+5G>A mutations, which produced the splicing abnormality in SH-SY5Y cells.

Our findings differ from those from a previously reported genome-wide association study.[21] We are

Panel: Research in context

Systematic review

We searched PubMed, in English, until Dec 11, 2014, for known genes for autosomal dominant Parkinson's disease using the terms "SNCA", "LRRK2", "VPS35", "EIF4G1", "DCTN1" and "DNAJC13". We also searched PubMed for studies published in English using the search terms "CHCHD2", "CHCHD", "Gene AND Parkinson's disease", "import AND assembly of IMS", and "Mic17" until Dec 11, 2014.

Interpretation

We show that (1) all affected individuals in family A who had genetic tests harboured a mutation in *CHCHD2*; (2) the log of odds score was greater than 3; (3) the detected mutations were not found in our control cohort or public variant databases; (4) different mutations in the same gene were found among four families with the same disease; and (5) all detected mutations were predicted to be pathogenic by a mutations algorithm. Although this is strong evidence that *CHCHD2* mutations are associated with Parkinson's disease, only one mutation (182C>T, Thr61Ile) was confirmed to cosegregate with autosomal dominant Parkinson's disease in this study. CHCHD2 has been implicated in mitochondrial respiration and is involved in cytochrome C oxidase activity,[22,23] but no previous reports had shown that *CHCHD2* mutations are associated with disease.

unsure whether our case-control study detected false positive results because of the small sample size or whether the genome-wide association study could not detect positive variants for Parkinson's disease risk because of the low allele frequencies of SNVs mapped on the *CHCHD2* region.

Contributors

MF, YM, KOhn, and NH were responsible for the concept and design of the study. MF, SS, and KOhe wrote the first draft of the paper. MF, KOhe, TA, NF, JY, SS, HY, WS, KM, KOhn, and NH revised the manuscript. MF, KOhe, TA, NF, JY, SS, YL, KOg, MA, HY, HT, KN, KH, HS, WS, KM, TT, YM, YU, KOhn, and NH acquired, analysed, and interpreted data. RS, YK, and SK collected and characterised control samples. All authors read and commented on drafts of the manuscript before submission.

Declaration of interests

MF and NH have a patent pending relating to this work. YM has received personal fees from FP Pharmaceutical, Otsuka Pharmaceutical, Abbvie, and Kyowa Hakko-Kirin. NH has received personal fees from Hisamitsu Pharmaceutical, Otsuka Pharmaceutical, Novartis Pharma, GlaxoSmithKline, Nippon Boehringer Ingelheim, FP Pharmaceutical, Dai-Nippon Sumitomo Pharma, Eisai, Kissei Pharmaceutical, Janssen Pharmaceutical, Nihon Medi-physics, Astellas Pharma, and Kyowa Hakko-Kirin. All other authors declare no competing interests.

Acknowledgments

We thank Yoko Imamichi for her assistance. We received a Grant-in-Aid for Scientific Research on Innovative Areas (25129707 to MF, 25111007 to SS, 25110720 to WS, 22129006 to TT, 23111004 to YU, 25118508 to KOhn, and 23111003 to NH), and a Grant-in-Aid for the Program for the Strategic Research Foundation at Private Universities from the Japanese Ministry of Education, Culture, Sports, Science and Technology; a Grant-in-Aid for Young Scientists (24790903 to TA, 25860725 to YL, 23689046 to SS, 25860726 to KN, 25713015 to WS, and, 26870175 to KM); a Grant-in-Aid for Challenging Exploratory Research (24659435 to SS, 25670420 to WS, 25670099 to YU and 25670164 to KOhn); a Grant-in-Aid for Scientific Research from the Japan Society for the Promotion of Science (25461291 to MF, 24591920 to KOhe, 24500868 to NF, 25305030 to YK, 24390221 to KOhn, and 24390224 to NH); a Grant-in-Aid for Health Labour Sciences Research Grant (H24-Nanchitou-Nan-Ippan-058 to YK, H26-Nanchitou-Nan-Ippan-085 to YK, TT, and NH; H23-Jitsuyouka-Nanbyou-Ippan-015 to TT; H26-Itaku-Nan-Ippan-037 to TT and NH; and H26-Itaku-Nan-Ippan-024 to KOhn) from the Japanese Ministry of Health, Labour and Welfare; and grants from the Life Science Foundation, the Takeda Scientific Foundation, the Cell Science Research Foundation, and the Nakajima Foundation (SS).

References

1 Shino MY, McGuire V, Van Den Eeden SK, et al. Familial aggregation of Parkinson's disease in a multiethnic community-based case-control study. *Mov Disord* 2010; **25:** 2587–94.
2 Singleton AB, Farrer MJ, Bonifati V. The genetics of Parkinson's disease: progress and therapeutic implications. *Mov Disord* 2013; **28:** 14–23.
3 Lautier C, Goldwurm S, Dürr A, et al. Mutations in the GIGYF2 (TNRC15) gene at the PARK11 locus in familial Parkinson disease. *Am J Hum Genet* 2008; **82:** 822–33.
4 Vilariño-Güell C, Rajput A, Milnerwood AJ, et al. DNAJC13 mutations in Parkinson disease. *Hum Mol Genet* 2014; **23:** 1794–801.
5 Schapira AH, Olanow CW, Greenamyre JT, Bezard E. Slowing of neurodegeneration in Parkinson's disease and Huntington's disease: future therapeutic perspectives. *Lancet* 2014; **384:** 545–55.
6 Hughes AJ, Daniel SE, Kilford L, Lees AJ. Accuracy of clinical diagnosis of idiopathic Parkinson's disease: a clinico-pathological study of 100 cases. *J Neurol Neurosurg Psychiatry* 1992; **55:** 181–84.
7 Fukuda Y, Nakahara Y, Date H, et al. SNP HiTLink: a high-throughput linkage analysis system employing dense SNP data. *BMC Bioinformatics* 2009; **10:** 121.
8 Abecasis GR, Cherny SS, Cookson WO, Cardon LR. Merlin—rapid analysis of dense genetic maps using sparse gene flow trees. *Nat Genet* 2002; **30:** 97–101.
9 Li H, Durbin R. Fast and accurate short read alignment with Burrows-Wheeler transform. *Bioinformatics* 2009; **25:** 1754–60.
10 Li H, Handsaker B, Wysoker A, et al. The Sequence Alignment/Map format and SAMtools. *Bioinformatics* 2009; **25:** 2078–79.
11 Saitsu H, Nishimura T, Muramatsu K, et al. De novo mutations in the autophagy gene *WDR45* cause static encephalopathy of childhood with neurodegeneration in adulthood. *Nat Genet* 2013; **45:** 445–49.
12 Masuda A, Shen XM, Ito M, Matsuura T, Engel AG, Ohno K. hnRNP H enhances skipping of a nonfunctional exon P3A in CHRNA1 and a mutation disrupting its binding causes congenital myasthenic syndrome. *Hum Mol Genet* 2008; **17:** 4022–35.
13 Ohe K, Mayeda A. HMGA1a trapping of U1 snRNP at an authentic 5′ splice site induces aberrant exon skipping in sporadic Alzheimer's disease. *Mol Cell Biol* 2010; **30:** 2220–28.
14 Sham PC, Purcell SM. Statistical power and significance testing in large-scale genetic studies. *Nat Rev Genet* 2014; **15:** 335–46.
15 Narahara M, Higasa K, Nakamura S, et al. Large-scale east-Asian eQTL mapping reveals novel candidate genes for LD mapping and the genomic landscape of transcriptional effects of sequence variants. *PLoS One* 2014; **9:** e100924.
16 Adzhubei IA, Schmidt S, Peshkin L, et al. A method and server for predicting damaging missense mutations. *Nat Methods* 2010; **7:** 248–49.
17 Schwarz JM, Rödelsperger C, Schuelke M, Seelow D. MutationTaster evaluates disease-causing potential of sequence alterations. *Nat Methods* 2010; **7:** 575–76.
18 Kumar P, Henikoff S, Ng PC. Predicting the effects of coding non-synonymous variants on protein function using the SIFT algorithm. *Nat Protoc* 2009; **4:** 1073–81.
19 Desmet, FO, Hamroun D, Lalande M, Collod-Beroud G, Claustres M, Beroud C. Human Splicing Finder: an online bioinformatics tool to predict splicing signals. *Nucleic Acid Res* 2009; **37:** e67.
20 Sahashi K, Masuda A, Matsuura T, et al. In vitro and in silico analysis reveals an efficient algorithm to predict the splicing consequences of mutations at the 5' splice sites. *Nucleic Acids Res* 2007; **35:** 5995–6003.
21 Satake W, Nakabayashi Y, Mizuta I, et al. Genome-wide association study identifies common variants at four loci as genetic risk factors for Parkinson's disease. *Nat Genet* 2009; **41:** 1303–07.
22 Aras S, Bai M, Lee I, Springett R, Hüttemann M, Grossman LI. MNRR1 (formerly CHCHD2) is a bi-organellar regulator of mitochondrial metabolism. *Mitochondrion* 2015 **20:** 43–51.

23 Baughman JM, Nilsson R, Gohil VM, Arlow DH, Gauhar Z, Mootha VK. A computational screen for regulators of oxidative phosphorylation implicates SLIRP in mitochondrial RNA homeostasis. *PLoS Genet* 2009; **5:** e1000590.

24 Longen S, Bien M, Bihlmaier K, et al. Systematic analysis of the twin cx(9)c protein family. *J Mol Biol* 2009; **393:** 356–68.

25 Liu Y, Clegg HV, Leslie PL, et al. CHCHD2 inhibits apoptosis by interacting with Bcl-x L to regulate Bax activation. *Cell Death Differ* 2014; published online Dec 5. DOI:10.1038/cdd.2014.194.

26 Fekete R, Jankovic J. Revisiting the relationship between essential tremor and Parkinson's disease. *Mov Disord* 2011; **26:** 391–98.

27 Puschmann A, Pfeiffer RF, Stoessl AJ, et al. A family with parkinsonism, essential tremor, restless legs syndrome, and depression. *Neurology* 2011; **76:** 1623–30.

28 Feyeux M, Bourgois-Rocha F, Redfern A, et al. Early transcriptional changes linked to naturally occurring Huntington's disease mutations in neural derivatives of human embryonic stem cells. *Hum Mol Genet* 2012; **21:** 3883–95.

29 Aras S, Pak O, Sommer N, et al. Oxygen-dependent expression of cytochrome c oxidase subunit 4-2 gene expression is mediated by transcription factors RBPJ, CXXC5 and CHCHD2. *Nucleic Acids Res* 2013; **41:** 2255–66.

30 Kondapalli C, Kazlauskaite A, Zhang N, et al. PINK1 is activated by mitochondrial membrane potential depolarization and stimulates Parkin E3 ligase activity by phosphorylating Serine 65. *Open Biol* 2012; **2:** 120080.

31 Koyano F, Okatsu K, Kosako H, et al. Ubiquitin is phosphorylated by PINK1 to activate parkin. *Nature* 2014; **510:** 162–66.

32 Bragoszewski P, Gornicka A, Sztolsztener ME, Chacinska A. The ubiquitin-proteasome system regulates mitochondrial intermembrane space proteins. *Mol Cell Biol* 2013; **33:** 2136–48.

The American Journal of Pathology, Vol. 185, No. 6, June 2015

ELSEVIER

The American Journal of
PATHOLOGY

ajp.amjpathol.org

NEUROBIOLOGY

Property of Lysosomal Storage Disease Associated with Midbrain Pathology in the Central Nervous System of *Lamp-2*—Deficient Mice

Akiko Furuta,* Hisae Kikuchi,† Hiromi Fujita,† Daisuke Yamada,† Yuuki Fujiwara,†‡ Tomohiro Kabuta,† Ichizo Nishino,§ Keiji Wada,† and Yasuo Uchiyama*

From the Department of Cellular and Molecular Neuropathology, Juntendo University Graduate School of Medicine, Tokyo; the Departments of Degenerative Neurological Diseases† and Neuromuscular Research,§ National Institute of Neuroscience, National Center of Neurology and Psychiatry, Kodaira, Tokyo; and the Department of Electrical Engineering and Bioscience,‡ Graduate School of Advanced Science and Engineering, Waseda University, Shinjuku, Tokyo, Japan*

Accepted for publication
February 12, 2015.

Address correspondence to Akiko Furuta, M.D., Ph.D., Department of Cellular and Molecular Neuropathology, Juntendo University Graduate School of Medicine, Hongo 2-1-1, Bunkyo-ku, Tokyo 113-8421, Japan.
E-mail: afuruta@juntendo.ac.jp.

Lysosome-associated membrane protein-2 (*LAMP-2*) is the gene responsible for Danon disease, which is characterized by cardiomyopathy, autophagic vacuolar myopathy, and variable mental retardation. To elucidate the function of LAMP-2 in the central nervous system, we investigated the neuropathological changes in *Lamp-2*—deficient mice. Immunohistochemical observations revealed that Lamp-1 and cathepsin D—positive lysosomal structures increased in the large neurons of the mouse brain. Ubiquitin-immunoreactive aggregates and concanavalin A—positive materials were detected in these neurons. By means of ultrastructural studies, we found various-shaped accumulations, including lipofuscin, glycolipid-like materials, and membranous structures, in the neurons and glial cells of *Lamp-2*—deficient brains. In deficient mice, glycogen granules accumulated in hepatocyte lysosomes but were not observed in neurons. These pathological features indicate lysosomal storage disease; however, the findings are unlikely a consequence of deficiency of a single lysosomal enzyme. Although previous study results have shown a large amount of autophagic vacuoles in parenchymal cells of the visceral organs, these findings were rarely detected in the brain tissue except for some axons in the substantia nigra, in which abundant activated microglial cells with increased lipid peroxidation were observed. Thus, LAMP-2 in the central nervous system has a possible role in the degradation of the various macromolecules in lysosomes and an additional function concerning protection from oxidative stress, especially in the substantia nigra. *(Am J Pathol 2015, 185: 1713—1723; http://dx.doi.org/10.1016/j.ajpath.2015.02.015)*

X-linked vacuolar cardiomyopathy and myopathy (Danon disease) are caused by the primary deficiency of lysosome-associated membrane protein-2 (LAMP-2).[1] Danon disease was first described as lysosomal glycogen storage disease with normal acid maltase because the cases closely resembled features of the infantile form of acid maltase deficiency (Pompe disease; glycogen storage disease type II), except that acid maltase activity was normal in the muscle.[2] The muscle malfunction of Danon disease has been well investigated with biopsied specimens characterized by autophagic vacuolar myopathy with sarcolemmal features.[3,4] Despite

Supported in part by Grant-in-Aid for Scientific Research (C) 23590244 from the Ministry of Education, Culture, Sports, Science and Technology (A.F.), Grant-in-Aid for Scientific Research 25290027 from the Japan Society for the Promotion of Science (K.W.), Grants-in-Aid for Scientific Research 05-32 from the Program for Promotion of Fundamental Studies in Health Sciences of the National Institute of Biomedical Innovation, Japan (K.W.), Grant-in-Aid for Creative Scientific Research 16GS0315 and Grants-in-Aid for Scientific Research on Innovative Areas 23111004 and 23110517 from the Japan Society for the Promotion of Science (Y.U.), and the Ministry of Education, Culture, Sports, Science and Technology, Japan-supported Program for the Strategic Research Foundation at Private Universities (Y.U.).

Disclosures: None declared.

http://dx.doi.org/10.1016/j.ajpath.2015.02.015

the presence of cognitive impairment in these patients, the neuropathological findings have not been investigated. Recently, we reported an autopsy case of genetically confirmed Danon disease and found distinct neuropathological changes, including features of lysosomal accumulation and senescence,[5] although the role of LAMP-2 in the central nervous system (CNS) is still under investigation.

The lysosomal membrane glycoproteins, LAMP-1 and LAMP-2, are type 1 membrane proteins that consist of a short cytoplasmic tail, one transmembrane domain, and a heavily glycosylated luminal domain.[6] Human LAMP-1 and LAMP-2 share 36.7% sequence identity and many structural and biochemical similarities.[7] The human *LAMP2* gene has three splice variants: *LAMP-2A*, *LAMP-2B*, and *LAMP-2C*.[6] LAMP-2A serves as a receptor for chaperone-mediated autophagy (CMA),[8] and CMA malfunction may be related to aging and lysosomal storage diseases, as well as neurodegenerative disorders such as Parkinson disease, Alzheimer disease, and polyglutamine disorders.[9] Fujiwara et al[10,11] discovered a novel function of LAMP-2C that mediates selective autophagy for nucleic acids. Despite the advancement of this field, results from relatively few studies confirm these functions of LAMP-2 *in vivo*.

Here, we examined the CNS of *Lamp-2*–deficient mice. All genes for *Lamp2* subtypes of the mice were deleted.[12] The neuropathological features were consistent with those of human Danon disease,[5] suggesting that *Lamp-2*–deficient mice are an appropriate *in vivo* model for human Danon disease and are, therefore, available to elucidate the mechanism and therapeutic intervention of the disease. Characteristic features, ie, accumulation of glycogen in lysosomes and enhancement of macroautophagy, are not noted in the brain. Different responses between neural cells of the CNS and parenchymal cells of visceral organs are discussed.

Materials and Methods

Experimental Animals

Littermates of male *Lamp2*-deficient mice and wild-type mice were used in this experiment. All of the animals were offspring from pairs of wild-type C57BL/6J male mice and hemizygote $Lamp2^{x/-}$ female mice because the *Lamp2* gene is located at X chromosome Xq24.[13] *Lamp-2*–deficient mice were provided by Dr. Paul Saftig[12] and were backcrossed with C57BL/6J mice >20 generations in our laboratory. The mice were maintained at Juntendo University and at the National Institute of Neuroscience, National Center of Neurology and Psychiatry (Tokyo, Japan). The experiments were approved by the institute's Animal Investigation Committee.

Antibodies

The following primary antibodies were used for Western blot analysis and immunohistochemical analysis: Lamp-2 (M3/84, rat monoclonal, 1:100, Abcam, Cambridge, UK), Lamp-1 (1D4B, rat monoclonal, 1:1000, Stressgen Bioreagents, Victoria, BC, Canada), cathepsin D (rabbit polyclonal, 1:1000, Dr. Yasuo Uchiyama), light chain 3 (LC3) (rabbit polyclonal, 1:1000, Abcam), α-synuclein (rabbit polyclonal, 1:1000 for Western blot analysis, 1:500 for immunohistochemical analysis, EMD Millipore, Billerica, MA), β-actin (mouse monoclonal, 1:10,000, Sigma-Aldrich, St. Louis, MO), ubiquitin (rabbit polyclonal, 1:200, Dako, Glostrup, Denmark), glial fibrillary acidic protein (rabbit polyclonal, 1:1000, Neomarkers, Fremont, CA), Mac-2 (rat monoclonal, 1:500, Cedarlane, Burlington, ON, Canada), GM130 (mouse monoclonal, 1:100, BD, Franklin Lakes, NJ), Rab7 (rabbit polyclonal, 1:100, Santa Cruz Biotechnology, Dallas, TX), microtubule-associated protein 2 (HM2, mouse monoclonal, 1:500, Sigma-Aldrich), ionized calcium-binding adapter molecule 1 (rabbit polyclonal, 1:200, Wako Pure Chemical Industries, Osaka, Japan), 2′,3′-cyclic-nucleotide 3′-phosphodiesterase (mouse monoclonal, 1:200, Covance, Princeton, NJ), SMI31 (mouse monoclonal, 1:1000, Covance), synaptophysin (mouse monoclonal, EMD Millipore), and 4 hydroxynonenal (mouse monoclonal, 1:200, Nikken Seil, Shizuoka, Japan).

Western Blot Analysis

Mice of both genotypes at the age of 12 weeks were deeply anesthetized with diethyl ether and decapitated, and then each tissue was dissected and lysed in radioimmunoprecipitation assay buffer [50 mmol/L Tris-HCl, pH 7.6; 150 mmol/L NaCl; 1% Triton X-100 (Nacalai Tesque, Kyoto, Japan); 0.5% sodium deoxycholate; 0.1% SDS] containing protease inhibitor cocktail (Nacalai Tesque) by means of a homogenizer (Polytron PT3100, Kinematica, Littau-Lucerne, Switzerland). After centrifuging at 10,500 × *g* for 10 minutes at 4°C, the protein concentration of the supernatants was determined by means of a microplate reader SpectraMax M2 (Molecular Devices Japan, Tokyo, Japan) by using bovine serum albumin as a standard. Proteins were separated on 10% or 15% SDS-polyacrylamide gels, transferred to polyvinylidene difluoride membranes (EMD Millipore), and incubated with 5% skim milk in phosphate-buffered saline (PBS) with Tween 20 [135 mmol/L PBS containing 0.05% Tween 20 (Nacalai Tesque)] for 1 hour at room temperature. The membranes were incubated overnight with each primary antibody, washed in PBS with Tween 20, and further incubated with anti-mouse or rabbit IgG horseradish peroxidase conjugate (1:1000, Dako). After washing in PBS with Tween 20, the membranes were developed with chemiluminescent horseradish peroxidase substrate (Immobilon Western, EMD Millipore) and analyzed using the LAS-4000 luminescent image analyzer (Fujifilm, Tokyo, Japan). β-Actin was used as a loading control. Statistical analyses ($n = 3$) were performed using a Student's *t*-test in Excel (Microsoft, Redmond, WA).

Immunohistochemical Analysis

For immunohistochemical studies, male mice of both genotypes at 12 and 32 weeks of age (total 12 mice) were deeply anesthetized with diethyl ether and perfused with 4% paraformaldehyde. The brain, heart, and liver were removed and postfixed overnight and then embedded in paraffin and sectioned. Sections (5 μm thick) were deparaffinized and treated with 1% hydrogen peroxide for 30 minutes, autoclaved at 105°C for 10 minutes, and then incubated with 5% normal serum in PBS (pH 7.4) for 1 hour at room temperature followed by incubation overnight at 4°C with each primary antibody. The sections were washed in PBS then incubated with biotinylated secondary antibodies diluted 1:500 in PBS containing 5% normal serum. The sections were treated with the VECTASTAIN Elite ABC kit (Vector Laboratories, Burlingame, CA) according to the manufacturer's protocol. Some sections were incubated with EnVision + System horseradish peroxidase—labeled polymer anti-rabbit or anti-mouse (Dako) as secondary antibodies. Sections were developed with 0.02% 3,3′-diaminobenzidine tetrahydrochloride solution containing 0.003% hydrogen peroxide. After visualization, sections were counterstained with hematoxylin.

For single or double immunofluorescent studies, sections were incubated with primary antibodies overnight, followed by secondary antibodies conjugated to Alexa Fluor 488 and/or 594 (1:200, Molecular Probes, Thermo Fisher Scientific, Eugene, OR) for 1 hour, then DAPI (250 nmol/L) for 5 minutes. Confocal microscopy was performed using the FluoView FV1000 confocal microscope system (Olympus, Tokyo, Japan). The percentage of intracellular particles that were immunoreactive for Lamp-2, Lamp-1, or Rab7 was counted in 100 particles of hippocampal large neurons for three candidates from each wild-type and *Lamp-2*—deficient mice groups.

Fluorescein Isothiocyanate Lectin Staining for Glycoanalysis

To identify the profiling of glycans for intracytoplasmic aggregates, we stained fluorescein isothiocyanate—conjugated lectins. Paraffin-embedded 4% paraformaldehyde-fixed sections were deparaffinized and incubated with 3% bovine serum albumin in PBSfor 1 hour at room temperature followed by incubation overnight at 4°C with each fluorescein isothiocyanate—conjugated lectin for concanavalin A, succinyl concanavalin A, wheat germ agglutinin, *Lens culinaris* agglutinin, *Psathyrella velutina* lectin, *Phaseolus vulgaris* erythrolectin, *Vicia villosa* lectin, *Galanthus nivalis* lectin, or *Bauhinia purpurea* lectin (Sigma-Aldrich) diluted 1:500 in 3% bovine serum albumin in PBS. The sections were observed with a confocal laser scanning microscope (FluoView FV1000, Olympus).

Electron Microscopic Analysis

Both genotypes of male mice at the age of 8 and 34 weeks (total eight mice) were deeply anesthetized with dimethyl ether and perfused with 2% paraformaldehyde and 2% glutaraldehyde in 0.1 mol/L phosphate buffer (pH 7.4). The brain and liver were removed, postfixed with the same fixative, and left overnight at 4°C. The specimens were trimmed and washed with PBS, incubated in phosphate-buffered 1% osmium tetroxide for 1 hour, dehydrated in ethanol, and embedded in resin (Epon 812, TAAB Laboratories Equipment, Berkshire, UK). Ultrathin sections were mounted on copper grids and stained with uranyl acetate and lead citrate. The sections were observed using an H-7000 electron microscope (Hitachi, Tokyo, Japan) or Tecnai transmission electron microscope (FEI, Hillsboro, OR).

Results

General Appearance of *Lamp-2*—Deficient Mice

The body weights of *Lamp-2*—deficient mice were significantly reduced when compared with those of wild-type mice at 16 weeks of age (Supplemental Figure S1). *Lamp-2*—deficient mice are reported to have increased mortality between 20 and 40 days of age.[12] In our observation, life spans of the mice that survived >40 days were also shortened (Supplemental Figure S2).

Localization of Lamp-2 in the CNS

Lamp-2 protein is abundant in the liver, and to a lesser extent, in the heart and brain of wild-type mice at the age of 12 weeks (Figure 1A). Expression of Lamp-2 was lacking in the *Lamp-2*—deficient mice (Figure 1, A—E). Double immunohistochemical analysis revealed that immunoreactivity for Lamp-2 largely colocalized in granules with immunoreactivity for Lamp-1 (89.3%), and some granules immunopositive for Lamp-2 colocalized with those for a late endosome marker, Rab7 (10.7%) (Figure 1, F and G). In the CNS, Lamp-2 was expressed ubiquitously in the neurons (microtubule-associated protein 2) (Figure 1, H—J), astrocytes (glial fibrillary acidic protein) (Figure 1, K—M), microglia (ionized calcium-binding adapter molecule 1) (Figure 1, N—P), and oligodendrocytes (2′,3′-cyclic-nucleotide 3′-phosphodiesterase) (Figure 1, Q—S), showing relatively prominent staining in large neurons (Figure 1D).

Morphological and Functional Changes in Lysosomes in *Lamp-2*—Deficient Mice

To study the structural and immunohistochemical changes in lysosomes, expression of another lysosomal membrane protein, Lamp-1 and a lysosomal aspartic proteinase, we examined cathepsin D. Western blot analysis showed that expression of Lamp-1 and cathepsin D was significantly increased in the brain of *Lamp-2*—deficient mice (Figure 2, A and B). Both Lamp-1 and cathepsin D—immunoreactive lysosomes were enlarged, especially in the large neurons of *Lamp-2*—deficient mice (Figure 2, C—H).

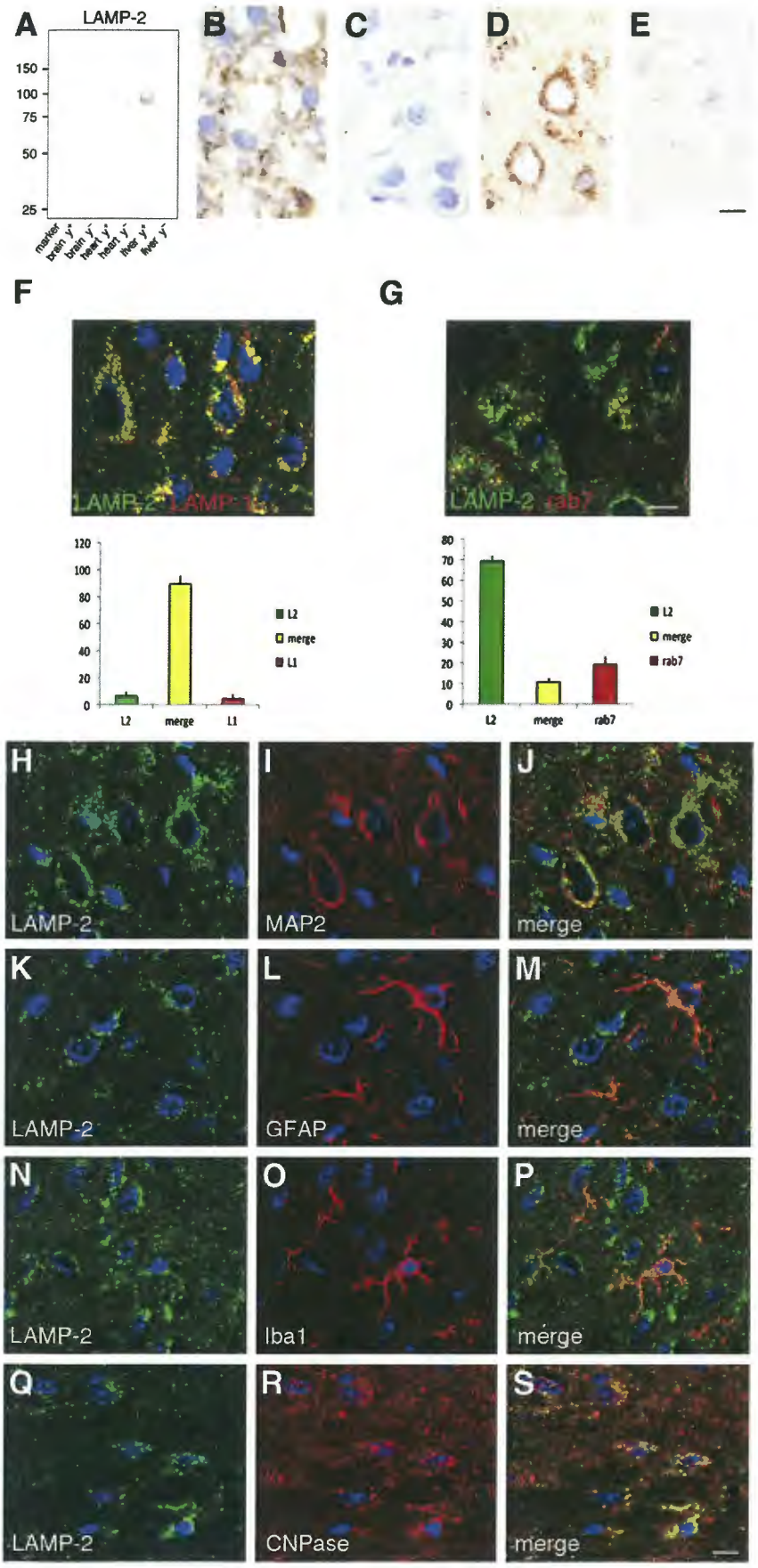

Figure 1 Lysosome-associated membrane protein-2 (Lamp-2) is expressed mainly in the lysosomes and enriched in the large neurons of the brain. **A:** Western blot analysis of Lamp-2 with lysates from the brain (30 μg per lane), heart (10 μg per lane), and liver (10 μg per lane) in wild-type and *Lamp-2*—deficient mice. The immunoreactive band for Lamp-2 is undetectable in *Lamp-2*—deficient mice. **B—E:** Immunoreactivity for Lamp-2 is observed in the liver (**B**) and neocortex (**D**) of the wild-type mice, whereas little immunoreactivity is seen in the liver (**C**) and neocortex (**E**) of the *Lamp-2*—deficient mice. **F** and **G:** Double immunohistochemical analysis reveals that Lamp-2 colocalizes with Lamp-1 (**F**; 89.3%) and with Rab7 (**G**; 10.7%). **H—S:** Lamp-2 partially colocalizes with microtubule-associated protein 2 (MAP2; **H—J**), glial fibrillary acidic protein (GFAP; **K—M**), ionized calcium-binding adapter molecule 1 (Iba1; **N—P**), and 2′,3′-cyclic-nucleotide 3′-phosphodiesterase (CNPase; **Q—S**). Scale bars: 10 μm.

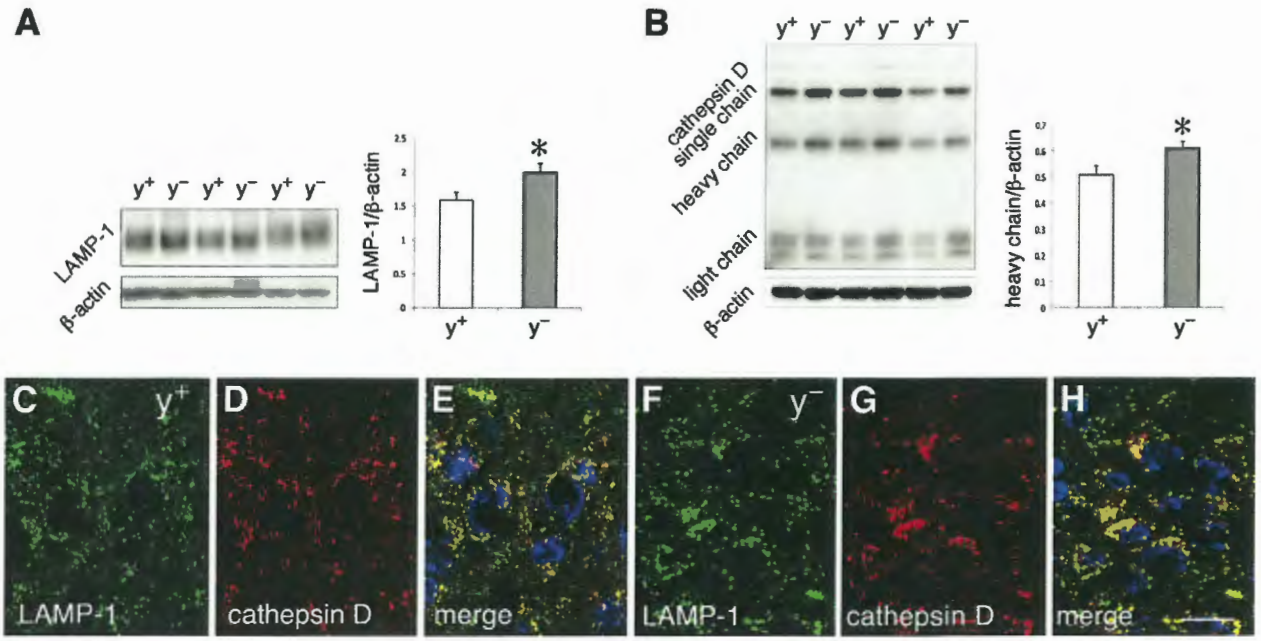

Figure 2 Expression of lysosome-associated membrane protein-2 (Lamp-1) and cathepsin D increases in the brain of *Lamp-2*—deficient mice. **A** and **B:** Western blot analysis reveals that expression of both Lamp-1 (**A**) and cathepsin D (**B**) significantly increases in the brain of *Lamp-2*—deficient mice (y^-) compared with in wild-type mice (y^+). Each value represents the means ± SEM. **C—H:** Double immunohistochemical analysis shows Lamp-1 and cathepsin D—immunoreactive lysosomes are enlarged in the CA3 of *Lamp-2*—deficient mice (12 weeks **F—H**). $^*P < 0.05$. Scale bar = 10 μm.

Electron microscopic observations showed primary lysosomes in wild-type mice (Figure 3, A and D) and accumulation of glycogen granules and membranous materials in lysosomes of the liver in *Lamp-2*—deficient mice at the age of 8 weeks (Figure 3, B and C). Although morphological changes in lysosomes were also observed in the hippocampal neurons of *Lamp-2*—deficient mice, glycogen granules did not accumulate in lysosomes (Figure 3, E and F). Lipofuscin in the large neurons was sometimes seen in the 34-week-old wild-type mice (Figure 3G). In addition to lipofuscin, vesicle-containing structures were seen in the cytoplasm of hippocampal neurons in *Lamp-2*—deficient mice (Figure 3H). Various materials accumulated not only in neurons but also in other cell types in the CNS of *Lamp-2*-deficient mice. Aggregates of membrane structures were detected in astrocytes (Figure 3I), whereas electron-dense materials packed in large granules that contained small electron-dense and -lucent vesicles were present in pericytes (Figure 3J).

To identify the properties of lysosomal accumulation, we performed immunohistochemical analysis for ubiquitin (Figure 4, A—D) and lectin staining (Figure 4, E and F). Ubiquitin-immunoreactive aggregates were found in the neuronal perikarya of the neocortex and hippocampal CA3 region (Figure 4, B and D). At confocal laser scanning microscopy, autofluorescence was detected in granular structures, some of which colocalized with positive staining for concanavalin A that interacts with D-mannose and D-glucose; these appeared more abundantly in the hippocampal CA3 neurons of *Lamp-2*—deficient mice than in those of wild-type mice (Figure 4, E and F).

Alterations of the Golgi Apparatus in Large Neurons

Besides morphological and functional changes in lysosomes, the structure of the Golgi apparatus was altered in the *Lamp-2*—deficient mice (Figure 5). Immunoreactivity for GM130, a Golgi matrix protein, increased in large neurons of *Lamp-2*—deficient mice at the age of 12 weeks (Figure 5, A and B). Ultrastructurally, the cisternae of the Golgi lamellae were dilated at the age of 8 weeks, and some cisternae took a circular form at the age of 32 weeks (Figure 5, C—F).

Cell-Type Specific Changes in Expression for LC3 in *Lamp-2*—Deficient Mice

Because skeletal muscle biopsy results for Danon disease exhibit autophagic vacuolar myopathy,[3,4] expression of LC3, a macroautophagy marker protein, was examined. Expression levels of LC3-II, a membrane-bound type, were significantly increased in the liver of the *Lamp-2*—deficient mice compared with that in control mice, as evidenced by Western blot analysis (Figure 6A) ($P < 0.05$), whereas expression levels of LC3-II were similar in the brain of both phenotypes (Figure 6B). Immunoreactivity for LC3 was detected in large granules in the cardiac myocytes and hepatocytes of *Lamp-2*—deficient mice (Figure 6, C—F). Electron micrographs showed a large amount of autophagic vacuoles and dense bodies in the liver of *Lamp-2*—deficient mice (Figure 6G). In the brain, expression of LC3 in *Lamp-2*—deficient mice was similar to that in wild-type mice

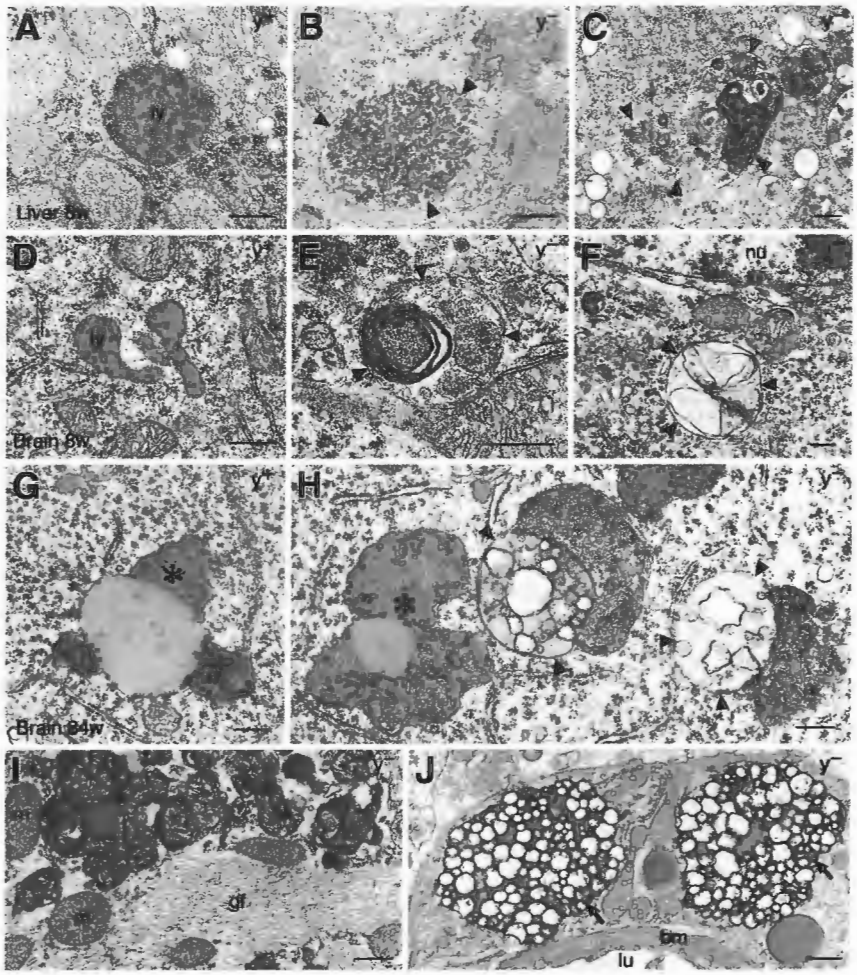

Figure 3 Ultrastructure of lysosomes and accumulation of various materials in the liver at 8 weeks (w) (**A—C**) and brain at 8 weeks (**D—F**) and 34 weeks (**G—J**) in wild-type mice (y^+; **A, D,** and **G**) and *Lamp-2*—deficient mice (y^-; **B, C, E, F,** and **H—J**). **A—C:** Lysosomes (ly) appear as electron-dense organelles in the liver of wild-type mice. Accumulations of glycogen (**arrowheads, B**) and membranous materials (**arrowheads, C**) in lysosomes are observed in the liver of *Lamp-2*—deficient mice. **D—F:** In contrast to lysosomes in neuronal cytoplasm of 8-week-old wild-type mice, lysosomal changes with membranous accumulations are found in the neurons of *Lamp-2*—deficient mice (**arrowheads, E** and **F**). **G—J:** In the brain at the age of 34 weeks, lipofuscin is observed in hippocampal CA3 neurons of both wild-type and *Lamp-2*—deficient mice (**asterisk, G** and **H**). In addition, vesicle-containing materials (**arrowheads, H**) are seen in the cytoplasm of neurons in *Lamp-2*—deficient mice. Membranous materials in astrocytes (**asterisks, I**) and electron-dense materials with small vesicles in pericytes (**arrows, J**) are also accumulated. bm, basement membrane; gf, glial filaments; lu, lumen; m, mitochondria; nu, nucleus. Scale bars: 250 nm (**A—H**); 500 nm (**I** and **J**).

(Figure 6, H and I) except for in the substantia nigra pars reticulata, where some LC3-immunoreactive large granular structures (Figure 6, J and K) and autophagic vacuole—containing axons were observed (Figure 6L). Although Western blot analysis for LC3-II with use of whole brain lysates did not show any difference between wild-type and *Lamp-2*—deficient mice (Figure 6B), analysis with midbrain lysates revealed increased expression of LC3-II in *Lamp-2*—deficient mice (Supplemental Figure S3A). Irrespective of such findings in the substantia nigra, neuronal loss of dopaminergic neurons was not observed with tyrosine hydroxylase staining (data not shown).

Midbrain Pathology with Extensive Glial Reactions

To further investigate the midbrain pathology, we performed immunohistochemical analysis for α-synuclein, one of the most important CMA substrates, and relevant proteins (Figure 7). First, we confirmed that the antibody for α-synuclein would not cross-react with β- or γ-synuclein (data not shown). Although expression of α-synuclein (Figure 7M) and a key regulator for CMA, Hsc70 (Supplemental Figure S3B), in the brain of *Lamp-2*—deficient mice was similar to that of wild-type mice, immunohistochemical studies revealed that large dotted structures positive for α-synuclein were found in the substantia nigra pars reticulata (Figure 7, A—D). Expression of α-synuclein in the dotted structures was not seen after proteinase K treatment (Supplemental Figure S4). Phosphorylated α-synuclein was not detected in the *Lamp-2*—deficient brain (data not shown). The structures were colocalized in part with SMI31, synaptophysin, Mac-2, and 4 hydroxynonenal (Figure 7, N—Q), suggesting that axons and activated microglia are associated with lipid peroxidation. In the substantia nigra, extensive reactive astrocytosis (Figure 7, E—H) and activated microglial infiltration (Figure 7, I—L) were observed.

Discussion

Expression of Lamps in the CNS

LAMPs are major components of lysosome membranes. In our observation, Lamp-2 was ubiquitously distributed to different cell types and enriched in the large neurons in the CNS. The majority of Lamp-2—immunoreactive vesicles colocalized with Lamp-1 in these large neurons. Although

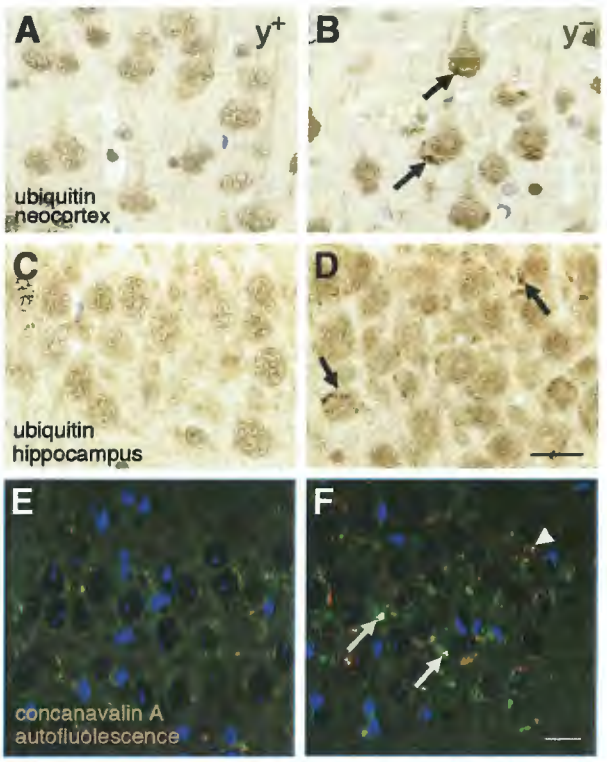

Figure 4 Expression of ubiquitin and concanavalin A increases in the large neurons of *Lamp-2*—deficient mice at the age of 32 weeks. **A**—**D:** Immunohistochemical images for ubiquitin in the neocortex (**A** and **B**) and hippocampal CA3 (**C** and **D**) in wild-type (y^+; **A** and **C**) and *Lamp-2*—deficient (y^-; **B** and **D**) mice reveals that large neurons in *Lamp-2*—deficient mice contain ubiquitin-immunoreactive aggregates (**arrows**, **B** and **D**). **E** and **F:** Concanavalin A staining (green; **arrows**, **F**) and autofluorescence (red; **arrowhead**, **F**) positive deposits in the hippocampal CA3 are abundant in *Lamp-2*—deficient mice (**F**) compared with those in wild-type mice (**E**). Scale bar = 20 μm.

Lamp-1—deficient mice exhibited mild gliosis and altered cathepsin D immunoreactivity in the brain with normal lysosomal morphology,[14] double deficiency of both Lamp-1 and Lamp-2 is embryonic lethal.[15] Because expression of Lamp-1 was elevated in the brains of *Lamp-2*—deficient mice, it is likely that these two proteins are interdependent in CNS neurons. Therefore, phenotypes of *Lamp-2*—deficient mice may indicate a specific function for Lamp-2.

Lamp-2—Deficient Mice as a Model of Lysosomal Storage Disease

Two-thirds of lysosomal storage diseases involve the CNS; however, their exact contribution to mental retardation remains unknown.[16] *LAMP-2*—deficient human Danon disease was first diagnosed as a glycogen storage disease because glycogen granules accumulated in the muscle.[2] We observed accumulations of electron-dense materials and ubiquitin-immunoreactive aggregates in the neuronal cytoplasm of the *Lamp-2*—deficient brain. Because various shaped materials accumulated in the different cell types of *Lamp-2*—deficient mice, these findings are likely not the consequence of deficiency of a single lysosomal enzyme but a disorder of enzyme trafficking or targeting or defective function of nonenzymatic lysosomal proteins. Results from functional studies have revealed that LAMP-2 deficiency leads to impaired recycling of 46-kDa mannose 6-phosphate receptors and partial mistargeting of lysosomal enzyme.[17] LAMP-2 also plays a critical role in endosomal cholesterol transport.[18] Our morphological studies are consistent with those in these reports.

Lectin staining revealed that intracellular aggregates were positive for concanavalin A, which binds D-mannose and

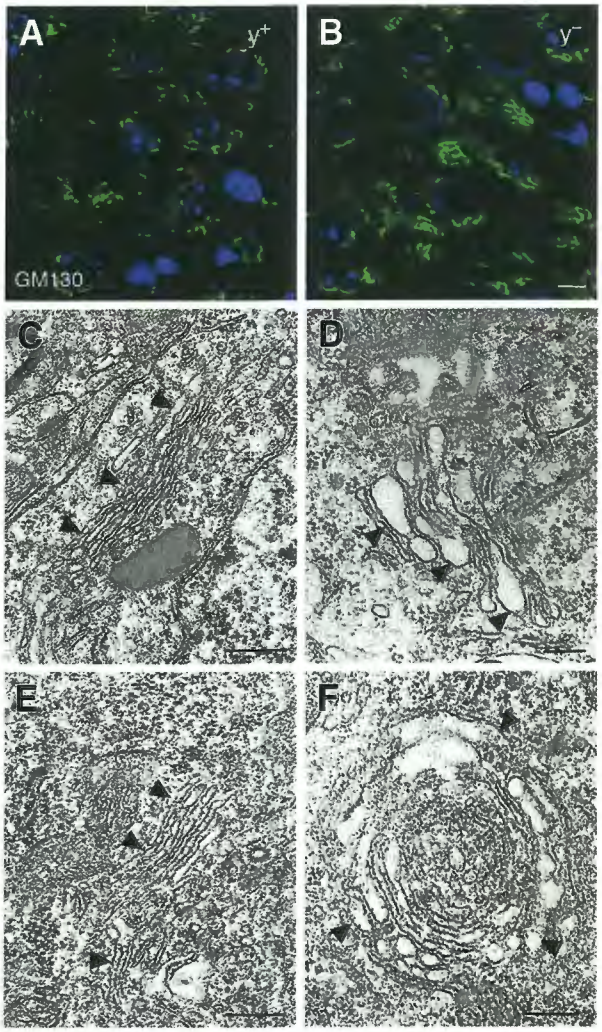

Figure 5 Structure of Golgi apparatus is altered in the neurons of *Lamp-2*—deficient mice. **A** and **B:** Immunoreactivity for GM130 is more abundant in the hippocampal pyramidal neurons of *Lamp-2*—deficient mice (y^-) than that in wild-type mice (y^+). **C**—**F:** Electron micrographs show that the Golgi apparatus appears as thin lamellar structures in the CA3 neurons of wild-type mice (8 weeks, **C**; 32 weeks, **E**; indicated by **arrowheads**). In the neurons of *Lamp-2*—deficient mice, dilatation of cisternae (8 weeks, **D**; indicated by **arrowheads**) and circular structures (32 weeks, **F**; indicated by **arrowheads**) are observed. Scale bars: 10 μm (**A** and **B**); 250 nm (**C**—**F**).

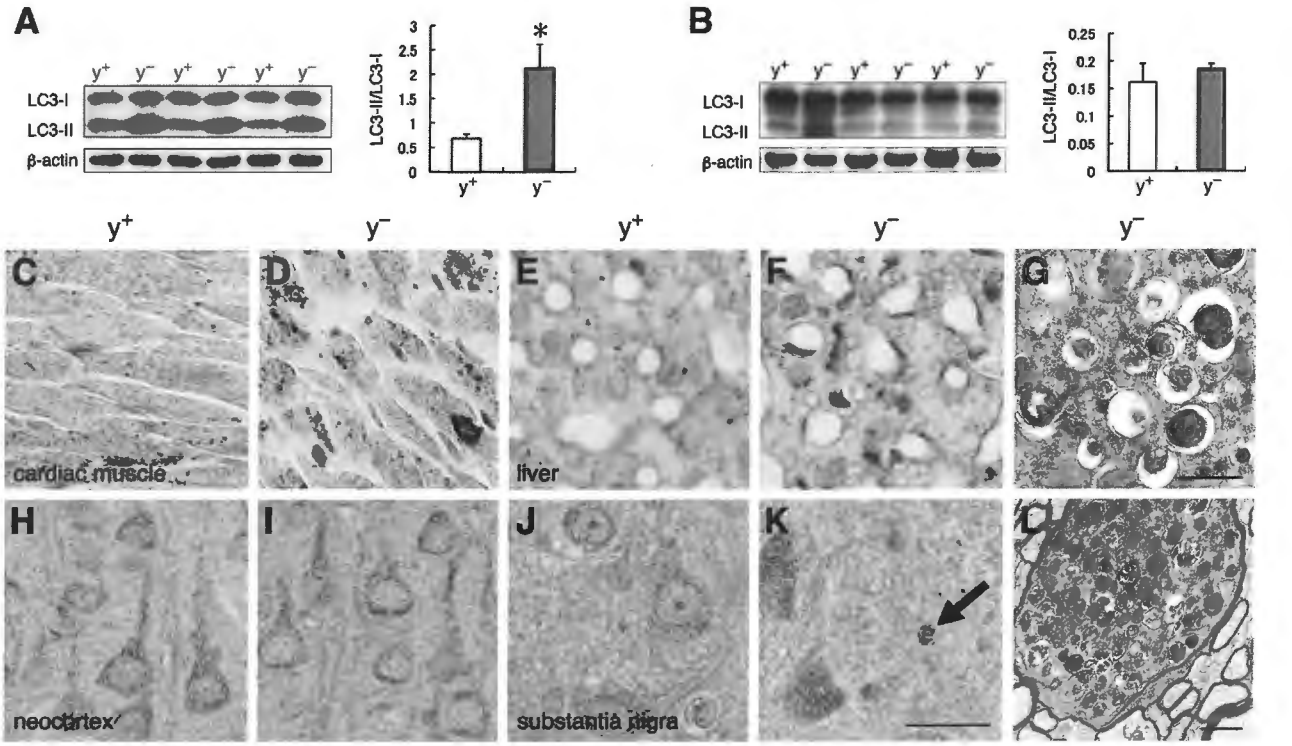

Figure 6 Macroautophagy is less affected in the brain of *Lamp-2*—deficient mice at the age of 12 weeks. **A** and **B:** Western blot analysis reveals that expression of membrane-bound type light chain 3 (LC3)-II significantly increases in the liver of *Lamp-2*—deficient mice (**A**); however, there is no significant change of LC3 expression in the central nervous system (CNS) (**B**). β-Actin was used as a loading control. **C**—**F** and **H**—**K:** Immunohistochemical analysis for LC3 in the cardiac muscle (**C** and **D**), liver (**E** and **F**), cerebral neocortex (**H** and **I**), and substantia nigra (**J** and **K**) of wild-type mice (y^+) and *Lamp-2*—deficient mice (y^-). In the *Lamp-2*—deficient mice, LC3-immunoreactive deposits are found in cardiac muscle (**D**) and hepatocytes (**F**); however, such immunoreactivity is not found in the CNS (**I** and **K**), except for LC3-positive large granular structures in the substantia nigra pars reticulata (**arrow**, **K**). **G** and **L:** Electron micrographs show accumulations of autophagic vacuoles and dense bodies in the hepatocytes (**G**) and axons of the substantia nigra (**L**) in *Lamp-2*—deficient mice. Each value represents the means ± SEM. $*P < 0.05$. Scale bars: 20 μm (**C**—**F**, **H**—**K**); 500 nm (**G**); 1 μm (**L**).

D-glucose. Virtanen et al[19] examined storage material in cultured fibroblasts by specific lectin binding in several lysosomal storage diseases and found that concanavalin A was positive for the materials in I-cell disease, which is a deficiency of phosphotransferase in the Golgi apparatus. In addition to the lysosomal changes, dysfunction of intracellular organelles, including the mitochondria, endoplasmic reticulum, and Golgi apparatus, has been described in lysosomal storage diseases.[16] Large neurons of *Lamp-2*—deficient mice showed increased immunoreactivity for GM130 and morphological changes in the cisternae of Golgi lamellae. Accumulation of GM130 leads to alterations of Golgi ribbon architecture.[20] Collectively, these findings in the CNS, in addition to growth retardation and low survival rate beyond postnatal day 40 (Supplemental Figures S1 and S2), are consistent with those of lysosomal storage disease. The main neuropathological feature—accumulation of lysosomes—is similar to that in human Danon disease.[5]

Region-Specific Differences in Macroautophagy

A large amount of autophagic vacuoles were found in the parenchymal cells of the various visceral organs both in Danon disease and *Lamp-2*—deficient mice.[1,12] Moreover, in the present study, we confirmed the elevation of autophagic activity in the heart and liver of *Lamp-2*—deficient mice. Multiple functions of LAMPs have been suggested so far: cholesterol traffic,[15] fusion of lysosomes with phagosomes,[21] and major histocompatibility complex class II antigen presentation.[22] Expression of LAMP-2 is also related to pathological processes such as neoplasms and inflammation,[23–25] although few experimental data on LAMP-2 have been shown in neuronal cells.

In the CNS, autophagic vacuoles were not observed in neurons except for some axons in the substantia nigra. Such cell-type specific alterations in the *Lamp-2*—deficient mice suggest that Lamp-2 may have distinct functions in each tissue or cell type. Constitutive autophagy is important in the CNS because lack of autophagy-related protein 7 or autophagy-related protein 5 in CNS tissue causes neuronal changes with ubiquitin-positive inclusion bodies.[26,27] It is uncertain why neurons do not show many autophagic vacuoles in the *Lamp-2*—deficient brains. Neurons may have protective mechanisms against excessive autophagic processes. Another possible mechanism may be that Lamp-2 has no effects on autophagosomes in neurons.

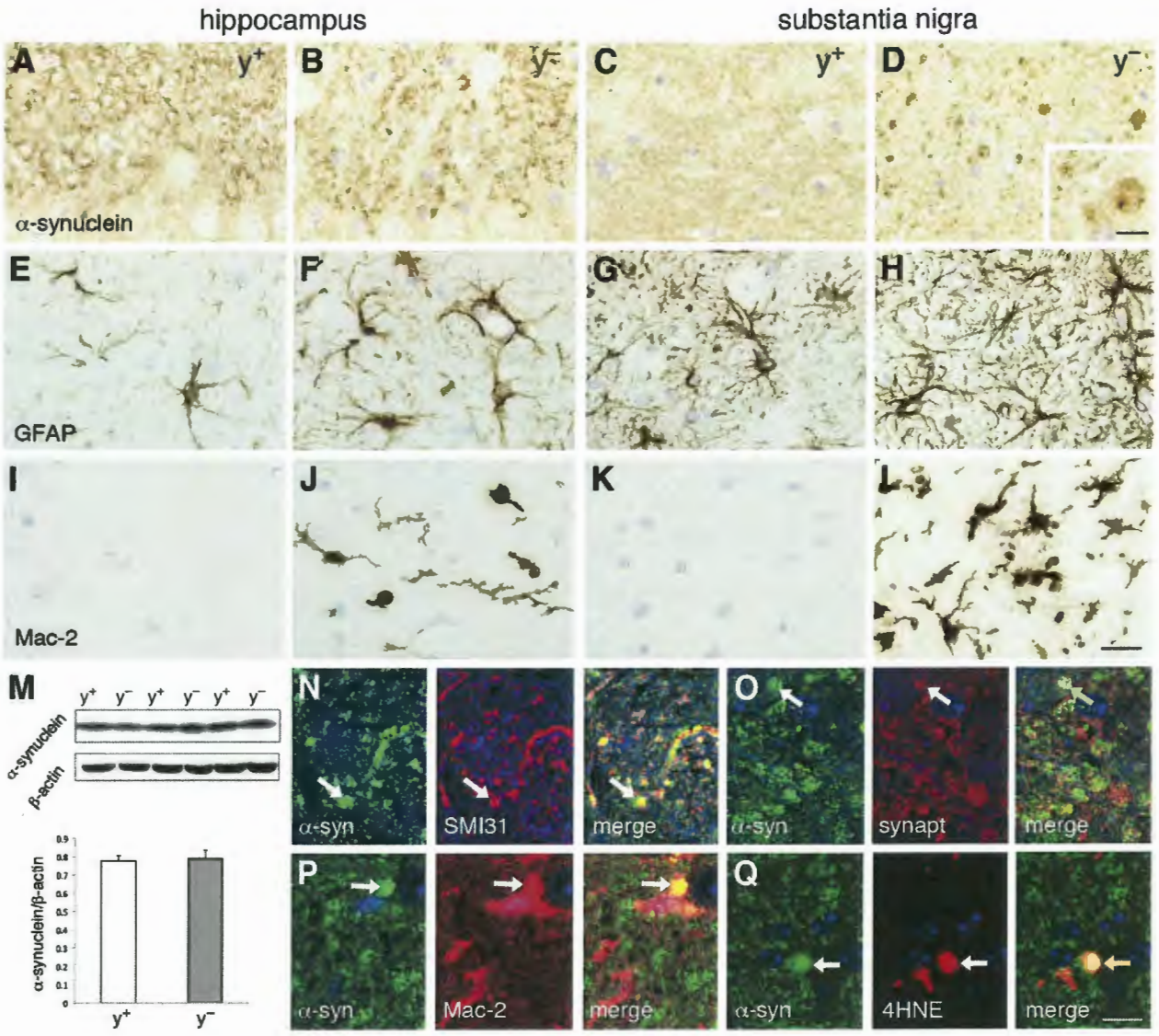

Figure 7 α-Synuclein–immunoreactive structures with extensive glial changes and oxidative stress are seen in the substantia nigra at the age of 12 weeks. **A–L:** Immunohistochemical analysis for α-synuclein (**A–D**), glial fibrillary acidic protein (GFAP; **E–H**), and Mac-2 (**I–L**) in the hippocampus (**A, B, E, F, I,** and **J**) and substantia nigra (**C, D, G, H, K,** and **L**). α-Synuclein–immunoreactive structures are found in the substantia nigra (**D; inset, D**). Extensive infiltration of GFAP-positive reactive astrocytes (**F** and **H**) and Mac-2-positive activated microglia (**J** and **L**) are seen in the substantia nigra and to a lesser extent in the hippocampus of *Lamp-2*–deficient mice. **M:** Western blot analysis for α-synuclein in the brain shows no significant changes between wild-type and *Lamp-2*–deficient mice. β-Actin is used as a loading control. **N–Q:** Double immunofluorescence for α-synuclein (α-syn; green) and SMI31 (**N**, red), synaptophysin (synapt; **O**, red), Mac-2 (**P**, red), and 4 hydroxynonenal (4HNE; **Q**, red) reveals colocalization of α-synuclein and each protein (**N–Q, arrows**). Scale bars: 20 μm (**A–L**); 10 μm (**inset, D**, and **N–Q**).

Evidence of Midbrain Pathology Associated with Excessive Glial Reactions and Lipid Peroxidation

We found intense astrocytic and microglial reactions in the substantia nigra and hippocampus of *Lamp-2*–deficient mice. Glial cells are also involved primarily in lysosomal storage diseases.[28] Accumulation of membranous materials was found in the astrocytes of *Lamp-2*–deficient mice (Figure 3I). Relationships between lysosomal disease and Parkinson disease, as well as oxidative stress, have been suggested.[29,30] Lysosomal dysfunction owing to LAMP-2 deficiency may cause lipid peroxidation, which enhances midbrain pathology; however, in *Lamp-2*–deficient mice, proteinase K–resistant α-synuclein did not accumulate, and a loss of dopaminergic neurons was not obvious.

Selective Degradation in the Lysosomes via Lamp-2 Subtypes

α-Synuclein is one of the most important substrates for CMA, and impaired degradation has been implicated in Parkinson disease.[31] Although some axonal swelling and

activated microglial cells were immunoreactive for α-synuclein, Western blot analysis for α-synuclein with whole brain or midbrain homogenates did not show any difference between wild-type and *Lamp-2*–deficient mice. Moreover, phosphorylated α-synuclein was not expressed in *Lamp-2*–deficient brains. Glyceraldehyde-3-phosphate dehydrogenase, another CMA substrate, also did not increase in *Lamp-2*–deficient mice.[10] CMA is activated during oxidative stress,[32] and protein degradation *in vivo* has an alternative pathway; eg, α-synuclein is also degraded by macroautophagy, the ubiquitin-proteasome system,[33] and other proteases such as calpains, neurosin, and metalloproteinases.[34] Although glyceraldehyde-3-phosphate dehydrogenase is known as a CMA substrate, 4 hydroxynonenal–modified glyceraldehyde-3-phosphate dehydrogenase could also be degraded by cathepsin G.[35] Therefore, a decrease in CMA activity owing to Lamp-2 deficiency could be compensated for by constitutive autophagy or the ubiquitin-proteasome system in the CNS of *Lamp-2*–deficient mice. Another possible explanation may be that unknown receptors are involved in CMA. LAMP-2C is mainly expressed in neurons in the CNS and mediates RNautophagy and DNautophagy.[10,11] Degradation of nucleic acids, in particular RNA, may be important in maintaining the neuronal environment. Another subtype, LAMP-2B is enriched in the liver and skeletal muscle. Because a patient with a frameshift of exon 9b shows full symptoms of Danon disease, including mental retardation, the function of LAMP-2B is crucial for Danon disease,[1] although the role of LAMP-2B in the CNS is unknown. Further investigation is required for understanding the specific function of each LAMP-2 subtype *in vivo*.

Acknowledgments

We thank Drs. Kiyomitsu Oyanagi, Kinuko Suzuki, and Koh Furuta for useful discussions, Drs. Paul Saftig and Judith Blanz for providing *Lamp-2*–deficient mice, Chihana Kabuta, Yohei Fujimoto, and Osamu Aizawa for technical assistance, and Robert Debold for editing the manuscript.

Supplemental Data

Supplemental material for this article can be found at *http://dx.doi.org/10.1016/j.ajpath.2015.02.015*.

References

1. Nishino I, Fu J, Tanji K, Yamada T, Shimojo S, Koori T, Mora M, Riggs JE, Oh SJ, Koga Y, Sue CM, Yamamoto A, Murakami N, Shanske S, Byrne E, Bonilla E, Nonaka I, DiMauro S, Hirano M: Primary LAMP-2 deficiency causes X-linked vacuolar cardiomyopathy and myopathy (Danon disease). Nature 2000, 406:906–910
2. Danon MJ, Oh SJ, DiMauro S, Manaligod JR, Eastwood A, Naidu S, Schliselfeld LH: Lysosomal glycogen storage disease with normal acid maltase. Neurology 1981, 31:51–57
3. Nishino I: Autophagic vacuolar myopathies. Curr Neurol Neurosci Rep 2003, 3:64–69
4. Sugie K, Noguchi S, Kozuka Y, Arikawa-Hirasawa E, Tanaka M, Yan C, Saftig P, von Figura K, Hirano M, Ueno S, Nonaka I, Nishino I: Autophagic vacuoles with sarcolemmal features delineate Danon disease and related myopathies. J Neuropathol Exp Neurol 2005, 64:513–522
5. Furuta A, Wakabayashi K, Haratake J, Kikuchi H, Kabuta T, Mori F, Tokonami F, Katsumi Y, Tanioka F, Uchiyama Y, Nishino I, Wada K: Lysosomal storage and advanced senescence in the brain of LAMP-2-deficient Danon disease. Acta Neuropathol 2013, 125:459–461
6. Eskelinen EL, Cuervo AM, Taylor MR, Nishino I, Blum JS, Dice JF, Sandoval IV, Lippincott-Schwartz J, August JT, Saftig P: Unifying nomenclature for the isoforms of the lysosomal membrane protein LAMP-2. Traffic 2005, 6:1058–1061
7. Fukuda M, Viitala J, Matteson J, Carlsson SR: Cloning of cDNAs encoding human lysosomal membrane glycoproteins, h-lamp-1 and h-lamp-2. Comparison of their deduced amino acid sequences. J Biol Chem 1988, 263:18920–18928
8. Cuervo AM, Dice JF: A receptor for the selective uptake and degradation of proteins by lysosomes. Science 1996, 273:501–503
9. Koga H, Cuervo AM: Chaperone-mediated autophagy dysfunction in the pathogenesis of neurodegeneration. Neurobiol Dis 2011, 43:29–37
10. Fujiwara Y, Furuta A, Kikuchi H, Aizawa S, Hatanaka Y, Konya C, Uchida K, Yoshimura A, Tamai Y, Wada K, Kabuta T: Discovery of a novel type of autophagy targeting RNA. Autophagy 2013, 9:403–409
11. Fujiwara Y, Kikuchi H, Aizawa S, Furuta A, Hatanaka Y, Konya C, Uchida K, Wada K, Kabuta T: Direct uptake and degradation of DNA by lysosomes. Autophagy 2013, 9:1167–1171
12. Tanaka Y, Guhde G, Suter A, Eskelinen EL, Hartmann D, Lüllmann-Rauch R, Janssen PM, Blanz J, von Figura K, Saftig P: Accumulation of autophagic vacuoles and cardiomyopathy in LAMP-2-deficient mice. Nature 2000, 406:902–906
13. Manoni M, Tribioli C, Lazzari B, DeBellis G, Patrosso C, Pergolizzi R, Pellegrini M, Maestrini E, Rivella S, Vezzoni P, et al: The nucleotide sequence of a CpG island demonstrates the presence of the first exon of the gene encoding the human lysosomal membrane protein lamp2 and assigns the gene to Xq24. Genomics 1991, 9:551–554
14. Andrejewski N, Punnonen EL, Guhde G, Tanaka Y, Lüllmann-Rauch R, Hartmann D, von Figura K, Saftig P: Normal lysosomal morphology and function in LAMP-1-deficient mice. J Biol Chem 1999, 274:12692–12701
15. Eskelinen EL, Schmidt CK, Neu S, Willenborg M, Fuertes G, Salvador N, Tanaka Y, Lüllmann-Rauch R, Hartmann D, Heeren J, von Figura K, Knecht E, Saftig P: Disturbed cholesterol traffic but normal proteolytic function in LAMP-1/LAMP-2 double-deficient fibroblasts. Mol Biol Cell 2004, 15:3132–3145
16. Bellettato CM, Scarpa M: Pathophysiology of neuropathic lysosomal storage disorders. J Inherit Metab Dis 2010, 33:347–362
17. Eskelinen EL, Illert AL, Tanaka Y, Schwarzmann G, Blanz J, von Figura K, Saftig P: Role of LAMP-2 lysosome biogenesis and autophagy. Mol Biol Cell 2002, 13:3355–3368
18. Schneede A, Schmidt CK, Hölttä-Vuori M, Heeren J, Willenborg M, Blanz J, Domanskyy M, Breiden B, Brodesser S, Landgrebe J, Sandhoff K, Ikonen E, Saftig P, Eskelinen EL: Role for LAMP-2 in endosomal cholesterol transport. J Cell Mol Med 2011, 15:280–295
19. Virtanen I, Ekblom P, Laurila P, Nordling S, Raivio KO, Aula P: Characterization of storage material in cultured fibroblasts by specific lectin binding in lysosomal storage diseases. Pediatr Res 1980, 14:1199–1203
20. Roy E, Bruyère J, Flamant P, Bigou S, Ausseil J, Vitry S, Heard JM: GM130 gain-of-function induces cell pathology in a model of lysosomal storage disease. Hum Mol Genet 2012, 21:1481–1495
21. Huynh KK, Eskelinen EL, Scott CC, Malevanets A, Saftig P, Grinstein S: LAMP proteins are required for fusion of lysosomes with phagosomes. EMBO J 2007, 26:313–324
22. Crotzer VL, Glosson N, Zhou D, Nishino I, Blum JS: LAMP-2-deficient human B cells exhibit altered MHC class II presentation of exogenous antigens. Immunology 2010, 131:318–330

23. Furuta K, Ikeda M, Nakayama Y, Nakamura K, Tanaka M, Hamasaki N, Himeno M, Hamilton SR, August JT: Expression of lysosome-associated membrane proteins in human colorectal neoplasms and inflammatory diseases. Am J Pathol 2001, 159:449–455
24. Fortunato F, Bürgers H, Bergmann F, Rieger P, Büchler MW, Kroemer G, Werner J: Impaired autolysosome formation correlates with Lamp-2 depletion: role of apoptosis, autophagy, and necrosis in pancreatitis. Gastroenterology 2009, 137:350–360, 360.e1-5
25. Peschel A, Basu N, Benharkou A, Brandes R, Brown M, Dieckmann R, Rees AJ, Kain R: Autoantibodies to hLAMP-2 in ANCA-negative pauci-immune focal necrotizing GN. J Am Soc Nephrol 2014, 25: 455–463
26. Komatsu M, Waguri S, Chiba T, Murata S, Iwata J, Tanida I, Ueno T, Koike M, Uchiyama Y, Kominami E, Tanaka K: Loss of autophagy in the central nervous system causes neurodegeneration in mice. Nature 2006, 441:880–884
27. Hara T, Nakamura K, Matsui M, Yamamoto A, Nakahara Y, Suzuki-Migishima R, Yokoyama M, Mishima K, Saito I, Okano H, Mizushima N: Suppression of basal autophagy in neural cells causes neurodegenerative disease in mice. Nature 2006, 441:885–889
28. Di Malta C, Fryer JD, Settembre C, Ballabio A: Astrocyte dysfunction triggers neurodegeneration in a lysosomal storage disorder. Proc Natl Acad Sci U S A 2012, 109:E2334–E2342
29. Dehay B, Martinez-Vicente M, Caldwell GA, Caldwell KA, Yue Z, Cookson MR, Klein C, Vila M, Bezard E: Lysosomal impairment in Parkinson's disease. Mov Disord 2013, 28:725–732
30. Subramaniam SR, Chesselet MF: Mitochondrial dysfunction and oxidative stress in Parkinson's disease. Prog Neurobiol 2013, 106-107: 17–32
31. Cuervo AM, Stefanis L, Fredenburg R, Lansbury PT, Sulzer D: Impaired degradation of mutant alpha-synuclein by chaperone-mediated autophagy. Science 2004, 305:1292–1295
32. Kiffin R, Christian C, Knecht E, Cuervo AM: Activation of chaperone-mediated autophagy during oxidative stress. Mol Biol Cell 2004, 15: 4829–4840
33. Vogiatzi T, Xilouri M, Vekrellis K, Stefanis L: Wild type alpha-synuclein is degraded by chaperone-mediated autophagy and macroautophagy in neuronal cells. J Biol Chem 2008, 283: 23542–23556
34. Xilouri M, Brekk OR, Stefanis L: Alpha-synuclein and protein degradation systems: a reciprocal relationship. Mol Neurobiol 2013, 47:537–551
35. Tsuchiya Y, Okuno Y, Hishinuma K, Ezaki A, Okada G, Yamaguchi M, Chikuma T, Hojo H: 4-Hydroxy-2-nonenal-modified glyceraldehyde-3-phosphate dehydrogenase is degraded by cathepsin G. Free Radic Biol Med 2007, 43:1604–1615

OPEN ACCESS Freely available online

PLOS | ONE

A Super-Ecliptic, pHluorin-mKate2, Tandem Fluorescent Protein-Tagged Human LC3 for the Monitoring of Mammalian Autophagy

Isei Tanida[1,2]*, Takashi Ueno[2], Yasuo Uchiyama[3]*

1 Department of Biochemistry and Cell Biology, National Institute of Infectious Diseases, Shinjuku, Tokyo, Japan, **2** Laboratory of Proteomics and Biomolecular Science, Research Support Center, Juntendo University Graduate School of Medicine, Bunkyo, Tokyo, Japan, **3** Department of Cellular and Molecular Neuropathology, Juntendo University School of Medicine, Bunkyo, Tokyo, Japan

Abstract

Tandem fluorescent protein-tagged LC3s that were comprised of a protein tag that emits green fluorescence (e.g., EGFP or mWasabi) fused with another tag that emits red fluorescence (e.g. mCherry or TagRFP) were used for monitoring the maturation step of mammalian autophagosomes. A critical point for this tandem fluorescent-tagged LC3 was the sensitivity of green fluorescence at an acidic pH. EGFP and mWasabi continue to emit a weak, but significant, fluorescence at a pH of approximately 6. To overcome this issue, we focused on super-ecliptic pHluorin, which is a more pH-sensitive GFP variation. The green fluorescence of EGFP and mWasabi in the cells was still observed at weakly acidic levels (pH 6.0–6.5). In contrast, the fluorescence of pHluorin was more significantly quenched at pH 6.5, and was almost completely abolished at pH 5.5–6.0, indicating that pHluorin is more suitable for use in a tandem fluorescent protein-tag for monitoring autophagy. A pHluorin-mKate2 tandem fluorescence protein showed pH-sensitive green fluorescence and pH-resistant far-red fluorescence. We therefore generated expression plasmids for pHluorin-mKate2-tagged human LC3 (PK-hLC3), which could be used as a modifier for LC3-lipidation. The green and far-red fluorescent puncta of PK-hLC3 were increased under starvation conditions. Puncta that were green-negative, but far-red positive, were increased when autolysosomes accumulated, but few puncta of the mutant PK-hLC3ΔG that lacked the carboxyl terminal Gly essential for autophagy were observed in the cells under the same conditions. These results indicated that the PK-hLC3 were more appropriate for the pH-sensitive monitoring of the maturation step of autophagosomes.

Citation: Tanida I, Ueno T, Uchiyama Y (2014) A Super-Ecliptic, pHluorin-mKate2, Tandem Fluorescent Protein-Tagged Human LC3 for the Monitoring of Mammalian Autophagy. PLoS ONE 9(10): e110600. doi:10.1371/journal.pone.0110600

Editor: Diane Bassham, Iowa State University, United States of America

Received June 3, 2014; **Accepted** September 24, 2014; **Published** October 23, 2014

Data Availability: The authors confirm that all data underlying the findings are fully available without restriction. All relevant data are within the paper.

Funding: This work was supported in part by Grants-in-Aids for Challenging Exploratory Research (10049091 to YU), Scientific Researches on Priority Areas "Proteolysis in the Regulation of Biological Processes" (18076005 to IT and TU), Scientific Researches on Innovative Area from the Japan Society for the Promotion of Science and the Ministry of Education, Science, Sports and Culture of Japan (MEXT) (23111004 and 23110517 to YU), a Grant-in-Aid for Scientific Research (C) (21570155 to IT), Grant-in-Aids for Scientific Research (B) (14380308 to TU; 23390041 to YU), a Grant-in-Aid for challenging Exploratory Research (25670099 to YU), a Grant-in-Aid for the "High-Tech Research Center" Project for Private Universities, a matching fund subsidy (TU) from the Ministry of Education, Culture, Sports, Science and Technology (MEXT) of Japan, the MEXT-supported Program for the Strategic Research Foundation at Private Universities (YU), a Grant-in-Aid for the Third-Term Comprehensive 10-Year Strategy for Cancer Control from the Ministry of Health, Labor and Welfare (16271401 to TU), a Research Grant from the Takeda Science Foundation (TU), and by the Ministry of Health, Labor and Welfare (IT). The funders had no role in study design, data collection and analysis, decision to publish, or preparation of the manuscript.

Competing Interests: The authors have declared that no competing interests exist.

* Email: tanida@nih.go.jp (IT); y-uchi@juntendo.ac.jp (YU)

Introduction

Autophagy is a bulk process involving degradation of the cytosol, which includes organelles [1,2]. During autophagy, isolation membranes/preautophagosomes are formed and elongated to engulf the cytosolic components. After elongation of the membranes, the isolation membranes are enclosed to form autophagosomes. Lysosomes are fused with autophagosomes to form autolysosomes. At this step, the lumenal pH of an autophagosome is acidified by the fusion with lysosomes, since the lumenal pH of a lysosome is 4.0–5.0. Intra-autophagosomal contents in autolysosomes are degraded by lysosomal hydrolases.

LC3 (microtubule-associated protein 1A and 1B light-chain 3; MAP-LC3/MAP1-LC3/MAP1A1B-LC3) is a unique modifier for ubiquitylation-like conjugation to localize to autophagosomes; LC3 is synthesized as proLC3. The carboxyl terminus of proLC3 is cleaved by Atg4B, a cysteine protease, to expose its carboxyl terminal Gly, which is essential for its conjugation reaction [3,4,5]. During autophagy, the cytosolic LC3 (LC3-I) is activated by Atg7 (an E1-like enzyme), transferred to Atg3 (an E2-like enzyme), and finally conjugated to phospholipids (phosphatidylethanolamine and/or phosphatidylserine) to form the LC3-phospholipid conjugate (LC3-II) [6,7,8,9]. LC3-II is localized to autophagosomes [4]. During the fusion of autophagosomes with lysosomes, LC3-II on the cytosolic face of autophagosomes is delipidated by Atg4B to form LC3-I, and LC3-II on the lumenal face of autophagosomes is degraded by lysosomal hydrolases. Therefore, LC3-II is a promising autophagosomal marker, and the lysosomal turnover of LC3-II is a marker for autophagic activity [4,10].

The formation of puncta by fluorescent protein-tagged LC3s (FP-LC3s) (EGFP-LC3, YFP-LC3, CFP-LC3, RFP-LC3, mCherry-LC3 and HcRed-LC3) are used to monitor autophagosome formation [11,12,13,14,15,16]. When autophagy is induced in the cells expressing a FP-LC3, the FP-LC3 is lipidated and localized to autophagosomes. The localization of FP-LC3 to autophagosomes was recognized as appropriate fluorescent puncta. Therefore, an increase in the puncta of FP-LC3 reflects an increase in autophagosomes and autolysosomes in the cells. The inhibition of lysosomal degradation results in a further increase in the puncta of FP-LC3, since autolysosomes in addition to autophagosomes are significantly accumulated by the inhibition [10]. An increase in the puncta that is promoted by the inhibition of lysosomal degradation is considered to be a reflection of autophagic flux. Mutant FP-LC3ΔGs (EGFP-LC3ΔG, YFP-LC3ΔG, CFP-LC3ΔG, and HcRed-LC3ΔG) lacking the carboxyl terminal Gly that is essential for LC3 lipidation are used as negative controls [12].

The FP-LC3s are considered to be a useful tool for the monitoring of autophagy, but there are limitations. It is difficult to use the fluorescent puncta of FP-LC3 to distinguish between autophagosomes and autolysosomes. In addition, Kimura *et al.* have found that EGFP-LC3 tends to lose fluorescence due to lysosomal acidic and degradative conditions, but mRFP-LC3 does not, indicating that the former mostly reflects only autophagosomes. The difference between EGFP-LC3 and mRFP-LC3 is a dependence on their pKa (pKa of EGFP is 5.9, and that of mRFP is 4.5) in addition to a degradation of EGFP by the lysosomal contents [17].

Based on these findings, a mRFP-EGFP tandem fluorescent protein-tagged LC3 (tfLC3) was generated for the monitoring of the autophagosomal maturation step [17]. The green and red double-positive fluorescent puncta of tfLC3 reflect autophagosomes (non-acidic compartments). The fluorescent puncta that are green-negative and red-positive reflect autolysosomes as acidic compartments, since EGFP tends to decrease its fluorescence at an acidic pH. An mCherry-EGFP-LC3 also was generated [18]. However, under acidic conditions (pH 4.0–5.0), EGFP has a weak fluorescence and acidic lysosomes [19,20]. Therefore, because the green fluorescent puncta of EGFP in tfLC3 still partially reflects autolysosomes in addition to autophagosomes, the pH-sensitivity of green fluorescent protein is important in order to distinguish autophagosomes from autolysosomes with a higher degree of sensitivity when using tfLC3.

To improve the problem of an EGFP-based tandem fluorescent protein-tagged LC3, mTagRFP-mWasabi-LC3 was generated, since the pKa of mWasabi (pKa = 6.5) was higher than that of EGFP [21,22]. mWasabi is a mutant of mTFP1, and mTFP1 is a pH-stable fluorescent protein [22,23]. As yet, the mechanism by which the fluorescence of mWasabi decreases under acidic conditions remains unknown, while the pKa of mWasabi has been reported.

The higher pH-sensitivity of a protein tag, which emits green fluorescence, is a critical point for monitoring the autophagosomal maturation step using a tandem, fluorescent, protein-tagged LC3. Therefore, we focused on a pH-sensitive green fluorescent protein, super-ecliptic pHluorin (pKa = 7.6) (hereafter simply referred to as pHluorin) [24]. In the present study, we compared the pH-sensitivity of green fluorescent proteins, including EGFP, mWasabi, and pHluorin, and constructed a tandem, fluorescent, protein-tagged LC3 and its negative control mutant using the most pH-sensitive protein.

Results

The pH-sensitive green fluorescent protein, super-ecliptic pHluorin, is the most sensitive to acidic pH among EGFP, mWasabi, and pHluorin

To investigate which is the most sensitive to acidic pH among EGFP, mWasabi, and pHluorin, we expressed each protein in Huh7.5.1 cells. After fixation, cells were permeabilized by digitonin, and the fluorescence derived from the fluorescent proteins was investigated with buffering at pH 5.5, 6.0, and 6.5 (Fig. 1). The fluorescence of EGFP was observed at pH 5.5–6.5 in addition to pH 7.2 (Fig. 1A–D). The fluorescence of mWasabi was slightly weakened at pH 6.0 and 6.5, and significantly decreased at pH 5.5 (Fig. 1E–H). The decreased fluorescence of mWasabi at pH 5.5 was detected via a three-time overexposure (Fig. 1H vs. I). The fluorescence of pHluorin was decreased significantly at pH 6.5, and little fluorescence was observed at pH 5.5 and 6.0 (Fig. 1L & M). A faint residual fluorescence of pHluorin was recognized at pH 5.5 and 6.0 using a ten-fold overexposure, while an autofluorescence of the cells was also observed under these conditions (Fig. 1O & P). When the pH of the incubated buffer was changed from 5.5 to 7.0, the green fluorescence of pHluorin was recovered (Fig. 1N). These results indicated that pHluorin was the most sensitive to an acidic pH among the three green fluorescent proteins.

pHluorin-mKate2 fusion protein showed pH-sensitive green fluorescence and pH-resistant far-red fluorescence

Using pHluorin, we next generated a plasmid for the expression of pHluorin-mKate2 (green and far-red) tandem fluorescent protein in order to investigate whether the pHluorin-mKate2 fusion protein would show both pH-sensitive green fluorescence derived from pHluorin and pH-stable far-red fluorescence derived from mKate2. A pHluorin-mKate2 protein was expressed in Huh7.5.1 cells. After fixation and mild permeabilization, cells were buffered at pH 5.5–6.5, and the green and far-red fluorescence of pHluorin-mKate2 in the cells was monitored (Fig. 2). As expected, both green and far-red fluorescence was observed at pH 7.2 (Fig. 2A & F). The green fluorescence of pHluorin-mKate2 was significantly decreased at pH 6.5 and almost completely abolished at pH 5.5, while its far-red fluorescence was easily detected even at pH 5.5 (Fig. 2B–D vs. G–I). The green fluorescence was recovered when cells were incubated at pH 7.2 after incubation at pH 5.5 (Fig. 2E). These results indicated that the tandem fluorescent protein, pHluorin-mKate2, showed pH-sensitive green and pH-resistant far-red fluorescence.

pHluorin-mKate2-tagged hLC3 is a modifier for LC3-conjugation

We then constructed mammalian expression plasmids for pHluorin-mKate2-tagged human LC3, which was designated PK-hLC3, under the control of a CAG promoter (Fig. 3A). As a negative control, we generated mammalian expression plasmids for PK-hLC3ΔG, which lacked the carboxyl terminal Gly of PK-hLC3 that is essential for LC3-lipidation. A FUGW plasmid is an expression vector for a 3rd generation lentiviral expression system [25]. A set of FUGW-based plasmids for the expression of PK-hLC3 and PK-hLC3ΔG under the control of the human polyubiquitin promoter C were also generated (Fig. 3B).

We investigated whether PK-hLC3 can form the Atg7-LC3 (E1-substrate) intermediate with Atg7 (Fig. 4A). When LC3-I activates Atg7, a transient E1-substrate intermediate is formed *via* a thioester bond between the carboxyl terminal Gly of LC3-I and

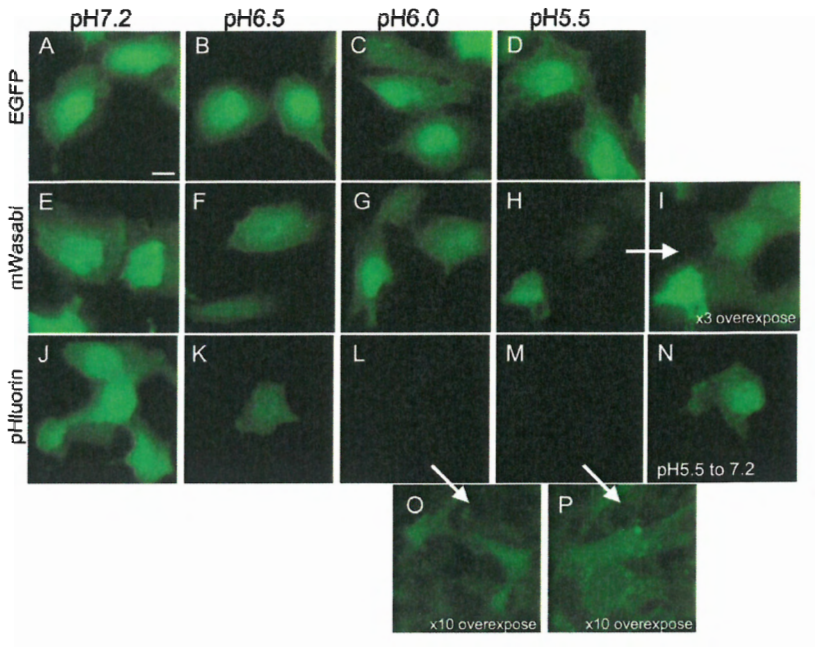

Figure 1. The pH sensitivity of the green fluorescence of EGFP, mWasabi, and super-ecliptic pHluorin. The green fluorescent proteins, EGFP (A–D), mWasabi (E–I), and pHluorin (J–P), were expressed in the Huh7.5.1 cells. After fixation and permeabilization of the cells, the cells were buffered at pH 5.5 (D, H, I, M, N, P), 6.0 (C, G, L, O), 6.5 (B, F, K), and 7.2 (A, E, J). The green fluorescence of each of the proteins in the cells were obtained with Biozero BZ-8000 using the filter set for GFP. The Images in A–H and J–N were obtained under the same conditions of the fluorescent microscope. The image in I was exposed three times longer than that in H. The images in O and P were exposed ten times longer than those in the respective L and M. In H, cells were incubated at pH 5.5, and the pH was changed to 7.2. Bar indicates 10 μm.
doi:10.1371/journal.pone.0110600.g001

the active site Cys^{572} in human Atg7 [7,26]. The E1-substrate intermediate is unstable in the cells, since LC3-I is transferred to Atg3. Therefore, an active site mutant $Atg7^{C572S}$ was employed to detect the formation of the E1-substrate intermediate. This mutant formed a stable E1-substrate intermediate *via* an *O*-ester bond with LC3 via Ser^{572} within the mutant $Atg7^{C572S}$ and the carboxyl Gly within LC3 [7]. The $Atg7^{C572S}$-LC3 intermediate was recognized by immunoblotting using appropriated antibodies when wild type PK-hLC3 was expressed together with $Atg7^{C572S}$ (Fig. 4A, wt). In contrast, no intermediate was recognized when PK-hLC3ΔG was expressed instead of the wild type (Fig. 4A, wt vs. ΔG).

We next investigated the formation of the E2-substrate intermediate of PK-hLC3 with Atg3 (Fig. 4B). The Atg3-LC3 (E2-substrate) intermediate is unstable, and LC3 is conjugated to phospholipids. To investigate if PK-hLC3 can form an E2-substrate intermediate with Atg3, we employed an active-site mutant, $Atg3^{C264S}$, since the mutant Atg3 forms an E2-substrate intermediate with LC3 *via* an *O*-ester bond instead of a thioester bond [8]. The Atg3-LC3 E2-substrate intermediate was recognized

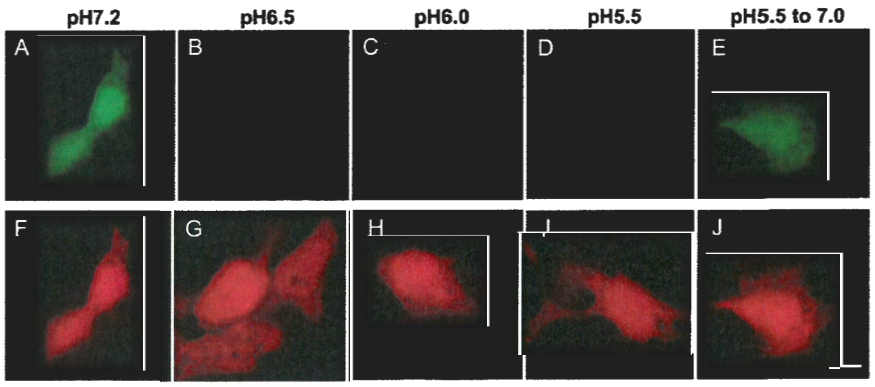

Figure 2. The pH sensitivity of the pHluorin-mKate2 tandem fluorescent protein. The pHluorin-mKate2 tandem fluorescent protein was expressed in the Huh7.5.1 cells. After fixation and permeabilization, cells were buffered at pH 5.5 (D, I), 6.0 (C, H), 6.5 (B, G), and 7.2 (A, F). In E and J, cells were incubated at pH 5.5, and the pH was changed to pH 7.2. The green and far-red fluorescence in the cells were obtained with Biozero BZ-8000 using the filter sets for GFP (A–E) and Texas Red (F–J). Bar indicates 10 μm.
doi:10.1371/journal.pone.0110600.g002

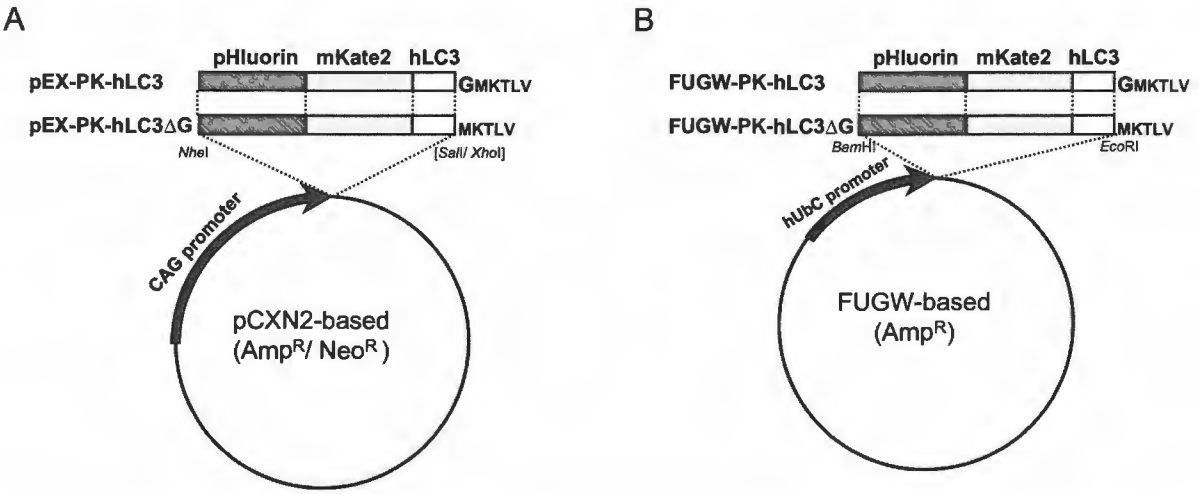

Figure 3. Schematic representation of the expression plasmids for wild type LC3 and mutant LC3ΔG fused to fluorescent proteins at the N-terminus. (A) The expression plasmids for wild type PK-hLC3, and mutant PK-hLC3ΔG under the control of chicken ß-actin (CAG) promoter. The name designated to each plasmid is shown in the left panel. (B) The plasmids for lentiviral packaging and transient expression for wild type PK-hLC3 and mutant PK-hLC3ΔG under the control of human polyubiquitin C (hUbC) promoter.
doi:10.1371/journal.pone.0110600.g003

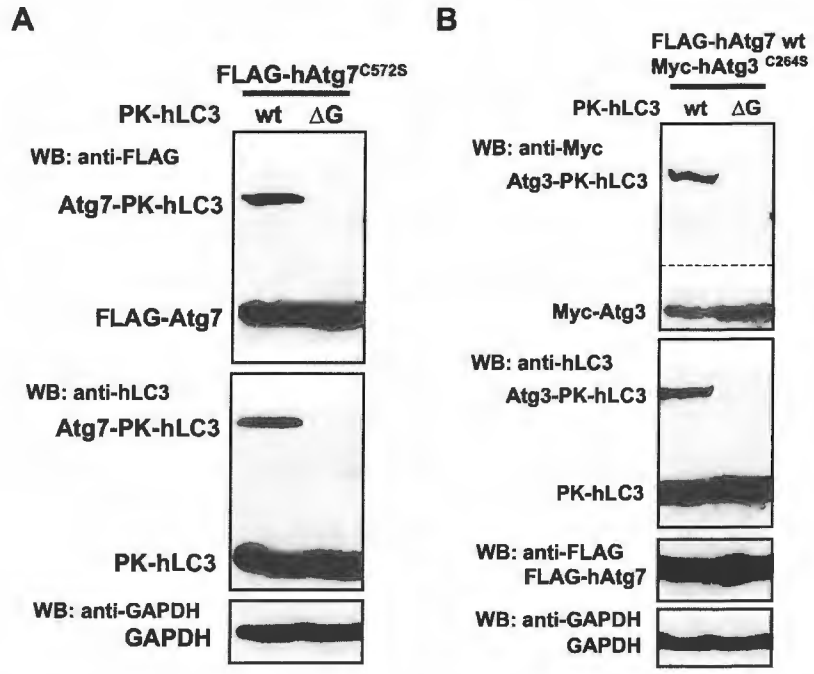

Figure 4. The formation of the Atg7-LC3 E1-substrate and Atg3-LC3 E2-substrate intermediates of fluorescent protein-tagged LC3. **(A)** The formation of the E1-substrate intermediate of Atg7 with fluorescent protein-tagged LC3s. The PK-hLC3 **(wt)** was expressed together with FLAG-tagged human **Atg7**^{C572S} in the Huh7.5.1 cells. After preparation of the cell lysate, total proteins were separated on SDS-PAGE. FLAG-hAtg7^{C572S} and PK-hLC3 were recognized by immunoblotting with appropriate antibodies. As a negative control, mutant PK-hLC3ΔG (**ΔG**) was expressed. As a loading control, **GAPDH** was employed. **Atg7-PK-hLC3** indicated the Atg7-LC3 (E1-substrate) intermediate with **Atg7**^{C572S}. **(B)** The formation of the E2-substrate intermediate of Atg3 with fluorescent protein-tagged LC3s. The PK-hLC3 was expressed together with wild type FLAG-tagged Atg7 and mutant Myc-Tagged Atg3^{C264S} in the Huh7.5.1 cells. FLAG-hAtg7, Myc-Atg3^{C264S} and PK-hLC3 were recognized by immunoblotting with appropriate antibodies. As a negative control, mutant PK-hLC3ΔG was expressed. As a loading control, **GAPDH** was employed. **Atg3-PK-hLC3** indicated their Atg7-LC3 intermediates with **Atg3**^{C264S}.
doi:10.1371/journal.pone.0110600.g004

when wild type PK-hLC3 was expressed together with $Atg3^{C264S}$ and Atg7. A scant level of E2-substrate intermediate was recognized when mutant PK-hLC3ΔG was expressed instead of wild type. These results demonstrated that PK-hLC3 has the ability to modify LC3-conjugation, and that mutant PK-hLC3ΔG is a suitable negative control of PK-hLC3.

Puncta of PK-hLC3 were increased during autophagy

To investigate whether the PK-hLC3 can form puncta under starvation conditions, we next examined the formation of PK-hLC3 puncta under starvation conditions (Fig. 5). If PK-hLC3 was lipidated and localized to autophagosomes like endogenous LC3, the green and far-red fluorescent puncta of PK-hLC3 could be detected in the cells expressing PK-hLC3 during autophagy. Huh7.5.1 cells expressing PK-hLC3 were incubated in a Krebs-Ringer buffer for 4h to simulate starvation conditions that would induce autophagy. PK-hLC3 puncta of green and far-red fluorescence was investigated. Under nutrient-rich conditions, a few green and far-red, double-positive, fluorescent puncta were observed in the cells (Fig. 5Aa–Ad). Under starvation conditions, the double-positive puncta were increased (Fig. 5Ca–Cd). The green-negative, but far-red-fluorescent-positive, puncta were also increased in the cells (Fig. 5Ca–Cd), indicating that PK-hLC3 forms intracellular puncta under starvation conditions.

To further investigate whether the green-negative, but far-red-positive, puncta of PK-hLC3 increase when autolysosomes are increased, we examined the formation of puncta in the cells expressing PK-hLC3 in the presence of inhibitors for major lysosomal proteases and cathepsins under starvation conditions. E64d is an inhibitor for cathepsins B, H and L, and pepstatin A is an inhibitor for cathepsin D [27,28,29]. Inhibition of the protease activities of these cathepsins leads to an inactivation of lysosomal hydrolases, since cathepsins B and D are major processing enzymes that are essential for lysosomal hydrolases in addition to proteases for the degradation of proteins. As a result, autolysosomes and autophagosomes significantly accumulated under starvation conditions in the presence of E64d and pepstatin A [10]. If PK-hLC3 reflects autolysosomes as the green-negative, but far-red-positive, fluorescent puncta, the far-red, single, fluorescent puncta of PK-hLC3 would accumulate in the presence of these inhibitors under starvation conditions. Huh7.5.1 cells expressing PK-hLC3 were incubated for 4 h under starvation conditions in the presence of these inhibitors, and the puncta of intracellular fluorescence in the cells were monitored. The green-negative, but far-red-positive, puncta of PK-hLC3 were significantly increased in the cells (Fig. 5Da–Dd). In contrast, few puncta were observed in the cells expressing PK-hLC3ΔG under the same conditions (Fig. 5Ea–Ed). The mTOR-signaling pathway negatively regulates autophagy. Rapamycin/sirolimus inhibits activities of mTORC1 complex *via* FKBP12, resulting in an induction of autophagy [30,31]. To investigate whether fluorescent puncta of PK-hLC3 are increased by rapamycin-induced autophagy, Huh7.5.1 cells expressing PK-hLC3 were incubated for 6 h under nutrient-rich conditions in the presence of 100 nM rapamycin, and the puncta of intracellular fluorescence in the cells were monitored (Fig. 5Fa–Fd). The green-negative, but far-red-positive, fluorescent puncta of PK-hLC3 and the double-positive puncta were increased in the cells.

We further investigated the formation of puncta of PK-hLC3 using a highly potent, selective and ATP-competitive mTOR inhibitor, torin1, that also induces autophagy [32]. As was the case in the rapamycin-treated cells, the green-negative, but far-red-positive, puncta and the double-positive puncta of PK-hLC3 were observed when the cells expressing PK-hLC3 were treated with 100 nM torin1 for 6 h (Fig. 5Ga–Gd).

The lysosomotropic agents, ammonium chloride and chloroquine, inhibit acidification of the intracellular compartments, leading to a defect in the fusion of autophagosomes with lysosomes during autophagy [33]. These reagents simultaneously induce the vacuolation of intracellular compartments including autophagic vacuoles [34]. If PK-hLC3 is localized to autophagosomes and autolysosomes, treatment of the cells with ammonium chloride and chloroquine should result in an increase in the green and far-red, double-positive, fluorescent puncta/vacuoles. The cells expressing PK-hLC3 were treated with 20 mM ammonium chloride or 20 μg/ml chloroquine for 4 h under starvation conditions (Fig. 5Ha Hd and Ia–Id, respectively). The green and far-red, double-positive, fluorescent puncta and vacuoles of PK-hLC3 were significantly increased. In contrast, only a few fluorescent-positive puncta and no vacuoles were observed in the cells expressing PK-hLC3ΔG in the presence of chloroquine (Fig. 5Ja–Jd). These results suggested that PK-hLC3 is suitable for monitoring autophagosomes and their maturation step.

Discussion

By comparison with EGFP and mWasabi, the super-ecliptic pHluorin, a pH-sensitive mutant GFP, was more sensitive to acidic pH. The green fluorescence of pHluorin was significantly decreased at pH 6.5, and the fluorescence was further decreased to a level similar to the autofluorescence of cells at pH 5.5–6.0. The pHluorin-mKate2 tandem fluorescent protein showed green and far-red fluorescence at pH 7.2, while it showed far-red, single-positive, fluorescence at pH 5.5–6.0, indicating the pHluorin-mKate2 tandem fluorescent protein is suitable as a tandem-fluorescence protein-tag for the monitoring of autophagosome maturation. The PK-hLC3 formed an E1-substrate intermediate with Atg7, and an E2-substrate intermediate with Atg3, suggesting that fluorescent, protein-tagged LC3 is a modifier of LC3-lipidation. The PK-hLC3 formed green and far-red, fluorescent puncta, and far-red, single-positive, fluorescent puncta were observed under starvation conditions. When autolysosomes were accumulated under starvation conditions by treatment with E64d and pepstatin A, far-red, single-positive puncta were significantly increased. Under the same conditions, few puncta of PK-hLC3ΔG were observed. These results suggested that PK-hLC3 and its negative control, PK-hLC3ΔG, are suitable to monitor the mammalian autophagosomal maturation step.

In general, the pH of the cytosol is 7.4, that of the endoplasmic reticulum is 7.0, that of the *cis*-Golgi is 6.5, the pH of secretory vesicles is 5.0–6.0, early endosomal pH is 5.9–6.8, and late endosomal pH is 5.4–5.6. When autophagosomes are formed, the intra-autophagosomal pH is considered to be near that of the cytosol. During the autophagosome-lysosome fusion, the intra-autophagosomal pH turns acidic. Considering that the green fluorescence of pHluorin is significantly decreased at pH 6.5, the green fluorescent puncta of PK-hLC3 will reflect autophagosomes and an early stage of autophagosome-lysosome fusion. Therefore, when using PK-hLC3, the signals of autophagosomes will be detected as green and far-red double positive puncta in a more sensitive manner. Using PK-hLC3ΔG as a negative control, artificial fluorescent signals that are independent of autophagy will be excluded in the cells.

Autophagy in the tissues of transgenic mice uses EGFP-LC3. Our results suggested that the puncta of EGFP-LC3 in the mouse tissues tends to be overestimated as autophagosome formation. Now we are generating PK-hLC3- and PK-hLC3ΔG-transgenic

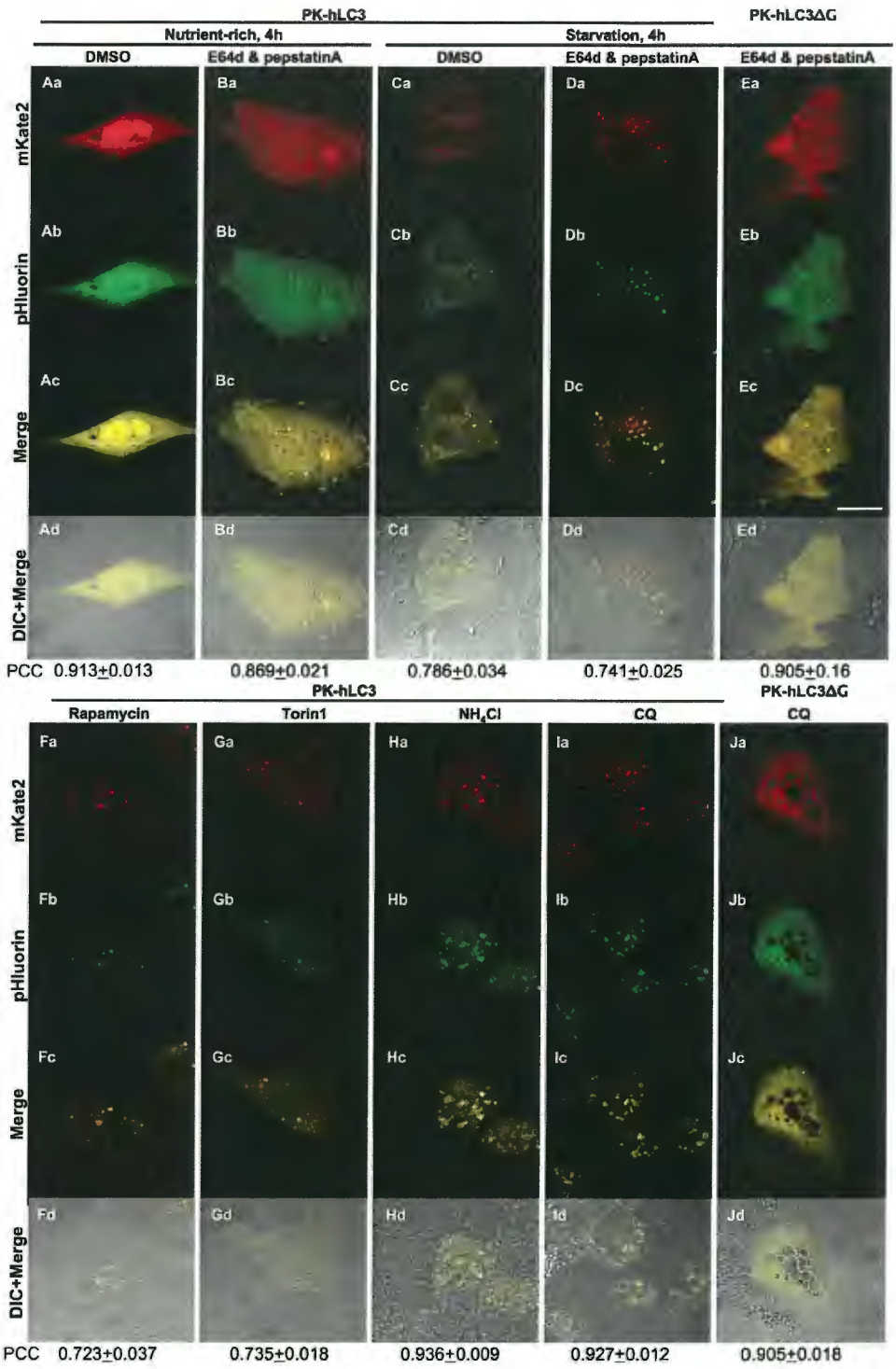

Figure 5. Formation of the puncta of PK-hLC3 during autophagy. The PK-hLC3 was expressed in Huh7.5.1 cells. The cells were incubated in the Krebs-Ringer buffer for 4 h as starvation conditions in the presence (**E64d & pepstatin A**) (Da–Dd) or absence (**DMSO**) (Ca–Cd) of 10 μg/ml E64d and 10 μg/ml pepstatin A (**Starvation, 4 h**). As nutrient-rich conditions, cells were incubated in the cultured medium (**Nutrient-rich, 4 h**) (Aa–Ad, Ba–Bd). For induction autophagy by the inhibition of mTOR-signaling pathway, cells were incubated in the cultured medium for 6 h in the presence of 100 nM **rapamycin** (Fa–Fd) or 100 nM **torin1** (Ga–Gd). To inhibit the fusion of autophagosome with lysosome, 20 mM ammonium chloride (**NH_4Cl**) (Ha–Hd) and 20 μg/ml chloroquine (**CQ**) (Ia–Id) were treated to the cells incubated in the Krebs-Ringer buffer for 4 h. The **PK-hLC3ΔG** (Ea–Ed and Ja–Jd) was expressed in the cells instead of the PK-hLC3 under the same conditions (Da–Dd and Ia–Id, respectively). The far-red (**mKate2**) and green (**pHluorin**) fluorescence in the cells were monitored using a Olympus FluoView FV1000 confocal laser scanning microscope.

"**Merge**" indicates the merging of the green (**pHluorin**) and far-red images (**mKate2**), and "**DIC+Merge**" indicates the overlaying the merged images on the DIC (differential interference contrast) images in the same field. Pearson's correlation coefficient (**PCC**) analysis with Costes' method was used as a measure of colocalization of mKate2 signals with pHluorin signals. The mean PCC value ± S.E. of at least 20 cells is shown on the bottom.
doi:10.1371/journal.pone.0110600.g005

mice. These mice will confer the problems derived from EGFP and EGFP-LC3 to further the study of autophagy. In future studies, we will report autophagic events in mouse tissues using these transgenic mice.

Materials and Methods

Cells, Media, Materials, and Antibodies

KOD-plus- (KOD-201) was employed for high-fidelity polymerase chain reactions (TOYOBO). Huh7.5.1 cells derived from the Huh7 cell line (ATCC CCL-185) were cultured in a Dulbecco's modified Eagle Medium (DMEM; Wako, 045-30285) containing 10% fetal calf serum (JRH biosciences/SIGMA, 12603C) and 1% nonessential amino acids (Invitrogen, 11140050). Polyclonal antibodies against human LC3 was described previously [10]. The mouse monoclonal antibody, clone M2, against FLAG peptide (DYKDDDDK) (F1804), ammonium chloride (254134), and chloroquine diphosphate salt (C6628) were purchased from SIGMA-ALDRICH, the mouse monoclonal antibodies against GAPDH (ab8245) were from Abcam, and the rabbit monoclonal antibody against Myc epitope tag (2278) was from Cell Signaling Technology. Protein concentrations were determined using the bicinchoninic acid protein assay reagent (Pierce, 23225). E64d (4321-v) and pepstatin A (4397-v) were purchased from Peptide Institute, and the rapamycin (#tlrl-rap) was from InvivoGen. Torin1 was a kind gift from Dr. Nathanael S. Gray at the Dana Farber Cancer Institute and Dr. David Sabatini at the Whitehead Institute for Biomedical Research. To introduce the plasmid into the cells, FuGENE HD transfection reagent (E2311) was used (Promega).

Construction of plasmids for the expression of pHluorin-based proteins

The plasmid containing DNA fragments encoding super-ecliptic pHluorin was kindly provided by Dr. James Edward Rothman [24]. pEX-GFPhLC3wt, pEX-GFPhLC3ΔG, pTag2B-hATG7, pTag2B-hATG7C572S, and pTag3B-hATG3C264S were described previously [8,12,35]. A pmKate2-C plasmid containing a DNA fragment of mKate2 (FP181) was purchased from Evrogen, the pmWasabi-C plasmid (ABP-FP-WCNCS10) was from Allele Biotechnology, and pEGFP-C1 (#6084-1) was from Clontech/TAKARA. FUGW (Addgene plasmid 14883) plasmid for 3rd generation lentiviral plasmid with the human polyubiquitin C (hUbC) promoter was obtained from Addgene [25]. Using two primers, pHluorin-NheI-F (5′-GCT AGC GCC ACC ATG AGT AAA GGA GAA GAA CTT TTC ACT GGA GTT G-3′) and pHluorin-GS-Bgl2-Rv (5′-AGA TCT ACC TCC TCC ACC TTT GTA TAG TTC ATC CAT GCC ATG TGT AAT C-3′), a DNA fragment was amplified via high-fidelity polymerase chain reaction using the pHluorin plasmid as a template to introduce the *Nhe*I site and the Kozak sequence just prior to the start codon of pHluorin and the Gly-Gly-Gly-Ser sequence and *Bgl*II site prior to the stop codon of pHluorin, and the amplified fragment was cloned into a pCRII-TOPO plasmid using a TA-cloning kit (K2050, Life Tech.), designated pCR-pHluorin. To introduce the *Bam*HI site before the start codon of mKate2 and the Gly-Gly-Gly-Ser linker and the *Xho*I-*Bgl*II site before the stop codon of mKate2, a DNA fragment was amplified via high-fidelity polymerase chain reaction using two primers, mKate2-BamHI-F (5′-GGA TCC ATG GTG AGC GAG CTG ATT AAG GAG AAC ATG CAC-3′) and mKate2GS-BglII-Rv (5′-CTC GAG ATC TGA GTC CGG AAC CTC CTC CAC CTC TGT G-3′) with pmKate2-C. The amplified DNA fragment was introduced into a pCRII-TOPO plasmid, designated pCR-mKate2. The *Nhe*I-*Bgl*II DNA fragment containing the open reading frame of EGFP in the pEGFP-C1 was replaced with the *Nhe*I-*Bgl*II DNA fragment containing the open reading frame of pHluorin in the pCR-pHluorin for the expression of pHluorin under the control of a cytomegalovirus immediate early promoter, designated pHluorin-G. The *Bam*HI-*Bgl*II DNA fragment containing mKate2 of pCR-mKate2 was inserted into the *Bgl*II site of the pHluorin-G plasmid for the expression of a pHluorin-mKate2 fusion protein under the control of a cytomegalovirus immediate early promoter, designated pHmK-G. For the expression of wild type PK-hLC3, the *Nhe*I-*Bgl*II DNA fragment containing the open reading frame of EGFP of pEX-GFP-hLC3WT (Addgene plasmid 24987, Addgene) [12] was replaced with the *Nhe*I-*Bgl*II DNA fragment containing the open reading frame of pHluorin-mKate2 fusion protein derived from pHmK-G plasmid, and the resultant plasmid was designated pEX-PK-hLC3. For the expression of mutant PK-hLC3ΔG, the *Nhe*I-*Bgl*II EGFP DNA fragment of pEX-GFP-hLC3ΔG (Addgene plasmid 24988, Addgene) [12] was replaced with the *Nhe*I-*Bgl*II DNA fragment encoding pHluorin-mKate2 fusion protein, and the resultant plasmid was designated pEX-PK-hLC3ΔG. For the lentiviral packaging system for the expression of PK-hLC3 fusion protein, the DNA fragment was amplified via a high-fidelity polymerase chain reaction using pEX-PK-hLC3, pH-Bam-Nhe-F (5′-AAA GGA TCC GCT AGC GCC ACC ATG AGT AAA GGA GAA G-3′), and hLC3-RI-Rv (5′-AAA GAA TTC TTA CAC TGA CAA TTT CAT CCC GAA CG-3′) primers. After the digestion of the amplified DNA fragment with *Bam*HI-*Eco*RI, the fragment was inserted into the *Bam*HI-*Eco*RI site of FUGW. The resultant plasmid was designated FUGW-PK-hLC3. For a lentiviral packaging system for the expression of mutant PK-hLC3ΔG, the hLC3ΔG-RI-Rv (5′-AAA GAA TTC TTA CAC TGA CAA TTT CAT GAA CG-3′) primer was employed instead of hLC3-RI-Rv, and the resultant plasmid was designated FUGW-PK-hLC3ΔG.

Immunoblotting analyses

Cells were washed twice in phosphate-buffered saline, lysed in lysis buffer (10 mM sodium phosphate, pH 7.2, 150 mM NaCl, and 1% sodium dodecyl sulfate) containing a Complete protease-inhibitor cocktail (Roche Diagnostics, 1697498). Proteins (10 μg) of the lysate were separated on sodium dodecyl sulfate polyacrylamide gel electrophoresis (SDS-PAGE). After transferring the proteins to a polyvinylidine difluoride membrane using a Trans-Blot SD transfer cell (Bio-Rad, 170-3940), FLAG-Atg7, Myc-Atg3, LC3 and GAPDH in the lysate were recognized using the appropriate antibodies. A chemiluminescent method was carried out according to standard protocols with SuperSignal West Dura Extended Duration Substrate (Pierce, 34075) or SuperSignal West Pico Chemiluminescent Substrate (Pierce, 34077).

Fluorescent Microscopy

Cells were fixed in a fixation solution (phosphate buffered saline containing 4% paraformaldehyde) at room temperature for 5 min, and permeabilized in a phosphate-buffered saline containing 50 μg/ml digitonin. After cells were buffered in 20 mM citrate phosphate buffer at pH 5.5, 6.0, and 6.5 containing 150 mM NaCl when indicated, the fluorescence of the fluorescent proteins was monitored using a Biozero BZ-8000 microscope (KEYENCE, Tokyo, Japan).

Laser scanning confocal microscopy

The fluorescence of the fluorescent proteins in the cells expressing PK-hLC3 was monitored using a Olympus FluoView FV1000 confocal laser scanning microscope. Pearson's correlation coefficient (PCC) analysis with Costes' method [36] was employed to estimate the colocalization of mKate2 signals with pHluorin signals of at least 20 independent images using ImageJ software (http://imagej.nih.gov/ij/) [37] with a JACoP (Just Another Colocalisation) plugin (http://www.blackwell-synergy.com/doi/pdf/10.1111/j.1365-2818.2006.01706.x) [38].

Acknowledgments

We thank Drs. James Edward Rothman and David Baltimore for providing respective pHluorin and FUGW plasmids, and thank Drs. Nathanael S. Gray at the Dana Farber Cancer Institute and Dr. David Sabatini at the Whitehead Institute for Biomedical Research for providing torin1.

Author Contributions

Conceived and designed the experiments: IT. Performed the experiments: IT. Analyzed the data: IT. Contributed reagents/materials/analysis tools: IT TU YU. Wrote the paper: IT TU YU.

References

1. Mizushima N, Komatsu M (2011) Autophagy: renovation of cells and tissues. Cell 147: 728–741.
2. Tanida I (2011) Autophagy basics. Microbiol Immunol 55: 1–11.
3. Mann SS, Hammarback JA (1994) Molecular characterization of light chain 3. A microtubule binding subunit of MAP1A and MAP1B. J Biol Chem 269: 11492–11497.
4. Kabeya Y, Mizushima N, Ueno T, Yamamoto A, Kirisako T, et al. (2000) LC3, a mammalian homologue of yeast Apg8p, is localized in autophagosome membranes after processing. EMBO J 19: 5720–5728.
5. Tanida I, Sou YS, Ezaki J, Minematsu-Ikeguchi N, Ueno T, et al. (2004) HsAtg4B/HsApg4B/autophagin-1 cleaves the carboxyl termini of three human Atg8 homologues and delipidates microtubule-associated protein light chain 3- and GABAA receptor-associated protein-phospholipid conjugates. J Biol Chem 279: 36268–36276.
6. Kabeya Y, Mizushima N, Yamamoto A, Oshitani-Okamoto S, Ohsumi Y, et al. (2004) LC3, GABARAP and GATE16 localize to autophagosomal membrane depending on form-II formation. J Cell Sci 117: 2805–2812.
7. Tanida I, Tanida-Miyake E, Ueno T, Kominami E (2001) The human homolog of *Saccharomyces cerevisiae* Apg7p is a Protein-activating enzyme for multiple substrates including human Apg12p, GATE-16, GABARAP, and MAP-LC3. J Biol Chem 276: 1701–1706.
8. Tanida I, Tanida-Miyake E, Komatsu M, Ueno T, Kominami E (2002) Human Apg3p/Aut1p homologue is an authentic E2 enzyme for multiple substrates, GATE-16, GABARAP, and MAP-LC3, and facilitates the conjugation of hApg12p to hApg5p. J Biol Chem 277: 13739–13744.
9. Sou YS, Tanida I, Komatsu M, Ueno T, Kominami E (2006) Phosphatidylserine in addition to phosphatidylethanolamine is an in vitro target of the mammalian Atg8 modifiers, LC3, GABARAP, and GATE-16. J Biol Chem 281: 3017–3024.
10. Tanida I, Minematsu-Ikeguchi N, Ueno T, Kominami E (2005) Lysosomal turnover, but not a cellular level, of endogenous LC3 is a marker for autophagy. Autophagy 1: 84–91.
11. Mizushima N, Yamamoto A, Hatano M, Kobayashi Y, Kabeya Y, et al. (2001) Dissection of autophagosome formation using Apg5-deficient mouse embryonic stem cells. J Cell Biol 152: 657–668.
12. Tanida I, Yamaji T, Ueno T, Ishiura S, Kominami E, et al. (2008) Consideration about negative controls for LC3 and expression vectors for four colored fluorescent protein-LC3 negative controls. Autophagy 4: 131–134.
13. Demarchi F, Bertoli C, Copetti T, Tanida I, Brancolini C, et al. (2006) Calpain is required for macroautophagy in mammalian cells. J Cell Biol 175: 595–605.
14. Bains M, Heidenreich KA (2009) Live-cell imaging of autophagy induction and autophagosome-lysosome fusion in primary cultured neurons. Methods Enzymol 453: 145–158.
15. Hailey DW, Rambold AS, Satpute-Krishnan P, Mitra K, Sougrat R, et al. (2010) Mitochondria supply membranes for autophagosome biogenesis during starvation. Cell 141: 656–667.
16. Iwai-Kanai E, Yuan H, Huang C, Sayen MR, Perry-Garza CN, et al. (2008) A method to measure cardiac autophagic flux in vivo. Autophagy 4: 322–329.
17. Kimura S, Noda T, Yoshimori T (2007) Dissection of the Autophagosome Maturation Process by a Novel Reporter Protein, Tandem Fluorescent-Tagged LC3. Autophagy 3: 452–460.
18. Pankiv S, Clausen TH, Lamark T, Brech A, Bruun JA, et al. (2007) p62/SQSTM1 binds directly to Atg8/LC3 to facilitate degradation of ubiquitinated protein aggregates by autophagy. J Biol Chem 282: 24131–24145.
19. Patterson GH, Knobel SM, Sharif WD, Kain SR, Piston DW (1997) Use of the green fluorescent protein and its mutants in quantitative fluorescence microscopy. Biophys J 73: 2782–2790.
20. Katayama H, Yamamoto A, Mizushima N, Yoshimori T, Miyawaki A (2008) GFP-like proteins stably accumulate in lysosomes. Cell Struct Funct 33: 1–12.
21. Zhou C, Zhong W, Zhou J, Sheng F, Fang Z, et al. (2012) Monitoring autophagic flux by an improved tandem fluorescent-tagged LC3 (mTagRFP-mWasabi-LC3) reveals that high-dose rapamycin impairs autophagic flux in cancer cells. Autophagy 8: 1215–1226.
22. Ai HW, Olenych SG, Wong P, Davidson MW, Campbell RE (2008) Hue-shifted monomeric variants of Clavularia cyan fluorescent protein: identification of the molecular determinants of color and applications in fluorescence imaging. BMC Biol 6: 13.
23. Ai HW, Henderson JN, Remington SJ, Campbell RE (2006) Directed evolution of a monomeric, bright and photostable version of Clavularia cyan fluorescent protein: structural characterization and applications in fluorescence imaging. Biochem J 400: 531–540.
24. Miesenbock G, De Angelis DA, Rothman JE (1998) Visualizing secretion and synaptic transmission with pH-sensitive green fluorescent proteins. Nature 394: 192–195.
25. Lois C, Hong EJ, Pease S, Brown EJ, Baltimore D (2002) Germline transmission and tissue-specific expression of transgenes delivered by lentiviral vectors. Science 295: 868–872.
26. Tanida I, Tanida-Miyake E, Nishitani T, Komatsu M, Yamazaki H, et al. (2002) Murine Apg12p has a substrate preference for murine Apg7p over three Apg8p homologs. Biochem Biophys Res Commun 292: 256–262.
27. Tamai M, Matsumoto K, Omura S, Koyama I, Ozawa Y, et al. (1986) *In vitro* and *in vivo* inhibition of cysteine proteinases by EST, a new analog of E-64. J Pharmacobiodyn 9: 672–677.
28. Tamai M, Yokoo C, Murata M, Oguma K, Sota K, et al. (1987) Efficient synthetic method for ethyl (+)-(2S,3S)-3-[(S)-3-methyl-1-(3-methylbutylcarbamoyl)butylcarbamoyl]-2-oxiranecarboxylate (EST), a new inhibitor of cysteine proteinases. Chem Pharm Bull (Tokyo) 35: 1098–1104.
29. Umezawa H, Takeuchi T, Linuma H, Suzuki K, Ito M (1970) A new microbial product, oudenone, inhibiting tyrosine hydroxylase. J Antibiot (Tokyo) 23: 514–518.
30. Noda T, Ohsumi Y (1998) Tor, a phosphatidylinositol kinase homologue, controls autophagy in yeast. J Biol Chem 273: 3963–3966.
31. Klionsky DJ, Abdalla FC, Abeliovich H, Abraham RT, Acevedo-Arozena A, et al. (2012) Guidelines for the use and interpretation of assays for monitoring autophagy. Autophagy 8: 445–544.
32. Thoreen CC, Kang SA, Chang JW, Liu Q, Zhang J, et al. (2009) An ATP-competitive mammalian target of rapamycin inhibitor reveals rapamycin-resistant functions of mTORC1. J Biol Chem 284: 8023–8032.
33. Tanida I, Waguri S (2010) Measurement of autophagy in cells and tissues. Methods Mol Biol 648: 193–214.
34. Fedorko ME, Hirsch JG, Cohn ZA (1968) Autophagic vacuoles produced in vitro II. Studies on the mechanism of formation of autophagic vacuoles produced by chloroquine. The Journal of cell biology 38: 392–402.
35. Komatsu M, Tanida I, Ueno T, Ohsumi M, Ohsumi Y, et al. (2001) The C-terminal region of an Apg7p/Cvt2p is required for homodimerization and is essential for its E1 activity and E1–E2 complex formation. J Biol Chem 276: 9846–9854.
36. Costes SV, Daelemans D, Cho EH, Dobbin Z, Pavlakis G, et al. (2004) Automatic and quantitative measurement of protein-protein colocalization in live cells. Biophys J 86: 3993–4003.
37. Schneider CA, Rasband WS, Eliceiri KW (2012) NIH Image to ImageJ: 25 years of image analysis. Nat Methods 9: 671–675.
38. Bolte S, Cordelieres FP (2006) A guided tour into subcellular colocalization analysis in light microscopy. J Microsc 224: 213–232.

Magn Reson Med Sci, Vol. 14, No. 2, pp. 159–162, 2015
doi:10.2463/mrms.2014-0142

TECHNICAL NOTE

See-through Brains and Diffusion Tensor MRI Clarified Fiber Connections: A Preliminary Microstructural Study in a Mouse with Callosal Agenesis

Aurelien KEREVER[1], Koji KAMAGATA[2*], Suguru YOKOSAWA[3], Yosuke OTAKE[3], Hisaaki OCHI[3], Taihei YAMADA[1], Masaaki HORI[2], Kouhei KAMIYA[4], Akira NISHIKORI[5], Shigeki AOKI[2], and Eri ARIKAWA-HIRASAWA[1]

[1]*Research Institute for Diseases of Old Age, Juntendo University Graduate School of Medicine 2–1–1 Hongo, Bunkyo-ku, Tokyo 113–8421, Japan*
[2]*Department of Radiology, Juntendo University Graduate School of Medicine*
[3]*Central Research Laboratory, Hitachi, Ltd.*
[4]*Department of Radiology, Graduate School of Medicine, The University of Tokyo*
[5]*Department of Radiological Sciences, Graduate School of Human Health Sciences, Tokyo Metropolitan University*
(Received December 8, 2014; Accepted January 28, 2015; published online March 31, 2015)

Clearing methods that render the brain optically transparent allow high-resolution three-dimensional (3D) imaging of neural networks. We used diffusion tensor imaging (DTI) and two-photon imaging of cleared brains to analyze white matter in BTBR mice. We confirmed corpus callosum agenesis and identified an abnormal commissure close to the third ventricle. DTI and cleared-brain two-photon imaging revealed that these commissural fibers constituted a frontal clustering of the ventral hippocampal commissure and provided a detailed assessment of white matter structure in mice.

Keywords: ***CLARITY, cleared brain, CUBIC, diffusion tensor imaging, mice***

Introduction

Various methods of rendering the mouse brain transparent (SCALEA2, CLARITY, SeeDB, 3DISCO, CUBIC) have recently been developed.[1,2] These techniques yield optical transparency and thus allow the creation of three-dimensional (3D) neural network images with single-cell resolution; they are therefore highly advantageous in neuroscience because they create novel perspectives completely different from those available with standard glass slide immunostaining. In addition, clinically oriented human brain imaging methods such as diffusion tensor imaging (DTI) have been applied to laboratory animals, enabling improvements in current experimental neuroscience. DTI allows researchers to measure the characteristics of local microstructural water diffusion in the brain,[3,4] taking advantage of the macroscopic geometric arrangement of white matter bundles.

*Corresponding author, Phone: +81-3-3813-3111, Fax: +81-3-5684-0476, E-mail: kkamagat@juntendo.ac.jp

The inbred BTBR T+tf/J (BTBR) mouse strain is a mouse model of autism that displays robust analogies to the diagnostic signs of this disorder in humans.[5] Neuroanatomical studies of the BTBR mouse brain have shown total agenesis of corpus callosum (CC) connective tissues, lack of a hippocampal commissure, and a putative accessory interhemispheric white matter tract that is implicated in abnormal behaviors.[6–8] Here, to better characterize the inter-hemispheric commissure in the BTBR strain of mice, we performed a neuroanatomical analysis by using both 3D high-resolution two-photon images of the transparent mouse brain and DTI. To our knowledge, this is the first report on the use of this dual procedure in the mouse brain.

Materials and Methods

Sample preparation

We performed two-photon analysis on the brains of five BTBR mice and five C57BL/6J (B6) mice (obtained from Jackson Laboratory, Bar Harbor, ME, USA) as controls. The brains of two of the

BTBR mice and two of the B6 mice were also scanned by MRI. Twelve-week-old male BTBR and B6 mice were deeply anesthetized and then perfused with 25 ml of ice-cold PBS-heparin (10 U/ml) solution followed by 25 ml of ice-cold paraformaldehyde (PFA) hydrogel solution (acrylamide 4%, bis 0.05%, Bio-Rad Laboratories, Inc., Hercules, CA, USA; PFA 4%, VA-044 initiator 0.25%, 145-05605, Wako Pure Chemical Industries Ltd., Osaka, Japan). The brain was carefully dissected and incubated in 10 ml of fresh hydrogel PFA solution in a sealed 50-ml conical tube for 2 days at 4°C. The tube containing the brain sample was then degassed and placed in a water bath for 3 h at 37°C for hydrogel polymerization. The brain was then carefully removed from the polymerized hydrogel and embedded in 1% agarose for MRI. All animal protocols were approved by the Animal Care and Use Committee of Juntendo University.

MRI

MR images were acquired within 2 weeks from perfusion using a 7T animal MRI system (MRI System, Agilent Technologies Inc., Palo Alto, CA, USA). The DTI sequence used was a 3D diffusion-weighted FSE, with TR = 300 ms, echo train length = 4, TE = 31.86 ms, two averages, field of view 19.2 × 19.2 × 19.2 mm, and matrix size 128 × 128 × 128, yielding an image with 150-μm isotropic voxels. The b value was 1,000 s/mm^2 (δ = 8 ms, Δ = 13.0 ms), and there were 30 diffusion directions. The total imaging time was 21 h and 10 min. Maps of fractional anisotropy (FA) and mean diffusivity (MD) were computed by using dTV II and VOLUMEONE 1.72, developed by Masutani et al.[9] Diffusion tensor tractography (DTT) of the BTBR mice and the B6 controls was performed with a deterministic fiber assignment by using a continuous tracking approach.[10] The FA threshold for tracking was set at 0.13, and the stop length was set at 160 steps. The bending angle of the tract was not allowed to exceed 45°.

In the B6 mice, we identified the corpus callosum (CC), dorsal hippocampal commissure (DHC), anterior commissure (AC), posterior commissure (PC), and ventral hippocampal commissure (VHC) as red areas on a mid-sagittal color-coded map (Fig. 1A). In BTBR mice, on the same type of map, we confirmed a total lack of the CC and DHC, although the AC and PC were present (Fig. 1E). We did not identify the VHC in BTBR mice, but we did find a red area in the rostral region of the third ventricle (Fig. 1E). The seed region of interest (ROI), including the entirety of the AC (blue), PC (yellow), and VHC (red) or abnormal commissure in the rostral region of the third ventricle (red), was placed manually on a reconstructed mid-sagittal isotropic diffusion-weighted image by referring to the mid-sagittal color-coded map (Fig. 1A, B, E, F). Because the habenular commissure (HBC) was a very small structure, we did not identify it in red on the mid-sagittal color-coded map; instead, we drew the seed ROI of the HBC on the mid-sagittal isotropic diffusion-weighted image while referring to a coronal non-diffusion-weighted image (Fig. 1C, G).

Tissue clearing and two-photon image acquisition

We used a modified version of the CLARITY[1] and CUBIC[2] protocols. The brain was removed from the agarose and washed in PBS-Triton X-100 (0.1%) for 1 h on a moving plate at 37°C. Sections (2 mm thick; coronal or sagittal) were obtained by using a mouse brain matrix (Muromachi Kikai Co., Ltd., Japan). Brain slices were incubated for 3 days at 37°C on a moving plate in a solution composed of 5 wt% urea (35904-45; Nacalai Tesque Inc., Japan), 25 wt% *N,N,N′,N′*-tetrakis(2-hydroxypropyl) ethylenediamine (T0781; Tokyo Chemical Industry Co., Ltd., Japan), and 15 wt% Triton X-100 (25987-85; Nacalai Tesque Inc.). The brain slices were washed in PBS-Triton X-100 (0.1%) overnight and then incubated with FluoroMyelin green (1:100; Invitrogen) for 5 days at 37°C on a moving plate. They were then washed in PBS-Triton X-100 (0.1%) overnight and incubated with a solution composed of 50 wt% sucrose (30403-55; Nacalai Tesque Inc.), 25 wt% urea, 10 wt% 2,20,20′-nitrilotriethanol (145-05605; Wako Pure Chemical Industries Ltd., Japan), and 0.1% (v/v) Triton X-100. Image acquisition was performed with a Carl Zeiss LSM 780 two-photon microscope (two-photon Chameleon laser; wavelength 800 nm) with a ×10 Plan Apochromat objective (numerical aperture 0.45; working distance 2 mm). Image processing was performed with Imaris Interactive Microscopy Image Analysis software (Bitplane).

Results

DTI and DTT revealed agenesis of the CC but intact inter-hemispheric tracts in the AC, PC, and HBC of all BTBR mice (Fig. 1), along with abnormal commissure fibers in the rostral region of the third ventricle. DTT revealed that these abnormal commissural fibers seemed to connect with the fimbria (Figs. 1H and 2B), which is the route followed by hippocampal axons to reach the hippocampal commissure at the midline. Therefore, we suspected that the abnormal inter-hemispheric commissure

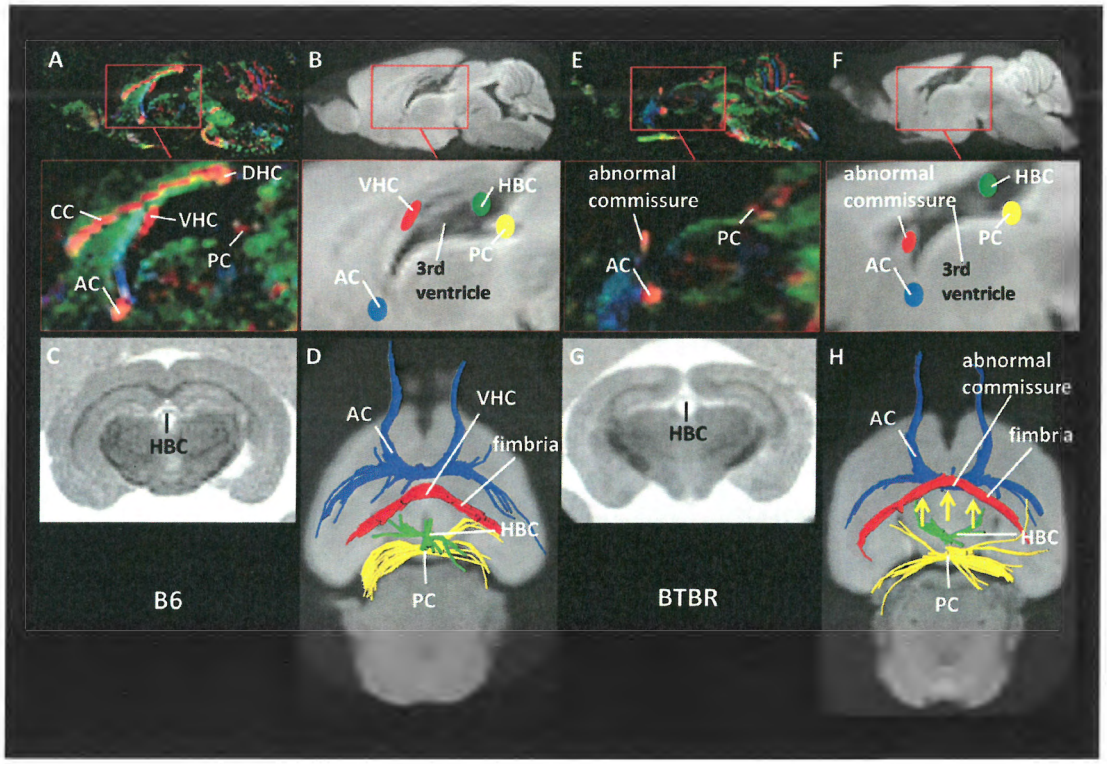

Fig. 1. Diffusion tensor imaging (DTI) and diffusion tensor tractography (DTT) of B6 mice and BTBR mice. Mid-sagittal color-coded fractional anisotropy (FA) map (**A**), isotropic diffusion-weighted image (**B**), coronal non-diffusion-weighted image (**C**), and DTT (**D**) in a B6 mouse. Mid-sagittal color-coded FA map (**E**), isotropic diffusion-weighted image (**F**), coronal non-diffusion-weighted image (**G**), and DTT (**H**) in a BTBR mouse.

was the VHC positioned more rostral than in B6 mice (Fig. 1D). By using two-photon imaging of cleared mouse brains, we assessed whether the abnormal commissural fibers were in fact connected to the fimbria. In all BTBR mice, they were indeed connected to it (Fig. 2A).

Discussion

There were two main findings of our analysis. First, in BTBR mice, we confirmed agenesis of the CC and found intact inter-hemispheric tracts in the AC, PC, and HBC. Second, we identified an abnormal inter-hemispheric commissure in the rostral region of the third ventricle, and we found that this abnormal commissure constituted a frontal clustering of the VHC.

The CC agenesis and intact inter-hemispheric tracts in the AC, PC, and HBC in BTBR mice were in line with the findings of previous reports.[6–8] In addition, Miller et al.[6] reported that the abnormal inter-hemispheric commissural fibers in the rostral region of the third ventricle constituted a novel connective inter-hemispheric structure between the left and right hemispheres that may contribute

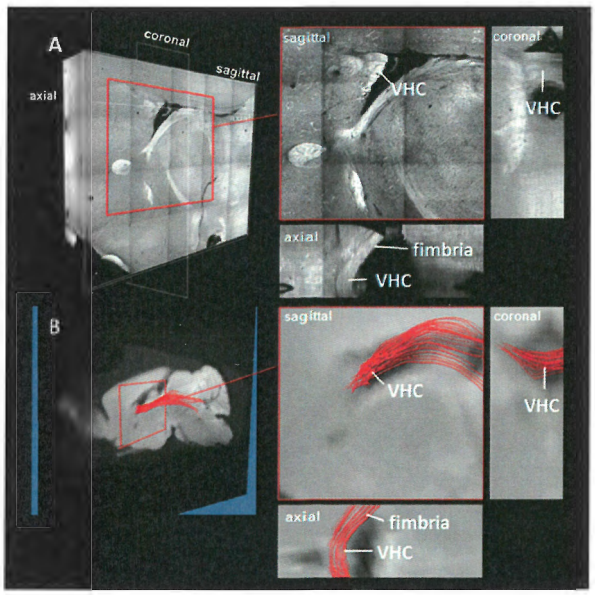

Fig. 2. Two-photon imaging of cleared BTBR mouse brain (**A**) and diffusion tensor tractography of BTBR mouse brain (**B**). In BTBR mice, the abnormal inter-hemispheric commissural fibers were connected to the fimbria; we considered them equivalent to the ventral hippocampal commissure (VHC).

to the behavioral abnormalities of BTBR mice. However, we confirmed by DTI and two-photon imaging that the abnormal inter-hemispheric commissural fibers in the rostral region of the third ventricle were connected to the fimbria. Wyss et al.[11] reported that the topographic organization of the fibers in the fimbria is reflected in the arrangement of the crossed components in the VHC. Therefore, the inter-hemispheric commissural fibers in the rostral region of the third ventricle in BTBR mice represent not a novel inter-hemispheric commissure, as reported by Miller et al.,[6] but the VHC.

White matter voxels in the brain contain multiple fiber bundles in tracts that are oriented in different directions (e.g., crossing, "kissing," and "fanning"); in these areas, DTT is not reliable.[12] DTT evaluations of the connectivity of nerve fibers can depict nerve fiber connectivity where none is present. By using 3D images of cleared mouse brains with single-cell resolution, we confirmed here that the inter-hemispheric fibers were connected to the fimbria. Because two-photon imaging of cleared mouse brains enables the evaluation of the brain microstructure with high resolution, it is useful for local-area characterization of the brain. However, evaluating macroscopic nerve fiber connectivity by this method is difficult. Therefore, combining DTI and two-photon imaging of cleared mouse brains improves the reliability of analyses of brain white matter connections.

Conclusion

DTI combined with two-photon imaging of the cleared mouse brains enables detailed assessment of white matter structure.

Acknowledgements

This work was supported by grants from MEXT-Supported Program for the Strategic Research Foundation at Private Universities (2011–2015) and a research grant from Hitachi, Ltd.

References

1. Chung K, Wallace J, Kim SY, et al. Structural and molecular interrogation of intact biological systems. Nature 2013; 497:332–337.
2. Susaki EA, Tainaka K, Perrin D, et al. Whole-brain imaging with single-cell resolution using chemical cocktails and computational analysis. Cell 2014; 157:726–739.
3. Basser PJ, Mattiello J, LeBihan D. Estimation of the effective self-diffusion tensor from the NMR spin echo. J Magn Reson B 1994; 103:247–254.
4. Kamagata K, Shimoji K, Hori M, et al Intersite reliability of diffusion tensor imaging on two 3T scanners. Magn Reson Med Sci 2015 Feb 12. [Epub ahead of print]
5. Scattoni ML, Ricceri L, Crawley JN. Unusual repertoire of vocalizations in adult BTBR T+tf/J mice during three types of social encounters. Genes Brain Behav 2011; 10:44–56.
6. Miller VM, Gupta D, Neu N, Cotroneo A, Boulay CB, Seegal RF. Novel inter-hemispheric white matter connectivity in the BTBR mouse model of autism. Brain Res 2013; 1513:26–33.
7. Wahlsten D, Metten P, Crabbe JC. Survey of 21 inbred mouse strains in two laboratories reveals that BTBR T/+ tf/tf has severely reduced hippocampal commissure and absent corpus callosum. Brain Res 2003; 971:47–54.
8. Dodero L, Damiano M, Galbusera A, et al. Neuroimaging evidence of major morpho-anatomical and functional abnormalities in the BTBR T+TF/J mouse model of autism. PLoS One 2013; 8:e76655.
9. Masutani Y, Aoki S, Abe O, Hayashi N, Otomo K. MR diffusion tensor imaging: recent advance and new techniques for diffusion tensor visualization. Eur J Radiol 2003; 46:53–66.
10. Mori S, Crain BJ, Chacko VP, van Zijl PC. Three-dimensional tracking of axonal projections in the brain by magnetic resonance imaging. Ann Neurol 1999; 45:265–269.
11. Wyss JM, Swanson LW, Cowan WM. The organization of the fimbria, dorsal fornix and ventral hippocampal commissure in the rat. Anat Embryol (Berl) 1980; 158:303–316.
12. Wiegell MR, Larsson HB, Wedeen VJ. Fiber crossing in human brain depicted with diffusion tensor MR imaging. Radiology 2000; 217:897–903.

Human Molecular Genetics, 2015, Vol. 24, No. 13 3651–3661

doi: 10.1093/hmg/ddv109
Advance Access Publication Date: 23 March 2015
Original Article

ORIGINAL ARTICLE

Perinatal *Gjb2* gene transfer rescues hearing in a mouse model of hereditary deafness

Takashi Iizuka[1], Kazusaku Kamiya[1], Satoru Gotoh[2], Yoshinobu Sugitani[2], Masaaki Suzuki[3], Tetsuo Noda[2,4], Osamu Minowa[2,4] and Katsuhisa Ikeda[1,*]

[1]Department of Otorhinolaryngology, Juntendo University Faculty of Medicine, Tokyo 113-8421, Japan, [2]Department of Cell Biology, Japanese Foundation for Cancer Research, Cancer Institute, Tokyo 135-8550, Japan, [3]Department of Otolaryngology, Teikyo University Chiba Medical Center, Ichihara 299-0111, Japan and [4]Team for Advanced Development and Evaluation of Human Disease Models, RIKEN BioResource Center, Tsukuba 305-0074, Japan

*To whom correspondence should be addressed at: Department of Otorhinolaryngology, Juntendo University Faculty of Medicine, 2-1-1 Hongo, Bunkyo-ku, Tokyo 113-8421, Japan. Tel: +81 358021094; Fax: +81 356890547; Email: ike@juntendo.ac.jp

Abstract

Hearing loss is the most widespread sensory disorder, with an incidence of congenital genetic deafness of 1 in 1600 children. For many ethnic populations, the most prevalent form of genetic deafness is caused by recessive mutations in the gene gap junction protein, beta 2, 26 kDa (*GJB2*), which is also known as connexin 26 (Cx26). Despite this knowledge, existing treatment strategies do not completely recover speech perception. Here we used a gene delivery system to rescue hearing in a mouse model of *Gjb2* deletion. Mice lacking Cx26 are characterized by profound deafness from birth and improper development of cochlear cells. Cochlear delivery of *Gjb2* using an adeno-associated virus significantly improved the auditory responses and development of the cochlear structure. Using gene replacement to restore hearing in a new mouse model of *Gjb2*-related deafness may lead to the development of therapies for human hereditary deafness.

Introduction

Severe-to-profound genetic hearing loss affects approximately one in 1600 children (1). Although early management of hearing impairment with hearing aids and cochlear implants often improves speech perception, profoundly deaf children cannot completely acquire the ability to develop spoken language, and thus intelligible speech is severely restricted (2). Gene therapy may become a powerful technology that could fundamentally correct the disease phenotype of genetic deafness. However, gene replacement approaches for animal models of inherited deafness have been extremely limited (3–7).

Currently 160 loci for the monogenic forms of human deafness have been reported, and 60 genes have been identified (see http://hereditaryhearingloss.org/). The most prevalent form of genetic hearing loss in many ethnic populations is due to defects in the gene encoding connexin26 (*GJB2*), which is expressed in the non-sensory cells of the cochlea. The *GJB2* mutations cause between one-third and 50% of prelingual genetic non-syndromic hearing loss, including dominant and recessive mutations (1).

In the inner ear of mice, both a spatially specific approach that targeted the deletion of the *Gjb2* in the cochlear sensory epithelium resulted in the death of different types in the inner ear after onset of hearing (8). On the other hand, a dominant-negative *Gjb2* R75W transgenic mouse created in our laboratories clearly showed incomplete development of the cochlear supporting cells, resulting in profound deafness from birth (9,10). The outer hair cells from the dominant-negative mutation of *Gjb2* showed normal development and maturation (11). Furthermore, three independent lines of conditional Cx26 null mice, which were generated by methods different from those of the previous study, revealed that postnatal development of the organ of Corti was

Received: February 13, 2015. **Revised and Accepted:** March 17, 2015

arrested before the occurrence of cell death in the organ of Corti (12). Thus, *Gjb2* appears to be indispensable in the postnatal development of the organ of Corti and normal hearing. Very recently, we developed a conditional Cx26-deficient mouse with a localized gene deletion in the inner ear under the control of the Protein 0 (P0) promoter. Wild-type mice revealed that both Cx26 and Cx30 were expressed at the cell border forming orderly pentagonal or hexagonal outlines in the whole-mount cochlear tissues. On the other hand, the punctate distribution of Cx30 alone was observed along the cell border in the Cx26-deficient mouse (13).

Gene delivery systems must be non-cytotoxic, and must be able to return to a normal physiological state after treatment (14). We developed a technique for successful transgene expression through the round window membrane in the supporting cells of the neonatal mouse cochlea using adeno-associated viral (AAV) vectors without causing additional damage to the cochlear function (15). Therefore, we investigated the efficiency and specificity of transcriptionally targeted AAV vectors to deliver Cx26 into the cochlea of *Gjb2*-deficient neonatal mice. We demonstrated efficient expression of Cx26 in the non-sensory cells of the organ of Corti. In addition, gene transfer prevented the progression into profound deafness as indicated by the functional assessment of hearing when the treatment was performed during the neonatal stage. The successful restoration of hearing mediated by gene replacement in the genetically created deaf mouse model of *Gjb2* could contribute to the development of clinical applications for human hereditary deafness.

Results

Creation of *Gjb2* conditional knockout mice

Mice lacking *Gjb2* exhibit embryonic lethality because of defective glucose transport across the placenta (16). To circumvent this lethality, we deleted *Gjb2* in a specific spatial pattern by crossing Cx26fl/fl mice with mice expressing Cre recombinase under the control of the P0 promoter (P0-Cre; Fig. 1A). P0 promoter activity was clearly observed at the otic vesicle of the mouse (17). To characterize Cx26 expression in the cochlea, we performed immunohistochemistry. High levels of Cx26 protein were detected in the supporting cells of the organ of Corti, spiral limbus and the lateral wall fibrocytes of littermate controls. However, Cx26 was not detected in the cochlear tissues of Cx26fl/flP0-Cre mice (Fig. 1B). To confirm the expression pattern of P0 in the inner ear lineage, P0-Cre mice were crossed with $R26R^{GFP}$ reporter mice, which contained GFP knocked into the *ROSA26* locus, allowing for the activation of GFP using Cre recombinase, and GFP signals were observed at the otocyst (13,17), which is consistent with the finding that Cx26 ablation disrupted gap junction networks within both epithelial and connective tissues.

The body weight and litter size of Cx26fl/flP0-Cre mice were normal, and the only apparent phenotypic difference exhibited by these mice was deafness. We evaluated the auditory function in Cx26fl/flP0-Cre mice by recording the auditory brainstem response (ABR), which is widely used to objectively determine hearing thresholds. Thresholds for the wave III component of the ABR were measured for click and tone burst stimuli of 8, 12, 16 and 20 kHz in adult Cx26fl/flP0-Cre ($n = 5$) and control ($n = 7$) mice; the evaluated mice were 5–6 weeks old (Fig. 1C). ABR thresholds in Cx26fl/flP0-Cre mice were ~100 dB sound pressure level (SPL) for click stimuli (data not shown) and >90 dB SPL for tone bursts. Control mice exhibited normal values for these thresholds (15–20 dB SPL). At P161, cochleae of Cx26fl/flP0-Cre mice showed normal gross anatomy with no obvious collapse or expansion of the Reissner's membrane. No defects were apparent in the tectorial membrane, stria vascularis or spiral ligament in mice lacking *Gjb2* expression, although a dramatic collapse of the organ of Corti including loss of hair cells and supporting cells was evident (Fig. 1D). Transmission electron microscopy showed collapse of both the tunnel of Corti and Nuel's space and deformities in the shapes of supporting cells, despite the presence of hair cells in the Cx26fl/flP0-Cre mice at P35. In contrast, fine structures of the stria vascularis and the spiral ligament were intact (Fig. 1E).

We then measured the endocochlear potential (EP), which is the resting DC potential in the scala media of the cochlea that is produced by the stria vascularis. These measurements were taken from the basal turn. The average EP value in Cx26fl/flP0-Cre mice was 40.3 ± 15.5 mV ($n = 8$), which was significantly reduced as compared with control mice (80.5 ± 10.7 mV, $n = 6$; $P < 0.01$; Fig. 1F). However, the presence of a residual EP value of ~40 mV cannot completely explain the reduced ABR thresholds that characterized the Cx26fl/flP0-Cre mice. The EP is determined by two K^+ diffusion potentials of the stria vascularis across the electrical barrier (18). The latter is closely related to tight junction proteins around the cochlear duct (19–21). Since the EP depression previously reported in *Gjb2*-deficient mice has been explained by the disruption of the reticular lamina (8), the tight junctions between the hair cells and supporting cells were observed. The fine structure of tight junctions within the organ of Corti was well preserved in the Cx26fl/flP0-Cre mice (Fig. 1G). Thus, the EP defects observed in Cx26fl/flP0-Cre mice may have resulted from insufficient K^+ recycling through the gap junction network rather than through a disruption of the intercellular barrier associated with the cochlear duct.

No correction of hearing by AAV-mediated delivery of *Gjb2* to adult *Gjb2*-deficient mice

To potentially rescue deafness using gene therapy, we generated an AAV vector that drove *Gjb2* expression with the cytomegalovirus promoter. This AAV vector that encoded the Cx26 protein was applied to the perilymph through the round window membrane in adult (P42) Cx26fl/flP0-Cre mice. Eight weeks after treatment, the ABR was measured, and cochlear sections were examined for Cx26 expression. Although the Cx26 gene was transduced moderately in the spiral ligament, the spiral limbus and, weakly, in the organ of Corti, the organ of Corti remained collapsed, and no sensory hair cells were observed. Non-treated cochleae did not show restored Cx26 expression and did not have rescued cochlear morphology (Fig. 2A). Furthermore, no significant change in the ABR threshold was measured in treated or non-treated cochleae (Fig. 2B). Thus, delivery of *Gjb2* to the perilymphatic space of adult Cx26fl/flP0-Cre cochleae failed to improve hearing despite the successful restoration of Cx26 expression in the organ of Corti, the spiral ligament and the spiral limbus. This suggests that the secondary degeneration of hair cells observed in adult Cx26fl/flP0-Cre mice was not arrested or repaired by *Gjb2* gene delivery.

Developmental changes associated with auditory function and cochlear morphology in *Gjb2*-deficient mice

We next compared the developmental course of the ABR thresholds between Cx26fl/flP0-Cre and control mice. In controls, the onset of hearing occurred between P11 and P12, and the ABR thresholds essentially reached adult levels between P18 and

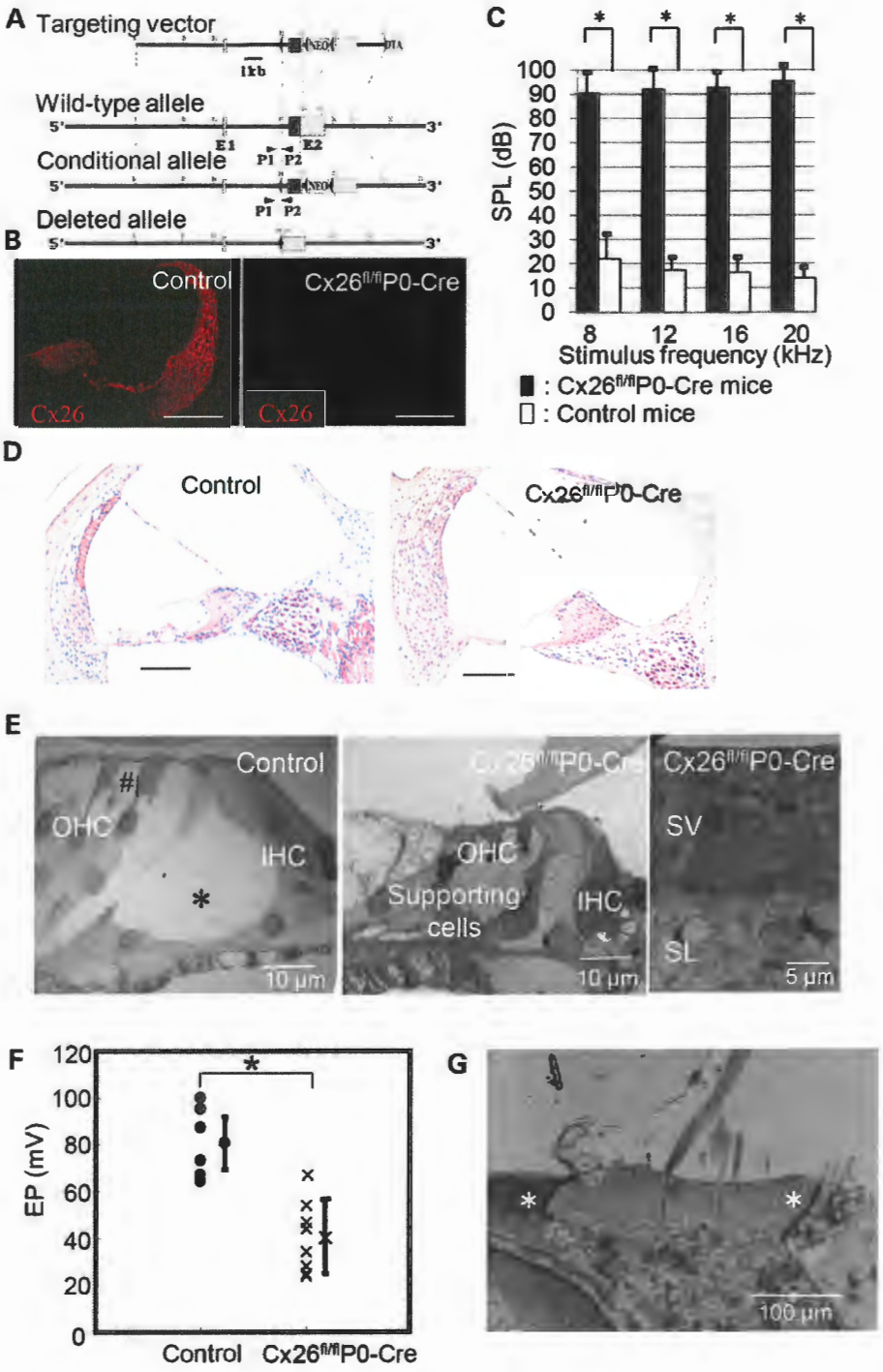

Figure 1. Generation and functional analyses of *Gjb2* conditional knockout mice. (A) Structure of the mutated alleles. A Cx26 conditional knockout allele was generated using a targeting vector containing floxed Cx26 coding sequences (filled box). LoxP sequences (triangles) and the neomycin resistance gene (NEO; pMC1-*neo*) are shown. B, BamHI; H, HindIII; Sc, SacI; X, XbaI; E1, exon 1; E2, exon 2; DTA, diphtheria toxin A; P1 and P2, PCR primers used for genotyping. (B) Cx26 distribution (red) in transverse sections of the cochlear duct of control and $Cx26^{fl/fl}$P0-Cre mice at postnatal day (P)56. (C) Average ABR thresholds (dB SPL) to pure tone bursts in control ($n = 7$) and $Cx26^{fl/fl}$P0-Cre ($n = 5$) mice (P35–P42). (D) Histological analysis of cochlear structure in control and $Cx26^{fl/fl}$P0-Cre mice (P161). (E) Electron micrographs of the organ of Corti in control and $Cx26^{fl/fl}$P0-Cre mice (left two panels). The organ of Corti in the control showed the tunnel of Corti (*) and Nuel's space (#) around the outer hair cells. The stria vascularis and spiral ligament from a $Cx26^{fl/fl}$P0-Cre mouse are shown in the right panel (P35). (F) EP in control ($n = 6$) and $Cx26^{fl/fl}$P0-Cre ($n = 8$) mice (P63–P84). *$P < 0.05$ calculated using the Student's *t*-test. (G) ZO-1 localization (green) in control and $Cx26^{fl/fl}$P0-Cre mice (top panels). Electron micrograph of tight junctions (*) around hair cells and supporting cells of $Cx26^{fl/fl}$P0-Cre mice (bottom panel). OHC, outer hair cell; IHC, inner hair cell; SV, stria vascularis; SL, spiral ligament; EP, endocochlear potential. Error bars represent the SEM. Scale bars = 100 μm (except for electron micrographs).

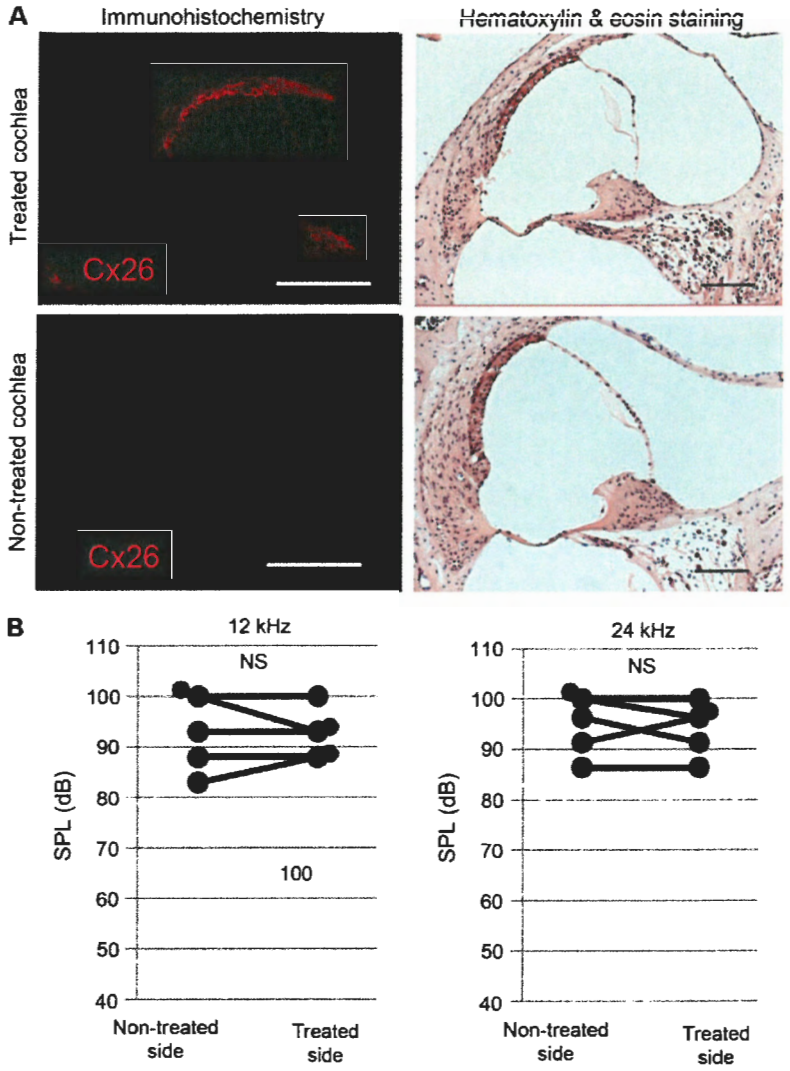

Figure 2. AAV-mediated delivery of *Gjb2* to adult Cx26$^{fl/fl}$P0-Cre mice (P42). (**A**) Cx26 localization (red, left panels) and light micrographs (right panels) of transverse sections of treated and non-treated cochleae from Cx26$^{fl/fl}$P0-Cre mice (P198). (**B**) Average ABR thresholds to pure tone bursts (12 and 24 kHz) in the treated and non-treated side of Cx26$^{fl/fl}$P0-Cre mice (P98; $n = 5$). Significance was calculated using the paired t-test. NS, not significant. Scale bars = 100 μm.

P20 (Fig. 3A). For Cx26fl/flP0-Cre mice, however, click stimuli never elicited detectable ABR waveforms, indicating that development of the auditory organ had been disrupted. Histological examination of cochleae from Cx26fl/flP0-Cre mice revealed that the tunnel of Corti, which normally opens by P10, failed to open before the organ of Corti degenerated (Fig. 3B), indicating a developmental defect. In the present mouse model of *Gjb2* deficiency, functional and morphological findings confirmed that *Gjb2* is indispensable during postnatal development of supporting cells in the organ of Corti. In other words, a well-timed transfer of functional *Gjb2* may rescue the postnatal development of the organ of Corti and prevent the secondary degeneration of hair cells.

Successful hearing correction after AAV-mediated delivery of *Gjb2* to neonatal *Gjb2*-deficient mice

We next used a different gene therapy strategy to prevent deafness caused by *Gjb2* deficiency. At P0 (rather than P42), an AAV vector containing wild-type *Gjb2* was introduced into the cochlear perilymph through the round window membrane. We measured the ABR and examined cochlear sections 10–12 weeks post-treatment. A significant improvement in the ABR thresholds was observed (Fig. 4A), together with the successful rescue of Cx26 expression in supporting cells of the organ of Corti, the spiral ligament fibrocytes and the spiral limbus (Fig. 4B). Non-rescued cochleae lacked Cx26 expression in these tissues (Fig. 4B). Fluorescence confocal images in the lateral wall fibrocytes showed that the Cx26 staining was punctate along the plasma membrane (Fig. 4C and D).

Histological examinations revealed proper formation of the tunnel of Corti and preservation of inner and outer hair cells, as well as supporting cells (Fig. 5A). These rescued phenotypes were more apparent at the basal turn than at the apical turn. Morphological differences between turns may have resulted from differential access to the perilymph through the round window membrane. AAV transduction lasted over 6 months (data not shown). Non-rescued cochleae showed unchanged

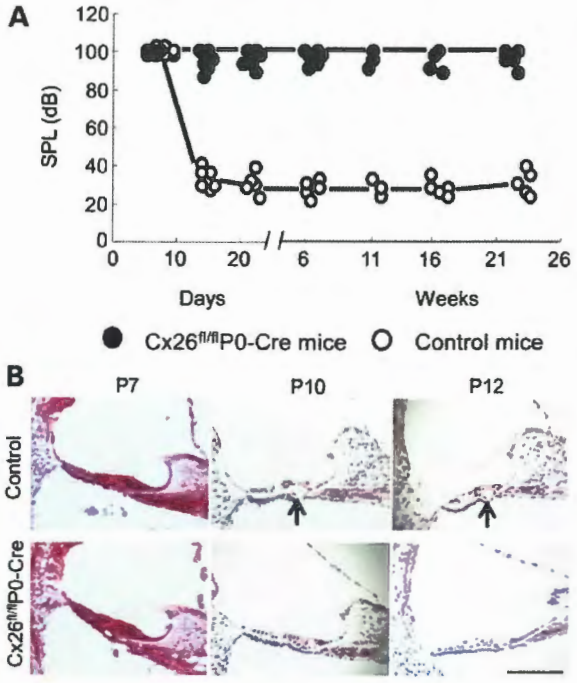

Figure 3. Developmental changes associated with auditory function and cochlear morphology in *Gjb2*-deficient mice. (**A**) Postnatal ABR thresholds to click tones in control and $Cx26^{fl/fl}$P0-Cre mice. (**B**) Transverse sections of the organ of Corti in control and $Cx26^{fl/fl}$P0-Cre mice at P7, P10 and P12. Arrows indicate the tunnel of Corti. Scale bar = 100 μm.

ABR thresholds (Fig. 4A) and collapsed organs of Corti and degenerated hair cells (Fig. 5A). Spiral ganglion neuron degeneration was examined by light microscopy (Fig. 5B). In non-rescued cochleae, both apical and middle turns showed a mild-to-moderate loss of spiral ganglion neurons, whereas a marked reduction in spiral ganglion neurons was observed at the basal turn. Spiral ganglion neurons at the middle and basal turns were apparently better preserved than those in non-rescued cochleae. Quantitative analysis of the height of the pillar cell and the number of spiral ganglion neurons was performed (Fig. 6). The height of the pillar cells of the basal turn in rescued cochleae, which failed to reach full maturation as compared with controls, was significantly increased as compared with that of non-rescued cochleae (Fig. 6A). Quantitative analysis showed that spiral ganglion neuron degeneration progressed from base to apex in *Gjb2*-deficient mice (Fig. 6B). *Gjb2* transfer resulted in a significant increase in the density of neurons at the middle and basal turns. Thus, prevention of both hair cell and spiral ganglion neuron degeneration well explains the preservation of the ABR responses in *Gjb2* transfected cochleae.

Discussion

Using the current mouse model of *Gjb2*-based deafness, we first identified a promising and novel strategy for restoring hearing. Gene therapy failed to rescue hearing in adult *Gjb2*-null mice because secondary hair cell loss was not restored by wild-type *Gjb2*. Performing the gene transfer at early stages of postnatal development, however, i.e. before hair cell degeneration, prevented the onset of deafness. In our laboratory, the gene expression in supporting cells of the neonatal mouse cochlea has been evaluated concerning virus vectors and application routes (15). The extent of adenovirus-GFP transfection was extremely limited in the mesenchymal cells. AAV-directed gene transfer after injection into the scala media through a cochleostomy showed transgene expression in the supporting cells, inner hair cells and lateral wall with resulting hearing loss. On the other hand, gene expression was observed in supporting cells, inner hair cells and lateral wall without hearing loss after the application of AAV into the scala tympani through the round window membrane. Thus, injection of AAV into the scala tympani of the neonatal mouse cochlea was considered to have the potential to efficiently and noninvasively introduce transgenes into the cochlear supporting cells and lateral wall fibrocytes of the neonatal mouse. A successful hearing rescue mediated by AAV-based delivery of a wild-type gene through the round window membrane during early postnatal stages in the present study is well comparable with a previous study to restore hearing in mice carrying a mutation in the vesicular glutamate transporter-3 (*VGLUT3*) (4). However, AAV-driven transfer of *Gjb2* into the scala media of early postnatal conditional *Gjb2* knockout mice did not show significant hearing improvement irrespective of the substantial reduction of both cell death in the organ of Corti and degeneration of spiral ganglion neurons (7). The electrochemical environment in the endolymph is extremely feasible since physiological experiments demonstrated that the injection of volumes >8 nl into the scala media suppressed EP with swollen outer hair cells and shrunken inner hair cells (22). The injection of sodium-based phosphate-buffered solution into potassium-rich endolymph is thought to disturb the mechanotransduction of the hair cells (23). Thus, the subtle change in the cochlear function is likely to be brought about by the endolymphatic application of the vector.

To deliver *Gjb2* to non-sensory cells of the neonatal cochlea, we used an AAV vector that was developed as a stable, efficient and potentially long-term transgene expression system for preserving hearing function in the neonatal cochlea (15) and fetal otocyst (24). The exogenous Cx26 protein in *Gjb2* null mice was expressed in various types of cochlear cells, similar to the expression pattern of GFP protein following AAV-GFP transfection in wild-type mice (15). The same results were also reported in a previous study using another type of *Gjb2*-deficient mice (7). However, in congenital deaf mice lacking *VGLUT3* the expression of VGLUT3 protein was restricted to the targeted cells, namely the inner hair cells (4). Although the underlying mechanism of the difference between *Gjb2* and *VGLUT3* genes is unknown, AAV-*Gjb2* delivery to the *Gjb2* null mice is expected to result in widespread expression in the cochlea. Among available viral vectors, AAV is one of the most promising for use in human clinical trials that involve gene therapy (25). However, the auditory systems of mouse and humans develop quite differently, as the human auditory end organ is almost completely matured by 26–28 weeks of gestation. Therefore, *in uterine* gene therapy must be considered to treat human *GJB2*-related deafness.

Data regarding the Cx function in the cochlea support two hypotheses: (i) the epithelial gap junction network supplies metabolites, nutrients and second messengers that are essential for postnatal development of the organ of Corti (biochemical or metabolic coupling), and (ii) the connective tissue gap junction network recycles K^+ to establish and maintain the ionic and electrical environments of the endolymph after hearing onset (ionic coupling) (9,12,25–31). The development and postnatal maturation of the organ of Corti are affected in a dominant-negative *Gjb2* R75W transgenic mouse (9) and in conditional *Gjb2*-null mice as shown previously (12) and in the present study. Both homomeric (e.g. Cx26 or Cx30) and hybrid (e.g.

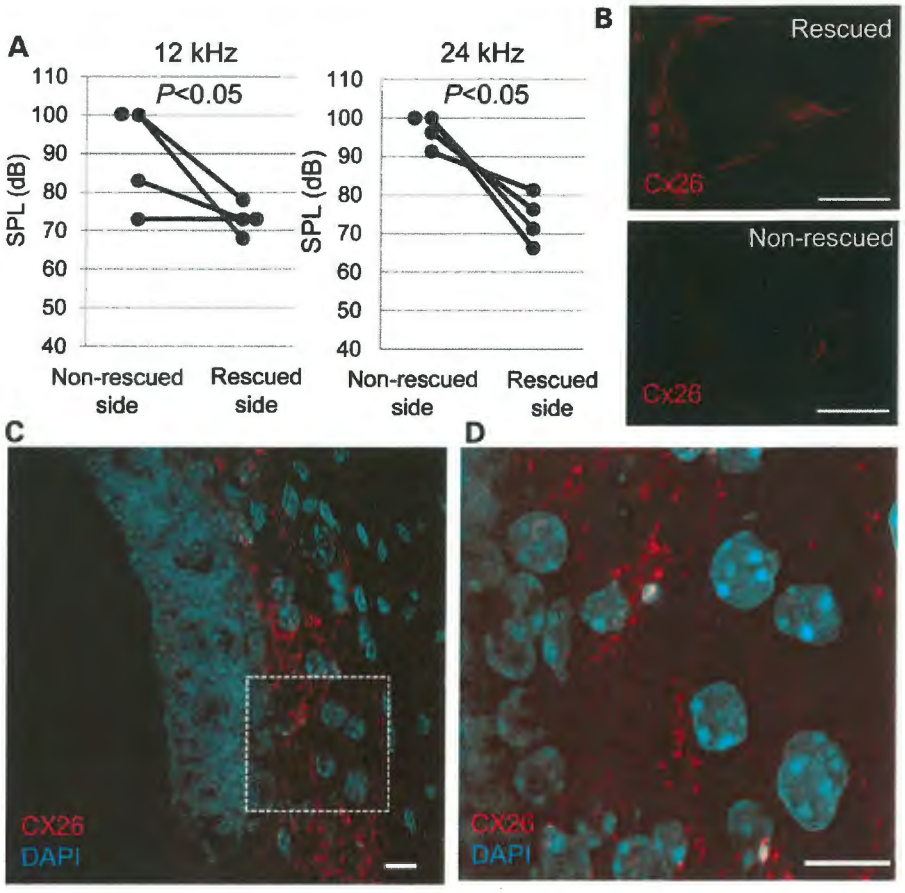

Figure 4. AAV-mediated delivery of *Gjb2* to neonatal (P0) Cx26-deficient mice. **(A)** ABR thresholds to pure tone bursts (12 and 24 kHz) for rescued and non-rescued cochleae of $Cx26^{fl/fl}$P0-Cre mice (P60–P90; $n = 5$). $P < 0.05$ was calculated using the paired *t*-test. **(B)** Cx26 localization (red) after *Gjb2* delivery to $Cx26^{fl/fl}$P0-Cre mice. Scale bars = 100 μm. **(C)** Cx26 distribution (in red) in lateral wall fibrocytes of $Cx26^{fl/fl}$P0-Cre mice cochlear cryosections at 10 weeks after AAV-Cx26 injection showing the cochlear gap junctions with Cx26. Scale bars: 10 μm. **(D)** A magnified image of region in (C). Nuclei were counterstained with DAPI (blue). Scale bars: 10 μm.

heterotypic and heteromeric Cx26/Cx30) gap junction channels form intercellular networks in non-sensory cells of the cochlea (32,33). Homotypic Cx26 channels, but not homotypic Cx30 channels, are permeable to anion tracers (34). Compared with homomeric channels, hybrid channels relay intercellular Ca^{2+} signals more rapidly (35) and are more permeable to neurobiotin (34). Overexpression of mouse *Gjb2* can rescue hearing loss in *Gjb6*/Cx30 null mice (36). In addition, a Cx30 knockout mouse model that preserved half of the Cx26 expression resulted in normal hearing (37). Thus, biochemical coupling in the cochlea requires hybrid Cx26/Cx30 or homotypic Cx26 gap junctions. Targeted deletion of Cx26 in a mouse model impairs *in vitro* biochemical coupling (7,38). Transducing the cochlear cultures (38) and the scala media (7) with an AAV vector containing Cx26 restores Cx26 expression and rescues biochemical coupling. The rescue of gap junction biochemical coupling may represent the mechanism by which gene transfer restored hearing in our mouse model of Cx26 deficiency. In the present study, gene therapy likely reconstitutes the hybrid Cx26/Cx30 and/or homotypic Cx26 gap junctions in the organ of Corti, as Cx30 was extensively expressed in Cx26-deficient mice (13). Restored biochemical or metabolic coupling in the organ of Corti may lead to appropriate postnatal development. To restore hearing, therefore, it may be sufficient to supply a wild-type version of Cx26 only during postnatal development. In contrast, permanent or repeated reconstitution of the K^+ recycling pathway would be required in connective tissue gap junctions. Timed conditional null of Cx26 in mice demonstrated that Cx26 plays essential roles in the maturation process of the organ of Corti prior to the establishment of high K^+ in the endolymph and the onset of hearing (39,40).

The absence of Cx26 or Cx30 is unlikely to disrupt endolymphatic K^+ recycling. The dominant-negative *Gjb2* R75W transgenic mouse is deaf but exhibits a normal EP (9). Normal EP in the dominant-negative R75W mouse can be explained by the fact that homotypic Cx26 channels are permeable to K^+ ions (34,41) and that gap junctions harboring Cx26 mutations associated with hearing loss have no abnormal electrophysiological characteristics, including K^+ permeability (35,36). In Cx30 null mice, the ionic coupling among cochlear supporting cells is indistinguishable from that in wild type (30), and is thought to be easily comparable to that of Cx26 null mice. These findings indicate that the movement of intercellular K^+ can be mediated by gap junction channels composed of Cx30 alone. Lower EP values measured in the current conditional *Gjb2* null mice may reflect reduced K^+ conductance in connective tissues that resulted from a decrease in the total number of gap junction proteins, i.e. the absence of Cx26. The transduction of wild-type Cx26 into cells of the pillar cells is unlikely to be completely sufficient on the basis of the

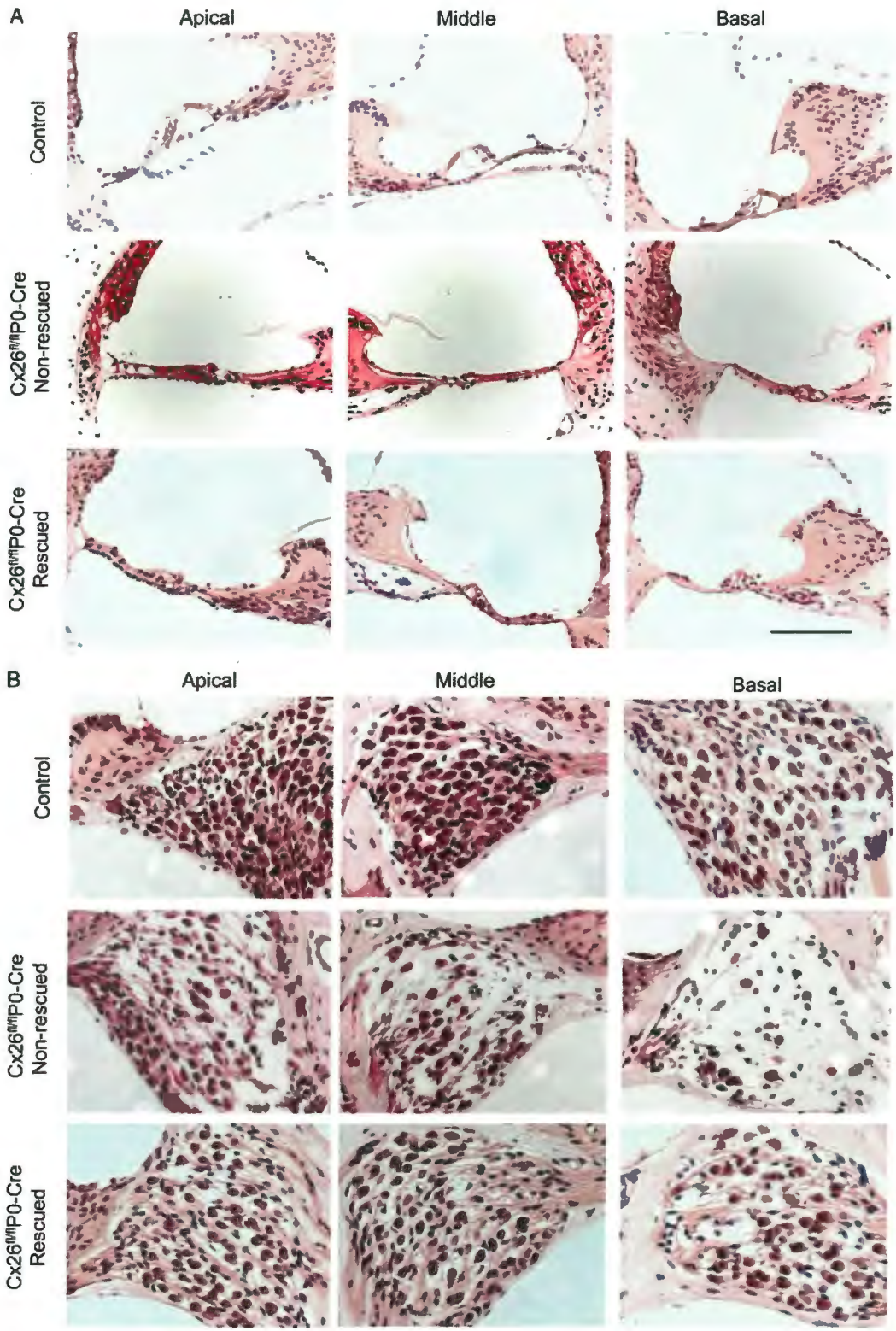

Figure 5. Light micrographs of the organ of Corti (A) and the spiral ganglion neurons (B) at the apical, middle and basal turns. Images from control mice, non-rescued $Cx26^{fl/fl}$P0-Cre mice and rescued $Cx26^{fl/fl}$P0-Cre mice are shown. Scale bars = 100 μm.

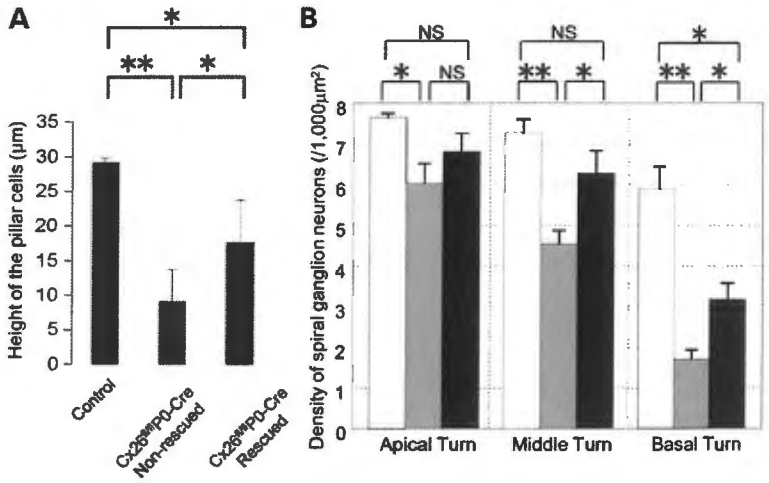

Figure 6. The morphometric analysis derived from Figure 5. (A) The height of the pillar cells at the basal turn among control mice and non-rescued and rescued cochleae of $Cx26^{fl/fl}$P0-Cre mice. (B) The density of the spiral ganglion neurons among control mice (white columns) and non-rescued (gray columns) and rescued cochleae (black columns) of $Cx26^{fl/fl}$P0-Cre mice. Error bars represent the SEM. Significance (*$P < 0.05$, **$P < 0.01$) was calculated using the Student's t-test.

height of the organ of Corti (Fig. 5). The wild-type Cx26 was transduced into type I and IV fibrocytes of the spiral ligament (Fig. 4B), which was consistent with the distribution of native Cx26 (33), suggesting that the EP would likely be partially recovered, although the EP was not measured in rescued cochleae.

Future experiments should focus on improving transduction efficiency to the supporting cells as well as the long-lasting transduction of wild-type Cx26, or replaceable genes such as Cx30 and Cx32 (34,42), in connective tissues.

Using a conditional knockout mouse and gene transfer techniques, we have clarified the molecular mechanisms by which *Gjb2* affects cochlear physiology. The epithelial gap junction network composed of hybrid Cx26/Cx30 channels is required for postnatal development of the organ of Corti and for normal hearing. In contrast, the K^+ recycling pathway, which is mediated by the gap junction network of connective tissues, can be supported by both hybrid and homomeric channels involving Cx26 and/or Cx30. These results will help begin a new era in the comprehensive treatment of hereditary deafness.

Materials and Methods

Generation of mice with a floxed Cx26 allele

A targeting vector of a floxed Cx26 allele was constructed using phage DNA clones that included exons 1 and 2 of Cx26 from a genomic library of J1 embryonic stem cells. An ~8.4 kb HindIII–BamHI fragment containing exon 1 and a 2.85 kb 'SacI–SacI' fragment containing the 3′ half of exon 2 (long and short homologous sequences, respectively) were isolated and used to construct the targeting vector. One loxP sequence was introduced at the end of intron 1, and the Neo cassette was introduced between two loxP sequences in exon 2. The diphtheria toxin A chain expression cassette was used as a negative selection marker. The linearized targeting vector was introduced into J1 embryonic stem cells by electroporation, and G418-resistant clones were analyzed by Southern blotting to isolate homologous recombinants as described (43). Recombinant embryonic stem cells were injected into C57/BL6J blastocysts. A mouse strain harboring the floxed Cx26 allele was established by crossing chimeras with C57/BL6J females to produce F1 heterozygotes ($Cx26^{fl/+}$). F2 offspring were generated by crossing two F1 double heterozygotes. Genotyping was performed via PCR amplification using tail lysates as templates and the primers shown in Figure 1A (P1: AAAC TACCGGGAAGCGACACGGGGT; P2: GGTTACGGGGTGCACCAAAG CACAG). No abnormalities were apparent in $Cx26^{fl/fl}$ mice. Otic vesicle-specific Cx26 knockout mice ($Cx26^{fl/fl}$P0-Cre) were generated by breeding $Cx26^{fl/fl}$ mice with P0-Cre mice. All animal work was carried out in accordance with institutional guidelines (see below).

Injection of the AAV-Cx26 viral vector

Animals were anesthetized with an intraperitoneal injection of ketamine (100 mg/kg) and xylazine (10 mg/kg) in all experiments. All experimental protocols were approved by the Institutional Animal Care and Use Committee at Juntendo University School of Medicine and were conducted in accordance with the US National Institutes of Health Guidelines for the Care and Use of Laboratory Animals.

The same protocol was used to treat both the adult and neonatal mice. An AAV serotype 5 vector was generated that used the CMV promoter to drive the expression of mouse Cx26. The coding region from mouse *Gjb2* cDNA (GenBank accession number BC013634.1) was inserted into the *pAAV-IRES-hr*GFP vector (Agilent Technologies, CA, USA). This AAV-Cx26 vector was injected into the perilymph through the round window membrane. Glass capillaries (Drummond Scientific Co., PA, USA) were drawn with a PB-7 pipette puller (Narishige, Tokyo, Japan) to achieve an outer tip diameter of ~10 μm. A polyethylene tube (outer diameter, 1.7 mm; Atom Medical Co., Saitama, Japan) was connected to the glass micropipette. The viral vector with a concentration of 8.6×10^{11} viral particles was injected into the perilymph at a rate of 0.05 μl/min in adult mice and 0.02 μl/min in neonatal mice for 10 min using a syringe connected to a polyethylene tube. To allow the vector to spread throughout the inner ear, the glass micropipette was left in place for 1 min after the injection procedure. The leakage of perilymph was confirmed to be nominal after removing the micropipette. It took ~20 min to complete the surgical procedure. After the surgery, the mice were kept in another cage until they awoke from anesthesia.

Auditory brainstem response

All electrophysiological measurements were performed within a grounded test room that was acoustically and electrically insulated. For the ABR measurement, mice were anesthetized and maintained in a headholder. Stainless steel needle electrodes were placed at the vertex and ventrolateral to the left and right ears. The ABRs were measured using waveform storing and stimulus control with Scope software on the Power Lab system (PowerLab4/25; AD Instruments, Castle Hill, Australia). Electrocardiogram recordings were performed using an extracellular AC Preamplifier (P-55; Astro-Med, Inc., RI, USA). Acoustic stimuli were delivered using a coupler type speaker (ES1spc; Bio Research Center, Nagoya, Japan). Thresholds were determined for click sounds and tone bursts (frequencies of 8, 12, 16, 20 and 24 kHz) from a set of responses at different intensities (5 dB intervals). Electrical signals were averaged over 512 repetitions. Hearing thresholds >95 dB were listed as 100 dB.

Endocochlear potential

For EP measurements, each mouse was artificially ventilated with a respirator through a tracheal cannula after deep anesthesia and muscular relaxation. Rectal temperature was maintained at 37°C, and an electrocardiometer was used to monitor the heart rate. A glass microelectrode filled with 150 mM KCl was inserted into the scala media of the basal turn through the lateral wall of the cochlea as previously reported (44). Output was recorded using a high-impedance dual electrometer.

Light microscopy

Animals were anesthetized and then perfused intracardially with 0.01 M phosphate-buffered saline (PBS; pH 7.2), followed by 4% paraformaldehyde (PFA; pH 7.4) in 0.1 M phosphate buffer (PB; pH 7.4). The mice were decapitated and their cochleae dissected under a microscope. Dissected cochleae were placed in 4% PFA at room temperature overnight. Cochleae were then placed in 0.12 M ethylenediaminetetraacetic acid (EDTA; pH 7.0) in PBS for 1 week for decalcification. Specimens were then dehydrated, embedded in paraffin and sectioned (6 μm). Serial sections were stained with hematoxylin and eosin staining.

Quantitative analyses of spiral ganglion neurons

To evaluate the survival of the spiral ganglion neurons, four animals from each group were used for cell counting. Five cross-sections of hematoxylin and eosin staining randomly selected from each animal were analyzed. The area of the Rosenthal's canal at the basal, middle and apical turns was measured using Image Pro Plus 6.0 software. The number of spiral ganglion neurons per 1000 μm^2 was calculated for each profile.

Transmission electron microscopy

Animals were anesthetized and then perfused intracardially with 0.01 M PBS, followed by 4% PFA and 2% glutaraldehyde (GA) in 0.1 M PB. The cochleae were opened and flushed with buffered 4% PFA and 2% GA and fixed for 2 h at room temperature. The specimens were washed and then post-fixed using 2% OsO_4 in 0.1 M PB for 1.5 h. Specimens were then dehydrated through graded concentrations of ethanol and embedded in Epon. Samples were sectioned (1 μm), stained with uranyl acetate and lead citrate and examined using an electron microscope (H-7100; Hitachi, Tokyo, Japan).

Immunohistochemistry

Mice were anesthetized and then perfused intracardially with PBS, followed by 4% PFA in PB. Cochleae were excised and fixed in 4% PFA for 2 h and then decalcified in 0.12 M EDTA for 7 d at room temperature. For frozen sections, specimens were cryo-protected in 30% sucrose in PBS overnight at 4°C and then embedded in OCT compound, frozen and sectioned (10 μm). For immunofluorescence, sections were incubated with 50% Block Ace (DC Pharma Biomedical, Osaka, Japan) in PBS/0.3% Triton X-100 for 60 min and then incubated overnight at 4°C with rabbit polyclonal antibodies directed against Cx26 and Cx30 (1:200; Zymed laboratories, CA, USA) that were diluted in PBS. Tissue specimens were then rinsed with PBS, incubated with goat anti-rabbit IgG antibodies conjugated with Alexa Fluor 594 (1:500; Molecular Probes, OR, USA) for 60 min and then rinsed with PBS. Specimens were mounted in Vectashield antifade mounting medium (Vector Laboratories, CA, USA). Images were captured using a Zeiss Axioplan2 microscope, an AxioCam HRc CCD camera and AxioVision Rel.4.5 software (Carl Zeiss, Esslingen, Germany). Fluorescence confocal images were obtained with a LSM510-META confocal microscope (Carl Zeiss, Jena, Germany).

Statistical analyses

Error bars represent the SEM. Statistical differences were calculated using the Student's t-test or paired t-test where indicated. Differences were considered significant for $P < 0.05$.

Authors' Contributions

K.I. and T.N. conceived of and designed the study. S.G., Y.S. and O.M. performed the molecular work. M.S. measured EP. T.I. and K.K. measured ABR and performed the histological experiments. K.I. wrote the paper.

Acknowledgements

We would like to thank H. Yamanaka and S. Ito-Kawashima (Department of Cell Biology, Japanese Foundation for Cancer Research, Cancer Institute) for their technical assistance. We also thank Y. Katori and T. Kudo (Department of Otolaryngology & Head and Neck Surgery, Tohoku University School of Medicine, Sendai); H. Mochizuki (Department of Neurology, Osaka University Graduate School of Medicine, Osaka); T. Nara (Department of Molecular and Cellular Parasitology, Juntendo University Faculty of Medicine, Tokyo); T. Nihira (Department of Neurology, School of Allied Health Sciences, Kitasato University, Sagamihara) and T. Okano, T. Nakagawa and J. Ito (Department of Otolaryngology-Head and Neck Surgery, Kyoto University, Kyoto) for technical advice and valuable discussions.

Conflict of Interest statement. None declared.

Funding

This work was supported in part by grants-in-aid (20390445 and 25293351) to K.I. and by grant-in-aid (12480253) to O.M. from the Ministry of Education, Sports, Science and Culture of Japan, the MEXT-support program for the Strategic Research Foundation at Private Universities, 2011–2013 to K.I. and a research grant from the Ministry of Health, Labor and Welfare of Japan to K.K.

References

1. Petit, C., Levilliers, J. and Hardelin, J.P. (2001) Molecular genetics of hearing loss. *Annu. Rev. Genet.*, **35**, 589–646.
2. Kral, A. and O'Donoghue, G.M. (2010) Profound deafness in childhood. *N. Engl. J. Med.*, **363**, 1438–1450.
3. Maeda, Y., Fukushima, K., Nishizaki, K. and Smith, R.J. (2005) In vitro and in vivo suppression of GJB2 expression by RNA interference. *Hum. Mol. Genet.*, **14**, 1641–1650.
4. Akil, O., Seal, R.P., Burke, K., Wang, C., Alemi, A., During, M., Edwards, R.H. and Lustig, L.R. (2012) Restoration of hearing in the VGLUT3 knockout mouse using virally mediated gene therapy. *Neuron*, **75**, 283–293.
5. Lentz, J.J., Jodelka, F.M., Hinrich, A.J., McCaffrey, K.E., Farris, H.E., Spalitta, M.J., Bazan, N.G., Duelli, D.M., Rigo, F. and Hastings, M.L. (2013) Rescue of hearing and vestibular function by antisense oligonucleotides in a mouse model of human deafness. *Nat. Med.*, **19**, 345–350.
6. Miwa, T., Minoda, R., Ise, M., Yamada, T. and Yumoto, E. (2013) Mouse otocyst transuterine gene transfer restores hearing in mice with connexin 30 deletion-associated hearing loss. *Mol. Ther.*, **21**, 1142–1150.
7. Yu, Q., Wang, Y., Chang, Q., Wang, J., Gong, S., Li, H. and Lin, X. (2014) Virally expressed connexin26 restores gap junction function in the cochlea of conditional Gjb2 knockout mice. *Gene Ther.*, **21**, 71–80.
8. Cohen-Salmon, M., Ott, T., Michel, V., Hardelin, J.P., Perfettini, I., Eybalin, M., Wu, T., Marcus, D.C., Wangemann, P., Willecke, K. and Petit, C. (2002) Targeted ablation of connexin26 in the inner ear epithelial gap junction network causes hearing impairment and cell death. *Curr. Biol.*, **12**, 1106–1111.
9. Kudo, T., Kure, S., Ikeda, K., Xia, A.P., Katori, Y., Suzuki, M., Kojima, K., Ichinohe, A., Suzuki, Y., Aoki, Y., Kobayashi, T. and Matsubara, Y. (2003) Transgenic expression of a dominant-negative connexin26 causes degeneration of the organ of Corti and non-syndromic deafness. *Hum. Mol. Genet.*, **12**, 995–1004.
10. Inoshita, A., Iizuka, T., Okamura, H.O., Minekawa, A., Kojima, K., Furukawa, M., Kusunoki, T. and Ikeda, K. (2008) Postnatal development of the organ of Corti in dominant-negative *Gjb2* transgenic mice. *Neuroscience*, **156**, 1039–1047.
11. Minekawa, A., Abe, T., Inoshita, A., Iizuka, T., Kakehata, S., Narui, Y., Koike, T., Kamiya, K., Okamura, H.O., Shinkawa, H. *et al.* (2009) Cochlear outer hair cells in a dominant-negative connexin26 mutant mouse preserve non-linear capacitance in spite of impaired distortion product otoacoustic emission. *Neuroscience*, **164**, 1312–1319.
12. Wang, Y., Chang, Q., Tang, W., Sun, Y., Zhou, B., Li, H. and Lin, X. (2009) Targeted connexin26 ablation arrests postnatal development of the organ of Corti. *Biochem. Biophys. Res. Commun.*, **385**, 33–37.
13. Kamiya, K., Yum, S.W., Kurebayashi, N., Muraki, M., Ogawa, K., Karasawa, K., Miwa, A., Guo, X., Gotoh, S., Sugitani, Y., Yamanaka, H. *et al.* (2014) Assembly of the cochlear gap junction macromolecular complex requires connexin 26. *J Clin Invest.*, **124**, 1598–1607.
14. Duan, M., Venail, F., Spencer, N. and Mezzina, M. (2004) Treatment of peripheral sensorineural hearing loss: gene therapy. *Gene Ther.*, **11**(Suppl 1), S51–S56.
15. Iizuka, T., Kanzaki, S., Mochizuki, H., Inoshita, A., Narui, Y., Furukawa, M., Kusunoki, T., Saji, M., Ogawa, K. and Ikeda, K. (2008) Noninvasive in vivo delivery of transgene via adeno-associated virus into supporting cells of the neonatal mouse cochlea. *Hum. Gene Ther.*, **19**, 384–390.
16. Gabriel, H.D., Jung, D., Bützler, C., Temme, A., Traub, O., Winterhager, E. and Willecke, K. (1998) Transplacental uptake of glucose is decreased in embryonic lethal connexin26-deficient mice. *J. Cell Biol.*, **140**, 1453–1461.
17. Hasegawa, S., Sato, T., Akazawa, H., Okada, H., Maeno, A., Ito, M., Sugitani, Y., Shibata, H., Miyazaki Ji, J., Katsuki, M. *et al.* (2002) Apoptosis in neural crest cells by functional loss of APC tumor suppressor gene. *Proc. Natl. Acad. Sci. U. S. A.*, **99**, 297–302.
18. Nin, F., Hibino, H., Doi, K., Suzuki, T., Hisa, Y. and Kurachi, Y. (2008) The endocochlear potential depends on two K+ diffusion potentials and an electrical barrier in the stria vascularis of the inner ear. *Proc. Natl. Acad. Sci. U. S. A.*, **105**, 1751–1756.
19. Gow, A., Davies, C., Southwood, C.M., Frolenkov, G., Chrustowski, M., Ng, L., Yamauchi, D., Marcus, D.C. and Kachar, B. (2004) Deafness in Claudin 11-null mice reveals the critical contribution of basal cell tight junctions to stria vascularis function. *J. Neurosci.*, **24**, 7051–7062.
20. Kitajiri, S., Miyamoto, T., Mineharu, A., Sonoda, N., Furuse, K., Hata, M., Sasaki, H., Mori, Y., Kubota, T., Ito, J. *et al.* (2004) Compartmentalization established by claudin-11-based tight junctions in stria vascularis is required for hearing through generation of endocochlear potential. *J. Cell Sci.*, **117**, 5087–5096.
21. Wangemann, P. (2006) Supporting sensory transduction: cochlear fluid homeostasis and the endocochlear potential. *J. Physiol.*, **576**, 11–21.
22. Salt, A.N., Thalmann, R., Marcus, D.C. and Bohne, B.A. (1986) Direct measurement of longitudinal endolymph flow rate in the guinea pig cochlea. *Hear. Res.*, **23**, 141–151.
23. Konishi, T., Kelsey, E. and Singleton, G.T. (1966) Effect of chemical alteration in the endolymph on the cochlear potentials. Acta Otolaryngol. (Stockh.), **62**, 393–404.
24. Bedrosian, J.C., Gratton, M.A., Brigande, J.V., Tang, W., Landau, J. and Bennett, J. (2006) In vivo delivery of recombinant viruses to the fetal murine cochlea: transduction characteristics and long-term effects on auditory function. *Mol. Ther.*, **14**, 328–335.
25. Sacheli, R., Delacroix, L., Vandenackerveken, P., Nguyen, L. and Malgrange, B. (2013) Gene transfer in inner ear cells: a challenging race. *Gene Ther.*, **20**, 237–247.
26. Kikuchi, T., Kimura, R.S., Paul, D.L. and Adams, J.C. (1995) Gap junctions in the rat cochlea: immunohistochemical and ultrastructural analysis. *Anat. Embryol. (Berl)*, **191**, 101–118.
27. Wangemann, P. (2002) K^+ cycling and the endocochlear potential. *Hear. Res.*, **165**, 1–9.
28. Beltramello, M., Piazza, V., Bukauskas, F.F., Pozzan, T. and Mammano, F. (2005) Impaired permeability to Ins(1,4,5)P3 in a mutant connexin underlies recessive hereditary deafness. *Nat. Cell Biol.*, **7**, 63–69.
29. Zhang, Y., Tang, W., Ahmad, S., Sipp, J.A., Chen, P. and Lin, X. (2005) Gap junction-mediated intercellular biochemical coupling in cochlear supporting cells is required for normal cochlear functions. *Proc. Natl. Acad. Sci. U. S. A.*, **102**, 15201–15206.
30. Chang, Q., Tang, W., Ahmad, S., Zhou, B. and Lin, X. (2008) Gap junction mediated intercellular metabolite transfer in the cochlea is compromised in connexin30 null mice. *PLoS One*, **3**, e4088.
31. Majumder, P., Crispino, G., Rodriguez, L., Ciubotaru, C.D., Anselmi, F., Piazza, V., Bortolozzi, M. and Mammano, F. (2010) ATP-mediated cell-cell signaling in the organ of Corti: the role of connexin channels. *Purinergic Signal.*, **6**, 167–187.

32. Ahmad, S., Chen, S., Sun, J. and Lin, X. (2003) Connexins 26 and 30 are co-assembled to form gap junctions in the cochlea of mice. *Biochem. Biophys. Res. Commun.*, **307**, 362–368.
33. Forge, A., Becker, D., Casalotti, S., Edwards, J., Marziano, N. and Nevill, G. (2003) Gap junctions in the inner ear: comparison of distribution patterns in different vertebrates and assessment of connexin composition in mammals. *J. Comp. Neurol.*, **467**, 207–231.
34. Yum, S.W., Zhang, J., Valiunas, V., Kanaporis, G., Brink, P.R., White, T.W. and Scherer, S.S. (2007) Human connexin26 and connexin30 form functional heteromeric and heterotypic channels. *Am. J. Physiol. Cell Physiol.*, **293**, C1032–C1048.
35. Sun, Y., Tang, W., Chang, Q., Wang, Y., Kong, W. and Lin, X. (2009) Connexin30 null and conditional connexin26 null mice display distinct pattern and time course of cellular degeneration in the cochlea. *J. Comp. Neurol.*, **516**, 569–579.
36. Ahmad, S., Tang, W., Chang, Q., Qu, Y., Hibshman, J., Li, Y., Söhl, G., Willecke, K., Chen, P. and Lin, X. (2007) Restoration of connexin26 protein level in the cochlea completely rescues hearing in a mouse model of human connexin30-linked deafness. *Proc. Natl. Acad. Sci. U. S. A.*, **104**, 1337–1341.
37. Boulay, A.C., del Castillo, F.J., Giraudet, F., Hamard, G., Giaume, C., Petit, C., Avan, P. and Cohen-Salmon, M. (2013) Hearing is normal without connexin30. *J. Neurosci.*, **33**, 430–434.
38. Crispino, G., Di Pasquale, G., Scimemi, P., Rodriguez, L., Galindo Ramirez, F., De Siati, R.D., Santarelli, R.M., Arslan, E., Bortolozzi, M., Chiorini, J.A. *et al.* (2011) BAAV mediated GJB2 gene transfer restores gap junction coupling in cochlear organotypic cultures from deaf Cx26Sox10Cre mice. *PLoS One*, **6**, e23279.
39. Chen, S., Sun, Y., Lin, X. and Kong, W. (2014) Down regulated connexin26 at different postnatal stage displayed different types of cellular degeneration and formation of organ of Corti. *Biochem Biophys Res Commun.*, **445**, 71–77.
40. Chang, Q., Tang, W., Kim, Y. and Lin, X. (2015) Timed conditional null of connexin26 in mice reveals temporary requirements of connexin26 in key cochlear developmental events before the onset of hearing. *Neurobiol Dis.*, **73**, 418–427.
41. Manthey, D., Banach, K., Desplantez, T., Lee, C.G., Kozak, C.A., Traub, O., Weingart, R. and Willecke, K. (2001) Intracellular domains of mouse connexin26 and -30 affect diffusional and electrical properties of gap junction channels. *J. Membr. Biol.*, **181**, 137–148.
42. Degen, J., Schütz, M., Dicke, N., Strenzke, N., Jokwitz, M., Moser, T. and Willecke, K. (2011) Connexin32 can restore hearing in connexin26 deficient mice. *Eur. J. Cell Biol.*, **90**, 817–824.
43. Shibata, H., Toyama, K., Shioya, H., Ito, M., Hirota, M., Hasegawa, S., Matsumoto, H., Takano, H., Akiyama, T., Toyoshima, K. *et al.* (1997) Rapid colorectal adenoma formation initiated by conditional targeting of the Apc gene. *Science*, **278**, 120–123.
44. Minowa, O., Ikeda, K., Sugitani, Y., Oshima, T., Nakai, S., Katori, Y., Suzuki, M., Furukawa, M., Kawase, T., Zheng, Y. *et al.* (1999) Altered cochlear fibrocytes in a mouse model of DFN3 nonsyndromic deafness. *Science*, **285**, 1408–1411.

THE JOURNAL OF BIOLOGICAL CHEMISTRY VOL. 289, NO. 48, pp. 33131–33136, November 28, 2014

Lysine 63-linked Polyubiquitination Is Dispensable for Parkin-mediated Mitophagy*

Received for publication, May 13, 2014, and in revised form, September 27, 2014
Published, JBC Papers in Press, October 21, 2014, DOI 10.1074/jbc.C114.580944

Kahori Shiba-Fukushima[‡], Tsuyoshi Inoshita[§], Nobutaka Hattori[‡§1], and Yuzuru Imai[§2]

From the Departments of [‡]Neurology and [§]Research for Parkinson's Disease, Juntendo University Graduate School of Medicine, Tokyo 113-8421, Japan

Background: Lys-63-linked ubiquitination in mitochondria occurs in PINK1/Parkin-mediated mitophagy, and its important roles have been proposed.
Results: The suppression of Lys-63-linked ubiquitination did not modulate PINK1/Parkin-mediated mitophagy and *Drosophila* mitochondrial phenotypes.
Conclusion: Lys-63-linked ubiquitination is dispensable for PINK1-Parkin pathway.
Significance: This is the first study to report the biological significance of Lys-63-linked ubiquitination in PINK1-Parkin pathway *in vitro* and *in vivo*.

PINK1/Parkin-mediated mitophagy is thought to ensure mitochondrial quality control in neurons as well as other cells. Upon the loss of mitochondrial membrane potential (ΔΨm), Lys-63-linked polyubiquitin chains accumulate on the mitochondrial outer membrane in a Parkin-dependent manner. However, the physiological significance of Lys-63-linked polyubiquitination during mitophagy is not fully understood. Here, we report that the suppression of Lys-63-linked polyubiquitination through the removal of Ubc13 activity essentially affects neither PINK1 activation nor the degradation of depolarized mitochondria. Moreover, the inactivation of Ubc13 did not modulate the mitochondrial phenotypes of *PINK1* knockdown *Drosophila*. Our data indicate that the formation of Lys-63-linked polyubiquitin chains on depolarized mitochondria is not a key factor for the PINK1-Parkin pathway as was once thought.

Mutations of the *Parkin* and *PINK1* genes cause selective degeneration of the midbrain dopaminergic neurons in autosomal recessive juvenile Parkinson disease (1, 2). The *Parkin* and *PINK1* genes encode a ubiquitin-ligase (E3)[3] and a serine/threonine protein kinase, respectively (3–7). Loss of the *Parkin* and *PINK1* genes in *Drosophila* leads to the degeneration of the mitochondria in tissues with high energy demands, such as the muscles and sperm, and genetic analysis has demonstrated that PINK1 is an upstream regulator of Parkin, suggesting an important role of Parkin and PINK1 in mitochondrial maintenance in the midbrain dopaminergic neurons that are affected in Parkinson disease (8–10).

A series of cell biological studies has provided strong evidence that Parkin cooperates with PINK1 to induce mitochondrial autophagy or mitophagy when the mitochondria are damaged (11–16). The reduction of ΔΨm leads to the accumulation and activation of PINK1 in the mitochondria (12, 17), which leads to the phosphorylation of a latent form of Parkin, priming its E3 activation (17, 18). PINK1 also phosphorylates ubiquitin (19–21), which in turn fully activates Parkin E3 activity, leading to Parkin translocation from the cytosol to the mitochondria and the subsequent ubiquitination of mitochondrial proteins (14, 15). Ubiquitin modification on the mitochondria induces the LC3-mediated autophagic elimination of the damaged mitochondria, a process known as mitophagy (11). The ubiquitination of mitochondrial proteins mainly produces Lys-63-linked polyubiquitin and only a small portion of Lys-48 linkages (22, 23). The Lys-63-linked polyubiquitin chain is proposed to activate PINK1 (24) and the mitochondrial translocation of Parkin (25). We examined the impact of Lys-63-linked polyubiquitination on PINK1/Parkin-mediated mitophagy in cells and mitochondrial maintenance in *Drosophila* and report that Lys-63-linked polyubiquitination is dispensable for PINK1 activation, mitochondrial clearance, and *Drosophila* mitochondrial homeostasis.

EXPERIMENTAL PROCEDURES

Antibodies, Reagents, Plasmids, and Cell Lines—The following antibodies were used in the Western blot analysis: anti-PINK1 (1:1,000 dilution; Novus Biologicals, BC100-494), anti-Mfn1 (1:1,000 dilution; Abnova, clone 3C9), anti-Ubc13 (1:1,000 dilution; Life Technologies, clone 4E11), anti-polyubiquitin (1:1,000 dilution; MBL International, clone FK2), anti-Lys-63-linked polyubiquitin (1:1,000 dilution; Cell Signaling Technology, clone D7A11), anti-Lys-48-linked polyubiquitin (1:1,000 dilution; Cell Signaling Technology, clone D9D5), anti-Tom20 (1:500 dilution; Santa Cruz Biotechnology, FL-145), anti-HA (1:1,000 dilution; Roche Applied Science, clone 3F10), anti-FLAG-HRP (1:2,000 dilution; Sigma-Aldrich, clone M2), anti-actin (1:10,000 dilution; Millipore, MAb1501),

* This work was supported by grants from the Takeda Science Foundation, (to Y. I.), the Life Science Foundation of Japan (to Y. I.), the Daiichi-Sankyo Foundation for Life Science (to Y. I.), the Mochida Memorial Foundation for Medical and Pharmaceutical Research (to Y. I.), and Otsuka Pharmaceutical (to N. H. and Y. I.).

[1] To whom correspondence may be addressed: Dept. of Neurology, Juntendo University Graduate School of Medicine, 2-1-1 Hongo, Bunkyo-ku, Tokyo 113-8421, Japan. Tel.: 81-3-3813-3111; Fax: 81-3-5800-0547; E-mail: nhattori@juntendo.ac.jp.

[2] To whom correspondence may be addressed: Dept. of Neuroscience for Neurodegenerative Disorders, Juntendo University Graduate School of Medicine, 2-1-1 Hongo, Bunkyo-ku, Tokyo 113-8421, Japan. Tel.: 81-3-3813-3111; Fax: 81-3-5800-0547; E-mail: yzimai@juntendo.ac.jp.

[3] The abbreviations used are: E1, ubiquitin-activating enzyme; E2, ubiquitin-conjugating enzyme; E3, ubiquitin-ligase; MEF, mouse embryonic fibroblast; Mfn1, Mitofusin1; Dox, doxycycline; CCCP, carbonyl cyanide *m*-chlorophenyl hydrazine; dMfn, *Drosophila* Mitofusin.

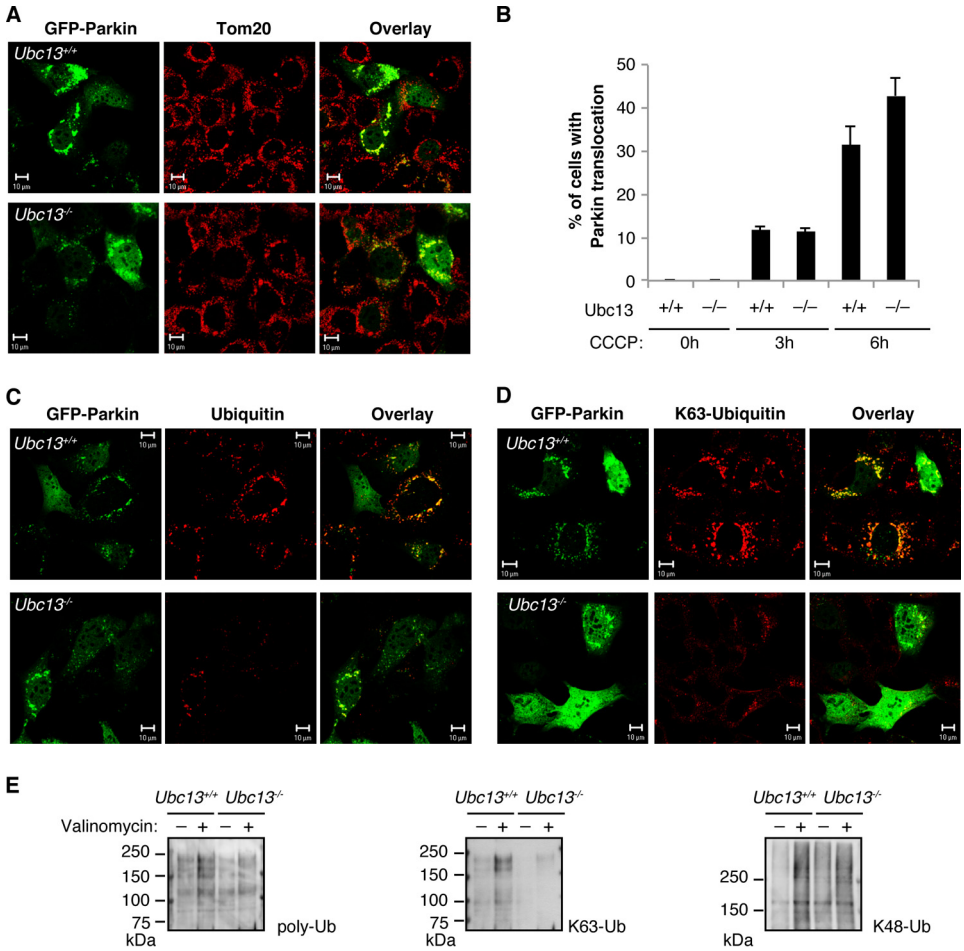

FIGURE 1. **The loss of Ubc13 activity impairs the accumulation of Lys-63-linked ubiquitin chains during Parkin-mediated mitophagy.** *A*, MEFs retrovirally introduced with GFP-Parkin were treated with Dox to remove *Ubc13* genes and then treated with 30 μM CCCP for 6 h. Parkin and mitochondria were visualized with GFP fluorescence (*green*) and anti-Tom20 (*red*), respectively. *B*, the mitochondrial translocation efficiency of Parkin treated as in *A* was graphed. The values represent the means ± S.E. of the percentages of cells exhibiting mitochondrial recruitment in three independent experiments. The translocation efficiency was similar in $Ubc13^{+/+}$ and $Ubc13^{-/-}$ (3 h, $p < 0.8024$; 6 h, $p < 0.1309$ by Student's *t* test). *C*, ubiquitin accumulation was detected with anti-polyubiquitin (*red*) in cells treated as in *A*. *D*, accumulation of a Lys-63-linked ubiquitin (*K63-Ubiquitin*) chain was detected with anti-Lys-63 linkage-specific ubiquitin antibody (*red*) in cells treated as in *A*. *Scale bars* = 10 μm. *E*, accumulation of Lys-63-linked polyubiquitin (*K63-Ub*) but not of Lys-48-linked polyubiquitin (*K48-Ub*) was reduced in the absence of Ubc13 activity. Crude mitochondrial fractions from MEFs expressing GFP-Parkin (1×10^6) treated with (+) or without (−) 30 μM valinomycin for 6 h were prepared. Polyubiquitin purified with TUBE1-agarose in the mitochondrial fractions was detected by Western blot. *poly-Ub*, polyubiquitin. All experiments were repeated at least three times in *A–D* and two times in *E*, and representative results were shown.

anti-Hsp60 (1:10,000 dilution; BD Biosciences, clone 24/Hsp60), anti-NDUFS3 (1:10,000 dilution; Abcam, 17D95), anti-*Drosophila* Hsp60 (1:1,000 dilution; Cell Signaling Technology, D307), and anti-*Drosophila* Mitofusin (dMfn) (1:2,000 dilution; made in-house). The following antibodies were used for immunocytochemistry analysis: anti-polyubiquitin (1:250 dilution; MBL International, clone FK2), anti-Lys-63-linked polyubiquitin (1:50 dilution; Millipore, clone Apu3), and anti-Tom20 (1:1,000 dilution; Santa Cruz Biotechnology, FL-145). Mouse embryonic fibroblasts (MEFs) harboring wild-type or homozygous *lox*P-flanked *Ubc13* alleles (26) were stably transfected with Cre recombinase controlled by Tet-On systems. *Ubc13* genes were floxed out following Cre-mediated excision by treatment with 1 μg/ml doxycycline (Dox) for 72 h to generate $Ubc13^{-/-}$ MEFs. Wild-type *Ubc13* MEFs were also treated with Dox as a control. The plasmids encoding GFP-Parkin, HA-Parkin, and PINK1-FLAG have been described previously (15, 27). MEFs and HeLa cells were retrovirally transfected with pMXs-puro harboring PINK1-FLAG, HA-Parkin, and GFP-Parkin, and the infected cells were selected with 1 μg/ml puromycin. The mitochondrial uncoupler carbonyl cyanide *m*-chlorophenyl hydrazine (CCCP) and the ubiquitin-activating enzyme (E1)-specific inhibitor UBEI-41 were purchased from Sigma-Aldrich. The mitochondrial uncoupler valinomycin and TUBE1-agarose were obtained from Wako and LifeSensors, respectively.

Immunocytochemical and Biochemical Analyses—Cells plated on 3.5-mm glass-bottom dishes (MatTek) were fixed with 4% paraformaldehyde in PBS and permeabilized with 50 μg/ml digitonin in PBS. The cells were stained with anti-Tom20 or anti-ubiquitin antibodies. The cells were imaged using laser-scanning microscope systems (LSM510 META, Carl Zeiss). Phos-tag (Wako Pure Chemical Industries) Western blotting was performed as described previously (18).

Drosophila Genetics—Fly experiments were performed as described (28). The w^{1118} (w^-) line was used as a wild-type

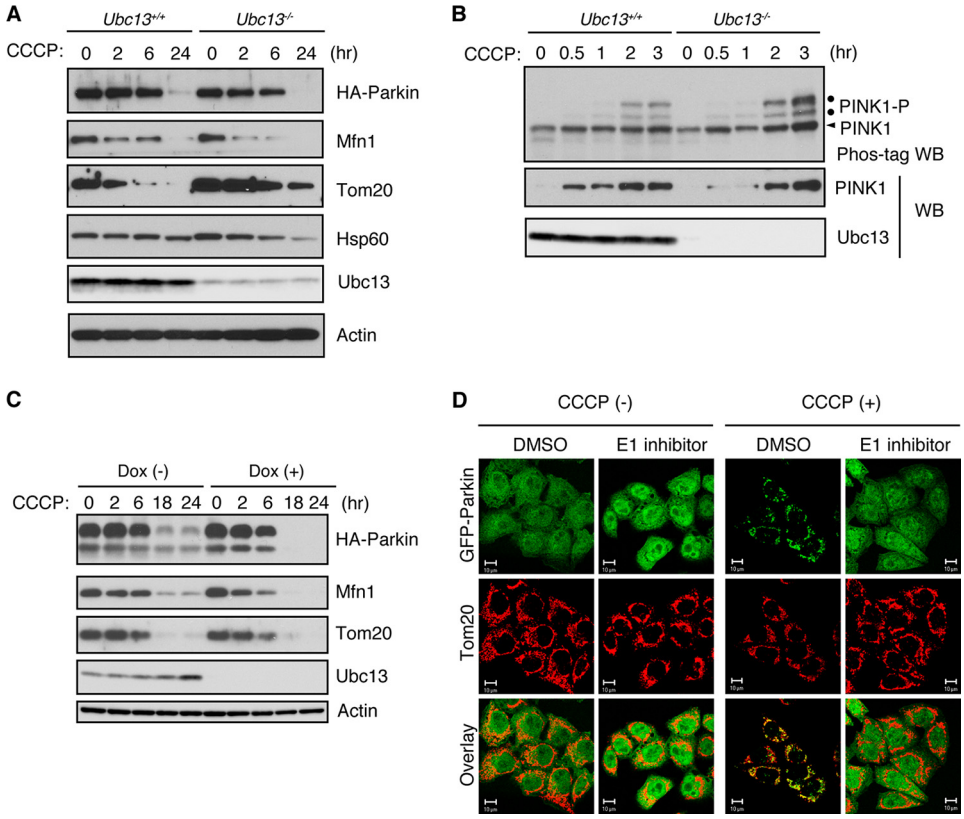

FIGURE 2. **Suppression of Lys-63-linked ubiquitin chain formation does not affect PINK1 activation or mitochondrial clearance.** *A*, MEFs expressing HA-Parkin were treated with 30 μM CCCP for up to 24 h and subjected to Western blot analysis. Mfn1 and Tom20 were used as markers of mitochondrial outer membrane proteins. Hsp60 was used as a marker of mitochondrial matrix proteins. Actin was used as a loading control. *B*, MEFs expressing PINK1-FLAG were treated with 30 μM CCCP as in *A*. The autophosphorylation of PINK1 and accumulation of PINK1 were estimated by Phos-tag Western blot with anti-PINK1 (*Phos-tag WB*) and conventional Western blot with anti-FLAG (*WB*). *C*, MEFs harboring *lox*P-flanked *Ubc13* were treated with (+) or without (−) Dox for 72 h and were further treated with CCCP for the indicated time periods. The degradation of Parkin, Mfn1, and Tom20 was analyzed by Western blot analysis. *D*, HeLa cells stably expressing GFP-Parkin were pretreated with 60 μM UBEI-41 (E1 inhibitor) or dimethyl sulfoxide (*DMSO*) solvent for 1 h and were further treated with or without 20 μM CCCP for 3 h. GFP-Parkin and mitochondria were visualized with GFP signal (*green*) and anti-Tom20 (*red*), respectively. *Scale bars* = 10 μm. All experiments were repeated at least three times in *A–C* and two times in *D*.

genetic background. The *Ubc13* RNAi line was obtained from the Vienna *Drosophila* RNAi Center and was characterized in Ref. 29. Other fly stocks used in this study have been described previously (8).

RESULTS AND DISCUSSION

Because Ubc13 is an E2 enzyme crucial for generating Lys-63-linked chains (30), we tested PINK1/Parkin-mediated mitophagy in Ubc13 mutant cells to estimate the effects of Lys-63-linked polyubiquitin chain formation. In the Ubc13 mutant cells harboring the *lox*P-flanked *Ubc13* gene, Ubc13 can be inactivated by Dox-induced flox-out. We inactivated Ubc13 by Dox treatment and induced the mitochondrial translocation of GFP-Parkin and the accumulation of ubiquitin chains using CCCP. The mitochondrial translocation of GFP-Parkin occurred with similar efficiency (Fig. 1, *A* and *B*). In contrast, the accumulation of total ubiquitin (Fig. 1, *C* and *E*) as well as Lys-63-linked polyubiquitin (Fig. 1, *D* and *E*) in the mitochondria was dramatically reduced in the absence of Ubc13 activity. Accumulation of Lys-48-linked polyubiquitin in the mitochondrial fractions was similar between $Ubc13^{+/+}$ and $Ubc13^{-/-}$ MEFs expressing GFP-Parkin (Fig. 1*E*).

Polyubiquitination induces the degradation of mitochondria outer membrane proteins through the proteasome and recruits LC3-mediated autophagy machinery (22). To test whether autophagy is altered in $Ubc13^{-/-}$ MEFs, we examined the levels of Mfn1, a known substrate of Parkin E3; a mitochondrial outer membrane protein, Tom20; and a matrix protein, Hsp60. The time-dependent degradation of Mfn1, Tom20, and Hsp60 in $Ubc13^{-/-}$ MEFs was comparable with that in $Ubc13^{+/+}$ MEFs (Fig. 2*A*). When Parkin is activated upon CCCP treatment, Parkin is subjected to autodegradation by the proteasome (18). The degradation efficiency of HA-tagged Parkin was similar between $Ubc13^{+/+}$ and $Ubc13^{-/-}$ MEFs, suggesting that the formation of Lys-63-linked polyubiquitin affects neither the activation of Parkin nor the autophagic clearance of mitochondria.

It has been proposed that Lys-63-linked ubiquitination of PINK1 by TRAF6 is required for the mitochondrial accumulation of PINK1 and mitochondrial translocation of Parkin upon a reduction of $\Delta\Psi$m (24). PINK1 stabilization on the mitochondrial outer membrane stimulates its dimerization and is closely correlated with its autophosphorylation at Ser-228 and Ser-402 in an intermolecular fashion (31), through which PINK1 kinase activity is thought to be activated (32). We estimated the extent of PINK1 accumulation and PINK1 autophosphorylation by conventional Western blot and Phos-tag Western blot analyses,

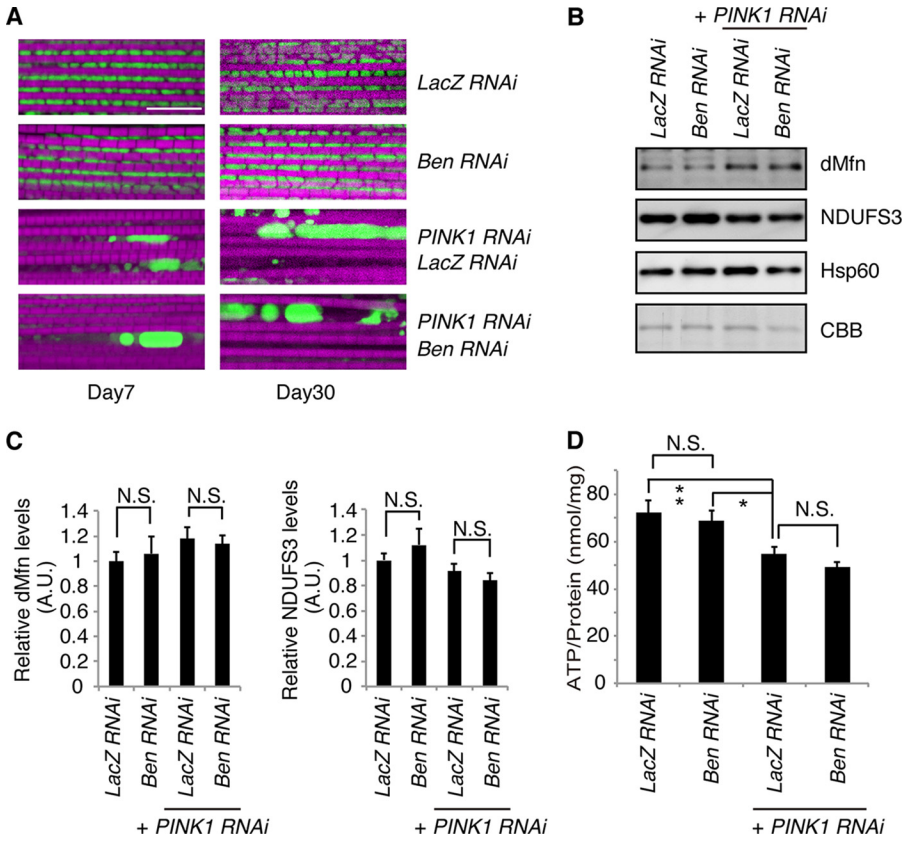

FIGURE 3. **Inhibition of Ubc13 does not modulate the mitochondrial phenotypes caused by PINK1 inactivation.** *A*, fluorescent images of the indirect flight muscle in 7- and 30-day-old adult flies expressing the indicated shRNAs are shown. To visualize the mitochondria, the mitoGFP (*green*) transgene was co-expressed, and the muscle tissue was counterstained with phalloidin (*magenta*). Representative images from three independent samples in each genotype are shown. Experiments were repeated two times. *Scale bar* = 10 μm in the fluorescent images. *B*, the protein levels of dMfn, complex I subunit NDUFS3, and Hsp60 from the thoraxes of 7-day-old adult flies were analyzed by Western blot. Coomassie Brilliant Blue (*CBB*) staining around the dMfn migration position confirms that approximately equivalent amounts of protein were loaded. *C*, the band intensities of dMfn and NDUFS3 were normalized to each Coomassie Brilliant Blue signal. The values (arbitrary units (*A.U.*)) represent the means ± S.E. from 4–5 independent samples as in *B*. Although dMfn and NDUFS3 levels showed increasing and decreasing tendencies, respectively, with PINK1 inactivation as reported (28), there were no statistical differences between any combinations. *N.S.*, not significant. $n = 4–5$. *D*, ATP contents of thorax muscle tissues of 7-day-old adult flies were measured. ATP contents were normalized against the protein levels. The values represent the means ± S.E. from five independent samples. *, $p < 0.05$, **, $p < 0.01$ by Tukey-Kramer test. Fly genotypes used in *A–D* are as follows: *UAS-mitoGFP/UAS-LacZ RNAi*; *MHC-GAL4/+* (*LacZ RNAi*), *UAS-mitoGFP/UAS-Ben RNAi*; *MHC-GAL4/+* (*Ben RNAi*), *UAS-mitoGFP/UAS-LacZ RNAi*; *MHC-GAL4, UAS-PINK1 RNAi/+* (*PINK1 RNAi, LacZ RNAi*), *UAS-mitoGFP/UAS-Ben RNAi*; *MHC-GAL4, UAS-PINK1 RNAi/+* (*PINK1 RNAi, Ben RNAi*).

respectively (Fig. 2*B*). However, there was no evidence that PINK1 accumulation and autophosphorylation were altered in the absence of *Ubc13* activity, suggesting that the formation of the Lys-63-linked polyubiquitin chain is not a key factor in PINK1 regulation in mitophagy.

Because MEFs are derived from a heterogeneous population of cells, the response to PINK1/Parkin-mediated mitophagy might differ among different batches of cells. To exclude this possibility, we used the same batch of Ubc13 mutant cells, which were treated with or without Dox. PINK1/Parkin-mediated mitophagy was induced by CCCP treatment for up to 24 h. We again confirmed that the efficiency of the degradation of HA-Parkin, Mfn1, and Tom20 is comparable between Dox-treated and untreated cells (Fig. 2*C*).

It has been reported that Parkin is also involved in xenophagy for *Mycobacterium tuberculosis*, in which the co-localization of a Lys-63-linked ubiquitin chain with phagosomes containing *M. tuberculosis* was observed (33). Because the formation of Lys-63-linked ubiquitination, the subsequent accumulation of the ubiquitin adaptors, and the autophagy machinery are Parkin-dependent, Lys-63-linked ubiquitination likely mediates the recruitment of autophagy-related proteins, as proposed in studies of mitophagy (14, 22). Lys-63-linked ubiquitination is also observed in *Salmonella* xenophagy (34). However, the recruitment of the autophagy machinery occurred with the same efficiency in *Salmonella* xenophagy (35). The results describing both mitophagy and xenophagy suggest that the autophagy machinery can recognize other polyubiquitin linkages in addition to Lys-63 or that Lys-63 linkage is not involved in this step. Although Lys-63-linked ubiquitination is not essentially required for mitochondrial translocation of Parkin, the inhibition of all of ubiquitination reactions by an E1-specific inhibitor completely suppresses Parkin translocation, suggesting that ubiquitination is part of the regulation in Parkin translocation (Fig. 2*D*).

The formation of Lys-63-linked polyubiquitination by Ubc13 and Uev1a is involved in the TNF signaling in both mammals (36) and *Drosophila* (29). Knockdown of *Bendless* (*Ben*), an ortholog of Ubc13, suppresses TNF signaling in *Drosophila*, suggesting that the formation of Lys-63-linked polyubiquitination is inhibited (29). Muscular mitochondria in the thorax, in which Ben was inactivated, showed a normal gross morphol-

ogy, implying that Lys-63-linked ubiquitination is dispensable for mitochondrial maintenance under steady-state conditions (Fig. 3*A*). In contrast, PINK1 activity is essential for maintaining mitochondrial homeostasis because inactivation of PINK1 largely leads to mitochondrial degeneration, as described previously (Fig. 3*A*) (8). The mitochondrial degeneration by PINK1 inactivation was no longer modulated by the suppression of Ben activity, even in old flies (Fig. 3*A*). Consistent with the histochemical analysis, levels of a mitochondrial outer membrane protein Mitofusin, which is a ubiquitination substrate of Parkin, as well as the mitochondrial complex I subunit NDUFS3, were not altered by Ben inactivation (Fig. 3, *B* and *C*). In addition, the absence of Ben did not affect mitochondrial ATP production (Fig. 3*D*).

In conclusion, this study revealed that Lys-63-linked ubiquitination is dispensable for the PINK1-Parkin pathway. Although Lys-63-linked ubiquitination by Parkin has been suggested to be important for the suppression of protein toxicity by Parkin, further investigations will be required to determine whether specific roles of Lys-63-linked ubiquitination in the PINK1-Parkin pathway exist (37, 38).

Acknowledgments—We thank Drs. S. Akira and M. Yamamoto for Ubc13 mutant cells, and T. Arano and T. Imura for technical assistance.

Addendum—After submission of this study, two studies using siRNA against Ubc13 reported that Ubc13 has a role for the autophagy process of Parkin-mediated mitophagy (39) and Parkin translocation (40). As we also observed some delay in mitophagy in our initial study using siRNA, we feel that certain sequences of siRNA affect mitophagy.

REFERENCES

1. Kitada, T., Asakawa, S., Hattori, N., Matsumine, H., Yamamura, Y., Minoshima, S., Yokochi, M., Mizuno, Y., and Shimizu, N. (1998) Mutations in the *parkin* gene cause autosomal recessive juvenile parkinsonism. *Nature* **392,** 605–608
2. Valente, E. M., Abou-Sleiman, P. M., Caputo, V., Muqit, M. M., Harvey, K., Gispert, S., Ali, Z., Del Turco, D., Bentivoglio, A. R., Healy, D. G., Albanese, A., Nussbaum, R., González-Maldonado, R., Deller, T., Salvi, S., Cortelli, P., Gilks, W. P., Latchman, D. S., Harvey, R. J., Dallapiccola, B., Auburger, G., and Wood, N. W. (2004) Hereditary early-onset Parkinson's disease caused by mutations in *PINK1*. *Science* **304,** 1158–1160
3. Imai, Y., Soda, M., and Takahashi, R. (2000) Parkin suppresses unfolded protein stress-induced cell death through its E3 ubiquitin-protein ligase activity. *J. Biol. Chem.* **275,** 35661–35664
4. Shimura, H., Hattori, N., Kubo, S. i., Mizuno, Y., Asakawa, S., Minoshima, S., Shimizu, N., Iwai, K., Chiba, T., Tanaka, K., and Suzuki, T. (2000) Familial Parkinson disease gene product, parkin, is a ubiquitin-protein ligase. *Nat. Genet.* **25,** 302–305
5. Beilina, A., Van Der Brug, M., Ahmad, R., Kesavapany, S., Miller, D. W., Petsko, G. A., and Cookson, M. R. (2005) Mutations in PTEN-induced putative kinase 1 associated with recessive parkinsonism have differential effects on protein stability. *Proc. Natl. Acad. Sci. U.S.A.* **102,** 5703–5708
6. Silvestri, L., Caputo, V., Bellacchio, E., Atorino, L., Dallapiccola, B., Valente, E. M., and Casari, G. (2005) Mitochondrial import and enzymatic activity of PINK1 mutants associated to recessive parkinsonism. *Hum. Mol. Genet.* **14,** 3477–3492
7. Sim, C. H., Lio, D. S., Mok, S. S., Masters, C. L., Hill, A. F., Culvenor, J. G., and Cheng, H. C. (2006) C-terminal truncation and Parkinson's disease-associated mutations down-regulate the protein serine/threonine kinase activity of PTEN-induced kinase-1. *Hum. Mol. Genet.* **15,** 3251–3262
8. Yang, Y., Gehrke, S., Imai, Y., Huang, Z., Ouyang, Y., Wang, J. W., Yang, L., Beal, M. F., Vogel, H., and Lu, B. (2006) Mitochondrial pathology and muscle and dopaminergic neuron degeneration caused by inactivation of *Drosophila* Pink1 is rescued by Parkin. *Proc. Natl. Acad. Sci. U.S.A.* **103,** 10793–10798
9. Park, J., Lee, S. B., Lee, S., Kim, Y., Song, S., Kim, S., Bae, E., Kim, J., Shong, M., Kim, J. M., and Chung, J. (2006) Mitochondrial dysfunction in *Drosophila PINK1* mutants is complemented by *parkin*. *Nature* **441,** 1157–1161
10. Clark, I. E., Dodson, M. W., Jiang, C., Cao, J. H., Huh, J. R., Seol, J. H., Yoo, S. J., Hay, B. A., and Guo, M. (2006) *Drosophila pink1* is required for mitochondrial function and interacts genetically with *parkin*. *Nature* **441,** 1162–1166
11. Narendra, D., Tanaka, A., Suen, D. F., and Youle, R. J. (2008) Parkin is recruited selectively to impaired mitochondria and promotes their autophagy. *J. Cell Biol.* **183,** 795–803
12. Narendra, D. P., Jin, S. M., Tanaka, A., Suen, D. F., Gautier, C. A., Shen, J., Cookson, M. R., and Youle, R. J. (2010) PINK1 is selectively stabilized on impaired mitochondria to activate Parkin. *PLoS Biol.* **8,** e1000298
13. Vives-Bauza, C., Zhou, C., Huang, Y., Cui, M., de Vries, R. L., Kim, J., May, J., Tocilescu, M. A., Liu, W., Ko, H. S., Magrané, J., Moore, D. J., Dawson, V. L., Grailhe, R., Dawson, T. M., Li, C., Tieu, K., and Przedborski, S. (2010) PINK1-dependent recruitment of Parkin to mitochondria in mitophagy. *Proc. Natl. Acad. Sci. U.S.A.* **107,** 378–383
14. Geisler, S., Holmström, K. M., Skujat, D., Fiesel, F. C., Rothfuss, O. C., Kahle, P. J., and Springer, W. (2010) PINK1/Parkin-mediated mitophagy is dependent on VDAC1 and p62/SQSTM1. *Nat. Cell Biol.* **12,** 119–131
15. Matsuda, N., Sato, S., Shiba, K., Okatsu, K., Saisho, K., Gautier, C. A., Sou, Y. S., Saiki, S., Kawajiri, S., Sato, F., Kimura, M., Komatsu, M., Hattori, N., and Tanaka, K. (2010) PINK1 stabilized by mitochondrial depolarization recruits Parkin to damaged mitochondria and activates latent Parkin for mitophagy. *J. Cell Biol.* **189,** 211–221
16. Kawajiri, S., Saiki, S., Sato, S., Sato, F., Hatano, T., Eguchi, H., and Hattori, N. (2010) PINK1 is recruited to mitochondria with parkin and associates with LC3 in mitophagy. *FEBS Lett.* **584,** 1073–1079
17. Kondapalli, C., Kazlauskaite, A., Zhang, N., Woodroof, H. I., Campbell, D. G., Gourlay, R., Burchell, L., Walden, H., Macartney, T. J., Deak, M., Knebel, A., Alessi, D. R., and Muqit, M. M. (2012) PINK1 is activated by mitochondrial membrane potential depolarization and stimulates Parkin E3 ligase activity by phosphorylating serine 65. *Open Biol.* **2,** 120080
18. Shiba-Fukushima, K., Imai, Y., Yoshida, S., Ishihama, Y., Kanao, T., Sato, S., and Hattori, N. (2012) PINK1-mediated phosphorylation of the Parkin ubiquitin-like domain primes mitochondrial translocation of Parkin and regulates mitophagy. *Sci. Rep.* **2,** 1002
19. Kazlauskaite, A., Kondapalli, C., Gourlay, R., Campbell, D. G., Ritorto, M. S., Hofmann, K., Alessi, D. R., Knebel, A., Trost, M., and Muqit, M. M. (2014) Parkin is activated by PINK1-dependent phosphorylation of ubiquitin at Ser^{65}. *Biochem. J.* **460,** 127–139
20. Kane, L. A., Lazarou, M., Fogel, A. I., Li, Y., Yamano, K., Sarraf, S. A., Banerjee, S., and Youle, R. J. (2014) PINK1 phosphorylates ubiquitin to activate Parkin E3 ubiquitin ligase activity. *J. Cell Biol.* **205,** 143–153
21. Koyano, F., Okatsu, K., Kosako, H., Tamura, Y., Go, E., Kimura, M., Kimura, Y., Tsuchiya, H., Yoshihara, H., Hirokawa, T., Endo, T., Fon, E. A., Trempe, J.-F., Saeki, Y., Tanaka, K., and Matsuda, N. (2014) Ubiquitin is phosphorylated by PINK1 to activate parkin. *Nature* **510,** 162–166
22. Chan, N. C., Salazar, A. M., Pham, A. H., Sweredoski, M. J., Kolawa, N. J., Graham, R. L., Hess, S., and Chan, D. C. (2011) Broad activation of the ubiquitin-proteasome system by Parkin is critical for mitophagy. *Hum. Mol. Genet.* **20,** 1726–1737
23. Haddad, D. M., Vilain, S., Vos, M., Esposito, G., Matta, S., Kalscheuer, V. M., Craessaerts, K., Leyssen, M., Nascimento, R. M., Vianna-Morgante, A. M., De Strooper, B., Van Esch, H., Morais, V. A., and Verstreken, P. (2013) Mutations in the intellectual disability gene *Ube2a* cause neuronal dysfunction and impair parkin-dependent mitophagy. *Mol. Cell* **50,** 831–843
24. Murata, H., Sakaguchi, M., Kataoka, K., and Huh, N. H. (2013) SARM1 and TRAF6 bind to and stabilize PINK1 on depolarized mitochondria. *Mol.*

Biol. Cell **24,** 2772–2784
25. Zheng, X., and Hunter, T. (2013) Parkin mitochondrial translocation is achieved through a novel catalytic activity coupled mechanism. *Cell Res.* **23,** 886–897
26. Yamamoto, M., Okamoto, T., Takeda, K., Sato, S., Sanjo, H., Uematsu, S., Saitoh, T., Yamamoto, N., Sakurai, H., Ishii, K. J., Yamaoka, S., Kawai, T., Matsuura, Y., Takeuchi, O., and Akira, S. (2006) Key function for the Ubc13 E2 ubiquitin-conjugating enzyme in immune receptor signaling. *Nat. Immunol.* **7,** 962–970
27. Shiba, K., Arai, T., Sato, S., Kubo, S., Ohba, Y., Mizuno, Y., and Hattori, N. (2009) Parkin stabilizes PINK1 through direct interaction. *Biochem. Biophys. Res. Commun.* **383,** 331–335
28. Shiba-Fukushima, K., Inoshita, T., Hattori, N., and Imai, Y. (2014) PINK1-mediated phosphorylation of Parkin boosts Parkin activity in *Drosophila*. *PLoS Genet.* **10,** e1004391
29. Ma, X., Huang, J., Yang, L., Yang, Y., Li, W., and Xue, L. (2012) NOPO modulates Egr-induced JNK-independent cell death in *Drosophila*. *Cell Res.* **22,** 425–431
30. Hofmann, R. M., and Pickart, C. M. (1999) Noncanonical *MMS2*-encoded ubiquitin-conjugating enzyme functions in assembly of novel polyubiquitin chains for DNA repair. *Cell* **96,** 645–653
31. Okatsu, K., Uno, M., Koyano, F., Go, E., Kimura, M., Oka, T., Tanaka, K., and Matsuda, N. (2013) A dimeric PINK1-containing complex on depolarized mitochondria stimulates Parkin recruitment. *J. Biol. Chem.* **288,** 36372–36384
32. Okatsu, K., Oka, T., Iguchi, M., Imamura, K., Kosako, H., Tani, N., Kimura, M., Go, E., Koyano, F., Funayama, M., Shiba-Fukushima, K., Sato, S., Shimizu, H., Fukunaga, Y., Taniguchi, H., Komatsu, M., Hattori, N., Mihara, K., Tanaka, K., and Matsuda, N. (2012) PINK1 autophosphorylation upon membrane potential dissipation is essential for Parkin recruitment to damaged mitochondria. *Nat. Commun.* **3,** 1016
33. Manzanillo, P. S., Ayres, J. S., Watson, R. O., Collins, A. C., Souza, G., Rae, C. S., Schneider, D. S., Nakamura, K., Shiloh, M. U., and Cox, J. S. (2013) The ubiquitin ligase parkin mediates resistance to intracellular pathogens. *Nature* **501,** 512–516
34. van Wijk, S. J., Fiskin, E., Putyrski, M., Pampaloni, F., Hou, J., Wild, P., Kensche, T., Grecco, H. E., Bastiaens, P., and Dikic, I. (2012) Fluorescence-based sensors to monitor localization and functions of linear and K63-linked ubiquitin chains in cells. *Mol. Cell* **47,** 797–809
35. Fujita, N., Morita, E., Itoh, T., Tanaka, A., Nakaoka, M., Osada, Y., Umemoto, T., Saitoh, T., Nakatogawa, H., Kobayashi, S., Haraguchi, T., Guan, J. L., Iwai, K., Tokunaga, F., Saito, K., Ishibashi, K., Akira, S., Fukuda, M., Noda, T., and Yoshimori, T. (2013) Recruitment of the autophagic machinery to endosomes during infection is mediated by ubiquitin. *J. Cell Biol.* **203,** 115–128
36. Deng, L., Wang, C., Spencer, E., Yang, L., Braun, A., You, J., Slaughter, C., Pickart, C., and Chen, Z. J. (2000) Activation of the IκB kinase complex by TRAF6 requires a dimeric ubiquitin-conjugating enzyme complex and a unique polyubiquitin chain. *Cell* **103,** 351–361
37. Olzmann, J. A., Li, L., Chudaev, M. V., Chen, J., Perez, F. A., Palmiter, R. D., and Chin, L. S. (2007) Parkin-mediated K63-linked polyubiquitination targets misfolded DJ-1 to aggresomes via binding to HDAC6. *J. Cell Biol.* **178,** 1025–1038
38. Lim, G. G., Chew, K. C., Ng, X. H., Henry-Basil, A., Sim, R. W., Tan, J. M., Chai, C., and Lim, K. L. (2013) Proteasome inhibition promotes Parkin-Ubc13 interaction and lysine 63-linked ubiquitination. *PLoS One* **8,** e73235
39. Geisler, S., Vollmer, S., Golombek, S., and Kahle, P. J. (2014) The ubiquitin-conjugating enzymes UBE2N, UBE2L3 and UBE2D2/3 are essential for Parkin-dependent mitophagy. *J. Cell Sci.* **127,** 3280–3293
40. Fiesel, F. C., Moussaud-Lamodière, E. L., Ando, M., and Springer, W. (2014) A specific subset of E2 ubiquitin-conjugating enzymes regulate Parkin activation and mitophagy differently. *J. Cell Sci.* **127,** 3488–3504

Lysine 63-linked Polyubiquitination Is Dispensable for Parkin-mediated Mitophagy

Kahori Shiba-Fukushima, Tsuyoshi Inoshita, Nobutaka Hattori and Yuzuru Imai

J. Biol. Chem. 2014, 289:33131-33136.
doi: 10.1074/jbc.C114.580944 originally published online October 21, 2014

Research article

Assembly of the cochlear gap junction macromolecular complex requires connexin 26

Kazusaku Kamiya,[1] Sabrina W. Yum,[2,3] Nagomi Kurebayashi,[4] Miho Muraki,[1] Kana Ogawa,[1] Keiko Karasawa,[1] Asuka Miwa,[1] Xueshui Guo,[2] Satoru Gotoh,[5] Yoshinobu Sugitani,[5] Hitomi Yamanaka,[5] Shioko Ito-Kawashima,[5] Takashi Iizuka,[1] Takashi Sakurai,[4] Tetsuo Noda,[5,6] Osamu Minowa,[5,6] and Katsuhisa Ikeda[1]

[1]Department of Otorhinolaryngology, Juntendo University Faculty of Medicine, Tokyo, Japan. [2]Division of Neurology, Children's Hospital of Philadelphia, Philadelphia, Pennsylvania, USA. [3]Department of Neurology, Perelman School of Medicine at the University of Pennsylvania, Philadelphia, Pennsylvania, USA. [4]Department of Cellular and Molecular Pharmacology, Juntendo University Graduate School of Medicine, Tokyo, Japan. [5]Department of Cell Biology, Japanese Foundation for Cancer Research, Cancer Institute, Tokyo, Japan. [6]Team for Advanced Development and Evaluation of Human Disease Models, RIKEN BioResource Center, Tsukuba, Japan.

Hereditary deafness affects approximately 1 in 2,000 children. Mutations in the gene encoding the cochlear gap junction protein connexin 26 (CX26) cause prelingual, nonsyndromic deafness and are responsible for as many as 50% of hereditary deafness cases in certain populations. Connexin-associated deafness is thought to be the result of defective development of auditory sensory epithelium due to connexion dysfunction. Surprisingly, CX26 deficiency is not compensated for by the closely related connexin CX30, which is abundantly expressed in the same cochlear cells. Here, using two mouse models of CX26-associated deafness, we demonstrate that disruption of the CX26-dependent gap junction plaque (GJP) is the earliest observable change during embryonic development of mice with connexin-associated deafness. Loss of CX26 resulted in a drastic reduction in the GJP area and protein level and was associated with excessive endocytosis with increased expression of caveolin 1 and caveolin 2. Furthermore, expression of deafness-associated *CX26* and *CX30* in cell culture resulted in visible disruption of GJPs and loss of function. Our results demonstrate that deafness-associated mutations in *CX26* induce the macromolecular degradation of large gap junction complexes accompanied by an increase in caveolar structures.

Introduction

Hearing loss is the most common congenital sensory deficit (1, 2). Approximately 1 child in 1,000 is affected at birth or during early childhood by severe hearing loss, which is defined as prelingual deafness (3, 4), with about half of the cases attributable to genetic causes (5). Among the more than 100 known forms of nonsyndromic deafness with identified genetic loci, by far the most common and best characterized is the one associated with *GJB2* (OMIM 121011), the gene encoding the connexin 26 (CX26) protein (6). This gap junction protein, which assembles to form channels between cells in the cochlear supporting cells, allows the rapid removal of K^+ away from the base of hair cells, resulting in the recycling of this ion back to the endolymph to maintain cochlear homeostasis (7). CX26 and CX30 are the two most abundantly expressed gap junction proteins in the cochlea (8) and form heteromeric and heterotypic channels in most of the cochlear gap junction plaques (GJPs) (9) as well as in in vitro experiments (10). In addition to their effects on K^+, gap junction proteins mediate the movement of Ca^{2+} and anions via inositol 1,4,5-trisphosphate, as well as the cell-signaling, nutrient, and energy molecules ATP and cAMP (11).

Connexins are assembled into hexameric connexons in the endoplasmic reticulum and are trafficked to the plasma membrane. Hemichannels dock head to head with partner hexameric channels positioned on neighboring cells (12). The resulting GJP may vary from 100 nm to several micrometers in diameter and can contain up to 10,000 connexons. Newly synthesized gap junctions always merge into the outside of existing GJPs, and the older gap junctions in the central area of the plaques are internalized in approximately 1 to 5 hours (13). Different types of connexin channels segregate into the different plaques forming both hetero- and homoconnexons (14). This dynamic process regulates gap junction assembly and disassembly in living cells.

In this study, we demonstrate that a mutation in CX26 induces the macromolecular degradation of large gap junction complexes accompanied by an increase in caveolar structures and that the assembly of this macromolecular complex requires CX26.

Results

In this study, we performed a detailed compositional analysis of cochlear GJPs using models of two major types of CX26-related hearing loss. The first model consists of a mouse that expresses human CX26 with the R75W dominant-negative mutation (*CX26*$^{R75W+}$; refs. 15–17 and Supplemental Figure 1, A and B; supplemental material available online with this article; doi:10.1172/JCI67621DS1). The other is a newly developed conditional *Cx26*-deficient mouse (*Cx26*$^{f/f}$ *P0-Cre*) with localized gene deletion in the inner ear under the control of the protein 0 (*P0*) promoter (ref. 18 and Supplemental Figure 1C). To confirm the expression pattern of P0 in the inner ear lineage, P0-Cre mice were crossed with R26R^{GFP} reporter mice, which contain GFP knocked into the *ROSA26* locus, allowing for the activation of GFP using Cre recombinase, and GFP signals were observed at the otocyst (Supplemental Figure 2). *Cx26*$^{f/f}$ *P0-Cre* mice had severe sensorineural hearing loss (Supplemental Figure 1D), although no abnormalities were observed in other organs (data not shown). Furthermore, these mice displayed an impaired ability to propagate Ca^{2+} oscillations from cell to cell at P5 (Supplemental Figure 3), which is probably related to an impaired function of gap junctions (19, 20) and

Conflict of interest: The authors have declared that no conflict of interest exists.
Citation for this article: *J Clin Invest.* 2014;124(4):1598–1607. doi:10.1172/JCI67621.

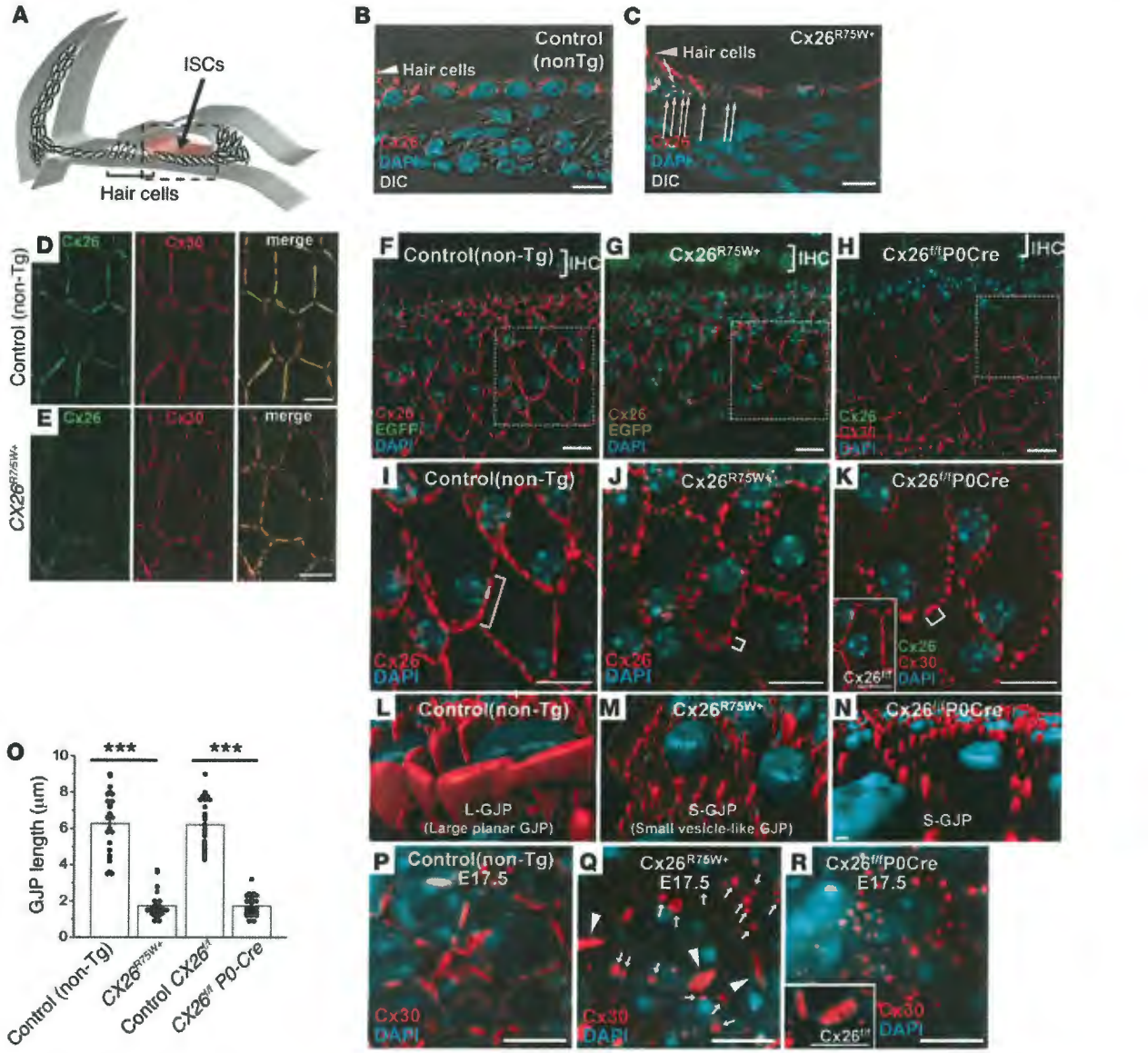

Figure 1

Drastic disruption of cochlear GJPs in two models of CX26-associated deafness. (**A**) Schematic illustration of cochlear ISCs. (**B** and **C**) CX26 distribution (in red) in ISCs (boxed region in **A**) in P12 cochlear cryosections from *CX26*$^{R75W+}$ mice show fragmented GJPs (**C**, small arrows) in contrast to GJPs in control mice (**B**). (**D** and **E**) Double staining of CX26 and CX30 in whole-mount cochlear tissue at 3 weeks showing that these GJPs are composed of both connexins in control (**D**) and *CX26*$^{R75W+}$ (**E**) mice. (**F–H**) GJP formation in 8-week-old adult cochleae from a *CX26*$^{R75W+}$ mouse (**G**), a non-Tg littermate control (**F**), and a *Cx26*$^{f/f}$ *P0-Cre* mouse (**H**). The partial EGFP signals in **G** indicate that it is a transgenic animal. (**I–K**) Image of each boxed region in **F–H**, respectively. Inset in **K** shows the GJPs in a *Cx26*$^{f/f}$ littermate control mouse. (**L–N**) Three-dimensional images reconstructed from the images in **I–K**, respectively. (**O**) Lengths of the largest GJPs (brackets in **I–K**) along a single cell border (mean ± SE, $n = 25$ for all four groups). ***$P = 4.7 \times 10^{-14}$ and 1.2×10^{-16} for *CX26*$^{R75W+}$ and *Cx26*$^{f/f}$ *P0-Cre* cochleae, respectively, relative to controls (Student's *t* test). (**P–R**) At E17.5, *CXx26*$^{R75W+}$ ISCs showed a number of S-GJPs (**Q**, arrows), including some L-GJPs (**Q**, arrowheads), as observed in the non-Tg control ISCs (**P**). *Cx26*$^{f/f}$ *P0-Cre* ISCs (**R**) showed totally disrupted GJPs, although the control ISCs (*Cx26*$^{f/f}$, inset in **R**) showed L-GJPs. Nuclei were counterstained with DAPI (blue). Scale bars: 10 μm.

which occurs before the onset of hearing. We note that although the propagation range was affected, the frequency of the Ca^{2+} oscillations did not change significantly (Supplemental Figure 3 and Supplemental Videos 4–7).

In a detailed analysis with a three-dimensional graphic construction of the GJP structure in the inner sulcus cells (ISCs; Figure 1A), WT adult mouse cochleae showed large, planar GJPs (L-GJPs; Figure 1I) at the cell border that formed orderly pentagonal or hexagonal outlines around normal ISCs (Figure 1, B, D, F, I, and L). In contrast, cochleae from *CX26*$^{R75W+}$ (Figure 1, C, E, G, J, M, and Supplemental Video 1) and *Cx26*$^{f/f}$ *P0-Cre* (Figure 1, H, K, and N) mice showed drastically fragmented, small vesicle–like GJPs (S-GJPs;

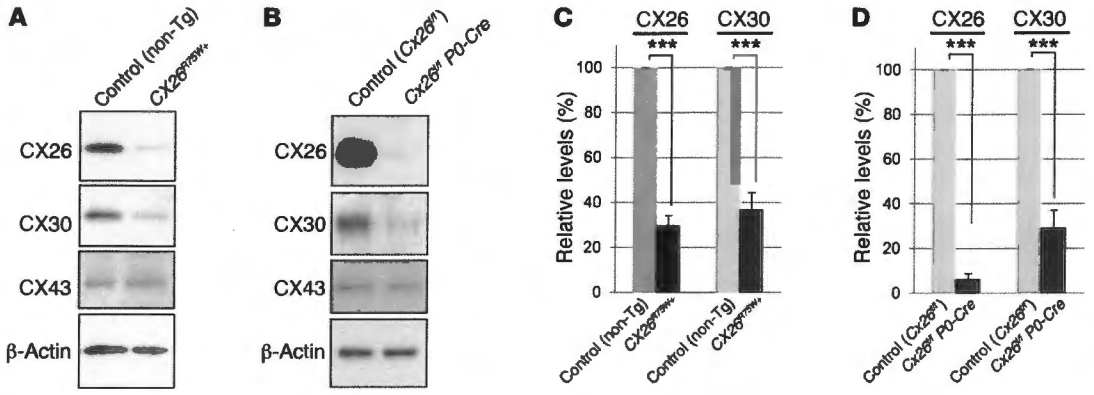

Figure 2

Changes in gap junction proteins in 8-week-old CX26-mutant mice. (**A** and **B**) Immunoblot analysis showed decreased protein expression not only for CX26, but also for CX30 in both *CX26^{R75W+}* (**A**) and *Cx26$^{f/f}$ P0-Cre* (**B**) mice. CX43 expression in the different cochlear cells was analyzed as a control. (**C** and **D**) CX26 and CX30 protein levels were normalized to the corresponding β-actin levels and were expressed relative to the amount present in each littermate control. Values represent the mean ± SEM (error bars; $n = 5$). $P = 7.0 \times 10^{-8}$ and 1.4×10^{-5} for CX26 and CX30, respectively, in *CX26^{R75W+}* mice; $P = 5.6 \times 10^{-11}$ and 8.7×10^{-6} for CX26 and CX30, respectively, in *Cx26$^{f/f}$ P0-Cre* mice. ***$P < 0.001$.

Figure 1, J, K, M, and N), resulting in an extremely diminished total plaque area as compared with that seen in control mice. In addition, the significant reduction in the protein levels of not only CX26 but also CX30 (Figure 2) suggested that the macromolecular complex had been degraded. The drastically dispersed plaques were observed from E17.5 (Figure 1, P–R). At the initial stage of cochlear GJP formation on E14.5, we observed that GJP disruption was already present. Two CX26-mutant mice did not show GJPs at many of the cell borders, although a part of the cells showed significantly shorter GJPs compared with the those of controls (Supplemental Figure 4). Since drastic GJP disruptions were observed even at E17.5 and the initial GJP formations were also abnormal at E14.5, which is the earliest histological change in this disease yet reported, we believe that this may be an initial phenotypic change that is followed by physiological disorder in the inner ear. As some undisrupted L-GJPs (Figure 1Q, arrowheads) were still present among the S-GJPs (Figure 1Q, arrows) in *CX26^{R75W+}* mice at E17.5, GJP disruption was thought to begin during embryonic development.

Since CX26 immunolabeling was rarely detected even in *Cx26$^{f/f}$ P0-Cre* mouse cochlea, the numbers of CX26-positive ISCs in 5 mice were counted at the middle turn of the cochlea. Approximately 1.6% (1.6 ± 0.3%, $n = 5$) of ISCs in *Cx26$^{f/f}$ P0-Cre* mice showed CX26 expression (Figure 3A, arrows), in contrast to 100% (100 ± 0%, $n = 5$) in their littermate controls (*Cx26$^{flox/flox}$*, referred to herein as *Cx26$^{f/f}$*). These CX26-positive cells in *Cx26$^{f/f}$ P0-Cre* mice may have invaded the cochlea from other tissues such as bone marrow and thus did not undergo Cre recombinase regulation (21). This cellular mosaicism enabled us to analyze differences in the cochlear GJPs formed by adjacent cells with and without the expression of CX26 and, critically, revealed the CX26-dependent differences in the formation of the two GJP types (L-GJP and S-GJP). Cochlear GJPs with both CX26 and CX30 formed L-GJPs, as compared with the S-GJPs that formed without CX26 (Figure 3, A–E, Supplemental Figure 5, E and F, and Supplemental Videos 2 and 3). Even in a single cell, the GJP type at each junctional side varied depending on the connexin expression in the adjacent cells (Figure 3D, arrowheads). The cells were classified as either CX26-positive cells (CX26 in Figure 3, B and C), which expressed CX26 in at least one GJP at the lateral cell junction site, or CX26-negative cells (KO in Figure 3, B and C). Based on this finding, we categorized the resulting GJPs as one of four types (Figure 3, F–I). It is notable that even though a cell expressed CX26, this protein was not able to assemble into a GJP when the adjacent cell did not also express CX26 (Figure 3H).

These GJP disruptions in the cochlea were also produced by human cDNA clones in HeLa cells (22, 23) that stably expressed mutant CX26 together with CX30 (Figure 4, A–E). Interestingly, these cell lines clearly showed functional differences in neurobiotin (NB) transfer analysis (Figure 4, I, J, O, and P) depending on the level of GJP disruption (Figure 4, F, G, L, and M), even when mutations at the same amino acid in CX26 were used (i.e., R75W and R75Q, which also cause hereditary deafness; ref. 24). The cells with smaller GJPs had less extensive NB dye transfer as compared with cells with larger GJPs (Figure 4, H–Q). To investigate whether supplementation with WT CX26 can rescue the GJP size in the two mutant mouse strains, we performed an overexpression experiment with adeno-associated virus (AAV) carrying WT CX26 tagged with FLAG in cochlear organ cultures from *CX26^{R75W+}* mice and *Cx26$^{f/f}$ P0-Cre* mice (Supplemental Figure 6). In this context, CX26-FLAG formed mainly small (0.93 ± 0.14 μm) vesicle-like GJPs in *CX26^{R75W+}* mouse cochleae, although it formed relatively large (3.7 ± 0.7 μm) GJPs in cochleae from *Cx26$^{f/f}$ P0-Cre* mice. Considering the original GJP size for the adult CX26-mutant mice shown in Figure 1O (~1 μm for both CX26-mutant mice and ~6 μm for the control littermate), the GJP size of *Cx26$^{f/f}$ P0-Cre* ISCs may be rescued by supplementation with WT CX26, while some mutants such as CX26R75W^{+} may not be rescued due to their dominant-negative effects. These results corresponded with the functional changes analyzed by fluorescence recovery after photobleaching (FRAP) or dye transfer analysis in HeLa cells in our previous reports (22, 23).

After extensive protein analysis with mutant cochleae (Supplemental Figure 7 and data not shown), we found that caveolin 1 (CAV1) and caveolin 2 (CAV2), components of the caveolae (which form during endocytosis), were molecules that were altered in the pathology. Interestingly, we observed a drastic isoform shift in CAV1 from CAV1α to CAV1β, which lacks the N-terminal

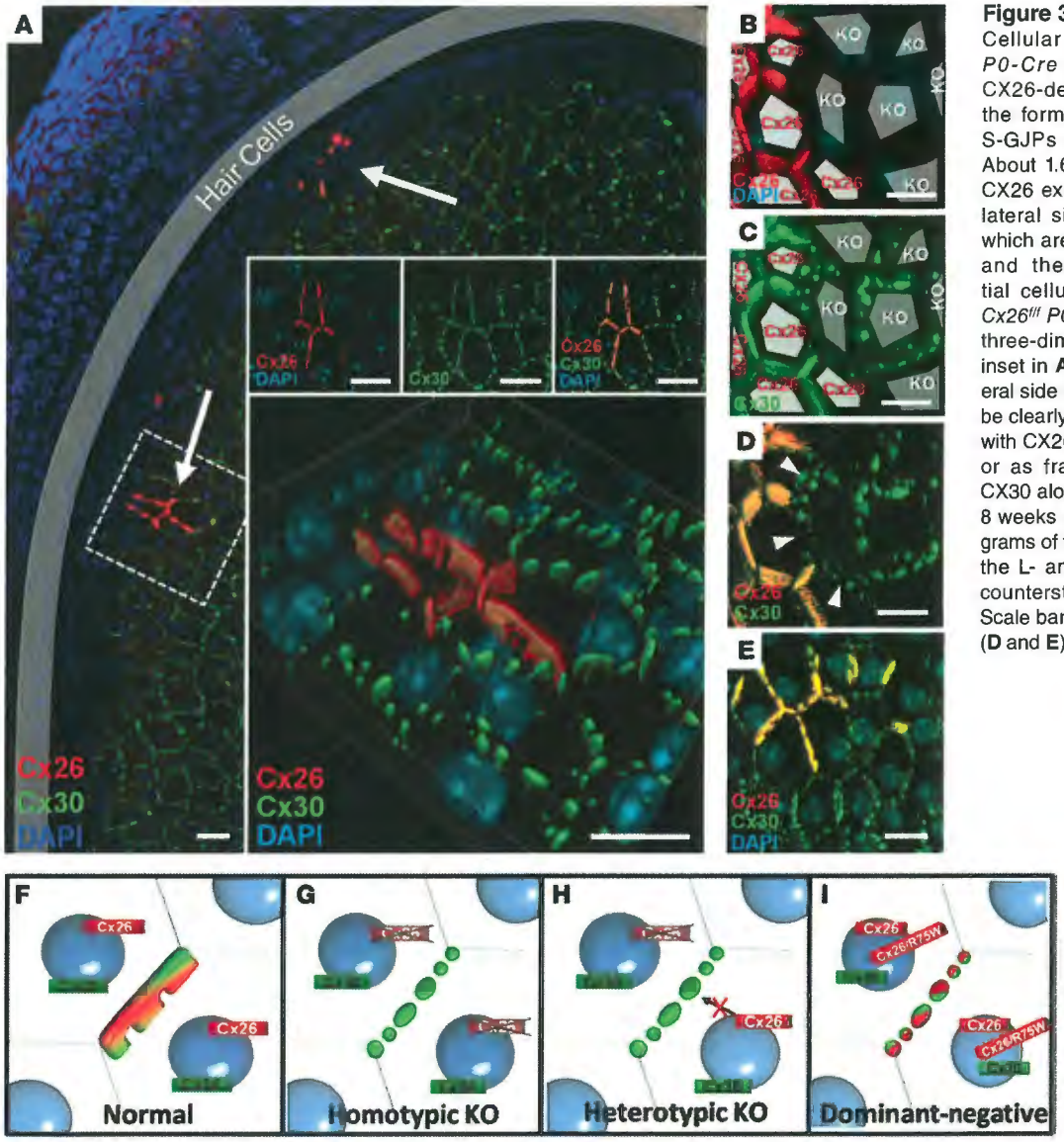

Figure 3
Cellular mosaicism in *Cx26$^{f/f}$ P0-Cre* mice revealed the CX26-dependent differences in the formation of L-GJPs versus S-GJPs shown in Figure 1. (**A**) About 1.6 % of the ISCs showed CX26 expression on at least one lateral side (arrows and insets, which are from the boxed region), and these cells showed partial cellular mosaicism in adult *Cx26$^{f/f}$ P0-Cre* mice. Confocal and three-dimensional images (large inset in **A**) revealed that each lateral side of the cell junctions could be clearly distinguished as L-GJPs with CX26 (red) and CX30 (green) or as fragmented S-GJPs with CX30 alone at 3 weeks (**A–D**) and 8 weeks (**E**). (**F–I**) Schematic diagrams of the rules used to organize the L- and S-GJPs. Nuclei were counterstained with DAPI (blue). Scale bars: 5 μm (**A–C**) and 10 μm (**D** and **E**).

hydrophilic region of CAV1α in *CX26^{R75W+}* cochleae, and found significantly increased expression of CAV1β and CAV2 in both *CX26^{R75W+}* and *Cx26$^{f/f}$P0-Cre* cochleae (Figure 5, A–D). CAV1 and CAV2 showed excessive accumulation (Figure 5, E–K) in 3-week-old *CX26^{R75W+}* cochleae. These cells that accumulated CAV1 or CAV2 were occasionally observed at the inter-GJP space or on the surface of the GJPs (Figure 5, G, H, J, and K) in 3-week-old *CX26^{R75W+}* cochleae, although no accumulated signals were observed in the control mice (Figure 5, E and I). We quantified the number of ISCs that had accumulated CAV1 and CAV2 in both CX26 mutants. There was no difference in their distribution pattern or in the number of positive cells (P = 0.16) with respect to CAV1 (7.3 ± 1.3%) and CAV2 (5.6 ± 0.9%) accumulation (Figure 5L). In the overexpression of CAV1β with WT CX26, CX26R75W, and CX30 in HEK293 cells, we observed that numerous GJPs at the cell borders and the connexin vesicles were accompanied by accumulated CAV1β, although WT CX26 with CAV1β did not show such a distribution pattern (Supplemental Figure 8). We also observed numerous CAV1- and CAV2-positive vesicles at the S-GJPs in the two mutant mice in the adult stage as compared with those seen at the L-GJPs in the control mice (Figure 5, M and N). These changes were associated with an increase in the caveolar structures (Figure 6, B and E–K) that are indicative of endocytosis, which leads to membrane retrieval and, perhaps, abnormal GJP formation.

Based on electron microscopic analysis of the ISCs, we observed that both *CX26^{R75W+}* and *Cx26$^{f/f}$P0-Cre* mice also formed gap junctions, although there were a number of discontinuous gap junctions (Figure 6, B, D, and K) with excessive endocytosis (Figure 6, B, E, F, and G–K) or abnormally condensed intermembrane layers (Figure 6, E and F) around the gap junctions in *Cx26$^{f/f}$P0-Cre* mice. In contrast with their littermate controls (Figure 6, A and C), significantly larger numbers of caveolae and vesicles were detected at cell borders in both *CX26^{R75W+}* mice and *Cx26$^{f/f}$P0-Cre* mice (Figure 6L). The distributions and the number of caveolae were nearly identical between both types of mutant mice and were consistent with the immunolabeling for CAV1 and CAV2 around GJPs (Fig-

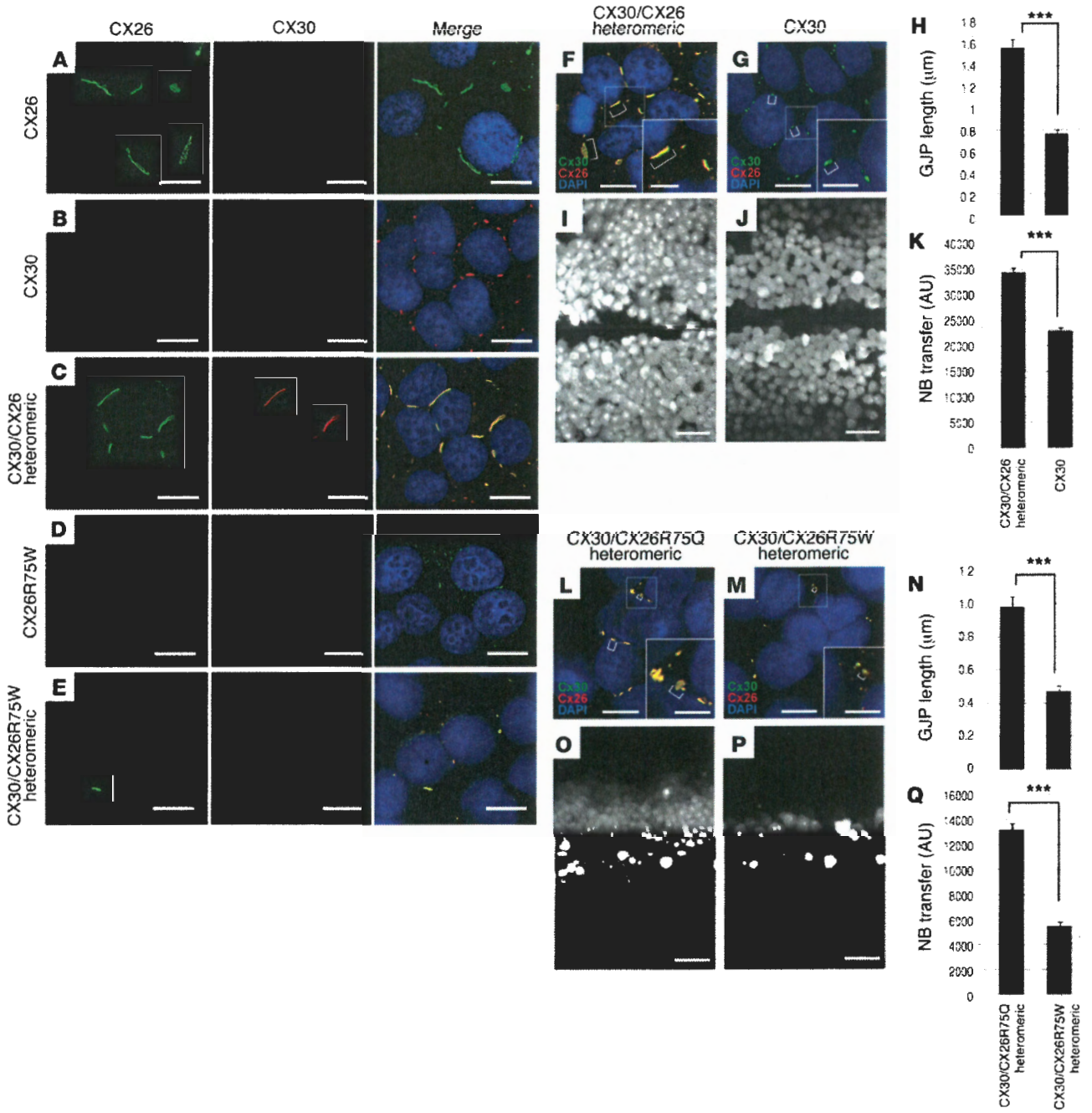

Figure 4

Disruption of cochlear GJPs is reproduced by human cDNA clones for CX30 and CX26, with or without mutations in HeLa cells, and leads to functional differences in dye transfer depending on the resultant GJP sizes. (**A**–**E**) Clear differences in GJP formation were observed in HeLa cells that expressed the indicated connexin(s), which made homomeric or heteromeric channels. Cells were colabeled with anti-CX26 (green) and anti-CX30 (red) antibodies and were counterstained with DAPI (blue). L-GJPs were observed only when normal CX26 was expressed alone (**A**) or was coexpressed with CX30 (**C**). The other combinations (**B**, **D**, and **E**) formed S-GJPs. (**F**–**Q**) In HeLa cells that expressed CX30 and CX26, cells with smaller GJPs demonstrated decreased NB transfer. (**F**, **G**, **L**, and **M**) Shown are HeLa cells that expressed WT CX30 alone (CX30) or coexpressed WT CX30 and WT CX26 (CX30/CX26), or the indicated CX26 mutants (CX30/Cx26R75Q or CX30/CX26R75W). CX26 and CX30 were colocalized, and the GJP size differed across cell lines. (**H** and **N**) Quantitative analysis of the GJP length (mean ± SEM). $^{***}P = 3.3 \times 10^{-17}$ (**H**) or $P = 7.7 \times 10^{-12}$ (**N**). (**I**, **J**, **O**, and **P**) Digital fluorescence images of HeLa cells expressing the indicated connexin(s) after NB scrape-loading. (**K** and **Q**) Quantitative analysis of intercellular NB transfer after scrape-loading. Columns represent the mean distance (± SEM) of NB transfer from the scrape line. $^{***}P = 9.6 \times 10^{-9}$ (**K**) or $P = 3.2 \times 10^{-11}$ (**Q**). Scale bars: 10 μm and 5 μm (insets).

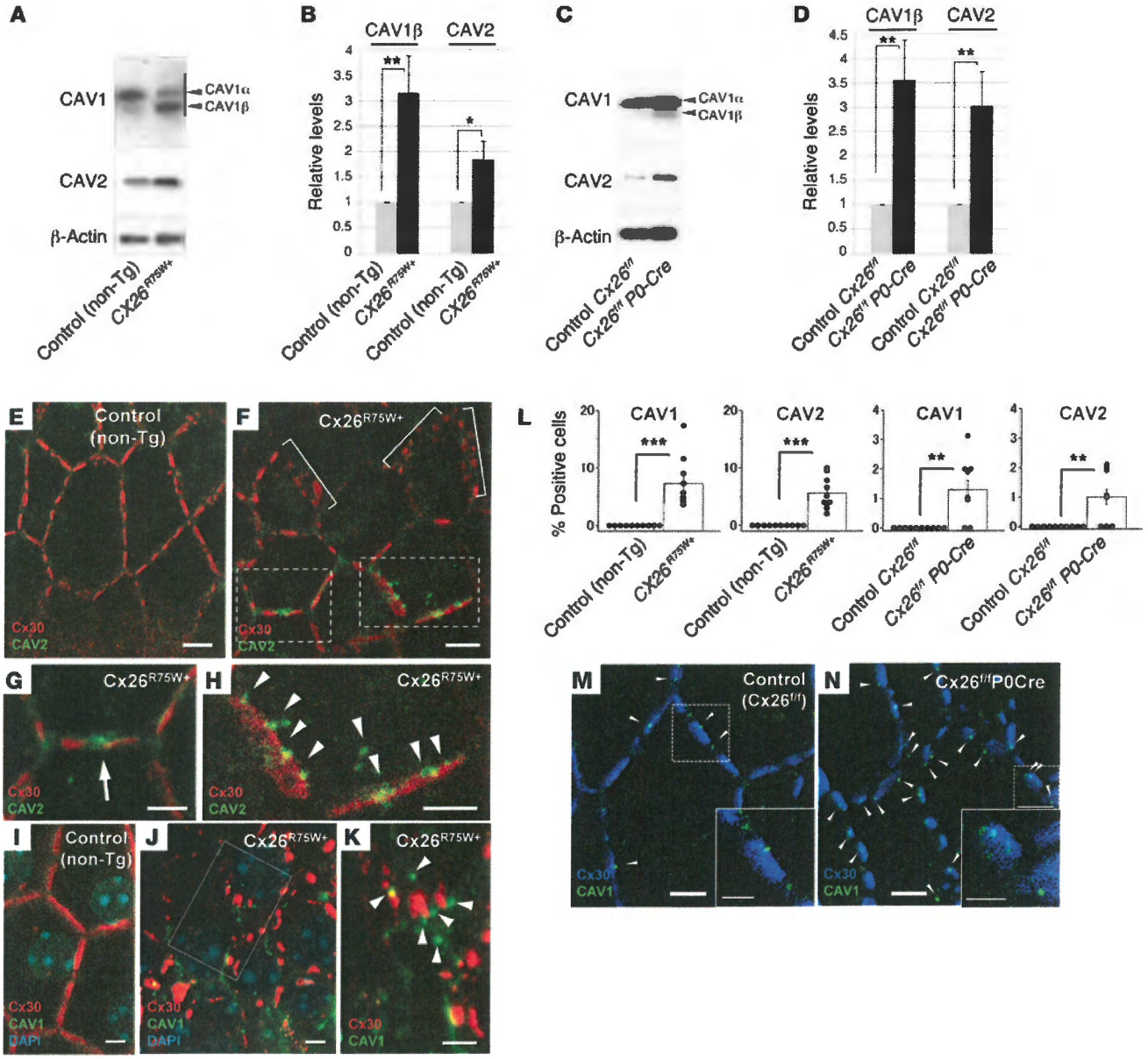

Figure 5

Changes in the endocytosis proteins CAV1 and CAV2 in CX26-mutant mouse cochlea. The CAV1 isoform preference shifted from α to β in *CX26*$^{R75W+}$ cochlea (**A**). The CAV1β and CAV2 increased in both mutant mice (**A** and **C**) at 8 weeks of age, as shown by Western blotting. Protein levels of CAV1β (**B**) and CAV2 (**D**) are expressed relative to the amount present in each littermate control (mean ± SEM, $n = 5$). $P = 0.009$ and 0.03 for CAV1β and CAV2, respectively, in *CX26*$^{R75W+}$ cochlea. $P = 0.007$ and 0.01 for CAV1β and CAV2, respectively, in *Cx26*$^{f/f}$ *P0-Cre* cochlea. (**E**–**K**) Accumulation of CAV2 and CAV1 in 3-week-old non-Tg littermate controls (**E** and **I**) and *CX26*$^{R75W+}$ mice (**F**–**H**, **J**, and **K**) with S-GJPs (brackets in **F**) was occasionally observed at the inter-GJP space (**G**, arrow) and on the surface of the GJPs (**H**, arrowheads), differing from that seen in littermate controls (**I** and **E**). The boxed regions in **F** and **J** are magnified in **G**, **H**, and **K**, respectively. (**L**) Numbers of cells with accumulated CAV1 or CAV2 were counted in five animals from each group (mean ± SEM, $n = 10$; $P = 0.0003$, 6.1×10^{-5}, 0.001 and 0.002, from left to right). (**M**–**N**) In adult mice, vesicles positive for CAV1 (arrowheads) were frequently detected on GJPs in *Cx26*$^{f/f}$ *P0-Cre* mice (**K**), but not in their littermate controls (**J**). Boxed regions are magnified in the bottom right corner. Scale bars: 10 μm and 5 μm (insets). $^*P < 0.05$; $^{**}P < 0.01$; $^{***}P < 0.001$.

ure 5, M and N) and the upregulation of the caveolin proteins (Figure 5, A–D). This may be associated with the membrane retrieval (Figure 6K) caused by excessive endocytosis and the formation of abnormal GJPs. In the labeling with cholera toxin subunit B (CTxB), it was shown that GJPs with CX26 and CX30 did not colocalize with lipid rafts in control mice (Supplemental Figure 9, A, C, and E). In contrast, the lipid raft signals in *Cx26*$^{f/f}$ *P0-Cre* mice localized between S-GJPs with no regularity and with more diffuse labeling and less clarity as compared with those in control mice (Supplemental Figure 9, B, D, and F).

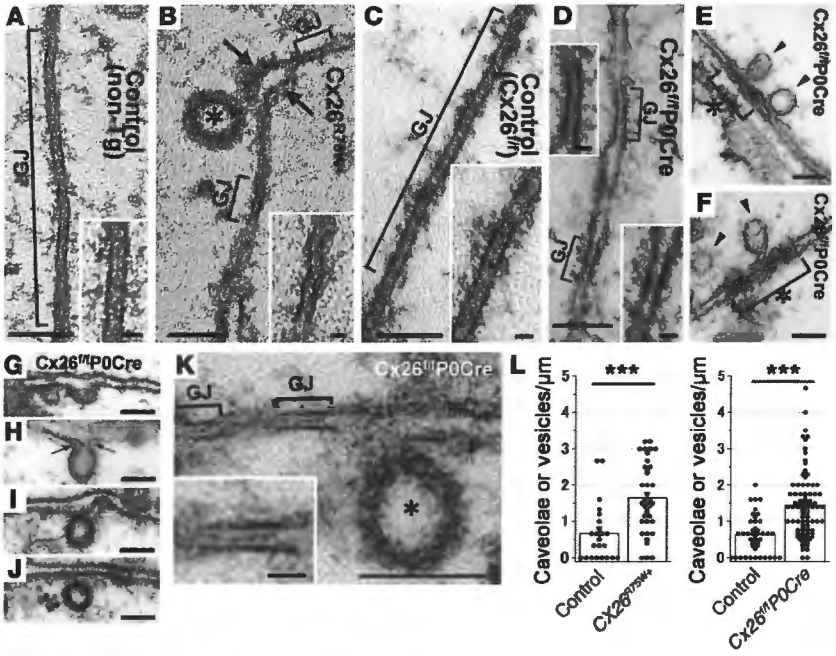

Figure 6

Discontinuous gap junctions with excessive endocytosis in CX26-mutant mice. (**A–K**) Ultrastructure of gap junctions and caveolae in 5-week-old *CX26^{R75W+}* (**B**) and *Cx26$^{f/f}$ P0-Cre* (**D–K**) mice compared with their respective littermate controls (**A** and **C**). Horizontal ultrathin sections of ISCs revealed that most of the gap junctions (GJs, brackets) were remarkably shorter or discontinuous (**B**, **D**, and **K**) compared with those of the control ISCs (**A** and **C**). (**B**) A caveolar vesicle (asterisk) with dissociated plasma membrane (arrows) around a short gap junction in a *CX26^{R75W+}* mouse. In both mutant mice, numerous caveolae and vesicles (**B** and **K**, asterisks; **E** and **F**, arrowheads; **G–J**) were observed. (**E** and **F**) Abnormally condensed intermembrane layers (asterisks with brackets) at the cell borders were observed in *Cx26$^{f/f}$ P0-Cre* mice. (**G–J**) In *Cx26$^{f/f}$ P0-Cre* mice, the plasma membrane showed a small cave-like shape (**G**), an invagination with a neck (**H**, arrows), and the formation of a vesicle-like structure (**I**); the vesicle was separated from the plasma membrane (**J**). (**K**) A caveolar vesicle (asterisk) is shown at the edge of discontinuous short gap junctions (inset) with clear internal layers. (**L**) Number of caveolae or caveolar vesicles that were counted around each cell border (mean ± SEM with dot plots): n = 23 and 39 cells for the littermate control and *CX26^{R75W+}* mice, respectively (***$P = 3.2 \times 10^{-5}$); n = 42 and 97 for the littermate control and *Cx26$^{f/f}$ P0-Cre* mice, respectively (***$P = 8.4 \times 10^{-10}$). Scale bars: 100 nm and 20 nm (insets).

With regard to this drastic GJP disruption, we hypothesized that the abnormal GJPs in both CX26-mutant mice populations were triggered by abnormalities in the formation of the protein complex associated with CX26 and that the resultant molecular changes could lead to the disruption of GJP formation. As for internalization of CX26 protein, we fractionated the cochlear proteins and analyzed them by immunoblotting. CX26 from CX26R75W$^+$ mice was, however, distributed in the plasma membrane fraction, as was CX26 from the control mice (Supplemental Figure 10A). To determine the affinity for other connexins or connexons, we performed coimmunoprecipitation using CX26 antibodies. CX30 was detected in both the CX26R75W$^+$ mice and control mice, and thus no substantive abnormality in the CX26-CX30 interaction in the macromolecular complex could be demonstrated (Supplemental Figure 10B). To examine the interactions with the cytoskeleton, we performed several in vitro experiments with cytochalasin D treatment, which destroys the cytoskeleton, in HEK cells transfected with CX26-EGFP with or without the R75W mutation. We did not, however, observe an effect on GJP formation resulting from disruption of the cytoskeleton (data not shown). As for ubiquitination and autophagy of the GJP, including CX26, we examined the association of ubiquitination and autophagy with GJP disruption in CX26 mutants by immunoblot analysis and transmission electron microscopy. We could not find convincing evidence to show that these processes were more prevalent in CX26-mutant cochleae than in control cochleae (data not shown). As for membrane retrieval at cell junctions, our ultrastructural pathology demonstrated that a significantly larger number of caveolae and vesicles were associated with the cell border (including small gap junctions) in *Cx26$^{f/f}$P0-Cre* mice as compared with those in the control mice (Figure 6). This may indicate that excessive endocytosis occurs in the presence of this CX26 mutation, leading to membrane retrieval that may accelerate GJP degradation.

Discussion

In this study, we demonstrated a novel molecular pathology in the cochlea, that of degradation of the gap junction macromolecular complex in CX26-associated deafness, as well as a novel mechanism of GJP formation into one of two types (L-GJPs or S-GJPs) that is dependent on CX26 expression. These findings were consistent not only in cochlear cells, but also in a human cell line with artificial connexin expression. Our data suggest that both the dominant-negative R75W mutation and the absence of CX26 affect the accumulation and assembly of gap junction units in the cell-cell junctions between cochlear supporting cells.

Regarding the initial phenotype of the hearing organ in the connexin mutants (Figure 1 and Supplemental Figure 4), we have previously described an early histological change in CX26-mutant mice, which showed an absence of the small space needed to form the future tunnel of Corti around P5 (15). As for hearing function, the earliest change detected by the auditory brainstem response occurs only after P11 (15), because hearing input to the mouse cochlea normally begins between P11 and P12 (25). With respect to the function of the cochlear gap junction, Ca^{2+} responses fail to propagate in organotypic cultures with defective expression of CX26 or CX30 from P3 through P6 (26). Thus, to the best of our knowledge, the phenotype at the embryonic stage shown in the present study (Figure 1 and Supplemental Figure 4) has not been previously reported.

The mosaicism generated by our newly developed *Cx26$^{f/f}$P0-Cre* mice revealed that the formation of L-GJPs versus S-GJPs critically depended on CX26 expression, and CX26 expression from both adjacent cells was essential to form normal L-GJPs — even if CX30 was highly expressed in the same cells (Figure 1, D and E). The in vivo (Figure 3) and in vitro (Figure 4) findings concerning GJP formation provided conclusive evidence demonstrating that the formation of

L-GJPs has a definite CX26 dependency and that CX26 is required to form the large macromolecular complex of gap junctions.

Regarding the association between connexins and caveolins (Figure 5 and Supplemental Figure 9), gap junction activity is regulated by protein kinase Cγ activity associated with CAV1-containing lipid rafts (27). Connexin family members (including CX26) are targeted to lipid raft domains, where they interact directly with caveolins such as CAV1 (28). Interestingly, in that experimental system, CX26 was targeted to lipid rafts only when CX26 was coexpressed with CAV1, suggesting that CAV1 recruits CX26 to lipid rafts, although other connexins such as CX32, CX36, CX43, and CX46 showed this lipid raft targeting without any artificial expression of CAV1 (28). These data showing that CX26 is excluded from the lipid raft fraction are in agreement with our present observation that the lipid raft signals in *Cx26$^{f/f}$ P0-Cre* mice localized between S-GJPs with no regularity and with more diffuse labeling and less clarity compared with those in control mice (Supplemental Figure 9). This suggests that the partial targeting to lipid rafts of connexins such as CX30 occurred to prevent the assembly or reassembly of GJPs in CX26-mutant mice.

In many tissues, CX26 is often coexpressed with another connexin in individual cells (29), and it can form heterotypic channels containing homomeric or heteromeric channels with CX30 (10). Hearing loss caused by CX30 deficiency in mice is rescued by the overexpression of CX26 (30). This observation demonstrates that CX26 can compensate for CX30. In contrast, when CX26 is absent in conditional CX26-null mice, CX30 overexpression does not rescue the severe hearing loss (31). Thus, it was concluded that CX26 plays an essential role in the development of the auditory sensory epithelium and that its unique developmental functions required for normal hearing cannot be replaced by CX30 (31). In lens fiber cells, although the expression of CX46 and CX50 overlap extensively, mice that lack one or the other of these connexins (and that serve as a model system for cataract formation) exhibit different phenotypes (32, 33). Macromolecular complex degradation in GJPs that affects other partner connexins and critically reduces functional plaque area may explain not only hearing loss, but also conditions such as cataracts resulting from gap junction dysfunctions with uncompensated connexin mutations.

Until now, hereditary deafness with connexin mutations was believed to be initiated by a single molecular dysfunction or dominant-negative effect on the connexin partners (34), and the primary pathology had never been observed at the embryonic stage. As for the cell degeneration in the connexin mutants, Liang et al. reported that cell degeneration was not a primary cause of CX26 deficiency–associated hearing loss (35). Using a CX26-deficient mouse model similar to the one used in the present study, they demonstrated that cochlear cells, including spiral ganglion neurons, had no significant degeneration throughout postnatal development, although auditory brainstem responses (ABRs) were absent in the whole frequency range (8–40 kHz) after birth.

Here, we demonstrate that connexin-associated deafness, which is the most frequent type of hereditary deafness, may be initiated not by a single molecular dysfunction of connexins, but by a macromolecular complex degradation of GJPs from the embryonic stage. This loss of GJP area may then abolish the proper ionic gradient needed for intercellular communication in the cochlea.

To the best of our knowledge, this is the first report demonstrating that a mutation in CX26 induces macromolecular degradation of large gap junction complexes accompanied by an increase in caveolar structures, which may lead to excessive membrane retrieval and result in a drastic reduction in the GJP area. This may represent a new molecular pathology for hereditary sensorineural deafness and for the general formation of gap junctions, and thus this machinery could be an effective target for drug design and chemical screening to reinforce the assembly of the other cochlear connexins such as CX30.

Methods

Dominant-negative CX26R75W (CX26^{R75W+}) transgenic mice. *CX26^{R75W+}* mice were obtained from a breeding colony of a previously reported line (16). *CX26^{R75W+}* mice were maintained on a C57BL/6J background and crossed with C57BL/6J animals to generate R75W rransgenic offspring. Nontransgenic (non-Tg) littermates on a C57Bl/6J background were always used as the control for *CX26^{R75W+}* mice.

Generation of novel conditional knockout mouse for CX26. A targeting vector of a floxed *Cx26* allele including exons 1 and 2 was consrructed using phage DNA clones from a genomic library of J1 ES cells. An approximately 8.4-kb HindIII-BamHI fragment with exon 1 and a 2.85-kb SacI-SacI fragment containing the 3′ half of exon 2 were isolated and used to construct a targeting vector with long and short homologous sequences, respectively. One loxP sequence was introduced at the end of inrron 1, and a Neo cassette was introduced between two loxP sequences in exon 2. The diphtheria toxin A (DT-A) chain expression cassette was used as a negative selection marker. The linearized targering vector was introduced into J1 ES cells by electroporation, and G418-resistant clones were analyzed by Southern blotting to isolate the homologous recombinant as described (18, 36). Identified recombinant ES cells were injected into C57/BL6J blastocysts. A mouse strain harboring the floxed *Cx26* allele was established by crossing chimeras with C57/BL6J females to produce F1 heterozygotes (*Cx26$^{flox/+}$*). F2 offspring were generated by crossing F1 heterozygotes, and their genotyping was performed by PCR amplification. No apparent abnormalities were detected in the *Cx26$^{f/f}$* mice. Otic vesicle–specific CX26-knockout mice were generated by breeding *Cx26$^{f/f}$* mice with mice that expressed the Cre recombinase gene under the control of the promoter of the *P0* gene (*P0-Cre* mice, on a C57BL/6J background), as described (18). To evaluate Cre recombinase expression and distribution, P0-Cre mice were crossed with ROSA26-GFP reporter mice (Gt-ROSA-26sortm1sor, R26R), and the four mice from rwo litters were analyzed by fluorescence and confocal microscopy (Supplemental Figure 2). *Cx26$^{f/f}$* on a C57Bl/6J background in the littermates was always used as the control for the *Cx26$^{f/f}$ P0-Cre* mice.

Immunohistochemistry. Mice were anestherized, killed, and the inner ear tissues were removed. The cochleae were further dissected and fixed in 4% PFA. Immunofluorescence staining with antibodies against CX26 (rabbit IgG from Life Technologies and mouse IgG from LifeSpan Biosciences), CX30 (rabbit IgG; Life Technologies), caveolin 1 (mouse IgG; BD Biosciences), and caveolin 2 (mouse IgG; BD Biosciences) was performed on whole-mount preparations of the finely dissected organ of Corti or cochlear cryosections (5-μm) that included ISCs. We incubated rhe tissues in the antibody solurions for 1 hour after blocking. The following secondary antibodies were used: Cy3-conjugated anti-rabbit IgG (Sigma-Aldrich) for anti-CX26 or -CX30 rabbit antibodies; Alexa Fluor 488–conjugated anti-mouse IgG (Life Technologies) for anti-CX26 mouse antibodies; Alexa Fluor 594–conjugated anti-mouse IgG (Life Technologies) for anti-CAV1 or -CAV2 mouse antibodies; and Alexa Fluor 633–conjugated anti-rabbit IgG (Life Technologies) for CX30 in double or triple staining. Lipid rafts were visualized with Alexa Flour 594–conjugated cholera toxin subunit B (CTxB, Life Technologies). Fluorescence confocal images were obtained with an LSM510-META confocal microscope (Zeiss). Some of the green fluorescence in *CX26^{R75W+}* mice indicates the pseudocolor obrained from

the Alexa Fluor 633–conjugated secondary antibody signal (Life Technologies), because these mice have ubiquitous EGFP expression from their transgene. *z*-stacks of images were collected at 0.5-μm intervals, and the single image stacks were constructed with the LSM Image Browser (Zeiss); three-dimensional images and videos were constructed using IMARIS software (Bitplane). We analyzed at least five samples from five animals at each age used, and representative images are shown. The compared images were photographed and processed using identical parameters. Three-dimensional images were constructed with *z*-stacked confocal images by IMARIS (Bitplane). Quantitative analysis of the GJP length (mean ± SEM) was performed with the LSM Image Browser (Zeiss), and data were compared using a Student's *t* test (Microsoft Excel).

Western blot analysis. The mouse cochlear proteins were extracted with T-PER Tissue Protein Extraction Reagent (Thermo Scientific) from at least six cochleae that included the organ of Corti, lateral wall, and stria vascularis. The proteins were resolved by SDS-PAGE with 4% to 20% mini-PROTEAN TGX gels (Bio-Rad Laboratories) and then transferred onto a PVDF membrane (Amersham Hybond-P; GE Healthcare). After blocking, the membranes were processed through sequential incubations with anti-caveolin 1 (1:1,000; BD) and anti-caveolin 2 (1:500; Sigma-Aldrich), rabbit anti-CX26 (1:1,000; Life Technologies), mouse anti-CX26 (1:1,000; Life-Span Biosciences), and monoclonal anti-β-actin (1:1,500; Sigma-Aldrich) with HRP-conjugated anti-rabbit or anti-mouse IgG (1:40,000; GE Healthcare) as the secondary antibody. Amersham ELC Prime Western Blotting Detection Reagent (GE Healthcare) was then used for visualization, and the signal was developed on x-ray film (Amersham Hyperfilm ECL; GE Healthcare). Each experiment was repeated at least three times. Densitometric analysis of the band intensities was performed with ImageJ software (NIH). The data were normalized to the corresponding β-actin levels, expressed relative to the amount present in each littermate control, and compared using a Student's *t* test (Microsoft Excel).

Transmission electron microscopy. Animals were deeply anesthetized and perfused intracardially with 0.01 M PBS, followed by 2% PFA and 2% glutaraldehyde in 0.1 M cacodylate buffer. The cochleae were opened and flushed with the fixative for 2 hours at room temperature. After washing, the specimens were postfixed for 1.5 hours in 2% osmium tetroxide in 0.1 M phosphate buffer and then dehydrated through a graded ethanol series and embedded in Epon. Horizontal sections of the surface of the cochlear membrane labyrinth were cut, stained with uranyl acetate and lead citrate, and examined by electron microscopy (H-7100; Hitachi). The numbers of caveolae and vesicles were counted and compared using a Student's *t* test (Microsoft Excel).

Expression constructs and cell lines expressing CX26, CX30, or CX26 mutants. Expression constructs and cell lines wete generated as previously described (10, 22). Briefly, human *GJB6* was obtained by RT-PCR (Superscript II; Life Technologies) from human corpus callosum RNA (Clontech) and subcloned into the pIRESpuro3 vector, then human *GJB2* was subcloned into the pIRESneo3 vector, and the *GJB2* mutations were introduced into the ORF of human *GJB2* cDNA by PCR site-directed mutagenesis using the QuickChange kit (Stratagene). Communication-incompetent HeLa cells were used to generate the stable cell lines expressing WT CX30. To generate cells expressing both WT CX30 and WT CX26 or CX26 mutants, one cloned cell line that stably expressed CX30 was transfected with *GJB2* in pIRESneo3. After selection with both 1 μg/ml of puromycin (Sigma-Aldrich) and 1 mg/ml of G418 (Life Technologies) for about 3 weeks, the colonies were trypsinized, and these bulk-selected cells were expanded for the subsequent studies. Quantitarive analysis of GJP length (mean ± SEM) was performed with ImageJ software.

Immunocytochemistry and GJP quantification. HeLa cells were grown on coverslips for 2 days ro a confluence of approximately 70% to 90%, fixed in acetone, and incubated with a monoclonal antibody (33-5800, diluted 1:500; Zymed Laboratories) and a rabbit antiserum against the C terminus of CX30 (71-2200, diluted 1:1,000; Zymed Laboratories); these did not cross-react with each other, as previously shown (10). The cells were visualized with tetramethylrhodamine isothiocyanate–conjugated (TRITC-conjugated) donkey anti-rabbit (Abcam) and FITC-conjugated donkey anti-mouse secondary antibodies (Abcam). The cells were photographed under a Leica fluorescence microscope with a Hamamatsu C4742-95 digital camera connected to a G5 Mac computer using OpenLAB 2.2 software for deconvolution. The images were analyzed for GJP length using ImageJ software. All GJPs from 30 to 35 cells of each cell line were measured, and the mean GJP length was compared between cells expressing CX30 alone and those expressing both CX30 and CX26, or between cells expressing both CX30 and CX26R75Q and those expressing both CX30 and CX26R75W, using a Student's *t* test (Stata).

Dye transfer with Scrape-loading. Dye transfer was investigated using a scrape-loading assay as previously described (10). Briefly, parental HeLa cells, bulk-selected cells that expressed WT CX30 alone, or cells that coexpressed WT CX30 and CX26 or one of the CX26 mutants (R75Q or R75W) were grown to confluence on coverslips. Following the scrape-loading with 2% NB and diffusion, the cells were washed, fixed, and the NB was visualized by TRITC-conjugated avidin (Sigma-Aldrich). Cells were photographed under a Leica fluorescence microscope with a Hamamatsu C4742-95 digital camera connecred to a G5 Mac computer, using OpenLAB 2.2 software. Dye transfer was quantified by measuring the distance from the scrape line to the point where the average fluorescence intensity dropped to 1.5 times the background intensity. Eleven to twelve images were acquired from each of three different plates of cells. The images were processed and analyzed with ImageJ software, and the mean distance was calculated using Microsoft Excel software and compared using a Student's *t* test (Stata).

Statistics. A one-tailed Student's *t* test, with a significance criterion of $P < 0.05$, was used to compare the GJP length, relative protein levels, number of cells positive for accumulated caveolins, ABR thresholds, propagation ranges of Ca^{2+} signaling, distance of dye transfer, and number of caveolae or vesicles.

Study approval. All experimental protocols were approved by the IACUC of Juntendo University School of Medicine and were conducted in accordance with the NIH guidelines for the care and use of laboratory animals.

Acknowledgments

This work was supported in part by a research grant from the Ministry of Education, Science and Culture (JSPS KAKENHI 25462563, to K. Kamiya); the Ministry of Health, Labor and Welfare of Japan (to K.Kamiya); the MEXT support program for the Strategic Research Foundation at Private Universities, 2011–2012 (to K. Ikeda); the Terumo Life Science Foundation (to K. Kamiya); and by NIH grant KO8DC005394 (to S.W. Yum). We thank M. Yoshida at the Laboratory of Ultrastructure Research for help with the transmission electron microscopy; Y. Fujitani for providing the reporter mouse line; H. Mochizuki for providing the AAV; Y. Yokoyama and B. Kuerban for experimental assistance; the staff of the Division of Proteomics and Biomolecular Sciences for help with our proteomic analysis; and Y. Uchiyama for helpful advice.

Received for publication November 1, 2012, and accepted in revised form January 2, 2014.

Address correspondence to: Kazusaku Kamiya, Department of Otorhinolaryngology, Juntendo University Faculty of Medicine, Hongo 2-1-1, Bunkyo-ku, Tokyo 113-8421, Japan. Phone: 81.3.5802.1229; Fax: 81.3.5840.7103; E-mail: kkamiya@juntendo.ac.jp.

1. Chan DK, Schrijver I, Chang KW. Connexin-26-associated deafness: phenotypic variability and progression of hearing loss. *Genet Med*. 2010; 12(3):174–181.
2. Mason JA, Herrmann KR. Universal infant hearing screening by automated auditory brainstem response measurement. *Pediatrics*. 1998;101(2):221–228.
3. Petersen MB, Willems PJ. Non-syndromic, autosomal-recessive deafness. *Clin Genet*. 2006;69(5):371–392.
4. Morton NE. Genetic epidemiology of hearing impairment. *Ann N Y Acad Sci*. 1991;630:16–31.
5. Birkenhäger R, Lüblinghoff N, Prera E, Schild C, Aschendorff A, Arndt S. Autosomal dominant prelingual hearing loss with palmoplantar keratoderma syndrome: Variability in clinical expression from mutations of R75W and R75Q in the GJB2 gene. *Am J Med Genet A*. 2010;152A(7):1798–1802.
6. Kelsell DP, et al. Connexin 26 murations in hereditary non-syndromic sensorineural deafness. *Nature*. 1997;387(6628):80–83.
7. Kikuchi T, Kimura RS, Paul DL, Takasaka T, Adams JC. Gap junction systems in the mammalian cochlea. *Brain Res Brain Res Rev*. 2000;32(1):163–166.
8. Ahmad S, Chen S, Sun J, Lin X. Connexins 26 and 30 are co-assembled to form gap junctions in the cochlea of mice. *Biochem Biophys Res Commun*. 2003;307(2):362–368.
9. Sun J, et al. Cochlear gap junctions coassembled from Cx26 and 30 show faster intercellular Ca2+ signaling than homomeric counterparts. *Am J Physiol Cell Physiol*. 2005;288(3):C613–C623.
10. Yum SW, et al. Human connexin26 and connexin30 form functional heteromeric and heterotypic channels. *Am J Physiol Cell Physiol*. 2007; 293(3):C1032–C1048.
11. Beltramello M, Piazza V, Bukauskas FF, Pozzan T, Mammano F. Impaired permeability to Ins(1,4,5) P3 in a mutant connexin underlies recessive hereditary deafness. *Nat Cell Biol*. 2005;7(1):63–69.
12. Bukauskas FF, et al. Clustering of connexin 43-enhanced green fluorescent protein gap junction channels and functional coupling in living cells. *Proc Natl Acad Sci U S A*. 2000;97(6):2556–2561.
13. Gaietta G, et al. Multicolor and electron microscopic imaging of connexin trafficking. *Science*. 2002;296(5567):503–507.
14. Sosinsky G. Mixing of connexins in gap junction membrane channels. *Proc Natl Acad Sci U S A*. 1995;92(20):9210–9214.
15. Inoshita A, et al. Postnatal development of the organ of Corti in dominant-negative Gjb2 transgenic mice. *Neuroscience*. 2008;156(4):1039–1047.
16. Kudo T, et al. Transgenic expression of a dominant-negative connexin26 causes degeneration of the organ of Corti and non-syndromic deafness. *Hum Mol Genet*. 2003;12(9):995–1004.
17. Minekawa A, et al. Cochlear outer hair cells in a dominant-negative connexin26 mutant mouse preserve non-linear capacitance in spite of impaired distortion product otoacoustic emission. *Neuroscience*. 2009;164(3):1312–1319.
18. Hasegawa S, et al. Apoptosis in neural crest cells by functional loss of APC tumor suppressor gene. *Proc Natl Acad Sci U S A*. 2002;99(1):297–302.
19. Schutz M, et al. The human deafness-associated connexin 30 T5M mutation causes mild hearing loss and reduces biochemical coupling among cochlear non-sensory cells in knock-in mice. *Hum Mol Genet*. 2010;19(24):4759–4773.
20. Tritsch NX, Yi E, Gale JE, Glowatzki E, Bergles DE. The origin of spontaneous activity in the developing auditory system. *Nature*. 2007;450(7166):50–55.
21. Lang H, et al. Contribution of bone marrow hematopoietic stem cells to adult mouse inner ear: mesenchymal cells and fibrocytes. *J Comp Neurol*. 2006;496(2):187–201.
22. Yum SW, Zhang J, Scherer SS. Dominant connexin26 mutants associated with human hearing loss have trans-dominant effects on connexin30. *Neurobiol Dis*. 2010;38(2):226–236.
23. Zhang J, Scherer SS, Yum SW. Dominant Cx26 mutants associated with hearing loss have dominant-negative effects on wild type Cx26. *Mol Cell Neurosci*. 2011;47(2):71–78.
24. Uygunet O, et al. The novel R75Q mutation in the GJB2 gene causes autosomal dominant hearing loss and palmoplantar keratoderma in a Turkish family. *Clin Genet*. 2002;62(4):306–309.
25. Kamiya K, Takahashi K, Kitamura K, Momoi T, Yoshikawa Y. Mitosis and apoptosis in postnatal auditory system of the C3H/He strain. *Brain Res*. 2001;901(1-2):296–302.
26. Anselmi F, et al. ATP release through connexin hemichannels and gap junction transfer of second messengers propagate Ca2+ signals across the inner ear. *Proc Natl Acad Sci U S A*. 2008;105(48):18770–18775.
27. Lin D, Zhou J, Zelenka PS, Takemoto DJ. Protein kinase Cgamma regulation of gap junction activity through caveolin-1-containing lipid rafts. *Invest Ophthalmol Vis Sci*. 2003;44(12):5259–5268.
28. Schubert AL, Schuberr W, Spray DC, Lisanti MP. Connexin family members target to lipid raft domains and interact with caveolin-1. *Biochemistry*. 2002;41(18):5754–5764.
29. Zhang JT, Nicholson BJ. The ropological structure of connexin 26 and its distribution compared to connexin 32 in hepatic gap junctions. *J Membr Biol*. 1994;139(1):15–29.
30. Ahmad S, et al. Restoration of connexin26 protein level in the cochlea completely rescues hearing in a mouse model of human connexin30-linked deafness. *Proc Natl Acad Sci U S A*. 2007;104(4):1337–1341.
31. Qu Y, et al. Early developmental expression of connexin26 in the cochlea contributes to its dominate functional role in the cochlear gap junctions. *Biochem Biophys Res Commun*. 2012;417(1):245–250.
32. White TW, Goodenough DA, Paul DL. Targeted ablation of connexin50 in mice results in microphthalmia and zonular pulverulent cataracts. *J Cell Biol*. 1998;143(3):815–825.
33. Gong X, et al. Disruption of alpha3 connexin gene leads to proteolysis and cararactogenesis in mice. *Cell*. 1997;91(6):833–843.
34. Zhang Y, Tang W, Ahmad S, Sipp JA, Chen P, Lin X. Gap junction-mediated intercellular biochemical coupling in cochlear supporting cells is required for normal cochlear functions. *Proc Natl Acad Sci U S A*. 2005;102(42):15201–15206.
35. Liang C, Zhu Y, Zong L, Lu GJ, Zhao HB. Cell degeneration is not a primary causer for Connexin26 (GJB2) deficiency associated hearing loss. *Neurosci Lett*. 2012;528(1):36–41.
36. Shibata H, et al. Rapid colorectal adenoma formation initiated by conditional targeting of the Apc gene. *Science*. 1997;278(5335):120–123.

Published January 12, 2012 as 10.3174/ajnr.A2860

White Matter Alteration of the Cingulum in Parkinson Disease with and without Dementia: Evaluation by Diffusion Tensor Tract-Specific Analysis

ORIGINAL RESEARCH

K. Kamagata
Y. Motoi
O. Abe
K. Shimoji
M. Hori
A. Nakanishi
T. Sano
R. Kuwatsuru
S. Aoki
N. Hattori

BACKGROUND AND PURPOSE: In PD, the neurodegenerative process begins in the brain stem and extends to the limbic system and finally into the cerebral cortex. We used diffusion tensor tractography to investigate the FA of the cingulate fiber tracts in patients with PD with and without dementia.

MATERIALS AND METHODS: Fifteen patients with PD, 15 patients with PDD, and 15 age-matched healthy controls underwent diffusion tensor imaging with a 3T MR imager. Diffusion tensor tractography images of the anterior and posterior cingulate fiber tracts were generated. Mean diffusivity and FA were measured along the tractography of the anterior and posterior cingulate fiber tracts. One-way ANOVA with the Scheffé post hoc test was used to compare results among the groups.

RESULTS: FA was significantly lower in patients with PDD than in healthy controls in both the anterior and the posterior cingulate fiber tracts ($P = .003$, $P = .015$) and significantly lower in patients with PD than in healthy controls ($P = .003$) in the anterior cingulate fiber tract. There were no significant mean diffusivity differences among the groups. MMSE and FA values of the anterior cingulate fiber tracts in patients with PDD were significantly correlated ($r = 0.633$, $P < .05$).

CONCLUSIONS: The reduced FA in patients with PD and PDD might reflect neuropathologic changes such as Lewy body pathology in the cingulate fibers. This abnormality might contribute to the dementing process in PD.

ABBREVIATIONS CFT = cingulate fiber tract; FA = fractional anisotropy; HSD = Honestly Significant Difference; MD = mean diffusivity; MMSE = Mini-Mental State Examination; PD = Parkinson disease; PDD = Parkinson disease with dementia; UPDRS = Unified Parkinson's Disease Rating Scale

BRAIN

ORIGINAL RESEARCH

PD is the second most frequent neurodegenerative disorder after Alzheimer disease.[1] It is clinically characterized by a complex motor disorder known as parkinsonism, which is manifested principally by resting tremor, slowness of initial movement, rigidity, and general postural instability.[2] In PD, the primary pathologic changes involve loss of nigrostriatal dopaminergic neurons and the presence of Lewy bodies (α-synuclein–immunoreactive inclusions), with neuronal loss in numerous brain regions.[3] The presence of these Lewy body aggregations, which result, in part, from protein misfolding, is mandatory for neuropathologic confirmation of the clinical diagnosis. The neurodegenerative process (Lewy body pathology) begins in the brain stem and extends into the limbic system and finally into the cerebral cortex.[3-6] Extension of the neurodegenerative process beyond the brain stem is probably the basis for some of the clinical features, including nonmotor deficits such as dementia. Although dementia frequently occurs in the late stages of PD and is associated with increasing disability, mainly in elderly cohorts,[7,8] its neuroanatomic basis is still controversial. In particular, it is unclear whether cognitive deterioration is primarily a cortical or a subcortical process.

To distinguish these pathophysiologic changes in PD, conventional MR imaging has so far been unsuccessful. A noninvasive technology such as diffusion tensor imaging would be helpful for understanding changes at the microstructural level, as well as for monitoring disease progression and improving prognosis in terms of these aspects of PD. A recent study including only patients with newly diagnosed PD used high-resolution diffusion tensor imaging at 3T to evaluate rostral, middle, and caudal ROIs within the substantia nigra on a single section of the midbrain. This study found that patients with PD could be completely distinguished from the control group on the basis of reduced FA values in the caudal ROI of the substantia nigra.[9] In another study, diffusion tensor imaging and ROI analyses revealed changes in FA in the cingulum in patients with PD without dementia relative to controls.[10] Changes in FA have also been found in the frontal lobes, including the supplementary motor area, the presupplementary motor area, and the cingulum, in patients with PD without dementia relative to controls by using statistical parametric mapping analysis in conjunction with diffusion tensor imaging.[11] In a diffusion tensor imaging study of subjects with PDD ($n = 11$), Matsui et al[12] reported a reduction in the FA in the posterior cingulate compared with the FA in subjects with PD ($n = 26$) and healthy controls ($n = 10$). These findings support the notion that the posterior cingulate may play an im-

Received June 6, 2011; accepted after revision August 4.

From the Departments of Radiology (K.K., K.S., M.H., A.N., R.K., S.A.) and Neurology (Y.M., T.S., N.H.), Juntendo University School of Medicine, Tokyo, Japan; and Department of Radiology (O.A.), Nihon University School of Medicine, Tokyo, Japan.

Koji Kamagata and Yumiko Motoi contributed equally to this study.

Please address correspondence to Koji Kamagata, MD, Department of Radiology, Juntendo University School of Medicine, 2–1-1, Hongo Bunkyo-ku Tokyo 113-8421 Japan; e-mail: kkamagat@juntendo.ac.jp

http://dx.doi.org/10.3174/ajnr.A2860

Table 1: Demographic characteristics of subjects

	Control (n = 15)	PD (n = 15)	PDD (n = 15)	P Value (Control vs PD)	P Value (Control vs PDD)	P Value (PD vs PDD)
Sex, male/female	6:9	9:6	8:7	NS	NS	NS
Age in years, (mean) (SD)	69.5 (6.9)	69.8 (5.9)	71.3 (5.6)	NS	NS	NS
Disease duration in months (mean) (SD)	NA	70.6 (58)	139.0 (96.5)	NA	NA	<.05
Hoehn and Yahr stage (SD)	0	2.3 (1.3)	3.0 (0.7)	NA	NA	<.05
MMSE (SD)	28.5	26.1 (3.2)	20.2 (4.0)	NS	<.01	<.01
UPDRS-III score (SD)	NA	19.0 (12.0)	27.1 (9.9)	NA	NA	<.05
Levodopa dosage (mg/day) (median) (SD)	0	409.1 (280.3)	687.0 (126.0)	NA	NA	<.05

Note:—NA indicates not applicable; NS, not significant ($P > .05$).

portant role in the pathologic process of PDD. On pathologic examination, Kövari et al[13] reported that there was a highly significant correlation between the clinical dementia rating scores and regional Lewy body densities in the entorhinal cortex and anterior cingulate gyrus.

The posterior cingulum is an important part of the Papez circuit, which is important for the processing of episodic memory. Posterior CFTs connect the anterior thalamus, cortical cingulum, association cortices, and hippocampus.[14] The importance of the cingulum goes far beyond episodic memory. As previously suggested, the perigenual anterior cingulate cortex is involved in affect; the subgenual subregion of the anterior cingulate cortex, in visceromotor control; the middle cingulate cortex, in response selection (including the dorsal middle cingulate cortex in skeletomotor control); the posterior cingulate cortex, in visuospatial processing; and the retrosplenial cingulate cortex, in memory access.[15]

The cause of dementia in PD is still under debate, but we consider that 1 underlying cause of dementia might be the process of neurodegeneration in the anterior and posterior cingulate gyrus over the brain stem, given the general role of the cingulate gyrus and the pathology of PD as described thus far.

We hypothesized that patients with PD with and without dementia show diffusion abnormalities in the cingulate fibers and that these diffusion abnormalities are an important part of the pathologic process of PD.

Almost all studies of diffusion tensor imaging in PD have used either ROI diffusion tensor imaging[10,12] or statistical parametric mapping methods.[11] Diffusion tensor tractography is one of the most promising imaging processing techniques because it enables both visualization of the fiber pathways in the brain and quantitative analysis of specific fiber bundles.[16,17]

We, therefore, compared diffusion abnormalities in the cingulate fibers in patients with PD with and without dementia and healthy controls by using diffusion tensor tractography.

Materials and Methods

Subjects

This study was approved by an institutional review board, and informed consent was obtained from all participants before evaluation. For subjects who, because of cognitive impairment, were determined by the clinician not to have the capacity to give consent, a legally authorized surrogate provided consent. The demographic characteristics of the subjects are shown in Table 1. In all patients with PD, the disease had been diagnosed by neurologists and fulfilled the UK Parkinson's Disease Society Brain Bank criteria.[18] PD was staged according to the Hoehn and Yahr scale, and the subjects underwent the Japanese version of the MMSE to assess cognitive dysfunction.[19] PDD was diagnosed in accordance with recently published guidelines,[20] and patients with probable PDD were selected. All patients with PD and PDD were taking levodopa at the time of the MR imaging and clinical examination. Eighteen months or more after scanning, all patients remained free of atypical parkinsonism and continued responding satisfactorily to antiparkinsonian therapy. Fifteen healthy subjects were recruited from the general population as control subjects, and they were carefully matched in age to the patients. Individuals with any history of hypertension, diabetes mellitus, cardiovascular disease, stroke, brain tumor, epilepsy, PD, dementia, depression, drug abuse, or head trauma were excluded as controls.

MR Imaging

The brains of all patients were examined with a 3T MR imaging unit (Achieva; Philips Healthcare, Best, the Netherlands) and an 8-channel-array receiving head coil for sensitivity encoding parallel imaging. Regular structural images such as T1-weighted spin-echo images, T2-weighted turbo-spin-echo images, and fluid-attenuated inversion recovery images were obtained before acquisition of diffusion tensor images. Diffusion tensor imaging was performed by using the spin-echo echo-planar technique (TR/TE, 5443/70 ms; matrix size, 128 × 128; FOV, 224 × 224 mm^2; section thickness, 3 mm with no gap). Images were obtained with both 32-direction diffusion encoding (b=1000 s/mm^2 for each direction) and no diffusion encoding (b=0 s/mm^2). A total of 50 axial section images were obtained, covering the whole cerebrum. Scanning time was 7 minutes 17 seconds.

Diffusion Tensor Data Postprocessing

Diffusion tensor imaging data were transferred to an off-line workstation. Maps of FA and MD were computed by using dTV II and Volume-One 1.72 (http://www.volume-one.org), developed by Masutani et al (University of Tokyo; diffusion tensor visualizer available at http://www.ut-radiology.umin.jp/people/masutani/dTV.htm).[17,21] Diffusion tensors were computed, and fiber tracts were created by using interpolation along the z-axis to obtain data (voxel size, 2.0 × 2.0 × 3.0 mm^3). Using 33 sets of images (32 sets of images with b=1000 s/mm^2, 1 set of images with b=0 s/mm^2), we created color-coded maps. On the color maps, red was assigned to left-right, green to the anteroposterior, and blue to the craniocaudal direction.[22] Fiber tracts were based on the fiber assignment made by using the continuous tracking approach[23] to obtain a 3D tract reconstruction. Identification of fiber tracts was initiated by placing a "seed" and a "target" area in anatomic regions through which the particular fibers

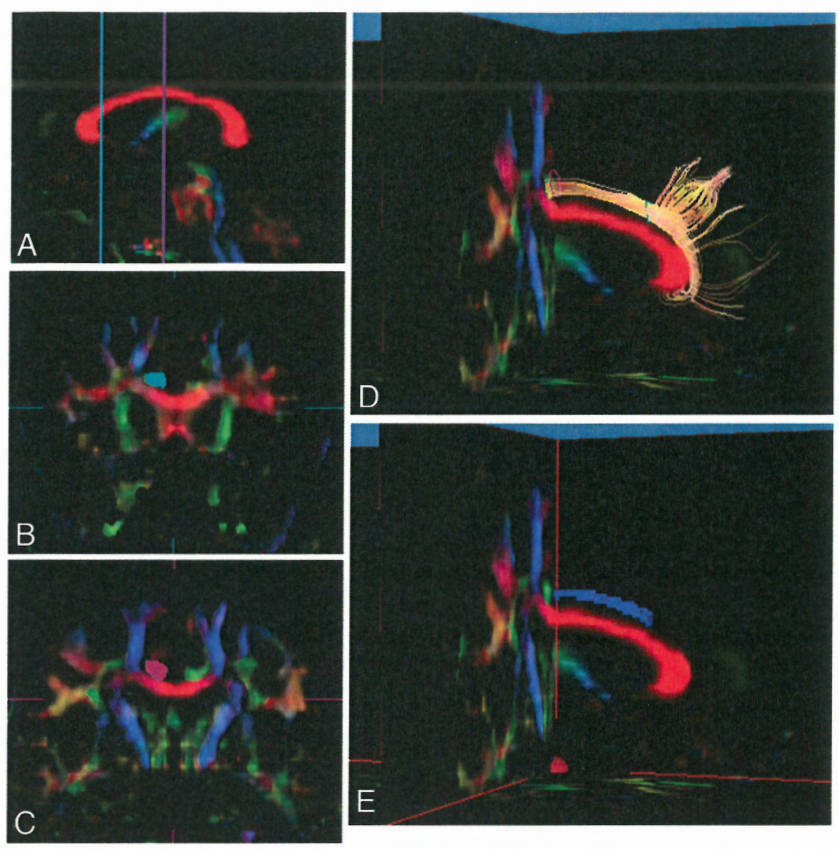

Fig 1. Diffusion tensor tractography images of the right cingulate, fiber tracts (CFTs), and voxelization along with diffusion tensor tractography images of the anterior CFTs. *A*, Sagittal section of the color-coded map was used to determine coronal sections at the level of the genu of the corpus callosum and the middle of the corpus callosum. *B*, The seed ROI, including the entirety of the CFTs (*light blue area*), was placed manually on a coronal section of the color maps at the level of the genu of the corpus callosum. *C*, The target ROI, including the entirety of the CFTs (*purple area*), was placed manually on a coronal section of the color maps at the level of the center of the corpus callosum in the sagittal plane. *D*, Tractographic image of the right anterior CFTs was generated from the seed ROI (light blue line) to the target region of interest (purple line). *E*, In this study, the anterior CFTs were defined as the CFTs between the seed ROI and the target ROI. Voxelization was performed along the right anterior CFTs between the seed ROI and the target ROI (blue voxels), and FA values in coregistered voxels were calculated.

were expected to course.[24] We performed diffusion tensor tractography of the anterior and posterior CFTs and also the corticospinal tracts as a control procedure. The FA threshold for tracking was set at 0.18, and the stop length was set at 160 steps, in accordance with a previous report by Yasmin et al.[25] Tract measurements were performed by 2 of the authors (K.S., K.K.), who were blinded to the disease status of the subjects.

Tractography of the anterior CFT was performed from the seed ROI in the anterior part of the CFT to the target ROI in the middle of the CFT, and tractography of the posterior CFT was performed from the seed ROI in the posterior part of the CFT to the target ROI in the middle of the CFT. Color maps were created to enable the exact and objective placement of these ROIs in the CFTs. Coronal sections at the level of the genu of the corpus callosum and the center of the corpus callosum were identified on a sagittal section of the color map (Fig 1*A*). The CFTs were shown as green in the coronal sections. The seed and target ROIs of the anterior CFTs were drawn manually. The seed region of interest included the entirety of the green part indicating the CFT on a coronal section of the color map at the level of the genu of the corpus callosum, with the green being replaced with light blue to mark the ROI (Fig 1*B*). The target ROI included the entirety of the green part on a coronal section of the color maps at the level of the center of the corpus callosum, with the green replaced by purple to mark the ROI (Fig 1*C*). A tractographic image of the anterior CFT was then generated (Fig 1*D*).

For the posterior CFTs, coronal sections at the level of the splenium of the corpus callosum and the center of the corpus callosum were identified on a sagittal section of the color map (Fig 2*A*). The seed and target ROIs of posterior CFTs were also drawn manually, including the entirety of the green part on a coronal section of the color maps at the level of the splenium of the corpus callosum for the seed (Fig 2*B*) and the center of the corpus callosum for the target (Fig 2*C*). A tractographic image of the posterior CFTs was then generated (Fig 2*D*). The trackline voxelization function of the dTV II software voxelizes the tracking line of the white matter tract by using the original tensor parameters. In this study, anterior and posterior CFTs were defined as the CFTs between the seed ROI and the target ROI. The anterior and posterior CFTs were voxelized between the seed ROI and the target region of interest (Figs 1*E* and 2*E*), and MD and FA values in coregistered voxels were calculated.

Tractography of the corticospinal tract was performed by placing the seed ROI on the cerebral peduncle and the target ROI on the superior precentral gyrus and adjacent white matter, in accordance with a previous report by Yasmin et al.[25] A tractographic image of the corticospinal tract was then generated. The corticospinal tract between the seed region of interest and the target region of interest was voxelized, and MD and FA values in coregistered voxels were calculated.

Statistical Analysis

Statistical analysis of demographic and clinical data was ANOVA with the Tukey HSD test for continuous variables and a χ^2 test for categoric data. The criterion of statistical significance was $P < .05$.

Statistical analyses were performed by using Statistical Package for the Social Sciences for Windows, Release 8.0 (SPSS, Chicago, Illinois). One-way ANOVA was used to compare the averaged MD and FA among patients with PD or PDD and healthy controls. The Scheffé correction was used for post hoc analysis. A Bonferroni correction was applied for the number of comparisons ($n = 3$: [anterior cingulum, posterior cingulum, corticospinal tract], setting the level of significance at $P < .05/3 = .016$). The Spearman rank-order correlation

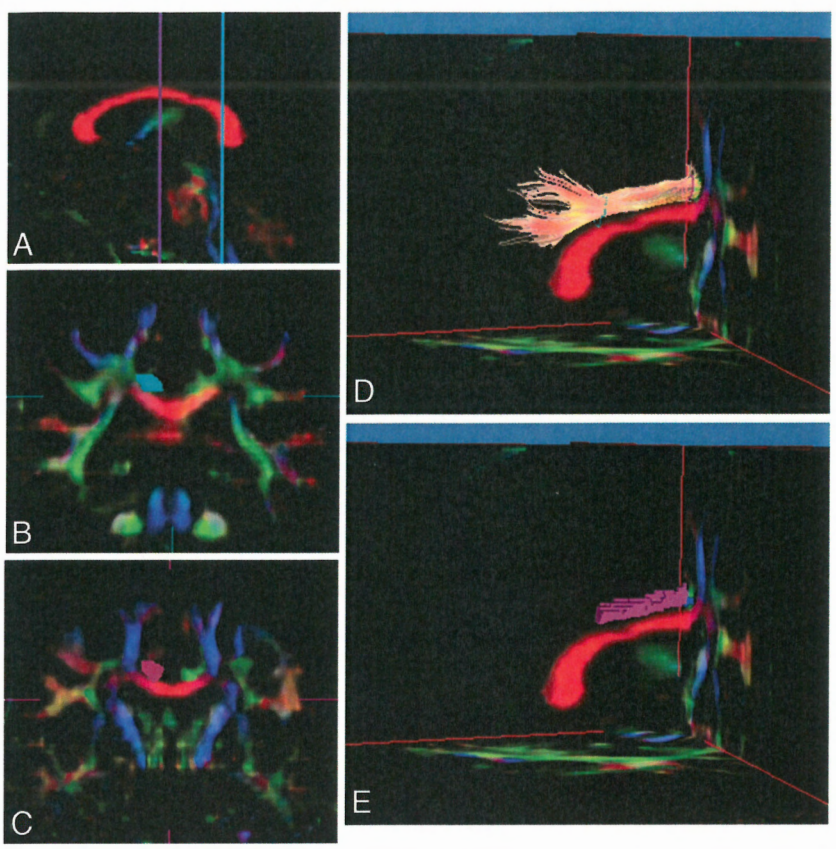

Fig 2. Diffusion tensor tractography images of the right cingulate. Fiber tracts (CFTs) and voxelization along with diffusion tensor tractography of the posterior CFTs. *A*, Sagittal section of the color-coded map was used to determine coronal sections at the level of the splenium of the corpus callosum and the middle of the corpus callosum. *B*, The seed ROI, including the entirety of the CFTs (light blue area), was placed manually on a coronal section of the color maps at the level of the splenium of the corpus callosum. *C*, The target region of interest, including the entirety of the CFTs (purple area), was placed manually on a coronal section of the color maps at the level of the center of the corpus callosum in the sagittal plane. *D*, A tractographic image of the right posterior CFTs was generated from the seed ROI (light blue line) to the target ROI (purple line). *E*, In this study, the posterior CFTs were defined as the CFTs between the seed ROI and the target ROI. Voxelization was performed along the right posterior CFTs between the seed ROI and the target ROI (purple voxels), and FA values in coregistered voxels were calculated.

test was used to investigate the correlations between the imaging measurements and continuous clinical variables.

Results

The 3 groups did not differ by age ($P > .53$, ANOVA) or sex distribution ($P > .68$, χ^2) (Table 1). As expected, patients with PDD scored significantly lower than patients with PD and control subjects on the MMSE ($P < .01$, $P < .01$, ANOVA with the Tukey HSD test), but patients with PD and control subjects did not differ significantly on the MMSE. There were significant differences in disease duration, Hoehn and Yahr stage, UPDRS-III score, and levodopa dosage (milligrams/day) between patients with PD and those with PDD (Table 1).

Reproducibility was determined on the basis of fiber counts and expressed as an intraclass correlation coefficient; the coefficient was 0.96 for the anterior CFTs, 0.94 for the posterior CFTs, and 0.96 for the corticospinal tracts. No significant differences were seen in either MD or FA between the right and left anterior or posterior CFTs ($P > .05$). Averaged values were, therefore, used for further statistical analyses.

There was a significant correlation between the MMSE score and FA value in the anterior CFTs ($r = 0.633$, $P < .05$) in patients with PDD (Fig 3). Measured FA and MD values of the anterior and posterior CFTs were not significantly correlated with disease duration or Hoehn and Yahr stage ($P > .05$) in patients with either PD or PDD.

FA measured in the anterior CFTs was significantly lower in patients with PD and PDD than in healthy controls ($P = .003$, $P = .003$) (Table 2). FA measured in the posterior CFTs was significantly lower in patients with PDD than in healthy controls ($P = .002$). There were no significant diffusion differences in the corticospinal tracts among the groups (Table 2).

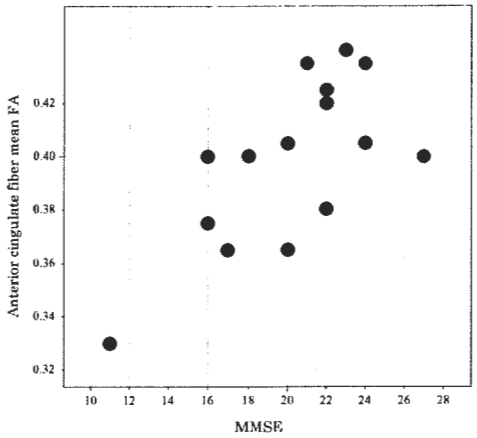

Fig 3. FA values in the anterior cingulate fiber tracts in patients with PDD were significantly correlated with the MMSE scores ($r = 0.633$, $P < .05$).

Discussion

We compared diffusion tensor imaging measurements of the cingulate fasciculi in patients with PD and PDD with those in healthy controls by using diffusion tensor tract-specific analyses. Our major findings were that the measured mean FA in the anterior CFTs was significantly lower in patients with PD and PDD than in healthy controls and that the measured mean FA in the posterior CFTs was significantly lower in patients with PDD than in healthy controls. Most interesting, there was

Table 2: Comparison of MD and FA in patients and control subjects[a]

	HC	PD	PDD	HC > PD	HC > PDD	PD > PDD
Anterior CFTs						
FA	0.441 ± 0.035[a]	0.399 ± 0.028	0.399 ± 0.031	$P = .003$[b]	$P = .003$[b]	$P = .90$
MD[c]	0.758 ± 0.025	0.789 ± 0.034	0.775 ± 0.031	$P = .031$	$P = .33$	$P = .47$
Posterior CFTs						
FA	0.519 ± 0.038	0.489 ± 0.040	0.477 ± 0.040	$P = .09$	$P = .015$[b]	$P = .72$
MD	0.755 ± 0.046	0.759 ± 0.022	0.770 ± 0.027	$P = .94$	$P = .32$	$P = .51$
Corticospinal tract						
FA	0.655 ± 0.020	0.651 ± 0.022	0.651 ± 0.024	$P = .89$	$P = .87$	$P = .99$
MD[c]	0.751 ± 0.026	0.775 ± 0.025	0.756 ± 0.031	$P = .077$	$P = .92$	$P = .17$

Note:—HC indicates healthy controls.
[a] Values are mean ± SD.
[b] Indicates statistical significance ($P < .016$).
[c] Mean diffusivity values are expressed as 10^{-3} mm^2/s.

also a significant correlation between MMSE scores and FA values of the anterior CFTs in patients with PDD.

Diffusion tensor imaging is capable of measuring the characteristics of local microstructural water diffusion in brain tissue. One representative diffusion tensor measurement is FA, which describes the degree of water molecule anisotropy or the directional preference of the water diffusion process. FA abnormalities in the brain are interpreted pathologically as being caused by loss of neurons or glia or by gliosis or demyelination.[26]

The existing literature already includes results showing diffusion abnormalities in the cingulum bundle.[10-12,27] However, there has been no report to date of the use of tractography to show diffusion abnormalities in the cingulum bundle in patients with PD and PDD. Diffusion tensor tractography enabled us to clearly identify the anterior CFTs and posterior CFTs and measure diffusion parameters more precisely than with a manually drawn ROI study. Use of diffusion tensor tractography avoided contamination of data by anterior and posterior CFTs from adjacent components such as CSF or callosal fibers. Taoka et al[28] compared a tract-specific method and an ROI method for evaluating the diffusion parameters of 3 cerebellar peduncles in subtypes of spinocerebellar degenerative disease. They found that the tract-specific method tended to show significant differences more clearly than the ROI method because instabilities in the placement of ROIs in anatomic structures directly result in instability of the values measured with the ROI method.[28] We consider the results of the tractography to be more reproducible and more accurate than those of other research in the existing literature.

The decreased FA in the anterior CFTs in patients with PD and PDD may be associated with the pathologic process of PD. Brains of patients with PD have Lewy bodies in various areas, including the cingulate cortex.[3-6] Neuropathologically, postmortem material from patients with PD is divided into 6 subgroups (stages 1–6) that differ from each other by virtue of changes in the topographic distribution pattern and severity of Lewy body involvement.[4-6] Postmortem material from patients with PD who manifest clinical findings consistent with sporadic PD can be assigned to 1 of 3 subgroups (stages 4–6). Because Lewy bodies appear in the anterior cingulate gyrus in stage 5,[3-6] neurodegeneration may occur in the anterior CFTs adjacent to the anterior cingulate gyrus.

The FA values of the anterior CFTs were significantly correlated with the MMSE scores. This result is in good agreement with that of a previous pathologic study in which Kövari et al[13] reported a highly significant correlation between the clinical dementia rating scores and regional Lewy body densities in the anterior cingulate gyrus.

The decreased FA values in the posterior CFTs of patients with PDD may be related to the pathologic processes responsible for dementia in PD. Atrophy in the limbic and paralimbic regions occurs in patients with PD without dementia, though less markedly so than in patients with PDD.[29,30] Metabolic abnormalities in the posterior cingulate regions[31,32] and cerebral blood flow reduction in the anterior cingulate cortex[33,34] have been reported in patients with PDD. A reduction in cerebral blood flow in the posterior cingulate cortex has also been reported in PDD.[33] In several previous studies of neuropsychologic diseases such as amyotrophic lateral sclerosis, posttraumatic stress disorder, and schizophrenia, metabolic and cerebral blood flow abnormalities in the cortex and diffusion abnormalities in the white matter tracts that connect the affected regions of the cortex have been reported.[16,35,36]

Our definition of the posterior cingulum bundle probably corresponds to the white matter directly below the posterior cingulate cortex and dorsal middle cingulate cortex, as described by Vogt et al.[15] They have also reported on the relationship between the posterior cingulate cortex and visuospatial perception. There have been reports of a general reduction in visuospatial perception in patients with PDD.[37,38] Diffusion impairment in the posterior cingulum bundle may reflect the particular pathophysiology of PDD.

The pathologic processes responsible for dementia in patients with PD are still controversial. Cortical Lewy bodies; striatal and extrastriatal dopamine deficiencies; loss of ascending noradrenergic, cholinergic, and serotonergic projections to the cortex; disruption of corticostriatal connections; coexistence of Alzheimer disease pathology; and frontal dysfunction have all been considered responsible for dementia in PD.[39-41] Although the pathologic processes responsible for dementia in PD may be multifaceted, our results show that the posterior CFT is important in the dementing process in PDD.

Some limitations of our study need to be addressed. First, because the diagnoses of PD and PDD were not histopathologically confirmed, the possibility of misdiagnosis remains. However, the validity of the diagnoses is supported by the fact that 18 months or more after being scanned, all the patients remained free of atypical parkinsonisms and continued to respond satisfactorily to antiparkinsonian therapy. Second, the

small size of our samples may have limited the detection of group differences, especially in the comparison of neuropsychological profiles and FA values. Third, the seed and target ROIs were drawn manually, and the reproducibility of the measurements was uncertain. However, rater bias was prevented by blinding, all ROIs were drawn by 2 of the authors, and the intraclass correlation coefficients were 0.94–0.96.

Conclusions

The decreased FA found in patients with PD on tract-specific analysis is likely due to neuronal loss, gliosis, or demyelination in the white matter of the cingulum. Our results suggest that these reduced values reflect neuropathologic changes—such as Lewy body pathology in the cingulate gyrus—that may play important roles in the dementing process in PD.

Acknowledgments

We thank Nozomi Hamasaki and Syuji Sato, MR imaging technologists, for their skillful performance in data acquisition; Toshino Suzuki, Tomomi Okamura, Yasmin Hasina, as research assistants; Yuriko Suzuki and Masaru Takashima, Philips Healthcare, for their technical assistance. We also thank Keisuke Sasai for administrative assistance.

References

1. de Lau LM, Breteler MM. **Epidemiology of Parkinson's disease.** *Lancet Neurol* 2006;5:525–35
2. Obeso JA, Rodriguez-Oroz MC, Rodriguez M, et al. **Pathophysiology of the basal ganglia in Parkinson's disease.** *Trends Neurosci* 2000;23:S8–19
3. Braak H, Del Tredici K. **Invited article: nervous system pathology in sporadic Parkinson disease.** *Neurology* 2008;70:1916–25
4. Braak H, Del Tredici K, Bratzke H, et al. **Staging of the intracerebral inclusion body pathology associated with idiopathic Parkinson's disease (preclinical and clinical stages).** *J Neurol* 2002;249(suppl 3):III/1–5
5. Braak H, Del Tredici K, Rub U, et al. **Staging of brain pathology related to sporadic Parkinson's disease.** *Neurobiol Aging* 2003;24:197–211
6. Braak H, Ghebremedhin E, Rub U, et al. **Stages in the development of Parkinson's disease-related pathology.** *Cell Tissue Res* 2004;318:121–34
7. Aarsland D, Tandberg E, Larsen JP, et al. **Frequency of dementia in Parkinson disease.** *Arch Neurol* 1996;53:538–42
8. Marder K, Tang MX, Cote L, et al. **The frequency and associated risk factors for dementia in patients with Parkinson's disease.** *Arch Neurol* 1995;52:695–701
9. Vaillancourt DE, Spraker MB, Prodoehl J, et al. **High-resolution diffusion tensor imaging in the substantia nigra of de novo Parkinson disease.** *Neurology* 2009;72:1378–84
10. Gattellaro G, Minati L, Grisoli M, et al. **White matter involvement in idiopathic Parkinson disease: a diffusion tensor imaging study.** *AJNR Am J Neuroradiol* 2009;30:1222–26
11. Karagulle Kendi AT, Lehericy S, Luciana M, et al. **Altered diffusion in the frontal lobe in Parkinson disease.** *AJNR Am J Neuroradiol* 2008;29:501–05
12. Matsui H, Nishinaka K, Oda M, et al. **Dementia in Parkinson's disease: diffusion tensor imaging.** *Acta Neurol Scand* 2007;116:177–81
13. Kövari E, Gold G, Herrmann FR, et al. **Lewy body densities in the entorhinal and anterior cingulate cortex predict cognitive deficits in Parkinson's disease.** *Acta Neuropathol* 2003;106:83–88
14. Duvernoy HM. *The Human Hippocampus: Functional Anatomy, Vascularization, and Serial Sections with MRI.* Berlin, Germany: Springer-Verlag; 2005
15. Vogt BA, Nimchinsky EA, Vogt LJ, et al. **Human cingulate cortex: surface features, flat maps, and cytoarchitecture.** *J Comp Neurol* 1995;359:490–506
16. Aoki S, Iwata NK, Masutani Y, et al. **Quantitative evaluation of the pyramidal tract segmented by diffusion tensor tractography: feasibility study in patients with amyotrophic lateral sclerosis.** *Radiat Med* 2005;23:195–99
17. Kunimatsu A, Aoki S, Masutani Y, et al. **Three-dimensional white matter tractography by diffusion tensor imaging in ischaemic stroke involving the corticospinal tract.** *Neuroradiology* 2003;45:532–35
18. Hughes AJ, Daniel SE, Kilford L, et al. **Accuracy of clinical diagnosis of idiopathic Parkinson's disease: a clinico-pathological study of 100 cases.** *J Neurol Neurosurg Psychiatry* 1992;55:181–84
19. Folstein MF, Folstein SE, McHugh PR. **"Mini-mental state": a practical method for grading the cognitive state of patients for the clinician.** *J Psychiatr Res* 1975;12:189–98
20. Goetz CG, Emre M, Dubois B. **Parkinson's disease dementia: definitions, guidelines, and research perspectives in diagnosis.** *Ann Neurol* 2008;64(suppl 2):S81–92
21. Kubicki M, Westin CF, Maier SE, et al. **Uncinate fasciculus findings in schizophrenia: a magnetic resonance diffusion tensor imaging study.** *Am J Psychiatry* 2002;159:813–20
22. Pajevic S, Pierpaoli C. **Color schemes to represent the orientation of anisotropic tissues from diffusion tensor data: application to white matter fiber tract mapping in the human brain.** *Magn Reson Med* 2000;43:921
23. Mori S, Crain BJ, Chacko VP, et al. **Three-dimensional tracking of axonal projections in the brain by magnetic resonance imaging.** *Ann Neurol* 1999;45:265–69
24. Wakana S, Jiang H, Nagae-Poetscher LM, et al. **Fiber tract-based atlas of human white matter anatomy.** *Radiology* 2004;230:77–87
25. Yasmin H, Aoki S, Abe O, et al. **Tract-specific analysis of white matter pathways in healthy subjects: a pilot study using diffusion tensor MRI.** *Neuroradiology* 2009;51:831–40
26. Abe O, Aoki S, Hayashi N, et al. **Normal aging in the central nervous system: quantitative MR diffusion-tensor analysis.** *Neurobiol Aging* 2002;23:433–41
27. Firbank MJ, Blamire AM, Krishnan MS, et al. **Atrophy is associated with posterior cingulate white matter disruption in dementia with Lewy bodies and Alzheimer's disease.** *Neuroimage* 2007;36:1–7
28. Taoka T, Kin T, Nakagawa H, et al. **Diffusivity and diffusion anisotropy of cerebellar peduncles in cases of spinocerebellar degenerative disease.** *Neuroimage* 2007;37:387–93
29. Nagano-Saito A, Washimi Y, Arahata Y, et al. **Cerebral atrophy and its relation to cognitive impairment in Parkinson disease.** *Neurology* 2005;64:224–29
30. Beyer MK, Janvin CC, Larsen JP, et al. **A magnetic resonance imaging study of patients with Parkinson's disease with mild cognitive impairment and dementia using voxel-based morphometry.** *J Neurol Neurosurg Psychiatry* 2007;78:254–59
31. Camicioli RM, Korzan JR, Foster SL, et al. **Posterior cingulate metabolic changes occur in Parkinson's disease patients without dementia.** *Neurosci Lett* 2004;354:177–80
32. Vander Borght T, Minoshima S, Giordani B, et al. **Cerebral metabolic differences in Parkinson's and Alzheimer's diseases matched for dementia severity.** *J Nucl Med* 1997;38:797–802
33. Mito Y, Yoshida K, Yabe I, et al. **Brain 3D-SSP SPECT analysis in dementia with Lewy bodies, Parkinson's disease with and without dementia, and Alzheimer's disease.** *Clin Neurol Neurosurg* 2005;107:396–403
34. Mito Y, Yoshida K, Yabe I, et al. **Brain SPECT analysis by 3D-SSP and phenotype of Parkinson's disease.** *J Neurol Sci* 2006;241:67–72
35. Abe O, Yamasue H, Kasai K, et al. **Voxel-based diffusion tensor analysis reveals aberrant anterior cingulum integrity in posttraumatic stress disorder due to terrorism.** *Psychiatry Res* 2006;146:231–42
36. Buchsbaum MS, Tang CY, Peled S, et al. **MRI white matter diffusion anisotropy and PET metabolic rate in schizophrenia.** *Neuroreport* 1998;9:425–30
37. Docherty MJ, Burn DJ. **Parkinson's disease dementia.** *Curr Neurol Neurosci Rep* 2010;10:292–98
38. Mahieux F, Fenelon G, Flahault A, et al. **Neuropsychological prediction of dementia in Parkinson's disease.** *J Neurol Neurosurg Psychiatry* 1998;64:178–83
39. Brown RG, Marsden CD. **How common is dementia in Parkinson's disease?** *Lancet* 1984;2:1262–65
40. Cooper JA, Sagar HJ, Jordan N, et al. **Cognitive impairment in early, untreated Parkinson's disease and its relationship to motor disability.** *Brain* 1991;114(pt 5):2095–122
41. Lees AJ, Smith E. **Cognitive deficits in the early stages of Parkinson's disease.** *Brain* 1993;106(pt 2):257–70